Univerza
v Ljubljani

Fakulteta *za*
gradbeništvo in
geodezijo

Doktorandka

BARBARA FORTUNA

RAČUNSKO IN EKSPERIMENTALNO DOLOČANJE NOSILNOSTI LAMELIRANIH LEPLJENIH NOSILCEV IZ BUKOVEGA LESA

Doktorska disertacija

COMPUTATIONAL AND EXPERIMENTAL ASSESSMENT OF LOAD BEARING CAPACITY OF GLUED LAMINATED BEAMS MADE OF BEECH WOOD

Doctoral disertation

Ljubljana, oktober 2022

Univerza
v Ljubljani
Fakulteta *za*
gradbeništvo in
geodezijo

Mentor: izr. prof. dr. Simon Schnabl, UL FKKT in UL FGG

Somentor: prof. dr. Goran Turk, UL FGG

Komisija za spremljanje doktorske študentke:

prof. dr. Tomaž Hozjan, UL FGG

prof. dr. Milan Šernek, UL BF

prof. dr. Jan Willem van de Kuilen, TUM

izr. prof. dr. Simon Schnabl, UL FKKT in UL FGG

prof. dr. Goran Turk, UL FGG

STRAN S POPRAVKI / ERRATA

Stran z napako	**Vrstica z napako**	**Namesto**	**Naj bo**
Page	**Line**	**Error**	**Correction**

“Blank page.”

BIBLIOGRAPHIC-DOCUMENTALISTIC INFORMATION AND ABSTRACT

UDC: 624.011.1:624.072.2:624.046.2(043)
Author: Barbara Fortuna
Supervisor: Assoc. Prof. Simon Schnabl, Ph.D.
Co-Supervisor: Prof. Goran Turk, Ph.D.
Title: Computational and Experimental Assessment of Load Bearing Capacity of Glued Laminated Beams made of Beech Wood.
Notes: 152 p., 101 fig., 36 tab., 269 eq.
Keywords: beech wood, glued laminated beams, adhesive, tension testing, finger joints, analytical model, numerical model

Abstract:

Study of the mechanical properties of glued laminated beech beams is presented in this doctoral thesis. The high strength and stiffness properties of beech wood require that special attention be paid to the tensile strength of different finger joint profiles with different adhesives used for longitudinal gluing of beech boards. The results of experimental testing of finger joints in tension have shown that longer and slimmer finger joints are required to increase the load bearing capacity of finger joints. The influence of the type of adhesive used decreases with the length of the finger joints, so that existing structural adhesives are suitable for use with glued laminated beech beams. Fourteen glued laminated beech beams were produced. The beams were then tested and the strength and stiffness properties were measured. In addition to flexural strength and flexural elastic modulus, shear modulus and contact stiffness between layers were measured. Analytical and numerical models for the analysis of glued laminated beech beams were established. The models are based on Reissner's planar beam theory and take into account the slip between laminations and the influence of finger joints. The analytical solution for Euler-Bernoulli and Timoshenko-Ehrenfest glued laminated beech beams is presented. The numerical model can be used for modelling glued laminated beams with an arbitrary number of laminations and an arbitrary number of finger joints. The model has been validated with the experimental results and the results agree well. Stochastic analysis of glued laminated beech beams is also performed using analytical and numerical model and the results showed a good agreement with the experimental results and that numerical model can simulate the mechanical behaviour of the glued laminated beech beams.

“Blank page.”

BIBLIOGRAFSKO-DOKUMENTACIJSKA STRAN IN IZVLEČEK

UDK:	624.011.1:624.072.2:624.046.2(043)
Avtor:	Barbara Fortuna
Mentor:	izr. prof. dr. Simon Schnabl
Somentor:	prof. dr. Goran Turk
Naslov:	Računsko in eksperimentalno določanje nosilnosti lameliranih lepljenih nosilcev iz bukovega lesa
Obseg in oprema:	152 str., 101 sl., 36 pregl., 269 en.
Ključne besede:	bukov les, lamelirani lepljeni nosilci, lepilo, natezni testi, zobati spoji, analitični model, numerični model

Izvleček:

V doktorski disertaciji je predstavljena analiza mehanskih lastnosti lameliranih lepljenih nosilcev iz bukovega lesa. Zaradi visokih mehanskih lastnosti bukovega lesa je potrebno posebno pozornost posvetiti zobatim spojem ter njihovi natezni nosilnosti. Pri tem sta geometrija zobatih spojev in lepilo, ki se uporablja za dolžinsko spajanje bukovih desk, bistvenega pomena. Rezultati eksperimentalnih testov so pokazali, da z daljšimi in ožjimi zobatimi spoji nosilnost zobatega spoja narašča pri tem pa se vpliv lepila zmanjšuje. Obstoječa konstrukcijska lepila so se izkazala kot ustrezna za uporabo v lepljenih lameliranih nosilcih iz bukovega lesa. Štirinajst lameliranih lepljenih nosilcev iz bukovega lesa je bilo testiranih v upogibu. Poleg upogibne trdnosti in upogibnega elastičnega modula lepljenih lameliranih nosilcev iz bukovega lesa, smo izmerili tudi strižni modul nosilcev in togost stika med lamelami. Za analizo lameliranih lepljenih nosilcev iz bukovega lesa sta pripravljena analitični in numerični model. Oba temeljita na Reissnerjevi teoriji ravninskih nosilcev. Pri analizi je upoštevan zdrs med sloji in vpliv zobatih spojev. Analitična rešitev je prikazana za Euler-Bernoullijev in Timoshenko-Ehrenfestov nosilec. Z numeričnim modelom je mogoče modelirati lamelirane lepljene nosilce s poljubnim številom lamel ter poljubnim številom zobatih spojev. Model je validiran z rezultati eksperimentalnih testov in pokazalo se je dobro ujemanje med izračunanimi in izmerjenimi vrednostmi. Za ovrednotenje rezultatov je bila opravljena tudi stohastična analiza, tako z analitičnim, kot tudi numeričnim modelom lameliranega lepljenega nosilca.

ABBREVIATIONS/ OKRAJŠAVE

CLT	cross laminated timber
FDS	fully debonded segment
FJ	finger joint
GL	glued laminated beam
GP	grip-pro (melamin-urea-formaldehyde type of adhesive)
LVDT	linear variable displacement transformers
MUF	melamin-urea-formaldehyde
MF	melamin-formaldehyde
PU	polyurethane
OSB	oriented strand board
PRF	phenol-resorcinol-formaldehyde

ZAHVALA

Ob zaključku pomembnega poglavja v mojem življenju se moram zahvaliti vrsti ljudi, ki so mi stali ob strani. Hvala mentorju izr. prof. dr. Simonu Schnablu in somentorju prof. dr. Goranu Turku za vodenje skozi doktorski študij. Hvala za vse vzpodbudne besede ob premagovanju izzivov, ki so se včasih zdeli preveliki. Hvala za vso ponujeno pomoč in vso potrpežljivost tekom mojega učenja. Hvala tudi zato, ker sta mi omogočila vpogled v zanimiv svet raziskovalnega dela.

Velik del raziskovalnega dela je bil opravljen v laboratoriju, kjer brez pomoči ne bi šlo. Zato se posebej zahvaljujem Mitji, ki je poleg dela v laboratoriju, s svojimi idejami v znatni meri oblikoval raziskovalno delo. Hvala za vso vzpodbudo. Hvala tudi Tamari, Žigi in Goranu za vse zabavne trenutke s katerimi smo si olepšali delo v laboratoriju. S skupnimi močmi smo rešili vsak nepričakovan izziv z bolj ali manj nasmejanim obrazom, kar mi bo za vedno ostalo v lepem spominu.

Seveda pa iskrena hvala prijateljem znotraj in zunaj fakultete. Vaše vzpodbudne besede so bile zame neprecenljivega pomena in so me prepričale, da zmorem in da bom. Hvala za vašo potrpežljivost. Hvala, da niste obupali. Najlepša hvala družini za vso podporo. Staršema hvala, da sta me vzgojila v trmasto osebo in da sta mi zagotovila možnosti za vztrajanje do konca. Brez vaju ne bi bilo nič.

Moja Izabela pa si zasluži posebno zahvalo za njeno sodelovanje pri dolgih urah študija. Vedno si mi znala narisati nasmeh in s svojim pisanim svetom olepšati mojega. Biti tvoj zgled je zame največja motivacija.

Vsem skupaj še enkrat iskrena hvala.

GRAPHICAL OVERVIEW

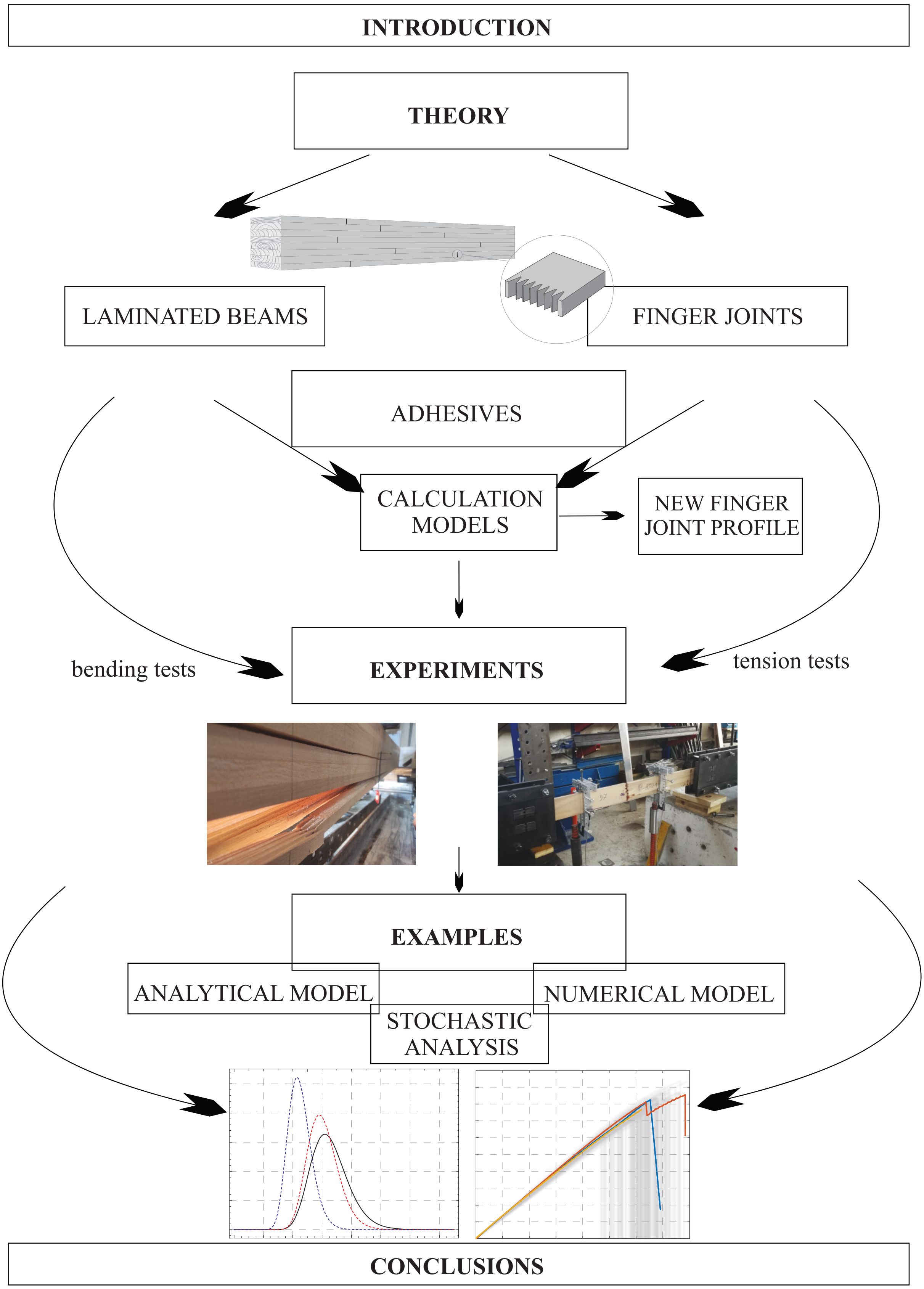

“Blank page.”

KAZALO VSEBINE

BIBLIOGRAPHIC-DOCUMENTALISTIC INFORMATION AND ABSTRACT III

BIBLIOGRAFSKO-DOKUMENTACIJSKA STRAN IN IZVLEČEK V

ABBREVIATIONS/OKRAJŠAVE VI

ZAHVALA VII

1 INTRODUCTION 1

1.1 Motivation . . . 1
1.2 Research Hypotheses and Goals . . . 2
1.3 State of the art in the research field . . . 2
1.4 Organisation of Work . . . 6

2 THEORY ON LAMINATED BEAMS AND FINGER JOINTS 8

2.1 Fundamental equations of laminated beams . . . 8
2.1.1 Kinematic equations . . . 8
2.1.2 Equilibrium equations . . . 10
2.1.3 Constitutive equations . . . 13
2.1.4 Boundary conditions . . . 15
2.2 Constraining equations . . . 15
2.2.1 Euler-Bernoulli laminated beam . . . 18
2.2.2 Timoshenko-Ehrenfest laminated beam . . . 20
2.2.3 Finger joints . . . 21
2.3 Analytical solution of laminated beam with finger joints . . . 22
2.3.1 Solution for the Euler-Bernoulli laminated beam without shear deformation . . 23
2.3.2 Solution for the Timoshenko-Ehrenfest laminated beam with shear deformation 25
2.4 Numerical solution of laminated beam with finger joints . . . 25
2.4.1 Modified principle of virtual work . . . 25
2.4.1.1 Euler-Lagrange equations of the Timoshenko-Ehrenfest laminated beam 28
2.4.2 Discretization of Euler-Lagrange equations of laminated Timoshenko-Ehrenfest beam . . . 30
2.4.2.1 Solution of the generalized discrete equilibrium equations of glued laminated beam . . . 32
2.5 Finger joints . . . 36
2.5.1 Preliminary research . . . 37
2.5.2 Numerical model of the finger joint . . . 39
2.5.3 Adhesives . . . 43
2.5.3.1 Classification of the adhesives . . . 44

2.5.3.2 Formation of the adhesive bond of wood 46

3 EXPERIMENTAL INVESTIGATION 50

3.1 Material and test configuration 51

3.1.1 10 mm finger joints 51

3.1.2 18 mm finger joints 54

3.1.3 40 mm finger joints 59

3.2 Bending tests of the laminated beams made of beech wood 66

3.2.1 Laminated beams with 18 mm finger joints 67

3.2.2 Laminated beams with 40 mm finger joints 69

4 ILLUSTRATIVE EXAMPLES 76

4.1 Analytical model 76

4.1.1 Simply supported two-layer Euler-Bernoulli beam with two finger joints-analytical model 76

4.1.2 Parametric study on two-layer simply supported Euler-Bernoulli beam 79

4.1.2.1 Parametric study on two-layer Euler-Bernoulli beam with one finger joint 79

4.1.2.2 Stiffness properties of the interlayer connection K_X and finger joints K_{FJ} 80

4.1.2.3 Position and length of the fully debonded segment 82

4.1.3 Continuous two-layer Euler-Bernoulli beam with finger joints in the two spans 83

4.1.4 Parametric study on continuous two-layer Euler-Bernoulli beam with finger joints in the two spans 87

4.2 Numerical model 91

4.2.1 Verification of numerical model 91

4.2.2 Validation of the numerical model 91

4.2.3 Verification of the influence of the finger joint 97

4.2.4 The robustness of the numerical model 100

4.2.5 Parametric study on multi-layer simply supported Timoshenko-Ehrenfest beam 101

4.2.5.1 Influence of number of laminations 101

4.2.5.2 Parametric study on ten-layer simply supported Timoshenko-Ehrenfest beam 102

4.3 Stochastic approach to modelling the laminated beams with finger joints 104

4.3.1 Simulations on two-layer simply supported Euler-Bernoulli beam with one finger joint 104

4.3.2 Simulations on ten-layer simply supported beam with finger joints 109

4.3.2.1 Linear material 109

4.3.2.2 Nonlinear material 112

5 CONCLUSIONS 117

6 RAZŠIRJENI POVZETEK 121

6.1 Uvod 121

6.2 Osnovne enačbe računskega modela lameliranega lepljenega nosilca z zobatimi spoji . 122
6.2.1 Analitična rešitev lameliranega nosilca z zobatimi spoji 126
6.2.2 Numerična rešitev lameliranega nosilca z zobatimi spoji 128
6.3 Zobati spoji 130
6.4 Konstrukcijska lepila 131
6.5 Laboratorijski testi 132
6.5.1 Natezno preizkušanje zobatih spojev 132
6.5.1.1 10 mm dolgi zobati spoji 132
6.5.1.2 18 mm dolgi zobati spoji 132
6.5.1.3 40 mm dolgi zobati spoji 133
6.5.2 Upogibno preizkušanje lameliranih nosilcev 134
6.5.2.1 Lamelirani nosilci z 18 mm dolgimi zobatimi spoji 134
6.5.2.2 Lamelirani nosilci s 40 mm dolgimi zobatimi spoji 134
6.6 Računski primeri 135
6.6.1 Analitična rešitev Euler-Bernoullijevega nosilca z zobatimi spoji 135
6.6.2 Numerična rešitev večslojnega nosilca z zobatimi spoji 137
6.6.3 Stohastična analiza deset slojnih nosilcev 137
6.7 Zaključki 139

VIRI **141**

“Blank page.”

LIST OF FIGURES

2.1 Undeformed and deformed configuration of laminated beam. 9
2.2 Contact tractions on contact surface, influencing on layer i. 11
2.3 Boundary loads and internal forces and moments. 13
2.4 A schematic presentation of the geometry of the slip between layers i and $i + 1$ in interlayer contact j. 16
2.5 A schematic presentation of the geometry of the slip and full debonding between layers i and $i + 1$ in interlayer contact j. 18
2.6 The influence of finger joint k in layer a. 21
2.7 Geometry of a scarf joint (left) and geometry of a finger joint (right). 37
2.8 Geometry of a half of a finger joint for analytical model. 38
2.9 Influence of geometric parameters of the finger joint l, p, and b_t on the tensile strength of finger joints based on the analytical solution. 39
2.10 Numerical model of half of the finger joint with boundary conditions. 39
2.11 The influence of the geometric parameters α, b_t, and l on the tensile strength of finger joints based on numerical solution. 41
2.12 Differences of maximum tensile strengths, Δ_{adh}, between adhesive 1 and adhesive 2 for different lengths (for $b_t = 1$ mm and $b_t = 2$ mm) 42
2.13 Comparison of calculated expected results of finger joints tension strengths f_t for different α, b_t, and l, obtained with analytical and numerical model (adhesive 1). 43
2.14 A schematic of adhesion and cohesion in the glueline. Adopted after Ülker (2016). . . 46
2.15 A schematic of typical failure modes of glued joints. Adopted after (Deng et al., 2015). 47

3.1 Histogram and probability density function of tensile strength f_t and modulus of elasticity in tension E_t of beech boards (Plos et al., 2022). 52
3.2 A schematic of construction for tensile tests. 52
3.3 The cutting head for the 10 mm finger joint (left) and the board with the 10 mm finger joint (right). 53
3.4 Pressing and curing of the 10 mm finger joint. 53
3.5 Results of tensile testing of 10 mm finger joints. 54
3.6 Failure in glue line (MUF adhesive, left) and wood failure (PRF adhesive, right). . . . 54
3.7 The cutting head for the 18 mm finger joint (left) and the board with the 18 mm finger joint. 55
3.8 Experimental measurements of elastic modulus in tension of 18 mm finger joint with MUF adhesive. 56
3.9 Diagram of the tension loading of the board for the determination of the static modulus of elasticiy in tension E_t. 56

3.10 Box and whiskers plots of tensile strengths for three groups of finger joints that failed in the glue line (left) and correlation of dynamic modulus of elasticity measured on joined boards and tensile strength of the finger joint specimens (right). 58
3.11 Correlation between the dynamic modulus of elasticity on boards (average of the two single boards) before gluing and dynamic modulus of elasticity on glued boards (left) and grading results, based on dynamic modulus of elasticity on glued boards and associated tensile strength (right). 59
3.12 Results of the grading based on the measurements of dynamic modulus of elasticity for single boards before gluing and dynamic modulus of elasticity on joined boards with associated tensile strength (specimens failed in finger joint). 60
3.13 The geometry of the chosen profile of the finger joint (cutting head). 61
3.14 The cutting head for the 40 mm finger joint mounted on a CNC machine. 62
3.15 Pressing device for pressing the finger joints with controlled pressure application, prototype on the left picture and final version on the right picture. 62
3.16 Glued 40 mm finger joint. 62
3.17 Test configurations and specimen after failure in tension. 63
3.18 An example of a specimen in GOM 2018 Professional software with tagged distances for the determination of the static modulus of elasticity in tension. 63
3.19 Maximal differences of moduli of elasticity within measurements in the same position (gray triangles) and between measurements over the width of the boards(green dots) in percent. 64
3.20 The longitudinal deformation ε_X of finger joint area a moment before a failure (left) and right after the rupture (right) from GOM software. 64
3.21 Box and Whiskers plots of tensile strengths for four groups of 40 mm finger joints divided by type of adhesive. 65
3.22 Failure of the 40 mm finger joint in the joint (left) and failure in wood (right). 66
3.23 Probability density function for lognormal distribution and histogram of measured moduli of elasticity $E_{t,\mathrm{FJ}}$ of the 40 mm finger joints. 66
3.24 Test configuration for determination of the local and global modulus of elasticity. Adopted after EN 408(CEN, 2010). 67
3.25 Gluing of the glued laminated beams with 18 mm finger joints. 68
3.26 Beam with 18 mm finger joints before failure (left) and after failure (right). 69
3.27 Failure of the 18 mm finger joint in the lower lamination of the beam. 69
3.28 Correlation of the local and global moduli of elasticity in bending. 70
3.29 Bending test configuration for the beams with 40 mm finger joints. 71
3.30 Failures of all four beams with 40 mm finger joints. 72
3.31 Comparison of the load/vertical displacements curves measured at three points in the middle of Beam 2 with 40 mm finger joints (targets on the front side of the beam). . . . 73
3.32 Measured load/displacement curve for vertical displacement at the mid-span of the beams. 73
3.33 A surface model of deformations of the beam at support for determination of the shear modulus. 75

4.1 Geometric and material data of a two-layer beam with two finger joints and fully debonded interlayer. 77
4.2 Equilibrium and kinematic quantities of a two-layer beam with two finger joints and fully debonded segment with L_{FDS} = 1 cm, shown for both laminations. 78
4.3 Equilibrium and kinematic quantities of a two-layer beam with two finger joints and fully debonded segment with L_{FDS} = 150 cm, shown for both laminations. 78
4.4 Geometric and material properties of the laminations, position and magnitude of the loading and the finger joint and material properties of the interlayer contact and the finger joint. 80
4.5 Vertical displacement in the middle of the span, $w(L/2)$, of glued laminated beam, as a function of different finger joint position and different finger joint stiffness, K_{FJ}. . . . 81
4.6 Axial stresses of lamination a (N^a) of finger jointed glued laminated beam, as a function of different finger joint position x_{FJ} and different finger joint stiffness K_{FJ}. 81
4.7 Horizontal and vertical displacement u^a and w^a at the mid-span of the beam as a function of the stiffness of the finger joint K_{FJ} and longitudinal stiffness of the interlayer contact K_X. 82
4.8 Internal axial force N^a and bending moment M^a at the mid-span of the beam as a function of the stiffness of the finger joint K_{FJ} and stiffness of the interlayer contact K_{X}. 83
4.9 Selected kinematic and equilibrium quantities as a function of the position of the fully debonded segment x_{FDS} for the three lengths of fully debonded segment L_{FDS} = 10, 50 and 100 cm. 84
4.10 Geometric data for the continuous two-layer beam with two spans and two finger joints. 85
4.11 Equilibrium quantities of two-layer continuous beam with two finger joints calculated with analytical model. 86
4.12 Kinematic quantities of two-layer continuous beam with two finger joints calculated with analytical model. 87
4.13 Equilibrium quantities in the laminations along the length of the two-layer beam for different interlayer contact stiffness K_{X}, calculated with analytical model. 88
4.14 Kinematic quantities in the laminations along the length of the two-layer beam for different interlayer contact stiffness K_{X}, calculated with analytical model. 89
4.15 Vertical displacement w and interlayer slip Δ_{X} along the beam for different finger joint stiffness K_{FJ}, calculated with analytical model. 89
4.16 Four-layer laminated beam used for the verification of numerical model. 91
4.17 Comparisson of slips in four-layer beam calculated with numerical model with the data from the literature (Kroflič, 2012; Sousa Jr and Silva, 2010). 92
4.18 Schematic presentation of positions of the non-destructively measured beech boards and positions of the finger joints in the ten-layer Beam 2, prepared for the numerical modelling. 93
4.19 Comparison of the measured and calculated load/vertical displacement curve for Beam 2 with finger joints, modelled only in the lower three laminations with averaged modulus of elasticity of upper seven laminations. 94

4.20 Comparison between the measured and calculated load/vertical displacement curve (same E_{dyn} for whole lamination). Left diagram is for the model with finger joint only in the lower three laminations and the right diagram is for the model with finger joints in all the laminations. 95
4.21 Comparison between the measured and calculated load/vertical displacement curve for Beam 1, Beam 3, and Beam 4. 96
4.22 Measured vertical displacement in the middle of the span, in front and on the back of the Beam 1. 97
4.23 Nonlinear constitutive law for interlayer contact (left) and nonlinear constitutive law for the laminations (right), input data for nonlinear numerical model of Beam 1. 98
4.24 Measured and calculated load/vertical displacement curve with nonlinear numerical model at the mid-span of Beam 1. 98
4.25 Slip Δ_{X} and vertical displacement w of two-layer beam with finger joint at $x_{\mathrm{FJ}} = 5/6L$ with finger joint stiffness $K_{\mathrm{FJ}} = 100$ kN/cm^2 (analytical and numerical model). 99
4.26 Slip Δ_{X} and vertical displacement w of two-layer beam with finger joint at $x_{\mathrm{FJ}} = L/2$ with finger joint stiffness $K_{\mathrm{FJ}} = 50$ kN/cm^2 (analytical and numerical model). 99
4.27 Dependence of the interlayer slip at the end of the beam (left) and vertical displacement in the middle of the span of the beam (right) on the number of finite elements. 100
4.28 Internal moment in the beam and internal axial forces in the laminations (left), axial deformations (upper right) and horizontal displacements of the laminations (bottom right). 101
4.29 Calculated slips between the individual laminations of the Beam 2. 102
4.30 Dependence of the interlayer slip at the end of the beam (left) and vertical displacement in the middle of the span of the beam (right) on the number of laminations. 102
4.31 Dependence of the interlayer slip at the end of the beam on the number of laminations for $K_{\mathrm{X}} = 10$ kN/cm^2. 103
4.32 Influence of the moduli of elasticity in tension of the laminations E_t and of the finger joints $E_{t,\mathrm{FJ}}$ on the vertical displacement at the mid-span of the glued laminated beam $w(L/2)$. 103
4.33 Influence of the shear modulus G and interlayer stiffness K_{X} on the vertical displacement in the middle of the span of the glued laminated Timoshenko-Ehrenfest beam. . . 104
4.34 Two-layer glued laminated beam with one finger joint for stochastic analysis. 105
4.35 Probability density function (left) and cumulative distribution function (right) of the vertical displacement at mid-span of two-layer beam for 100 simulations for three different mean values of K_{X}. 107
4.36 Probability density function (left) and cumulative distribution function (right) of the vertical displacement in the middle of two-layer beam for 100 simulations for three different mean values of K_{FJ}. 107
4.37 Probability density function (left) and cumulative distribution function (right) of the interlayer slip at the end of two-layer beam for 100 simulations for three different mean values of K_{FJ}. 109
4.38 Probability density function with histogram (left) and cumulative distribution function (right) of the vertical displacement at given load for 500 simulations. 110

4.39 Probability density function with histogram (left) and cumulative distribution function (right) of the vertical displacement at mid-span of Beam 2 for three different mean values of K_{X}. 111
4.40 Load/vertical displacement curves (50 simulations) and deterministically calculated (left) and measured (right) vertical displacement of three beams at given load. 112
4.41 Example of constitutive law of one lamination in finite element (left) load/vertical displacement curve for 150 simulations together with measured beams (right). 113
4.42 Probability density function with histogram (left) and cumulative distribution function (right) of the vertical displacement in the middle of the span of the beams for 150 simulations with nonlinear material. 114
4.43 Probability density function with histogram (left) and cumulative distribution function (right) of final load bearing capacity for 150 simulations with nonlinear material. . . . 114

6.1 Undeformed and deformed configuration of laminated beam. 123
6.2 A schematic presentation of the internal forces due to the influence of finger joint k in layer a. 126
6.3 Geometry of a scarf joint (left) and geometry of a finger joint (right). 130
6.4 The geometry of the chosen profile of the finger joint. 131
6.5 Beam with 18 mm long finger joints before failure (left) and after failure (right). 135
6.6 Measured load/displacement curve for vertical displacement at the mid-span of the beams. 135
6.7 Geometric and material properties of the layers, position and magnitude of the loading and the finger joint and material properties of the interlayer contact and the finger joint. 136
6.8 Axial force in the lower layer, N^a, and vertical displacement in the middle of the span, $w(L/2)$, of glued laminated beam, as a function of different finger-joint position and different finger-joint stiffness, K_{FJ}. 136
6.9 Comparison between the measured and calculated curve load with vertical displacement for Beam 1, Beam 3 and Beam 4. 138
6.10 Load/vertical displacement curve for 250 simulations (left) and probability density function with histogram (right). 139

“Blank page.”

LIST OF TABLES

2.1 Mechanical properties of beech wood (mean values used for the Abaqus model). 40

2.2 Parameters used for the cohesive elements and cohesive surface in Abaqus model. . . . 40

3.1 The number of test specimens for individual length of finger joints and used adhesive. . 50

3.2 Strength class assignment for Slovenian beech wood according to previous study (Fortuna et al., 2018a) 56

3.3 Statistical values for tensile strength, modulus of elasticity in tension and dynamic modulus of elasticity for specimens divided into six groups by the type of adhesive, assembling pressure and type of failure for 18 mm finger joints. 57

3.4 Strength class assignment for separate boards on the basis of settings from Tab. 3.2 (tensile strength of the corresponding finger joint). 59

3.5 Statistical values for tensile strength and modulus of elasticity in tension for 40 mm finger joints, divided into four groups by the type of adhesive and type of failure. . . . 65

3.6 Statistical values for the experimentally measured bending strength and bending strength adjusted with k_h factor (CEN, 2013e), of the glued laminated beech beams with standard finger joint geometry. 68

3.7 Statistical values for the of the global and local modulus of elasticity in bending of the laminated beams with standard finger joint geometry. 70

3.8 Bending strengths measured with experimental testing and bending strengths adjusted with k_h factor (CEN, 2013e), of the glued laminated beech beams with 40 mm finger joints. 71

3.9 Global and local elastic moduli in bending for the laminated beams with 40 mm finger joints. 74

3.10 Shear moduli for the laminated beams with 40 mm finger joints at both supports. . . . 75

3.11 Measured slip between the middle laminations and corresponding shear stress of the laminated beams with 40 mm finger joints at both supports. 75

4.1 Kinematic quantities of two-layer Euler-Bernoulli beam with finger joints evaluated with analytical model at five points along the span for $L_{\text{FDS}} = 0$ cm. 79

4.2 Kinematic quantities of two-layer Euler-Bernoulli beam with finger joints evaluated with analytical model at five points along the span for $L_{\text{FDS}} = 1$ and 150 cm. 80

4.3 Selected kinematic and equilibrium quantities of two-layer beam with finger joints evaluated with numerical model for different K_X and K_{FJ} at different locations for $L_{\text{FDS}} = 50$ cm and comparison with results of analytical model by Schnabl (2007) . . 84

4.4 Selected kinematic and equilibrium quantities of two-layer beam with finger joints evaluated with numerical model for different K_X and K_{FJ} at different locations for $L_{\text{FDS}} = 50$ cm and comparison with results of analytical model by Schnabl (2007) . . 85

4.5 Kinematic and equilibrium quantities of two-layer continuous beam with finger joints evaluated with analytical model for different K_X and at different locations along the beam. . . . 90

4.6 Interlayer slips Δ_X^j at the beginning of the four-layer beam and vertical displacement w at the middle of the beam span calculated with the proposed analytical and numerical model and comparison with the results from the literature (Sousa Jr and Silva, 2010; Kroflič, 2012). . . . 92

4.7 List of boards, their lengths and dynamic moduli of elasticity in laminations of Beam 2 used in numerical model of Beam 2. . . . 93

4.8 List of measured dynamic moduli of elasticity of the laminations in four beams (input data in the numerical models). . . . 96

4.9 Values of measured and calculated maximum vertical displacements of the glued laminated beams with 40 mm finger joints. . . . 97

4.10 Values of measured and calculated maximum load and vertical displacements of the Beam 1 with nonlinear material model. . . . 99

4.11 Statistical values and distribution type of variables, used for stochastic analysis of two-layer beam with finger joint for different values of K_X with analytical model. . . . 105

4.12 Parameters m and s for the evaluation of probability that vertical displacement at mid-span of the beam reaches a certain value $w_{L/2}$, determined under the assumption that the mid-span vertical displacement is lognormally distributed, for three mean values K_X. 106

4.13 Mean values and standard deviations from the results of stochastic analysis of two-layer beam with analytical model, where μ_{K_X} was varied. . . . 107

4.14 Statistical values and distribution type of variables, used for stochastic analysis of two-layer beam with finger joint with analytical model for different values of K_FJ. . . . 108

4.15 Mean values and standard deviations from the results of stochastic analysis of two-layer beam with analytical model, where μ_{K_FJ} was varied. . . . 108

4.16 Statistical values and distribution type of variables, used for stochastic analysis of ten-layer beam with finger joint with numerical model. . . . 110

4.17 Statistical values and distribution type of variables, used for stochastic analysis of ten-layer beam with finger joint with numerical model for different values of μ_{K_X}. . . . 111

4.18 Mean values and standard deviations from the results of stochastic analysis of ten-layer beam with numerical, where μ_{K_XJ} was varied. . . . 112

4.19 Statistical values and distribution type of variables, used for stochastic analysis of ten-layer beam with finger joints with numerical model and nonlinear material model. . . . 113

4.20 Probability of failure of ten-layer beam with finger joints for given load, determined based on stochastic analysis with numerical model and nonlinear material model, for the normal distribution and empirical distribution estimate. . . . 115

6.1 Calculated interlayer slips Δ_X^j for $j = (1, 2, 3)$ at the begining of the four-layer beam and vertical displacement at the middle of the beam span calculated with the proposed analytical and numerical model and comparison with the results from the literature (Sousa Jr and Silva, 2010; Kroflič, 2012). . . . 137

6.2 Statistical values and distribution type of selected variables for simulations with non-linear constitutive material law. 138

“Blank page.”

KAZALO SLIK

2.1 Nedeformirana in deformirana konfiguracija lameliranega nosilca. 9
2.2 Kontaktna obtežba na stiku j, ki deluje na sloj i. 11
2.3 Robna obtežba ter notranje sile in momenti v nosilcu. 13
2.4 Shematski prikaz geometrije zdrsa slojev i in $i + 1$ v stiku j. 16
2.5 Shematski prikaz geometrije zdrsa in popolne razslojitve slojev i in $i + 1$ v stiku j. . . 18
2.6 Vpliv zobatega spoja k v sloju a. 21
2.7 Geometrija poševnega spoja (levo) in geometrija zobatega spoja (desno). 37
2.8 Geometrija polovice zobatega spoja za analitični model. 38
2.9 Vpliv geometrijskih parametrov zobatega spoja l, p, and b_t na natezno trdnost zobatih spojev po analitični rešitvi. 39
2.10 Numerični model polovice zobatega spoja z robnimi pogoji. 39
2.11 Vpliv geometrijskih parametrov α, b_t in l zobatega spoja glede na numerično rešitvev. . 41
2.12 Razlike med maksimalni natezni trdnosti, Δ_{adh}, doseženi z lepilom 1 ter lepilom 2 (za $b_t = 1$ mm in $b_t = 2$ mm). 42
2.13 Primerjava izračunanih pričakovanih nateznih trdnosti zobatih spojev f_t za različne α, b_t in l, dobljenih z analitičnim in numeričnim modelom (lepilo 1). 43
2.14 Shematski prikaz adhezije in kohezije v lepljenem spoju. Povzeto po Ülker (2016). . . 46
2.15 Shematski prikaz tipičnih porušitev v lepljenem spoju. Povzeto po (Deng et al., 2015). 47

3.1 Histogram in gostota porazdelitve nateznih trdnosti f_t in nateznih modulov elastičnosti E_t desk iz bukovine, (Plos et al., 2022). 52
3.2 Shematski prikaz konstrukcije za izvedbo nateznih testov. 52
3.3 Rezkalna glava za 10 mm dolg zobati spoj (levo) in deska z 10 mm dolgim zobatim spojem (desno). 53
3.4 Stiskanje in utrjevanje 10 mm dolgih zobatih spojev. 53
3.5 Rezultati nateznih testov 10 mm dolgih zobatih spojev. 54
3.6 Porušitev v lepljenem spoju (lepilo MUF, levo) in porušitev v lesu (PRF, desno). 54
3.7 Rezkalna glava za 18 mm dolg zobati spoj (levo) in deska z 18 mm dolgim zobatim spojem. 55
3.8 Eksperimentalne meritve nateznega modula elastičnosti 18 mm dolgega zobatega spoja z lepilom MUF. 56
3.9 Diagram obremenjevanja deske v nategu za določitev statičnega modula elastičnosti v nategu E_t. 56
3.10 Škatlasti diagram nateznih trdnosti za tri skupine zobatih spojev, s porušitvijo v stiku (levo) in korelacija med dinamičnim modulom elastičnosti zlepljenih desk in natezno trdnostjo zobatega spoja (desno). 58

3.11 Korelacija med dinamičnim modulom elastičnosti desk (povprečje dveh posameznih desk) pred lepljenjem in dinamičnim modulom elastičnosti zlepljenih desk (levo) in rezultati razvrščanja na osnovi dinamičnega modula elastičnosti na zlepljenih deskah in pripadajoča natezna trdnost. 59
3.12 Rezultati razvrščanja na osnovi dinamičnega modula elastičnosti posameznih desk pred lepljenjem in na osnovi dinamičnega modula elastičnosti zlepljenih desk s pripadajočo natezno trdnostjo (preizkušanci s porušitvijo v zobatem spoju). 60
3.13 Geometrija izbranega profila zobatega spoja (rezkalna glava). 61
3.14 Rezkalna glava za 40 mm dolg zobati spoj nameščena na CNC stroj. 62
3.15 Naprava za stiskanje zobatih spojev pod kotroliranim nanosom pritiska, prototip na levi sliki in končna izvedba na desni sliki. 62
3.16 Zlepljen 40 mm dolg zobati spoj. 62
3.17 Postavitev testa in preizkušanec po natezni porušitvi. 63
3.18 Primer vzorca v programu GOM 2018 Professional z označenimi razdaljami za določitev statičnega modula elastičnosti v nategu. 63
3.19 Največja odstopanja modulov elastičnosti znotraj meritev na istem mestu (sivi trikotniki) in znotraj meritev po širini desk (temno zelene pike) v odstotkih. 64
3.20 Osna deformacija ε_X območja zobatega spoja trenutek pred porušitvijo (levo) in takoj po porušitvi (desno) iz programa GOM. 64
3.21 Škatlasti diagram nateznih trdnosti za štiri skupine 40 mm dolgih zobatih spojev razdeljenih glede na vrsto lepila. 65
3.22 Porušitev 40 mm dolgega zobatega spoja po stiku (levo) in porušitev po lesu (desno). . 66
3.23 Gostota porazdelitve po logaritemsko normalni porazdelitvi ter histogram izmerjenih modulov elastičnosti $E_{t,\mathrm{FJ}}$ 40 mm dolgih zobatih spojev. 66
3.24 Testna postavitev za določitev lokalnega in globalnega modula lastičnosti. Povzeto po EN 408(CEN, 2010). 67
3.25 Lepljenje lameliranih nosilcev z 18 mm dolgimi zobatimi spoji. 68
3.26 Nosilec z 18 mm dolgimi zobatimi spoji pred porušitvijo (levo) in po poruštivi (desno). 69
3.27 Porušitev 18 mm dolgega zobatega spoja v spodnji lameli nosilca. 69
3.28 Korelacija med lokalnimi in globalnimi upogibnimi moduli elastičnosti. 70
3.29 Postavitev upogibnega testa za nosilce z 40 mm dolgimi zobatimi spoji. 71
3.30 Porušitve vseh štirih nosilcev z 40 mm dolgimi zobatimi spoji. 72
3.31 Primerjava krivulj obtežba/navpični pomik izmerjenih v treh točkah na sredini Nosilca 2 s 40 mm dolgimi zobatimi spoji (tarč na sprednji strani nosilca). 73
3.32 Izmerjena krivulja obtežba/navpični pomik na sredini razpona za vse štiri nosilce. . . . 73
3.33 Model deformirane površine nosilca pri podporah v programu GOM, za določitev strižnega modula. 75

4.1 Geometrijski in materialni podatki za dvoslojni nosilec z dvema zobatima spojema in popolno razslojenim stikom. 77
4.2 Ravnotežne in kinematične količine dvoslojnega nosilca z dvema zobatima spojema in popolno razslojenim delom z L_{FDS} = 1 cm, prikazane za oba sloja. 78

4.3 Ravnotežne in kinematične količine dvoslojnega nosilca z dvema zobatima spojema in popolno razslojenim delom z L_{FDS} = 150 cm, prikazane za oba sloja. 78
4.4 Geometrijske in materialne lastnosti slojev, pozicije in velikosti obtežbe in zobatega spoja ter materialne lastnosti stika med sloji in zobatega spoja. 80
4.5 Navpični pomik na sredini razpona, $w(L/2)$, lepljenega slojevitega nosilca z zobatim spojem, kot funkcija različnih pozicij zobatega spoja, x_{FJ}, in različnih togosti zobatega spoja, K_{FJ}. 81
4.6 Osne napetosti v sloju a (N^a) lepljenega nosilca z zobatim spojem, kot funkcija različnih pozicij zobatega spoja x_{FJ} in različnih togosti zobatega spoja K_{FJ}. 81
4.7 Vodoravni in navpični pomik u^a in w^a na sredini razpona nosilca kot funkcija togosti zobatega spoja K_{FJ} in vzdolžne togosti stika K_X. 82
4.8 Notranje osne sile N^a in upogibni moment M^a na sredini razpona dvoslojnega nosilca kot funkcija togosti zobatega spoja K_{FJ} in togosti stika med lamelami K_{X}. 83
4.9 Izbrane kinematične količne kot funkcija pozicije popolnoma razslojenega dela x_{FDS} za tri dolžine popolnoma razslojenega dela L_{FDS} = 10, 50 and 100 cm. 84
4.10 Geometrijski podatki za dvoslojni nosilec z dvema razponoma in dvema zobatima spojema. 85
4.11 Ravnotežne količine dvoslojnega kontinuirnega nosilca z dvema zobatima spojema izračunane z analitičnim modelom. 86
4.12 Kinematične količine dvoslojnega kontinuirnega nosilca z dvema zobatima spojema izračunane z analitičnim modelom. 87
4.13 Ravnotežne količine v slojih vzdolž dvoslojnega kontinuirnega nosilca za različne togosti stika K_{X}, izračunani z analitičnim modelom. 88
4.14 Kinematične količine v slojih vzdolž dvoslojnega kontinuirnega nosilca za različne togosti stika K_{X}, izračunani z analitičnim modelom. 89
4.15 Navpični pomiki w in zdrs med slojema Δ_{X} vzdolž nosilca za različne togosti zobatega spoja K_{FJ}, izračunani z analitičnim modelom. 89
4.16 Štirislojni lamelirani nosilec uporabljen za verifikacijo numeričnega modela. 91
4.17 Primerjava zdrsov štirislojnega nosilca, izračunanih z numeričnim modelom s podatki iz literature (Kroflič, 2012; Sousa Jr and Silva, 2010). 92
4.18 Shematski prikaz položajev bukovih desk in položajev zobatih spojev v deset slojnem Nosilcu 2, pripravljen za numerično modeliranje. 93
4.19 Primerjava med izmerjeno in izračunano krivuljo obtežbo/navpični pomik za Nosilec 2, z upoštevanjem zobatih spojev samo v spodnjih treh slojih ter povprečnim modulom elastičnosti zgornjih sedmih slojev. 94
4.20 Primerjava med izmerjeno in izračunano krivuljo obtežba/navpični pomik (enak E_{dyn} za celotni sloj). Levi diagram velja za model z zobatimi spoji samo v spodnjih treh slojih in desni diagram velja za model z zobatimi spoji v vseh desetih slojih. 95
4.21 Primerjava med izmerjeno in izračunano krivuljo obtežba/navpični pomik za Nosilec 1, Nosilec 3 in Nosilec 4. 96
4.22 Izmerjen navpični pomik Nosilca 1 na sredini razpona na sprednji in zadnji strani. . . . 97
4.23 Nelinearni konstitutivni zakon stika med sloji (levo) in nelinearni konstitutivni zakon lamel (desno), vhodni podatki za nelinearni numerični model Nosilca 1. 98

4.24 Izmerjen in izračunana krivulja obtežba/navpični pomik z nelinearnim numeričnim modelom na sredini razpona Nosilca 1. 98
4.25 Zdrs Δ_{X} in navpični pomik w dvoslojnega nosilca z zobatim spojem pri $x_{\mathrm{FJ}} = 5/6L$ s togostjo zobatega spoja $K_{\mathrm{FJ}} = 100$ kN/cm^2 (analitični in numerični model). 99
4.26 Zdrs Δ_{X} in navpični pomik w dvoslojnega nosilca z zobatim spojem pri $x_{\mathrm{FJ}} = L/2$ s togostjo zobatega spoja $K_{\mathrm{FJ}} = 50$ kN/cm^2 (analitični in numerični model). 99
4.27 Odvisnost zdrsa med slojema na koncu nosilca (levo) in navpičnega pomika na sredini razpona nosilca (desno) od števila končnih elementov. 100
4.28 Notranji moment v nosilcu in notranja osna sila v posameznih slojih (levo), osne deformacije (desno zgoraj) in vodoravni pomik slojev (desno spodaj). 101
4.29 Izračunani zdrsi med posameznimi sloji Nosilca 2. 102
4.30 Odvisnost zdrsa med slojema na koncu nosilca (levo) in navpičnega pomika na sredini razpona nosilca (desno) od števila slojev. 102
4.31 Odvisnost zdrsa med slojema na koncu nosilca od števila slojev za $K_{\mathrm{X}} = 10$ kN/cm^2. . 103
4.32 Vpliv nateznih modulov elastičnosti slojev E_t in zobatih spojev $E_{t,\mathrm{FJ}}$ na navpični pomik na sredini lameliranega lepljenega nosilca $w(L/2)$. 103
4.33 Vpliv strižnega modula G in togostjo vzdolžnega stika K_{X} na navpični pomik na sredini lameliranega lepljenega Timoshenko-Ehrenfestovega nosilca. 104
4.34 Dvoslojni lepljeni nosilec z enim zobatim spojem za stohastično analizo z analitičnim modelom. 105
4.35 Gostota verjetnosti (levo) in porazdelitvena funkcija (desno) za navpični pomik na sredini dvoslojnega nosilca za 100 simulacij pri treh različnih srednjih vrednostih K_{X}. . . 107
4.36 Gostota verjetnosti (levo) in porazdelitvena funkcija (desno) za navpični pomik na sredini dvoslojnega nosilca za 100 simulacij pri treh različnih srednjih vrednostih K_{FJ}. . . 107
4.37 Gostota verjetnosti (levo) in porazdelitvena funkcija (desno) za zdrs med slojema na koncu dvoslojnega nosilca za 100 simulacij pri treh različnih srednjih vrednostih K_{FJ}. 109
4.38 Gostota verjetnosti s histogramom (levo) in porazdelitvena funkcija (desno) za navpični pomik pri dani obtežbi za 500 simulacij. 110
4.39 Gostota verjetnosti s histogramom (levo) in porazdelitvena funkcija (desno) za navpični pomik na sredini Nosilca 2 pri treh različnih srednjih vrednostih K_{X}. 111
4.40 Krivulje obtežba/navpični pomik (50 simulacij) in deterministično izračunan (levo) in izmerjeni (desno) navpični pomik za tri nosilce pri dani obtežbi. 112
4.41 Primer konstitucijskega zakona posamezne laminacije končnega elementa (levo) in krivulja obtežba/pomik za 150 simulacij skupaj z izmerjenimi nosilci (desno). 113
4.42 Gostota verjetnosti s histogramom (levo) in porazdelitvena funkcija (desno) navpičnih pomikov na sredini nosilcev za 150 simulacij z nelinearnim materialom. 114
4.43 Gostota verjetnosti s histogramom (levo) in porazdelitvena funkcija (desno) končne trdnosti nosilcev za 150 simulacij z nelinearnim modelom. 114

6.1 Nedeformirana in deformirana konfiguracija lameliranega nosilca. 123
6.2 Shematski prikaz notranjih sil zaradi vpliv zobatega spoja k v sloju a. 126
6.3 Geometrija poševnega spoja (levo) in geometrija zobatega spoja (desno). 130
6.4 Geometrija izbranega profila zobatega spoja. 131

6.5 Nosilec z 18 mm dolgimi zobatimi spoji pred porušitvijo (levo) in po porušitvi (desno). 135
6.6 Izmerjena krivulja obtežba/navpični pomik na sredini razpona za vse štiri nosilce. . . . 135
6.7 Geometrijske in materialne lastnosti slojev, pozicije in velikosti obtežbe in zobatega spoja ter materialne lastnosti stika med sloji in zobatega spoja. 136
6.8 Osna sila v spodnjem sloju ,N^a, in navpični pomik na sredini razpona, $w(L/2)$, lepljenega slojevitega nosilca z zobatim spojem, kot funkcija različnih pozicij zobatega spoja, x_{FJ}, in različnih togosti zobatega spoja, K_{FJ}. 136
6.9 Primerjava med izmerjeno in izračunano krivuljo obtežbe z navpičnim pomikom za Nosilec 1, Nosilec 3 in Nosilec 4. 138
6.10 Krivulja obtežba/pomik za 250 simulacij skupaj z izmerjenimi nosilci (levo) in gostota verjetnosti s histogramom (desno). 139

"Blank page."

KAZALO PREGLEDNIC

2.1 Mehanske lastnosti bukovega lesa (srednje vrednosti količin uporabljenih v modelu v Abaqusu). 40
2.2 Parametri uporabljeni za kohezivne elemente in kohezivno površino za model v Abaqusu. 40

3.1 Število preizkušancev za posamezno dolžino zobatega spoja in uporabljeno lepilo. . . . 50
3.2 Razvrstitev lesa slovenskega bukovega lesa v trdnostne razrede v skladu s predhodnimi raziskavami (Fortuna et al., 2018a). 56
3.3 Statistične vrednosti nateznih trdnosti, nateznega modula elastičnosti in dinamičnega modula elastičnosti preizkušancev razdeljenih v šest skupin glede na tip lepila, pritiska pri stiskanju in načina porušitve za 18 mm dolge zobate spoje. 57
3.4 Razvrstitev v trdnostne razrede posameznih desk glede na nastavitve iz Tab. 3.2 (natezne trdnosti pripadajočega zobatega spoja). 59
3.5 Statistične vrednosti o natezni trdnosti in statičnih modululov elastičnosti 40 mm dolgih zobatih spojev, razdeljenih v štiri skupine glede na vrsto lepila in tip porušitve. 65
3.6 Statistične vrednosti o eksperimentalno izmerjenih upogibnih trdnostih ter trdnostih z upoštevanjem k_h faktorja (CEN, 2013e), lameliranih lepljenih nosilcev s standardno geometrijo zobatih spojev. 68
3.7 Statistične vrednosti o globalnem in lokalnem upogibnem modulu elastičnosti lameliranih nosilcev s standardno geometrijo zobatih spojev. 70
3.8 Upogibne trdnosti izmerjene z eksperimentalnimi testi ter trdnost z upoštevanim k_h faktorjem (CEN, 2013e), lameliranih lepljenih nosilcev s 40 mm dolgimi zobatimi spoji. 71
3.9 Globalni in lokalni elastičbi upogibni moduli lameliranih nosilcev s 40 mm dolgimi zobatimi spoji. 74
3.10 Strižni moduli lameliranih nosilcev s 40 mm dolgimi zobatimi spoji pri obeh podporah. 75
3.11 Izmerjen zdrs med sredinskima lamelama in pripadajoča strižna napetost v lameliranem nosilcu s 40 mm dolgimi zobatimi spoji. 75

4.1 Kinematične količine dvoslojnega Euler-Bernoullijevega nosilca z zobatima spojema izračunane z analitičnim modelom v petih točkah vzdolž nosilca za $L_{\mathrm{FDS}} = 0$ cm. . . . 79
4.2 Kinematične količine dvoslojnega Euler-Bernoullijevega nosilca z zobatima spojema izračunane z analitičnim modelom v petih točkah vzdolž nosilca za L_{FDS} = 0 cm. . . . 80
4.3 Izbrane kinematične in ravnotežne količine dvoslojnega nosilca z zobatima spojema izvrednotene z analitičnim modelom pri različnih K_X in K_{FJ} in različnih pozicijah $L_{\mathrm{FDS}} = 50$ cm in primerjava rezultatov z rezultati analitičnega modela po (Schnabl, 2007). 84
4.4 Izbrane kinematične in ravnotežne količine dvoslojnega nosilca z zobatima spojema izvrednotene z analitičnim modelom pri različnih K_X in K_{FJ} in različnih pozicijah $L_{\mathrm{FDS}} = 50$ cm in primerjava rezultatov z rezultati analitičnega modela po Schnabl (2007). 85

4.5 Kinematične in ravnotežne količine dvoslojnega kontinuirnega nosilca z zobatima spojema izvrednotene z analitičnim modelom pri različnih K_X in pri različnih lokacijah vzdolž nosilca. 90
4.6 Zdrsi med sloji Δ_X^j na začetku štirislojnega nosilca in navpični pomik w na sredini razpona nosilca izračunani z izdelanim analitičnim in numeričnim modelom ter primerjava z rezultati iz literature (Sousa Jr and Silva, 2010; Kroflič, 2012). 92
4.7 Seznam desk, njihovih dolžin in dinamičnih modulov v lamelah Nosilca 2 uporabljenih v numeričnem modelu Nosilca 2. 93
4.8 Seznam izmerjenih dinamičnih modulov elastičnosti laminacij v štirih nosilcih (vhodni podatki za numerične modele). 96
4.9 Vrednosti izmerjenih in izračunanih največjih pomikov lepljenih lameliranih nosilcev s 40 mm dolgimi zobatimi spoji. 97
4.10 Vrednosti izmerjene in izračune maksimalne sile in pomika Nosilca 1 z nelinearnim materialnim modelom. 99
4.11 Statistične vrednosti in tip porazdelitve spremenljivk uporabljenih za stohastično analizo dvoslojnega nosilca z zobatim spojem za različne srednje vrednosti K_X z analitičnim modelom. 105
4.12 Parametra m in s, za izvrednotenje verjetnosti, da navpični pomik na sredini nosilca doseže izbrano vrednost $w_{L/2}$, določeni ob predpostavki, da je navpični pomik na sredini nosilce porazdeljen po lognormalni porazdelitvi, za tri srednje vrednosti μ_{K_X}. 106
4.13 Srednje vrednosti in standardne deviacije iz rezultatov stohastične analize dvoslojnega nosilca z analitičnim modelom pri spreminjanju μ_{K_X}. 107
4.14 Statistične vrednosti in tip porazdelitve spremenljivk uporabljenih za stohastično analizo dvoslojnega nosilca z zobatim spojem z analitičnim modelom za različne srednje vrednosti K_FJ. 108
4.15 Srednje vrednosti in standardne deviacije iz rezultatov stohastične analize dvoslojnega nosilca z analitičnim modelom pri spreminjanju μ_{K_FJ}. 108
4.16 Statistične vrednosti in tip porazdelitve spremenljivk uporabljenih za stohastično analizo desetslojnega nosilca z zobatim spojem z numeričnim modelom. 110
4.17 Statistične vrednosti in tip porazdelitve spremenljivk uporabljenih za stohastično analizo desetslojnega nosilca z zobatim spojem z numeričnim modelom za različne srednje vrednosti μ_{K_X}. 111
4.18 Srednje vrednosti in standardne deviacije iz rezultatov stohastične analize desetslojnega nosilca z numeričnim modelom pri spreminjanju μ_{K_X}. 112
4.19 Statistične vrednosti in tip porazdelitve spremenljivk uporabljenih za stohastično analizo desetslojnega nosilca z zobatimi spoji z numeričnim modelom in nelinearnim materialnim modelom. 113
4.20 Verjetnost porušitve desetslojnega nosilca z zobatimi spoji, pri dani obtežbi določena na osnovi stohastične analize z numeričnim modelom in nelinearnim materialnim modelom ob predpostavki normalne porazdelitve in empirične porazdelitve porušitve nosilca. 115

6.1 Zdrsi med sloji Δ_X^j za $j = (1, 2, 3)$ na začetku štirislojnega nosilca in navpični pomik na sredini razpona nosilca izračunani z izdelanim analitičnim in numeričnim modelom ter primerjava z rezultati iz literature (Sousa Jr and Silva, 2010; Kroflič, 2012). 137
6.2 Statistične vrednosti in tip porazdelitve izbranih spremenljivk za simulacije z nelinearnim konstitucijskim zakonom materiala. 138

1 INTRODUCTION

1.1 Motivation

Ensuring comfortable living conditions and being environmentally friendly are just two of many factors influencing the increasing use of wood as a building material. Wood is characterized by a number of other factors, which to some extent also depend on the type of wood. According to the reports of the Slovenian Forest Service, the volume of coniferous and deciduous stands in Slovenia is comparable (ZGS, 2020). Spruce and fir (*Picea Abies and Abies Alba*) are the most common conifers, and beech (*Fagus Sylvatica*) dominates among deciduous trees. The latter is rarely found as a building material in today's built environment, as coniferous wood, especially spruce and fir, is most commonly used in Central Europe. Coniferous wood is characterized by relatively fast growth, high load bearing capacity (in relation to material density), ease of wood processing, and manageable response to temperature fluctuations, high moisture content, and other external influences. Because of its light weight, the construction technology is also relatively easier for softwoods than for hardwoods. This is an important advantage in the construction of (prefabricated) buildings. Beech wood, on the other hand, is very sensitive to changes in humidity and temperature, which leads to changes in the moisture content of the material which results in dimensional changes. The beech wood has a higher density and hardness, so its processing is more demanding. Elements made from beech wood are also more susceptible to fungal attack, so additional protection is required (Peperko, 2006). All these factors have an influence on the current low share of beech wood in built environment. However, beech wood is characterized by significantly higher mechanical properties and could therefore be very useful as a building material. The idea of using beech wood as a building material is not new. In the region of southeastern Slovenia, beech wood was used for structural purposes. We find the reports of still standing beech structures (Peperko, 2006) built in the middle of the 19$^{\text{th}}$ century. This is a proof that beech wood, if properly implemented, can be used as a building material. Beech wood is a species native to southeastern Europe, and beech stands are adapted to the climatic conditions and more resistant to extreme environmental conditions (e.g. sled) and possible pests (e.g., bugs and beetles). Due to the extreme winds and snowfalls that led to pest epidemics, the most extensive sanitary deforestation in Slovenian forests was performed from 2014 to 2020. The most affected tree species was spruce (almost 70 % of the felling), while the share of beech was much lower, around 5 % (ZGS, 2020). The latter facts are an additional reason for the introduction of beech wood as one of the possible species for structural purposes, but there are many unknowns that still need to be investigated. Due to the relatively small database on the mechanical behaviour of beech wood (Franke et al., 2014) and the lack of accurate computational models, there are currently no comprehensive standards regulating the use of beech and hardwood in general for structural purposes.

Adhesives and other bonding methods are essential for wood composites. By gluing wood, we can make the most of the wood without irregularities to obtain stronger products and products with more uniform mechanical properties. The more primitive forms of gluing were already used by the Egyptians, who used gelatin based on animal bones and skins (Aicher, 2003). More modern forms of gluing emerged in the early 20$^{\text{th}}$ century when the first laminated, glued structural element was patented (Serrano, 2003).

This was the beginning of the increasing use of glued wood-based composites in modern construction where glued timber elements are replacing solid timber elements. The construction industry has become one of the largest consumers of adhesives, as they are used for most structural and non-structural wood elements, such as glued laminated beams, cross-laminated timber, fiberboards, OSB panels, etc. The load bearing capacity of such structural elements is increased, and adhesives are one of the most important factors in the construction of multi-storey buildings with a timber structure. In the production of these elements lower quality wood can also be used, which reduces the amount of waste, which, of course, is a great advantage for manufacturers.

1.2 Research Hypotheses and Goals

In the framework of the doctoral thesis, the following hypothesis were addressed:

- The load bearing capacity of the glued finger joints made from beech wood can be significantly increased by using longer and thinner finger joints, i.e., modified geometry. This could enable full utilization of glued elements.
- The load bearing capacity is increased to such an extent that there is no need for a new type of adhesive that should be developed for application to the beech wood.
- The proposed numerical model of the glued laminated beam will simulate the actual bending behaviour of composite glued beams made of beech wood.

1.3 State of the art in the research field

One of the main advantages of using wood in composite structural elements is the ability to use smaller components, such as boards, and eliminate the weak parts, thus achieving a higher load bearing capacity. Composite structures in general offer a wide range of possibilities and thus a wide range of problems to be solved. This is reflected in an extensive area of research dealing with layered structures. For layered systems, Newmark's beam theory (Newmark, 1951) is considered one of the pioneering and widely accepted theories for composite beams with partial interaction. In addition, a general theory on layered systems with interlayer slip was presented by Ko et al. (1972) and Goodman and Popov (1968), who presented the numerical solution procedure for a layered beam with deformable connection between layers in the longitudinal direction. Adekola (1968) presented a solution of a composite beam without restriction of curvature of the layers.

The application to the wooden laminated composite was actually one of the main motivations for the Goodman model, but the application to other materials, such as steel-concrete systems, often require geometrically and materially nonlinear models (Kroflič et al., 2011; Čas, 2004; Hozjan et al., 2013; Lolić et al., 2020; Adam and Furtmüller, 2019, 2020) and models with time-dependent behaviour (Ranzi and Bradford, 2006; Wu et al., 2016a,b). Some models are based on Bernoulli beam theory and neglect the shear deformation of the layers (Girhammar and Gopu, 1993; Xu and Wu, 2009; Adam and Furtmüller, 2019), while others consider the more exact stress and displacement fields (Wu et al., 2016a; Schnabl, 2007; Schnabl and Planinc, 2011; Xu and Wang, 2013; Ecsedi and Baksa, 2016; Siciliano et al., 2021) and thus the shear deformations. Besides planar models, some three-dimensional solutions of beams/columns with interlayer sliding were also presented by Schnabl and Planinc (2011); Challamel and Girhammar (2012, 2013); Čas et al. (2018).

The analytical solutions for layered beams have been presented recently by several authors focusing on different properties of the model. Girhammar and Gopu (1993) showed the exact solution for composite beams and columns with interlayer slip, considering the second-order analysis. Later, he also presented a simplified solution (Girhammar, 2009). Models developed for different applications of the constitutive laws for interlayer contact (Xu and Wu, 2009; Wu et al., 2016a; Galuppi and Royer-Carfagni, 2012; Siciliano et al., 2021) and different (continuous or discrete) types of interlayer interaction for two- or multi-layer beams (Focacci et al., 2015; Foraboschi, 2009; Sousa Jr and Silva, 2010; Siciliano et al., 2021) can be found in the literature. In composite timber beams, contact between layers is often assumed to consist of discrete connections via dowel type fasteners, which may be considered brittle or ductile. In the literature (Goodman and Popov, 1968; Milner and Tan, 2001; Rassam et al., 1970), the timber laminations are connected by dowel type fasteners with linear constitutive laws, although the interlayer contact behaviour is nonlinear (Foschi and Bonac, 1977). Alternatively, the continuous connection between the laminations, e.g., glued interlayer contact, is not analysed as frequently in the literature. Mostly, only the strength of the glued connections is reported (Aicher and Ohnesorge, 2011; Derikvand and Pangh, 2016) and no information about the corresponding deformation of the interlayer contact can be found. We assume that this is because the deformations on thin layers of the bonded joint are very small and also difficult to measure. However, with new technologies, some attempts to determine the deformations have been found using optical measurement methods (Serrano; Sebera et al., 2021; Sandhaas, 2012). This is introduced together with new modelling techniques offered by commercial finite element programmes (Smith, 2009; DeSalvo and Swanson, 1985), where cohesive zone finite elements are implemented by fracture mechanics and the dissipated energy information is essential data for the models (fracture energy). These methods are used to model local damage in the material (crack initiation) and predict the maximum force and character of failure (Qiu et al., 2014; Sebera et al., 2021). As for numerical models of the glued laminated beams, some of the most important and well-known models are based on computer simulations (Foschi and Barrett, 1980; Ehlbeck et al., 1985b,a,c; Serrano). The first, model of Foschi and Barrett (1980) is based on the assumption of a linearly elastic material in tension and compression and the lamellae consist of finite elements with predefined and fixed dimensions ($l = 150$ mm). The so-called Karlsruhe model (Ehlbeck et al., 1985b,a,c) is similar to the model of Foschi and Barrett (1980). It is somewhat improved, since the nodes and finger joints can be considered so that the stochastically selected finite element has the properties of the finger joint or a node. The nonlinear behaviour of the wood under compression is also considered and the progressive failure of the beam can be modelled. However, the failure criterion is assumed only in tension, so compressive failure cannot occur. The stresses are calculated in the centroidal axes of the finite elements as the average stresses of the cross-section of the lamina (Serrano, 2003). This assumption can be justified by the fact that laminated beams in fact usually fail in tension due to rupture of the laminations or finger joints.

Finger joints are regularly used to connect the shorter parts of the layer longitudinally. Finger joints are therefore an anomaly in the lamination and can significantly alter the performance of the laminated beam. Although any type of connection in the structure or member must overcome the load bearing capacity of the primary material, this is not always the case with hardwood. On the contrary, failure of the laminated beam is often due to local failure of the finger joints. Due to the pronounced scatter of material properties of wood and a complex geometry, modelling of finger joints is still an active research area, both from modelling (Aicher and Klöck, 1991; Aicher and Radović, 1999; Serrano, 2001; Tran et al., 2014; Franke et al., 2014) and experimental (Aicher and Klöck, 2001; Aicher and Ohnesorge, 2011; Fortuna et al., 2020) point of view. In general, the results of numerical models of laminated beams with finger joints are validated with the experimental results of the modelled element, usually with the calibration of the model (Ehlbeck et al., 1985b,a,c; Serrano, 2003). Exact analytical models for finger joints, are rarely found (Erdogan and Ratwani, 1971; da Silva et al., 2009) and furthermore, no analytical or exact model for the laminated beam with finger joints has been found in the literature. Therefore, an exact solution could be useful as a benchmark for numerical models.

In recent years, research throughout Europe has focused on various aspects of application of beech wood as a building material. Research has focused primarily on determining the mechanical properties of structural sized solid wood, i.e., the strength, modulus of elasticity, and density of the wood, as well as its assignment into strength classes. Some experimental studies show that the average tensile strength of beech can be almost three times that of spruce (Ehrhart et al., 2016, 2018b; Fortuna et al., 2018a; Plos et al., 2018b). The modulus of elasticity of beech wood is also higher than that of spruce, but the difference is slightly less than that of tensile strength. This has shown the great potential of beech wood, but as a construction material it presents a unique challenge. However, under given conditions, it can be used in load bearing elements, especially in glued load bearing elements (Aicher et al., 2001). Thinner lamellas are used to ensure a sufficiently high load bearing capacity. The stability and consequentially the durability of the elements is increased by the use of adhesives, as they reinforce the damaged cells and thus contribute to a more uniform stress distribution over the larger contact area (Šernek et al., 1999). Therefore, another research focus is on the different types of bonding. Glued laminated timber (GLT), along with cross-laminated timber (CLT), is one of the most commonly used glued laminated timber elements for use in load bearing structures. Both GLT and CLT elements consist of longitudinally connected boards. The most common type of longitudinal connection is finger jointing.

The requirements of the standards dealing with the manufacturing of finger joints were developed with regard to the properties of softwoods (CEN, 2001, 2013a,e). SIST EN 385 standard (CEN, 2001) specifies that the load bearing capacity of the finger joint must be determined by bending and/or tensile tests. Due to the stress distribution over the height of the beam under bending load, tension stresses are induced mainly in the outer laminations (bottom or top depending on the load position). Therefore, sufficient tension capacity of the finger joints must be ensured. In the literature, finger joints are mostly tested in bending tests (Tran et al., 2014; Franke et al., 2014), while adhesives are tested in tensile shear tests (Ammann et al., 2016; Konnerth et al., 2016), as defined in SIST EN 301 (CEN, 2006). In tensile shear tests, shear stresses dominate in the adhesive joint and no information is available on pure tensile strengths. At the University of Bern (Franke et al., 2014) a study was carried out on the production of finger joints on beech wood. The influence of various parameters was analysed, namely finger joint geometry, type and amount of adhesive used, method of adhesive application, and time and pressure during gluing. Melamine-urea-formaldehyde (MUF), polyurethane (PUR) and emulsion polymer isocyanate (EPI) and four different geometries were used. The length of the finger joints was 10, 15, 20 and 50 mm. The joints were tested for both bending and pure tension. The results showed that the highest tension and bending strengths were obtained with the MUF adhesive and a finger length of 20 mm (the mean value of the tensile strength was 95 N/mm^2) and a finger joint length of 15 mm (the mean value of the bending strength was 100 N/mm^2), while the strengths of the PUR and EPI adhesives were comparable. The maximum bending strength for a 50 mm finger joint with MUF adhesive was over 120 N/mm^2. Within

the TIGR4smart project (Fortuna et al., 2018a), the highest tension strengths of Slovenian beech wood were measured between 120 and 140 N/mm^2. Variations in the mechanical properties of wood are generally considerable, even within the same species so assessment of the quality of the finger joint isn't straightforward and the type of failure has proven to be a useful quality evaluation criterion (Aicher et al., 2001; Franke et al., 2014; Ammann et al., 2016; Konnerth et al., 2016). The quality of the finger joint is considered to be sufficient if the rupture occurs in the glued material and not in the glue line. In the study of Aicher et al. (2001), where the tensile strength of the 20 mm finger joints with MUF adhesive was tested in tension, the average value of the tensile strengths of the finger joints was 70 ± 11 N/mm^2.
Based on the known mechanical properties of the beech wood and the mechanical properties of the longitudinally bonded boards, research on glued laminated elements, i.e. structural elements, continues. In the literature, bending tests on glued laminated beams (Frese and Blass, 2006; Ehrhart et al., 2018a; Kržan et al., 2019) are usually performed to determine the bending strength, an essential basis for structural design. Various numerical models of glued laminated beams and simulations of bending tests are presented in addition to experimental tests in the literature. Glued laminated beams are in most cases modelled in finite element programmes such as Abaqus (Smith, 2009; Tran et al., 2014; Sandhaas, 2012; Qiu et al., 2014; Franke et al., 2014; Kržan et al., 2019; Sandhaas et al., 2019; Sebera et al., 2021).
The derivation of the computational model can generally be divided into three parts. In the first part, a study of the mechanical properties of the material and its behaviour under load is of great importance. Heterogeneity and anisotropy are characteristic phenomena for the properties of the wood (Sandhaas, 2012; Qiu et al., 2014; Sandhaas et al., 2019) and, moreover, the behaviour of the wood depends on the loading conditions. Wood behaves like a brittle material when loaded in tension or shear, while it behaves like a ductile material when loaded in compression. In the research by Sandhaas (2012) various combinations of models describing different behaviours are presented. The author has outlined the possibilities for modelling complex behaviours using what is known as micromechanical modelling, in which the material is modelled at multiple levels, starting with modelling the chemical composition of the material. Such models are too complex for use in engineering and are not yet sufficiently developed for wood. Therefore, a 3-dimensional model was developed (Sandhaas, 2012) that takes into account all the above wood-specific phenomena in the framework of Continuum Damage Mechanics - CDM. In the framework of the above damage mechanics, the nonlinear behaviour of a wood material is taken into account by changing the stiffness matrix. The stiffness matrix is gradually changed according to the damage evolution in the material. Therefore, the response of the material to loading is bilinear, with the displacement increasing linearly in the first part of the loading and decreasing linearly in the second part after the damage has occurred. The author (Sandhaas, 2012) has implemented the material model in Abaqus (Smith, 2009). The results of the model have successfully described the complex behaviour of the material under different loading conditions, i.e., ductile behaviour under compression and brittle behaviour under tensile and shear loading. Comparisons with experimental results have shown that while the model predicts the elastic properties of the material well, the displacements obtained are somewhat underestimated. In the model, the load-carrying capacity is characterised by a so-called numerical failure, which does not reflect the actual behaviour. In reality, after the failure of the first element, the neighbouring elements would break. This was implemented with further development of the model implementing the deletion of the failed finite elements thus redistributing the stresses in the model (Sandhaas et al., 2019).
The second part deals with the modelling of finger joints, especially the glue line in the finger joint. In

order to correctly determine the strength of the finger joint, the appropriate stress distribution must be proposed and suitable failure criteria determined. The latter depends on the geometry of the finger joint and the loading conditions (da Silva et al., 2009). When modelling finger joints in glued laminated beams, it is critical to determine the load-carrying capacity in tension. This is due to the stress distribution along the cross-section of the beam loaded in bending, where the tensile strength in the lower laminations is critical. The choice of the model depends on the complexity of the problem. The latter depends on the geometrical and material properties as well as on the loading conditions. For basic problems, an analytical approach is sufficient. Two-dimensional planar models are most commonly used, taking into account the linear behaviour of the adhesive and also the material of the bonded elements. In the work of da Silva et al. (2009) a detailed overview of different analytical models of various adhesively bonded joints and their applicability is given. As the complexity of the problem increases, the differential equations can no longer be solved analytically, so a numerical approach is required. A brief overview of the established numerical models for glued laminated beams can be found in Serrano (2001). In the models, finger joints are considered as a local weak point in the context of the variability of the mechanical properties of wood. The authors presented their own model in which a more accurate description of the finger joints is implemented based on nonlinear fracture mechanics. Although the mechanical properties of finger joints are considered stochastic, the lamellar material is described deterministically.

The third important step in the modelling of glued laminated elements is the formulation of the interlayer contacts i.e. the contact between the surfaces of the individual laminations. Glued laminated beams consist of a series of laminations bonded together by adhesive. Therefore, the stresses and deformations that occur in the individual lamination are directly related to the stresses in the glued joint. The deformations of the latter represent constraints in solving the equations and determining the deformations and stresses in the material lamination. The constraining equations are used to describe the behaviour of the adhesive at the contact between the layers of a glued beam. In the study performed by Kroflič (2012), the equations of the numerical model for geometrically nonlinear analysis of planar multilayer glued beams are presented, focusing on the equations for modelling the contact between layers. Delamination of two adjacent layers of the glued beam in both longitudinal and transverse directions is considered (Kroflič, 2012). The usual approach is target modelling to match the results of experimental tests and simulations. Wood exhibits highly variable mechanical properties, which are also reflected in the large variability of the properties of the glued finger joints, i.e., the glued elements. It is therefore essential to take this scatter of properties into account in the modelling, as this greatly increases the overall validity of the model, i.e., its usefulness. Unfortunately, this is not very common in the literature dealing with composite beams with interlayer slip.

1.4 Organisation of Work

The aim of the dissertation was to investigate as comprehensively as possible the various aspects of the glued laminated beams made of Slovenian beech timber. This field of research is relatively unexplored, so the intention of the present work was to obtain the basic information about the material and to formulate suitable and useful computational tools that can be used for research purposes and also in the design process of the glued laminated beams made of beech timber or even timber in general. This dissertation is roughly divided into three main parts.

The first part presents the theoretical basis of the calculations. The fundamental equations are presented, on the basis of which the computational models were formulated. First, the analytical solution of the multi-layer beam is shown. The interlayer slip between the laminations is allowed. The laminations can have multiple finger joints and a fully debonded segment of the interlayer contact. The equations are based on the Euler-Bernoulli theory for planar beams as well as the somewhat more general Timoshenko-Ehrenfest beam theory, where shear deformations are taken into account. The appendix contains the explicit expressions of the analytical solution for a two-layer beam with two finger joints and a fully debonded segment. Since the complexity of the analytical expression increases with the number of laminations and the number of finger joints, the calculation can become time consuming. Therefore, the theoretical part continues with the formulation of the numerical model, in which the equations for locking-free finite element are presented. The formulation is based on the same fundamental equations as for the analytical model, i.e. on the first order theory. The behaviour of the finite element is defined only by the interpolation of its deformations. The model is therefore more robust and more applicable. The elements of the tangential stiffness matrix are given, which are the bases of the numerical model of the planar, multilayer Timoshenko-Ehrenfest beam with arbitrary number and position of finger joints. The calculation is efficient and fast, and compared to the analytical formulation, has no limitation on the number of the laminations or the number of finger joints. The material of the lamination and interlayer contact can be defined with an arbitrary constitutive law.

The theoretical part of the dissertation deals also with the preliminary studies on finger joints and adhesives. For the analysis of finger joints, a simple analytical model of the finger joint is used to assess the influence of the geometrical parameters of the finger joint profile on its tensile strength. A more detailed analysis was also performed using the numerical model of one half of the finger joint profile, and the tensile strength capacities were evaluated for different finger joint profiles. Based on the results, the optimum geometry of the finger joint profile was selected to be used in the experimental part. Different adhesive types were investigated based on a literature review. Based on the information obtained and the feasibility of producing finger joints and later glued laminated beams, three different adhesive types were selected to be used in the experimental part of the research.

The second major part of the dissertation is the experimental part, in which first the experimental results of tensile tests of different finger joint profiles and adhesive types are presented. Tensile strength capacities and moduli of elasticity in tension of the finger joints were measured. Prior to destructive testing, single boards were non-destructively tested and the dynamic modulus of elasticity was measured. Measurements were also made on glued boards. Similarly, the laminations for the glued laminated beams were also non-destructively tested. The glued laminated beams were produced in two batches with two different finger joint profiles and were then tested in bending. The bending strength and static modulus of elasticity were measured for all 14 beams. For the smaller batch of 4 glued laminated beams, the shear deformations and interlayer displacements were measured so that the shear modulus and interlayer contact stiffness could be determined.

In the third part, the mathematical models are verified with other similar studies on the laminated beams and then validated with the measurements and the results of the performed experimental tests. Although the measured and calculated results agreed quite well, it is reasonable to adopt a stochastic approach when the scatter of mechanical properties is so large, as is characteristic of wood. The stochastic simulations were performed for a two-layer beam using the analytical model and for a ten-layer beam using the numerical model, where nonlinear material properties were also taken into account.

2 THEORY ON LAMINATED BEAMS AND FINGER JOINTS

The basic equations of the laminated beams with an arbitrary number of layers are presented in this chapter. The equations provide the theoretical background and the basis for the derivation of an analytical model of a laminated beam and for the derivation of the new finite element of the N-layer laminated beam used in the numerical model presented in the following chapter. The formulation of the equations is based on the kinematically exact Reissner theory for planar beams (Reissner, 1972). The deformation of the beam is limited to small displacements and small rotations. Timoshenko-Ehrenfest theory is also considered. Therefore, the originally straight cross-sections in the undeformed state remain straight in the deformed configuration, but not necessarily perpendicular to the reference axis of the beam (Timoshenko, 1921).

2.1 Fundamental equations of laminated beams

Before listing the equations, we must introduce some important assumptions that will be considered. The basic subject of our problem is a geometrically linear composite beam with an arbitrary number of layers N. The layers are denoted by i, where $i = (1, 2, ..., N)$. They are connected with interlayer contact layer, which has negligible thickness and known material properties. The interlayer contact is continuous along the length of the beam L. All layers are initially undeformed and have the same length, i.e. $L^i = L$. The beam is defined in Cartesian space $\mathbb{R}^3 = \{X, Y, Z\}$ with fixed orthonormal global basis vectors $\mathbf{E}_X, \mathbf{E}_Y$ and $\mathbf{E}_Z$, where $\mathbf{E}_Z = \mathbf{E}_X \times \mathbf{E}_Y$. The global reference axis of the straight, undeformed beam is assumed to be at the lowest edge of the beam. For simplicity, the reference axis coincides with the X axis of the global coordinate system and the reference axes of all layers are common to the global reference axis. The arbitrary particle of layer i is defined with material coordinates (x^i, y^i, z^i). The shape of the cross-section A^i of the layer i is considered prismatic, defined with thickness h^i and width b^i in the plane Y, Z. The cross-sections of the layers are homogeneous and their shape does not change during deformation.

2.1.1 Kinematic equations

In general, the displacement of the arbitrary particle of the beam with coordinates (x^i, y^i, z^i) is described with the position vector $\mathbf{R^i}(x^i, y^i, z^i)$ as shown in Fig. 2.1 and written as:

$$\mathbf{R^i}(x^i, y^i, z^i) = x^i\,\mathbf{E}_X + \mathbf{U^i}(x^i, y^i, z^i), \tag{2.1}$$

where $\mathbf{U^i}(x^i, y^i, z^i)$ is the displacement vector of a particle (x^i, y^i, z^i) and is defined as:

$$\mathbf{U^i}(x^i, y^i, z^i) = u^i(x^i)\,\mathbf{E_X} + w^i(x^i)\,\mathbf{E_Z} + \boldsymbol{\varphi}^i(x^i, y^i, z^i), \tag{2.2}$$

where $u^i(x^i)$ and $w^i(x^i)$ are the horizontal and vertical displacements of the particle at the reference axis of the layer i in X and Z directions, respectively. The $\boldsymbol{\varphi}^{\mathbf{i}}(x^i, y^i, z^i)$ represents the rotation vector in the

XZ plane and defines the position of the arbitrary particle of the cross-section and is determined as:

$$\boldsymbol{\varphi}^i(x^i, y^i, z^i) = y^i\,\mathbf{e}_y^i(x^i) + z^i\,\mathbf{e}_z^i(x^i). \tag{2.3}$$

The $\mathbf{e}_x^i(x^i)$, $\mathbf{e}_y^i(x^i)$ and $\mathbf{e}_x^i(x^i)$ define the local material basis of the cross-section and are determined in the global coordinate space, as shown in Eqs. (2.4) – (2.6). Since it is assumed that the reference axis coincide with the X axis of the global coordinate system, i.e., $y^i = 0$ and $z^i = 0$, the $u^i(x^i)$ and $w^i(x^i)$ are determined only by the material coordinate $x^i \in \{0, L^i\}$. The material basis is defined as:

$$\mathbf{e}_x^i(x^i) = \cos\,\varphi^i(x^i)\,\mathbf{E}_X - \sin\,\varphi^i(x^i)\,\mathbf{E}_Z, \tag{2.4}$$

$$\mathbf{e}_y^i(x^i) = \mathbf{E}_Y, \tag{2.5}$$

$$\mathbf{e}_z^i(x^i) = \sin\,\varphi^i(x^i)\,\mathbf{E}_X + \cos\,\varphi^i(x^i)\,\mathbf{E}_Z, \tag{2.6}$$

where the $\varphi^i(x^i)$ denotes the rotation of the cross-section at position x^i. Under the assumptions of geometrically linear theory where rotations are small and it is true that

$$\cos\,\varphi^i \approx 1 \qquad \text{and} \qquad \sin\,\varphi^{\mathrm{i}} \approx \varphi^{\mathrm{i}}. \tag{2.7}$$

The deformation vector in Eq. (2.1), of any particle along the beam taking into account Eqs. (2.4) – (2.6) and (2.7) can be written as shown in Eq. (2.8). Since we are dealing with a plane model of the beam, the argument y^i is further omitted from expressions.

$$\mathbf{R}^i(x^i, z^i) = (x^i + u^i(x^i) + z^i\,\varphi^i(x^i))\mathbf{E}_X + (z^i + w^i(x^i))\,\mathbf{E}_Z. \tag{2.8}$$

In this way, the deformed configuration of the beam is kinematically described by the basic kinematic functions $u^i(x^i)$, $w^i(x^i)$ and $\varphi^i(x^i)$. Based on the Reissner planar beam theory (Reissner, 1972), the kinematic equations are defined to relate the kinematic quantities, i.e., the displacements and the rotations, to the deformations ε^i, γ^i and κ^i of the layer i. General form of the kinematic equations, according to the Reissner beam theory (Reissner, 1972), are a first order differential equations and can be used to solve mechanical problems without regard to the magnitude of displacements and rotations and have been presented in detail in the past (Schnabl, 2007; Rodman, 2009; Kroflič, 2012). However, in civil engineering, the expected deformations of the structural elements are small compared to their dimensions and the equations can be simplified. The geometry of the structural element does not change significantly during deformation. If the partial derivatives of the kinematic functions over all variables are expressed using the Taylor series at an arbitrary point x_0 (in the undeformed configuration $f(x) = 0$) and truncated at the first differentiated member, this gives a sufficiently accurate result (Bonet and Wood, 1997):

$$f(x_0 + e) \approx f(x_0) + \left.\frac{df}{dx}\right|_{x_0} e, \tag{2.9}$$

where the e defines the neighbourhood of x:

$$e = (x - x_0). \tag{2.10}$$

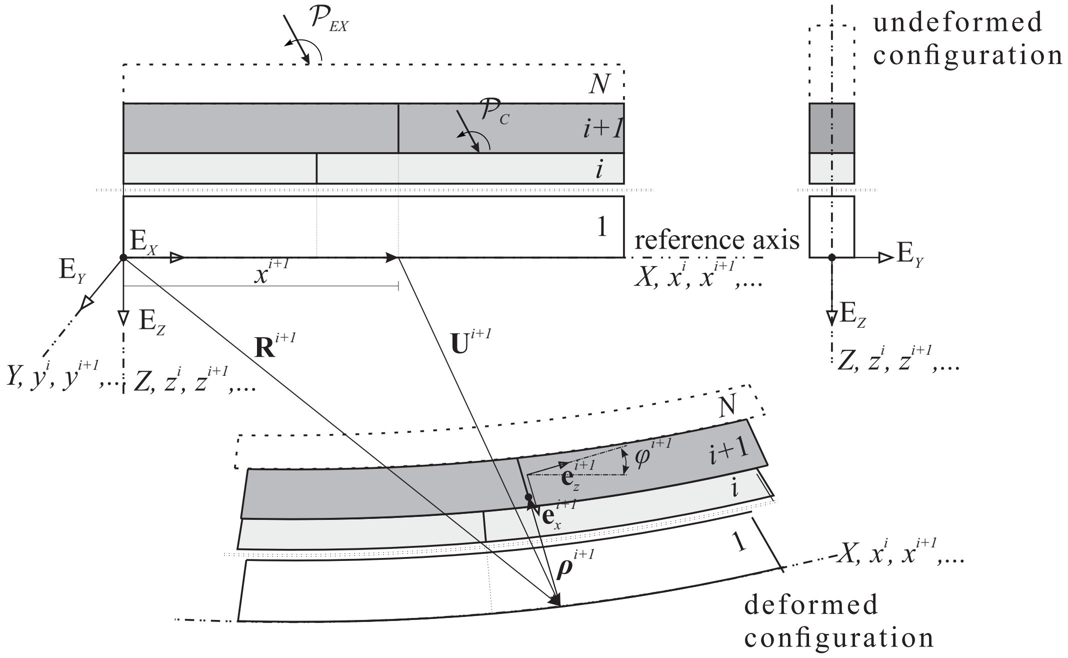

Figure 2.1: Undeformed and deformed configuration of laminated beam.
Slika 2.1: Nedeformirana in deformirana konfiguracija lameliranega nosilca.

By Eq. (2.9), the initial, nonlinear differential equation $f(x)$, representing the condensed kinematic equations, becomes a simple, linear differential equation. This process is known as consistent linearization (Hughes and Pister, 1978; Bonet and Wood, 1997) and it was used here on the generalized kinematic equations so they can be written in simplified form, for $i = \{1, 2, ..., N\}$:

$$\frac{du^i(x^i)}{dx^i} - \varepsilon^i(x^i) = 0, \tag{2.11}$$

$$\frac{dw^i(x^i)}{dx^i} + \varphi^i(x^i) - \gamma^i(x^i) = 0, \tag{2.12}$$

$$\frac{d\varphi^i(x^i)}{dx^i} - \kappa^i(x^i) = 0. \tag{2.13}$$

The deformations appearing in Eq. (2.11) – (2.13) are the longitudinal deformation of the material, $\varepsilon^i(x^i)$, the shear deformation, $\gamma^i(x^i)$, and the pseudocurvature or bending deformation of the cross-section of the beam, $\kappa^i(x^i)$. When $\gamma^i(x^i) = 0$, the $\varepsilon^i(x^i)$ also represents the specific length change of the reference axis of the layer i and when $\varepsilon^i(x^i) = 0$, the pseudocurvature $\kappa^i(x^i)$ represents the actual curvature of the reference axis of the layer i (Vratanar and Saje, 1998; Čas, 2004). The longitudinal deformation D^i of the material at arbitrary position over the height of the beam can be determined with the following equation:

$$D^i(x^i, z^i) = \varepsilon^i(x^i) + z^i\,\kappa^i(x^i), \tag{2.14}$$

where $i = \{1, 2, ..., N\}$.

2.1.2 Equilibrium equations

The beam is subjected to the generalised load $\mathcal{P}$. The equilibrium equations are used to connect the internal forces and moments caused by the external load. For multilayer elements, according to the origin, there are two types of loads acting on the internal forces and moments of each layer i. These are the external load $\mathcal{P}_{EX} = \{\mathbf{p}^i(x^i), \mathbf{m}^i(x^i)\}$ and the load, induced by adjacent layers and transmitted through the contact between the layers and therefore denoted as *contact* load, $\mathcal{P}_c = \{\mathbf{p}^i_c(x^i), \mathbf{m}^i_c(x^i)\}$. Additionally, the external load can be either distributed along an arbitrarily long section of the beam $L_P \in [0, L]$, see Eqs. (2.15) – (2.18), or concentrated in one point. The concentrated load S^i_j, where $i = (1, 2, ..., N)$ and $j = (1, 2, ..., 6)$, can be applied only at the extreme ends of the beam element, i.e. $x^i = 0$ and/or $x^i = L$.

$$\mathbf{p^i}(x^i) = p^i_X(x^i)\,\mathbf{E}_X + p^i_Z(x^i)\,\mathbf{E}_Z, \tag{2.15}$$

$$\mathbf{m^i}(x^i) = m^i_Y(x^i)\,\mathbf{E}_Y. \tag{2.16}$$

As already indicated, the multilayer beams consist of N layers whose mechanical behaviour is interdependent. Therefore, deformation of one layer leads to deformation of other layers. Laminated beam with N layers have $N-1$ interlayer contact surfaces. The notation $j = \{1, 2, ..., N-1\}$ is used to define the interlayer contact surface and it is assumed that, for $i < N$, $i = j$ so that the contact area at the top of the layer has the same notation as the layer. This means that for the first layer $i = 1$ the contact tractions $p^{i,j-1}_{c,X}(x^i)$ and $p^{i,j-1}_{c,Z}(x^i)$ as well as the moment $m^{i,j-1}_{c,Y}(x^i)$ are equal to 0. In this way, the traction in the contact surface j acts on the layers i and $i+1$, as shown in Fig. 2.2. The distributed contact load is defined by Eqs. (2.17) – (2.18).

$$\begin{aligned}\mathbf{p}^i_c(x^i) &= p^i_{c,X}(x^i)\,\mathbf{E}_X + p^i_{c,Z}(x^i)\,\mathbf{E}_Z = \\ &= \left(p^{i,j}_{c,X}(x^i) - p^{i,j-1}_{c,X}(x^i)\right)\mathbf{E}_X + \left(p^{i,j}_{c,Z}(x^i) - p^{i,j-1}_{c,Z}(x^i)\right)\mathbf{E}_Z,\end{aligned} \tag{2.17}$$

$$\begin{aligned}\mathbf{m}^i_c(x^i) &= m^i_{c,Y}(x^i)\,\mathbf{E}_Y = \left(m^{i,j}_{c,Y}(x^i) + m^{i,j-1}_{c,Y}(x^i)\right)\mathbf{E}_Y = \\ &= \Bigg(z^j\left(p^{i,j}_{c,Z}(x^i)\sin\varphi^i(x^i) - p^{i,j}_{c,X}(x^i)\cos\varphi^i(x^i)\right) + \\ &\quad + z^{j-1}\left(p^{i,j-1}_{c,X}(x^i)\cos\varphi^i(x^i) - p^{i,j-1}_{c,Z}(x^i)\sin\varphi^i(x^i)\right)\Bigg)\,\mathbf{E}_Y\end{aligned} \tag{2.18}$$

According to the Reissner beam theory (Reissner, 1972), the load of the layer i is applied to the deformed reference axes, see Fig. 2.3. The equilibrium equations for the layers are defined with first order differential equations, adopted after Simo (1985) and presented, where z^j and z^{j-1} denote the z coordinates of the interlayer contact j and $j-1$, respectively:

$$\frac{dR^i_X(x^i)}{dx^i} + p^i_X(x^i) + p^{i,j}_{c,X}(x^i) - p^{i,j-1}_{c,X}(x^i) = 0, \tag{2.19}$$

$$\frac{dR^i_Z(x^i)}{dx^i} + p^i_Z(x^i) + p^{i,j}_{c,Z}(x^i) - p^{i,j-1}_{c,Z}(x^i) = 0, \tag{2.20}$$

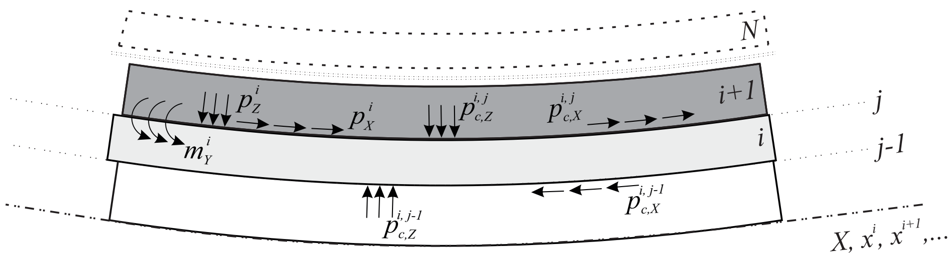

Figure 2.2: Contact tractions on contact surface, influencing on layer i.
Slika 2.2: Kontaktna obtežba na stiku j, ki deluje na sloj i.

$$\begin{aligned}&\frac{dM^i(x^i)}{dx^i} - \left(1 + \varepsilon^i(x^i)\right) Q^i(x^i) + \gamma^i(x^i)\, N^i(x^i) + m_Y(x^i) + \\ &+ \left(z^{j-1}\, p_{c,X}^{i,j-1}(x^i) - z^j\, p_{c,X}^{i,j}(x^i)\right) \cos\varphi^i(x^i) - \\ &- \left(z^{j-1}\, p_{c,Z}^{i,j-1}(x^i) + z^j\, p_{c,Z}^{i,j}(x^i)\right) \sin\varphi^i(x^i) = 0,\end{aligned} \tag{2.21}$$

where the equilibrium quantities $R^i_X(x^i)$, $R^i_Z(x^i)$, $M^i(x^i)$, $N^i(x^i)$ and $Q^i(x^i)$ represent the internal forces and moments of the layer i in global directions $\mathbf{E}_X$, $\mathbf{E}_Z$, $\mathbf{E}_Y = \mathbf{e}_y$ and local material directions $\mathbf{e}^i_x$ and $\mathbf{e}^i_z$, respectively. As a result of selected global and local coordinate basis, Eq. (2.5), the internal bending moments are in global and local basis identical, while in the case of longitudinal and transversal force, the rotation of the cross-section $\varphi^i(x^i)$ has to be considered. The relations are written in:

$$\mathbf{N}^i = R^i_X(x^i)\,\mathbf{E}_X + R^i_Z(x^i)\,\mathbf{E}_Z = N^i(x^i)\,\mathbf{e}_x + Q^i(x^i)\,\mathbf{e}_z \tag{2.22}$$

$$\mathbf{M}^i = M^i\,\mathbf{E}_Y = M^i\mathbf{e}_y. \tag{2.23}$$

If Eqs. (2.4) – (2.6) are considered in Eqs. (2.22) – (2.23), the components of internal forces in different coordinate basis are related as shown in Eqs. (2.24) – (2.25).

$$N^i(x^i) = R^i_X(x^i)\, \cos\varphi^i(x^i) - R^i_Z(x^i)\, \sin\varphi^i(x^i), \tag{2.24}$$

$$Q^i(x^i) = R^i_X(x^i)\, \sin\varphi^i(x^i) + R^i_Z(x^i)\, \cos\varphi^i(x^i), \tag{2.25}$$

As for the kinematic equations, also the equilibrium equations can be written in linearized form according to the principle of consistent linearization, see Eq. (2.9). In this case the function $f(x)$ now represents the condensed equilibrium equations, Eqs. (2.19) – (2.21). Together with the assumption of small displacements and rotations, Eq. (2.7), of the layers, the Eqs. (2.19) – (2.21) are now defined on undeformed configuration:

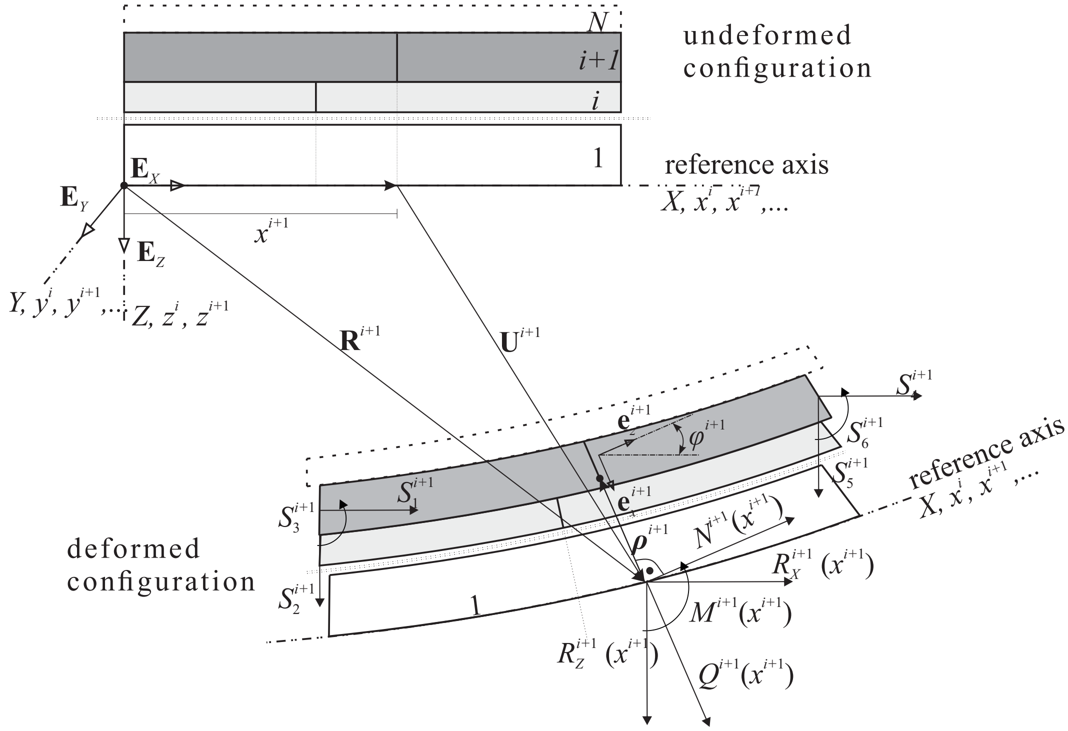

Figure 2.3: Boundary loads and internal forces and moments.
Slika 2.3: Robna obtežba ter notranje sile in momenti v nosilcu.

$$\frac{dN^i(x^i)}{dx^i} + p_X^i(x^i) + p_{c,X}^{i,j}(x^i) - p_{c,X}^{i,j-1}(x^i) = 0, \tag{2.26}$$

$$\frac{dQ^i(x^i)}{dx^i} + p_Z^i(x^i) + p_{c,Z}^{i,j}(x^i) - p_{c,Z}^{i,j-1}(x^i) = 0, \tag{2.27}$$

$$\frac{dM^i(x^i)}{dx^i} - Q^i(x^i) + m_Y^i(x^i) + z^{j-1}\, p_{c,X}^{i,j-1}(x^i) - z^j\, p_{c,X}^{i,j}(x^i) = 0. \tag{2.28}$$

2.1.3 Constitutive equations

For the beam to be in static equilibrium, the internal forces and moments induced by the external load must be undertaken by the material of the glued laminated beam. The constitutive equations define the relationship between the deformation of the beam and the internal forces. It is important that the equilibrium quantities are expressed in the local (material) coordinate system $(\mathbf{e}_x, \mathbf{e}_y, \mathbf{e}_z)$, (Reissner, 1972). Therefore, the general form of the constitutive equations for the layer $i = (1, 2, ..., N)$ is presented as in Eqs. (2.29) – (2.31), taking into account the assumption of homogeneous cross-section of the layers. A generalized representation of the constitutive equations for layered beams can also be found in (Schnabl, 2007).

$$N^i(x^i) = N_C^i\big(\varepsilon^i(x^i), \kappa^i(x^i)\big) = \int_{\mathcal{A}^i} \sigma^i(x^i, z^i)\, dA = \int_{\mathcal{A}^i} \sigma^i(D^i(x^i, z^i))\, dA, \tag{2.29}$$

$$Q^i(x^i) = Q_C^i\big(\gamma^i(x^i)\big) = \int_{\mathcal{A}^i} \tau^i(x^i, z^i)\, dA = \int_{\mathcal{A}^i} \tau^i(\gamma^i(x^i, z^i))\, dA, \tag{2.30}$$

$$M^i(x^i) = M_C^i\big(\varepsilon^i(x^i), \kappa^i(x^i)\big) = \int_{\mathcal{A}^i} z^i\, \sigma^i(x^i, z^i)\, dA = \int_{\mathcal{A}^i} z^i\, \sigma^i(D^i(x^i, z^i))\, dA. \tag{2.31}$$

where N_C^i, Q_C^i and M_C^i are the constitutive axial and shear forces and the constitutive bending moment of layer i, respectively, and are defined as resultants of the normal and shear components of the stress tensor. The tensor consists of the normal stress σ^i and the shear stress τ^i and is defined with Eqs. (2.32) – (2.33). The functions $\mathcal{F}_1^i$ and $\mathcal{F}_2^i$ are defined with uniaxial compression and/or tensile tests and experimental shear tests and generally describe any arbitrary material model (linear elastic, hyperelastic, plastic material, etc.).

$$\sigma^i(x^i, z^i) = \mathcal{F}_1^i\big(D^i(x^i, z^i)\big), \tag{2.32}$$

$$\tau^i(x^i, z^i) = \mathcal{F}_2^i\big(\gamma^i(x^i, z^i)\big). \tag{2.33}$$

In engineering, Eq. (2.34) is commonly used to determine of the constitutive shear force. The expression and was adopted from (Cowper, 1966), where the constitutive the force is calculated for a given shear modulus G^i and shear cross-section A_s^i, defined in terms of the shape of the cross-section A^i and it holds $A_s^i < A^i$:

$$Q_C^i(\gamma^i(x^i)) = \int_{\mathcal{A}^i} \tau^i(x^i, z^i)\, dA = G^i\, A_s^i\, \gamma^i(x^i). \tag{2.34}$$

With Eqs. (2.32) – (2.34) a very general expressions are given. However, when modelling laminated beams, the constitutive quantities N_C^i, Q_C^i and M_C^i can also be linearized. When applying the principle defined by Eqs. (2.9) – (2.10), the constitutive quantities are defined with simpler linear equations. The variations of the constitutive quantities δN_C^i, δQ_C^i, and δM_C^i:

$$\begin{aligned} \delta N_C^i\big(\varepsilon^i(x^i), \kappa^i(x^i)\big) &= \left(\int_{\mathcal{A}^i} \frac{\partial \sigma^i}{\partial \varepsilon^i}\, dA\right) \delta\varepsilon^i + \left(\int_{\mathcal{A}^i} z^i\, \frac{\partial \sigma^i}{\partial \kappa^i}\, dA\right) \delta\kappa^i = \\ &= C_{11}^i\, \delta\varepsilon^i + C_{12}^i\, \delta\kappa^i, \end{aligned} \tag{2.35}$$

$$\begin{aligned} \delta M_C^i\big(\varepsilon^i(x^i), \kappa^i(x^i)\big) &= \left(\int_{\mathcal{A}^i} z^i\, \frac{\partial \sigma^i}{\partial \varepsilon^i}\, dA\right) \delta\varepsilon^i + \left(\int_{\mathcal{A}^i} (z^i)^2\, \frac{\partial \sigma^i}{\partial \kappa^i}\, dA\right) \delta\kappa^i = \\ &= C_{21}^i\, \delta\varepsilon^i + C_{22}^i\, \delta\kappa^i, \end{aligned} \tag{2.36}$$

$$\delta Q_C^i\big(\gamma^i(x^i)\big) = \left(\int_{\mathcal{A}^i} \frac{\partial \tau^i}{\partial \gamma^i}\, dA\right) \delta\gamma^i = C_{33}^i\, \delta\, \gamma^i. \tag{2.37}$$

The derivatives $\partial\sigma^i/\partial D^i$,$\partial\sigma^i/\partial\varepsilon^i$ and $\partial\sigma^i/\partial\kappa^i$ represent the tangential material modulus E^i of layer i and the quantities C^i_{11}, C^i_{22}, $C^i_{12} = C^i_{21}$ and C^i_{33} are the components of the tangential material matrix $\mathbf{C}^i$ of the cross-section of layer i:

$$\mathbf{C}^i = \begin{bmatrix} C^i_{11} & C^i_{12} & 0 \\ C^i_{21} & C^i_{22} & 0 \\ 0 & 0 & C^i_{33} \end{bmatrix} \tag{2.38}$$

2.1.4 Boundary conditions

The kinematic equations, Eqs. (2.11) – (2.13), equilibrium equations, Eqs. (2.26) – (2.28), and constitutive equations, Eqs. (2.32) – (2.34), represent the fundamental system of $6\,N$ first-order differential equations and $3\,N$ algebraic equations, giving $6\,N$ unknown integration constants. To obtain the complete solution for the unknowns $u^i(x^i)$, $w^i(x^i)$, $\varphi^i(x^i)$, $N^i(x^i)$, $Q^i(x^i)$, and $M^i(x^i)$, the boundary conditions must be defined. As the name implies, the conditions define selected mechanical quantities at the boundaries of the layers, i.e. $x^i = 0$ and $x^i = L$. In general, boundary conditions are divided into Neuman (or natural) and Dirichlet (or essential) boundary conditions and differ by the type of quantity used in the condition. Neuman conditions are defined with equilibrium quantities, while Dirichlet conditions are defined with kinematic quantities. The conditions are usually predefined by the geometry of the model (e.g., the type of supports), but using only one type of the boundary conditions does not necessarily lead to a unique solution of the system. Therefore, the combination of Neuman and Dirichlet conditions must be used. For each degree of freedom, only one of the two types may be used, either Neuman's or Dirchlets. This is determined by Eqs. (2.39) – (2.40) at the beginning and end of the layers.

$x = 0:$

$$\begin{aligned} &U^i_1 - u^i(0) = 0 \quad \text{or} \quad S^i_1 + N^i(0) = 0, \\ &U^i_2 - w^i(0) = 0 \quad \text{or} \quad S^i_2 + Q^i(0) = 0, \\ &U^i_3 - \varphi^i(0) = 0 \quad \text{or} \quad S^i_3 + M^i_Y(0) = 0. \end{aligned} \tag{2.39}$$

$x = L:$

$$\begin{aligned} &U^i_4 - u^i(L) = 0 \quad \text{or} \quad S^i_4 - N^i(L) = 0, \\ &U^i_5 - w^i(L) = 0 \quad \text{or} \quad S^i_5 - Q^i(L) = 0, \\ &U^i_6 - \varphi^i(L) = 0 \quad \text{or} \quad S^i_6 - M^i_Y(L) = 0. \end{aligned} \tag{2.40}$$

The first column of the Eqs. (2.39) – (2.40) presents the essential boundary conditions with prescribed generalized boundary displacements U^i_k for the six degrees of freedom $k = (1, 2, ..., 6)$. The second column of the Eqs. (2.39) – (2.40) represents the natural boundary conditions with prescribed generalized boundary loads S^i_k, $k = (1, 2, ..., 6)$.

2.2 Constraining equations

As mentioned earlier, the deformations of the layers of the beam are generally not independent and the layers are constrained against each other. If we define three options for the interaction between the layers, the first would be the connection with infinitely high stiffness properties. In this case, there would be no deformation in the interlayer, i.e. no sliding between the layers and no delamination. Such cases are very unlikely. The second and also extreme option would be completely debonded layers, i.e. no interaction between the layers. In this case, each layer can deform independently of the other. The third option is the most realistic in practice, i.e. partial interaction, where the connection between the layers exists but has limited stiffness and is therefore deformable. To define the connection, the constraining equations are used.

In the context of this work, we are interested in the last two options of interlayer connections. The adhesives used to join the laminations, which are most commonly used in the manufacture of glued laminated beams are deformable and are a very simple representative of the partial (in terms of glueline rigidity) interaction option . However, in this dissertation we restrict ourselves to the partial interaction, where only sliding between layers is allowed, while delamination between layers i and $i+1$ is restricted in the interlayer contact j, see Eq. (2.41), where $i = (1, 2, ..., N)$ and $j = (1, 2, ..., N-1)$.

$$\mathbf{R}^i(x^i, y^i, z^j) = \mathbf{R}^{i+1}(x^{i+1}, y^{i+1}, z^j). \tag{2.41}$$

$\mathbf{R}^i$ and $\mathbf{R}^{i+1}$ are the position vectors of any arbitrary particles T^i and T^{i+1} in layers i and $i+1$, respectively, and are chosen to have different positions in the undeformed configuration but the same position after deformation, see Fig. 2.4. If Eq. (2.8) is taken into account, considering $y^i = y^{i+1} = 0$ and

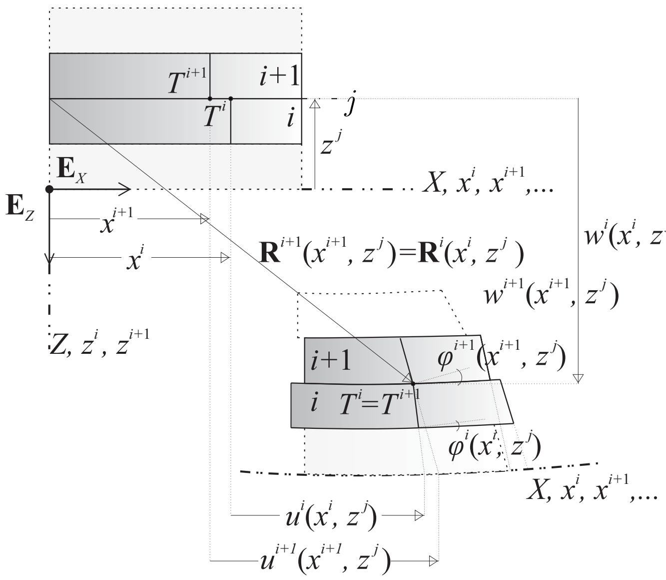

Figure 2.4: A schematic presentation of the geometry of the slip between layers i and $i+1$ in interlayer contact j.
Slika 2.4: Shematski prikaz geometrije zdrsa slojev i in $i+1$ v stiku j.

the fact that for contact j, z^j, the Eq. (2.41) is written:

$$\begin{aligned}&\big(x^i + u^i(x^i) + z^j\,\varphi^i(x^i)\big)\mathbf{E}_X + \big(z^j + w^i(x^i)\big)\,\mathbf{E}_Z = \\ &= \big(x^{i+1} + u^{i+1}(x^{i+1}) + z^j\,\varphi^{i+1}(x^{i+1})\big)\mathbf{E}_X + \big(z^j + w^{i+1}(x^{i+1})\big)\,\mathbf{E}_Z,\end{aligned} \tag{2.42}$$

or in rearranged component form

$$x^i - x^{i+1} + u^i(x^i) - u^{i+1}(x^{i+1}) + z^j\left(\varphi^i(x^i) - \varphi^{i+1}(x^{i+1})\right) = 0, \tag{2.43}$$

$$w^i(x^i) - w^{i+1}(x^{i+1}) = 0. \tag{2.44}$$

By Eq. (2.44) it is shown, that no delamination between the layers is allowed. The deformation of the interlayer contact between particles T^i and T^{i+1} with coordinates x^i and x^{i+1}, respectively, on the undeformed reference axes, respectively, is now defined only by the interlayer slip $\Delta^j_{\mathrm{X}}(x^i)$:

$$\Delta^j_X(x^i) = x^i - x^{i+1} \neq 0, \tag{2.45}$$

$$\Delta^j_Z(x^i) = 0. \tag{2.46}$$

If the expression for slip $\Delta^j_X(x^i)$ of the interlayer contact j is implemented in Eq. (2.43), following equation is obtained:

$$\Delta^j_X(x^i) = u^{i+1}(x^{i+1}) - u^i(x^i) + z^j\,(\varphi^{i+1}(x^{i+1}) - \varphi^i(x^i)). \tag{2.47}$$

As mentioned earlier, in civil engineering, the expected deformation of structural elements is limited by the serviceability limit state, so displacements and rotations are small. In addition, similar assumptions can be considered for the interlayer slips. The connection between layers in structural elements usually has a relatively high stiffness, so that the expected slips are also small. Such simplifications are therefore commonly used (Čas et al., 2004; Schnabl, 2007; Sousa Jr and Silva, 2010; Xu and Wu, 2009) and are justified later in the dissertation with experimental results.

With respect to the production of glued laminated beams from (any type of) wood, the ”no interaction” option is also interesting. Although it is highly undesirable, defects can occur in the production process that lead to an interruption of the adhesive application. This means that there is a certain risk that parts of the beam my remain fully debonded, like shown in Fig. 2.5. In this case, the deformation vectors for the particles T^i and T^{i+1}, $\mathbf{R}^i(x^i)$ and $\mathbf{R}^{i+1}(x^{i+1})$ will no longer be identical, Eq. (2.48) and for the interlayer contact j $z^i \neq z^{i+1}, z^i \neq z^j$.

$$\mathbf{R}^i(x^i, y^i, z^i) \neq \mathbf{R}^{i+1}(x^{i+1}, y^{i+1}, z^{i+1}). \tag{2.48}$$

This leads to a slightly different definition of the kinematic field in the Z direction compared to that defined by the Eqs. (2.42) – (2.47):

$$\Delta^j_X(x^i) = x^i - x^{i+1} \neq 0, \tag{2.49}$$

$$\Delta^j_Z(x^i) = z^i - z^{i+1} \neq 0. \tag{2.50}$$

In this case, the horizontal component of the displacement remains as shown in Eq. (2.47), while the vertical component is no longer 0:

$$\Delta^j_Z(x^i) = w^{i+1}(x^{i+1}) - w^i(x^i). \tag{2.51}$$

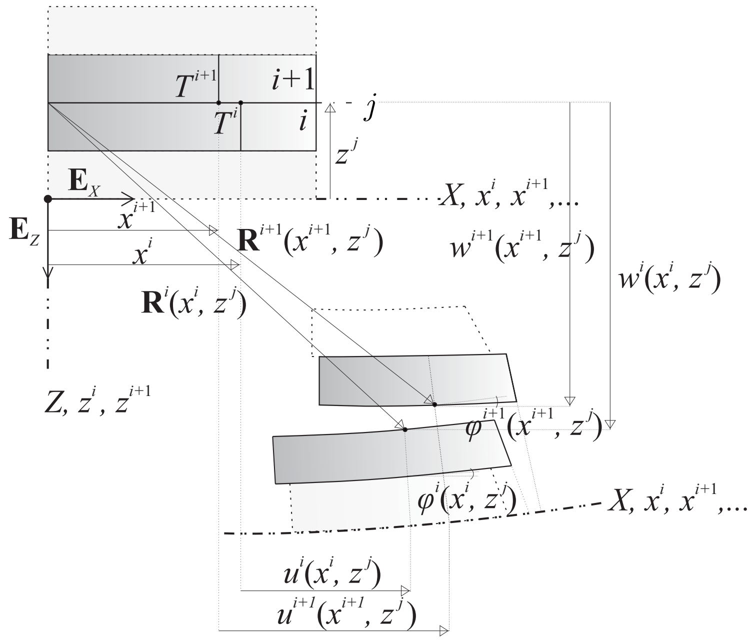

Figure 2.5: A schematic presentation of the geometry of the slip and full debonding between layers i and $i+1$ in interlayer contact j.
Slika 2.5: Shematski prikaz geometrije zdrsa in popolne razslojitve slojev i in $i+1$ v stiku j.

The kinematic aspect of the mechanical behaviour of the interlayer contact is described by Eq. (2.47). Like the material of the layers, the material of the interlayer contact can deform arbitrarily, e.g., elastic, plastic, hyperelastic, etc. The behaviour is defined by the constitutive law of the interlayer contact. This information, similar to the constitutive laws of the layers, is also determined by experimental tests. In general, the results of the tests are arbitrary constitutive functions $\mathcal{S}_{\mathrm{X}}^{j}$ and $\mathcal{S}_{\mathrm{Z}}^{j}$ in the material coordinates $\mathbf{e}_x$ and $\mathbf{e}_z$, respectively, $j = (1, 2, ..., N-1)$. Since delamination is neglected in this model, Eq. (2.44), only the constitutive law for the horizontal component of slip is defined:

$$p_{c,X}^{i,j}(x^i) = \mathcal{S}_{\mathrm{X}}^{j}\big(x^i, \Delta_X^j(x^i)\big), \tag{2.52}$$

where the $p_{c,X}^{i,j}(x^i)$ is the interlayer traction in the interlayer contact $j = (1, 2, ...N-1)$ to which layer $i = (1, 2, ...N)$ is subjected. The simplest form of the constitutive law applies to the linear-elastic interlayer contact, which we will use for our analytical model in the following chapters and is associated with a constant stiffness value $K_{\mathrm{X}}^{i,j}$, for the interlayer contact j:

$$p_{c,X}^{i,j}(x^i) = K_{\mathrm{X}}^{j}\,\Delta_X^j(x^i). \tag{2.53}$$

According to the third Newton law, the interconnected layers act on each other in equilibrium with forces of equal magnitude and opposite direction. The result is:

$$p_{c,X}^{i,j}(x^i) - p_{c,X}^{i+1,j}(x^{i+1}) = 0. \tag{2.54}$$

In case there is no interaction between the layers, there is of course no constitutive law and consequently no interlayer tractions.

2.2.1 Euler-Bernoulli laminated beam

The expressions in this section are obtained assuming that the shear deformations γ^i of the layers $i = (1, 2, ..., N)$ are neglected. This assumption is justified when shear stresses are not predominant, which is the case for slender beams where the height of the beam h is much smaller than the length of the beam L. This assumption implicitly defines the beam as an Euler-Bernoulli beam, where the original straight cross-section A of the beam remains straight and perpendicular to the reference axis after deformation. This provides room for further simplification of the basic equations of the laminated beam presented in the previous sections 2.1.1, 2.1.2, 2.1.3 and 2.1.4.

$$\gamma^i(x^i) = \gamma^{i+1}(x^{i+1}) = \gamma(x^i) = 0. \tag{2.55}$$

From the Eq. (2.44) and the assumption of small displacements, rotations and deformations it follows that the vertical displacements of all layers can be regarded as equal:

$$w^i(x^i) = w^{i+1}(x^{i+1}) = w(x^i). \tag{2.56}$$

Considering the Eqs. (2.55) and (2.56), we can further assume that also the rotations and pseudosurvatures φ^i and κ^i from Eqs. (2.12) and (2.13), respectively, are the same for all the layers i, where $i = (1, 2, ..., N)$ and N is the total number of layers:

$$\varphi^i(x^i) = \varphi^{i+1}(x^{i+1}) = \varphi(x^i), \tag{2.57}$$

$$\kappa^i(x^i) = \kappa^{i+1}(x^{i+1}) = \kappa(x^i). \tag{2.58}$$

Because of Eqs. (2.55) and (2.58) the equilibrium equations can also be simplified. The internal shear forces $Q^i(x^i)$ and bending moments $M^i(x^i)$ of individual layers i can now be represented by the total shear force $Q(x^i)$ and total bending moment $M(x^i)$ for all layers of the glued laminated beam.

$$Q(x^i) = \sum_{i=1}^{N} Q^i(x^i), \tag{2.59}$$

$$M(x^i) = \sum_{i=1}^{N} M^i(x^i), \tag{2.60}$$

With these simplifications, the kinematic and equilibrium and constitutive equations are modified. The boundary conditions are also reformulated taking into account the simplifications:
Kinematic equations:

$$\frac{du^i(x^i)}{dx^i} - \varepsilon^i(x^i) = 0, \tag{2.61}$$

$$\frac{dw(x^i)}{dx^i} + \varphi(x^i) = 0, \tag{2.62}$$

$$\frac{d\varphi(x^i)}{dx^i} - \kappa(x^i) = 0. \tag{2.63}$$

Equilibrium equations:

$$\frac{dN^i(x^i)}{dx^i} + p^i_X(x^i) + p^{i,j}_{c,X}(x^i) - p^{i,j-1}_{c,X}(x^i) = 0, \tag{2.64}$$

$$\frac{dQ(x^i)}{dx^i} + \sum_{i=1}^{N} p^i_Z(x^i) = 0, \tag{2.65}$$

$$\frac{dM(x^i)}{dx^i} - Q(x^i) + \sum_{i=1}^{N} m^i_Y(x^i) = 0. \tag{2.66}$$

Boundary conditions:

$x = 0:$

$$\begin{aligned} U^i_1 - u^i(0) &= 0 \quad \text{or} \quad S^i_1 + N^i(0) = 0, \\ U_2 - w(0) &= 0 \quad \text{or} \quad S_2 + Q(0) = 0, \\ U^i_3 - \varphi^i(0) &= 0 \quad \text{or} \quad S_3 + M_Y(0) = 0. \end{aligned} \tag{2.67}$$

$x = L:$

$$\begin{aligned} U^i_4 - u^i(L) &= 0 \quad \text{or} \quad S^i_4 - N^i(L) = 0, \\ U_5 - w(L) &= 0 \quad \text{or} \quad S_5 - Q(L) = 0, \\ U_6 - \varphi(L) &= 0 \quad \text{or} \quad S_6 - M_Y(L) = 0. \end{aligned} \tag{2.68}$$

2.2.2 Timoshenko-Ehrenfest laminated beam

The Timoshenko-Ehrenfest theory is the basic theory for planar beams that takes into account the shear deformation of the beam. This is important for short beams where the shear stresses are high. The influence of shear deformations on the mechanical behaviour of the composite beams with interlayer slips was shown by Schnabl (2007). In this dissertation, some illustrative examples will be shown where shear deformation is considered. However, we assume that the layer of the beam deform uniformly in the transverse direction, so that the vertical displacements, the rotations of the finger joints, the pseudocurvatures and consequently the shear deformations are identical for all layers:

$$\gamma^i(x^i) = \gamma^{i+1}(x^{i+1}) = \gamma(x^i) \neq 0, \tag{2.69}$$

$$w^i(x^i) = w^{i+1}(x^{i+1}) = w(x^i), \tag{2.70}$$

$$\varphi^i(x^i) = \varphi^{i+1}(x^{i+1}) = \varphi(x^i), \tag{2.71}$$

$$\kappa^i(x^i) = \kappa^{i+1}(x^{i+1}) = \kappa(x^i). \tag{2.72}$$

Kinematic equations:

$$\frac{du^i(x^i)}{dx^i} - \varepsilon^i(x^i) = 0, \tag{2.73}$$

$$\frac{dw(x^i)}{dx^i} + \varphi(x^i) - \gamma(x^i) = 0, \tag{2.74}$$

$$\frac{d\varphi(x^i)}{dx^i} - \kappa(x^i) = 0. \tag{2.75}$$

All the equilibrium equations, Eqs. (2.26) – (2.28) remain unchanged.

2.2.3 Finger joints

The analytical model is based on the system of equations presented in the previous sections. The equations define the mechanical behaviour of the layers connected in the transverse direction, but the finger joint is used to connect the parts of the layers in the longitudinal direction. The finger joint has not yet been implemented in the model and is defined here. The planar beams are usually subjected to vertical loading, which causes bending moments in the beams. The distribution of stresses across the cross-section is such that the top edge is in compression and the bottom edge is in tension. Experimental tests of glued laminated beams made of wood have shown that the finger joints, which are located in the areas of highest tension stresses, are usually the weak points and therefore determine the final load bearing capacity of the glued laminated beams. For this reason, the influence of the finger joints is included in the model only in the axial direction. Since the length of the finger joints is small compared to the length of the laminations, it is reasonable to consider them as a concentrated influence in a planar model of the beam, as shown in Fig. 2.6, where the beam consists of only two layers for transparency. It is assumed that the finger joint is located in layer a, where $a = (1, 2, ..., N)$ and layer b has no finger joints and it holds that $b = (1, 2, ..., N)$.

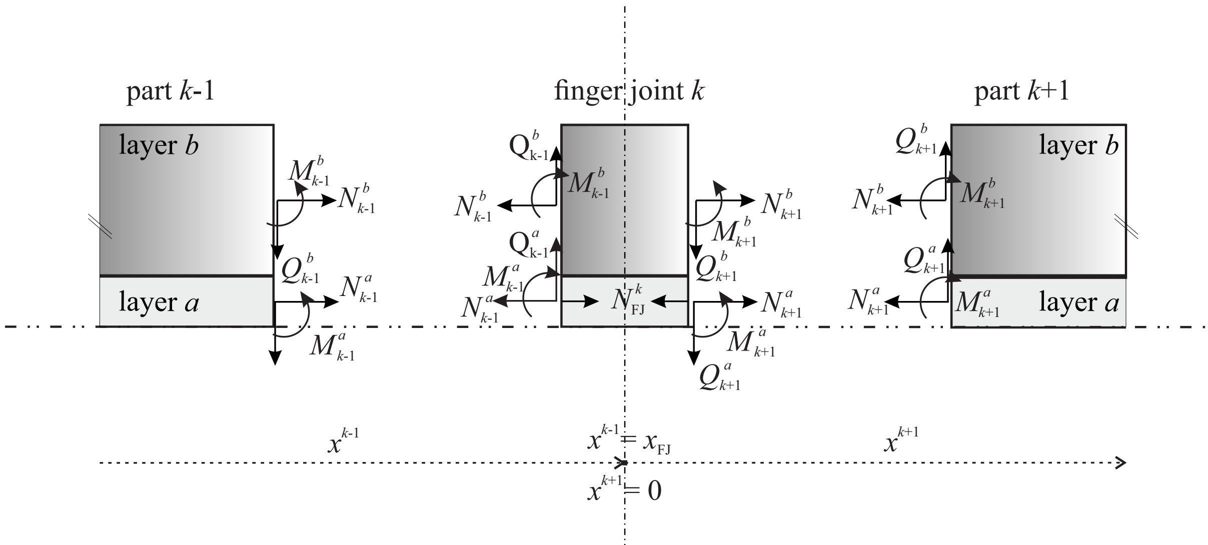

Figure 2.6: The influence of finger joint k in layer a.
Slika 2.6: Vpliv zobatega spoja k v sloju a.

In Section 2.1.2, the equilibrium of the laminated beam was presented and it was found that the concentrated load is introduced into the model only at the edges of the layers of the beam, i.e., at $x = 0$ and/or

$x = L$. The finger joint k is implemented into the model as a concentrated force N^k_{FJ}, as it is presented in Fig. 2.6. In general, the mechanical behaviour of the finger joint can be determined using its constitutive model. This is an arbitrary function $\mathcal{K}^k_{\mathrm{FJ}}$ that defines the relationship between the axial stress and the axial deformation in the finger joint. Since it is a concentrated, point load, the constitutive function defines the relation between the axial force in the finger joint N^k_{FJ} and displacement in the finger joint Δ^k_{FJ}, Eq. (2.76). If the finger joint is considered as linear elastic material, the function $\mathcal{K}^k_{\mathrm{FJ}}$ is further simplified and has a constant value K^k_{FJ}

$$N^k_{\mathrm{FJ}} = K^k_{\mathrm{FJ}}\,\Delta^k_{\mathrm{FJ}}. \tag{2.76}$$

$$\Delta^k_{\mathrm{FJ}} = N^k_{\mathrm{FJ}}/K^k_{\mathrm{FJ}}. \tag{2.77}$$

With this definition, the finger joint k automatically divides the model into two parts: part $k-1$ on the left side and $k+1$ on the right side of the finger joint. The basic equations for the layers of the two parts remain unchanged, but at $x^{k-1} = x_{\mathrm{FJ}}$ the continuous kinematic and equilibrium field must be maintained. At this point the continuity conditions are defined:

$$-N^a_{k-1}(x_{\mathrm{FJ}}) + N^a_{k+1}(0) = 0, \tag{2.78}$$
$$-N^b_{k-1}(x_{\mathrm{FJ}}) + N^b_{k+1}(0) = 0, \tag{2.79}$$
$$-Q^a_{k-1}(x_{\mathrm{FJ}}) + Q^a_{k+1}(0) = 0, \tag{2.80}$$
$$-Q^b_{k-1}(x_{\mathrm{FJ}}) + Q^b_{k+1}(0) = 0, \tag{2.81}$$
$$-M^a_{k-1}(x_{\mathrm{FJ}}) + M^a_{k+1}(0) = 0, \tag{2.82}$$
$$-M^b_{k-1}(x_{\mathrm{FJ}}) + M^b_{k+1}(0) = 0, \tag{2.83}$$

$$u^a_{k-1}(x_{\mathrm{FJ}}) - u^a_{k+1}(0) - \Delta^k_{\mathrm{FJ}} = 0, \tag{2.84}$$
$$u^b_{k-1}(x_{\mathrm{FJ}}) - u^b_{k+1}(0) = 0, \tag{2.85}$$
$$w^a_{k-1}(x_{\mathrm{FJ}}) - w^a_{k+1}(0) = 0, \tag{2.86}$$
$$w^b_{k-1}(x_{\mathrm{FJ}}) - w^b_{k+1}(0) = 0, \tag{2.87}$$
$$\varphi^a_{k-1}(x_{\mathrm{FJ}}) - \varphi^a_{k+1}(0) = 0, \tag{2.88}$$
$$\varphi^b_{k-1}(x_{\mathrm{FJ}}) - \varphi^b_{k+1}(0) = 0, \tag{2.89}$$

where $a = (1, 2, ..., N)$ and $b = (1, 2, ..., N)$.

2.3 Analytical solution of laminated beam with finger joints

The derivation of the analytical solution presented in this dissertation is done under the assumptions that simplify the model. The main assumptions have been mentioned earlier in the text. However, some additional assumptions are introduced here. For clarity, we have summarised them in a more compact form:

1. the layers are prismatic, homogeneous and linearly elastic;

2. the contact between the layers is linear elastic;
3. a linearized planar Reissner beam theory (Reissner, 1972) is used for the layers;
4. the contact area between the layers has negligible thickness and finite stiffness and only relative sliding of the layers is allowed. If the fully debonded segment exists, delamination of the layers is also allowed;
5. the cross-sections of the layers' are symmetrical about the z axis, and do not change their shape and size during deformation;
6. no type of instability (local or global) can occur;
7. all displacements and deformations are small;
8. the generalized interlayer slips are small;
9. the finger joints are modelled as linear springs i.e. as linear elastic material.

The algorithm is based on the fact that there is only one general unknown of the problem. Although the system of algebraic and differential equations has $6 \times N$ basic unknowns ($u^i(x^i)$, $w^i(x^i)$, $\varphi^i(x^i)$, $N^i(x^i)$, $Q^i(x^i)$, $M^i(x^i)$), it turns out that they can all be expressed from a single unknown, namely the interlayer slip $\Delta_X^j(x^i)$. The derivation of the analytical solution has already been presented by Schnabl (2007).

In the first step, the interlayer slip $\Delta_X^j(x^i)$ is differentiated twice with respect to x^i. If Eqs. (2.57) and (2.58) are considered in Eq. (2.47), one can see that $\varphi^{i+1} - \varphi^i = 0$. Thus, a new expression for $\Delta_X^j(x^i)$ is obtained:

$$\Delta_X^j(x^i) = u^{i+1}(x^i) - u^i(x^i) \tag{2.90}$$

and the second derivative of the interlayer slip is

$$\frac{d^2\Delta_X^j(x^i)}{dx^{i2}} = \frac{d\varepsilon^{i+1}(x^i)}{dx^i} - \frac{d\varepsilon^i(x^i)}{dx^i}, \tag{2.91}$$

where $i = (1, 2, ..., N)$ and $j = (1, 2, ..., N-1)$. The analytical solution depends on the assumption whether the shear deformation is considered in the model or not, therefore it is presented separately for the two options.

2.3.1 Solution for the Euler-Bernoulli laminated beam without shear deformation

The specific longitudinal deformations ε^i and the pseudocurvature κ are obtained from the constitutive equations defined in section 2.2. Taking into account all simplifications, the constitutive equations can be written in matrix form, leading to the following results:

$$\left\{\begin{matrix} \dfrac{N^i(x^i)}{dx^i} \\ \dfrac{M(x^i)}{dx^i} \end{matrix}\right\} = \mathbf{C} \left\{\begin{matrix} \dfrac{d\varepsilon^i(x^i)}{dx^i} \\ \dfrac{\kappa(x^i)}{dx^i} \end{matrix}\right\}. \tag{2.92}$$

With inverting the system:

$$\begin{Bmatrix} \dfrac{d\varepsilon^i(x^i)}{dx^i} \\ \dfrac{\kappa^i(x^i)}{dx^i} \end{Bmatrix} = \mathbf{C}^{-1} \begin{Bmatrix} \dfrac{N^i(x^i)}{dx^i} \\ \dfrac{M(x^i)}{dx^i} \end{Bmatrix}, \tag{2.93}$$

where $i = (1, 2, ..., N)$ and $\mathbf{C}$ is the matrix of constitutive constants and $\mathbf{C}^{-1}$ its inverse:

$$\mathbf{C}^{-1} = \begin{bmatrix} D_{11} & D_{12} & ... & D_{1,N+1} \\ D_{21} & D_{22} & ... & D_{2,N+1} \\ \vdots & \vdots & \ddots & \vdots \\ D_{N+1,1} & D_{N+1,2} & ... & D_{N+1,N+1} \end{bmatrix}. \tag{2.94}$$

The next step is to integrate the equilibrium equations fro 0 to x^i

$$N^i(x^i) = N^i(0) - \int_0^{x^i} \left(p_X^i(\eta) + p_{c,X}^i(\eta) \right) d\eta, \tag{2.95}$$

$$Q(x^i) = Q(0) - \sum_{i=1}^{N} \int_0^{x^i} p_Z^i(\eta) d\eta, \tag{2.96}$$

$$M(x^i) = M(0) + \int_0^{x^i} \left(Q(\eta) - \sum_{i=1}^{N} m_Y^i(\eta) \right) d\eta. \tag{2.97}$$

and insert them into Eq. (2.91). The next step is to differentiate the expression in Eq. (2.90) with respect to x^i and express the result as a third order, linear ordinary differential equation, Eq. (2.98). For the derivation with respect to x^i the notation $(\cdot)'$ is used.

$$\Delta_X^{j\,'''} + A\Delta_X^{j\,'} - B\Delta_X^{j-1'} + C\Delta_X^{j+1'} + F = 0 \tag{2.98}$$

where A, B, and C are constants of the geometric and material parameters. F consists is the external load and depends in general on x^i. The quantities are defined as:

$$A = (D_{i+1,i} - D_{i,i} - D_{i+1,i+1} + D_{i,i+1})\, K_{\mathrm{X}}^{j}, \tag{2.99}$$

$$B = (D_{i+1,i} - D_{i,i})\, K_{\mathrm{X}}^{j-1}, \tag{2.100}$$

$$C = (D_{i+1,i+1} - D_{i,i+1})\, K_{\mathrm{X}}^{j+1} \tag{2.101}$$

and

$$\begin{aligned} F = {} & p_X^i\,(D_{i+1,i} - D_{i,i}) + p_X^{i+1}\,(D_{i+1,i+1} - D_{i,i+1}) + \\ & + \left(\sum_{i=1}^{N} p_Z^i - \sum_{i=1}^{N} m_Y^{i\,'} \right) (D_{i+1,N+1} - D_{i,N+1}). \end{aligned} \tag{2.102}$$

The system of linear differential equations Eq. (2.98) can be uniquely determined only if the boundary conditions for the interlayer slip $\Delta_X^j(x^i = 0)$ and $\Delta_X^j(x^i = L)$ are given, where $i = (1, 2, ..., N)$ and $j = (1, 2, ..., N-1)$. The system of equations defined by Eq. (2.98) was solved using Wolfram MATHEMATICA (Wolfram Research). Once the interlayer slips $\Delta_X^j(x^i)$ are known, the analytic expressions for all other unknown functions can be determined from the system of algebraic equations:

$$\mathbf{K}\,\mathbf{U_0} = \mathbf{f}, \tag{2.103}$$

where $\mathbf{U}_0$ is the vector of constant values of the unknown equilibrium functions evaluated at the endpoints of layers i, $\mathbf{K}$ is the tangent stiffness matrix of the model, and $\mathbf{f}$ is the load vector. With the presented method the unknown functions $\varepsilon^i(x^i)$, $\kappa(x^i)$, $u^i(x^i)$, $w(x^i)$, $\varphi(x^i)$, $N^i(x^i)$, $Q(x^i)$, $M(x^i)$ can be evaluated. The explicit expressions for all unknown functions can be found in (Fortuna et al., 2021) for the two-layer Euler-Bernoulli beam with two finger joints and full debonded segment. The shear force $Q^i(x^i)$ and the bending moment $M^i(x^i)$ of individual layer i are determined by the constitutive equations, Eqs. (2.35) – (2.37).

2.3.2 Solution for the Timoshenko-Ehrenfest laminated beam with shear deformation

In this dissertation, the analytical solution for laminated beams with shear deformation is presented under the assumption that all layers i have the same shear deformation, see Eq. (2.55). This leads to a solution that is similar to the one where shear was not considered at all. The matrix form of the inverted constitutive equations (2.104) has one additional member, as does the inverted constitutive matrix in Eq. (2.105).

$$\begin{Bmatrix} \dfrac{d\varepsilon^i(x^i)}{dx^i} \\ \dfrac{d\kappa(x^i)}{dx^i} \\ \dfrac{d\gamma(x^i)}{dx^i} \end{Bmatrix} = \mathbf{C}^{-1} \begin{Bmatrix} \dfrac{N^i(x^i)}{dx^i} \\ \dfrac{M(x^i)}{dx^i} \\ \dfrac{Q(x^i)}{dx^i} \end{Bmatrix}, \tag{2.104}$$

where $i = (1, 2, ..., N)$ and now the inverted matrix of constitutive constants, $\mathbf{C}^{-1}$, takes the form:

$$\mathbf{C}^{-1} = \begin{bmatrix} D_{i,i} & D_{i,i+1} & \dots & D_{i,N+1} & D_{i,N+2} \\ D_{i+1,i} & D_{i+1,i+1} & \dots & D_{i+1,N+1} & D_{i+1,N+2} \\ \vdots & \vdots & \ddots & \vdots & \\ D_{N+1,i} & D_{N+1,i+1} & \dots & D_{N+1,N+1} & D_{N+1,N+2} \\ D_{N+2,i} & D_{N+2,i+1} & \dots & D_{N+2,N+1} & D_{N+2,N+2} \end{bmatrix}. \tag{2.105}$$

The system of third-order equation remains the same as before, Eq. (2.98), but the parameter F is determined differently:

$$\begin{aligned} F = {} & p_X^i \left(D_{i+1,i} - D_{i,i}\right) + p_X^{i+1} \left(D_{i+1,i+1} - D_{i,i+1}\right) + \\ & + \left(\sum_{i=1}^{N} (p_Z^i - m_Y^{i\,\prime})\right) \left(D_{i+1,N+1} - D_{i,N+1}\right) + \sum_{i=1}^{N} p_Z^{i\,\prime\prime} \left(D_{i+2,N+2} - D_{i,N+2}\right). \end{aligned} \tag{2.106}$$

As can be seen, Eq. (2.106) is extended by the part that leads to the second derivative of the vertical load $p_Z^{i\,\prime\prime}$. If the load is uniformly distributed along the length of the beam, this part is equal to 0.

Otherwise, the algorithm remains the same as for the case of the laminated beam without shear deformation. However, the kinematic quantities must be evaluated using the Eqs. (2.73) — (2.75). The analytical solution for the Timoshenko-Ehrenfest laminated beam, where the shear deformation γ^i is not the same for all layers $i = (1, 2, ..., N)$, can be found in (Schnabl, 2007).

2.4 Numerical solution of laminated beam with finger joints

2.4.1 Modified principle of virtual work

The basic equations presented in Section 2.1 are very complex to solve in general form, and the analytical solution is possible only if the model is somewhat simplified with a limited number of lamination and a limited number of finger joints. The system of equations can be solved numerically using the finite element method. For our numerical model, we used the finite elements based on the approximation of strains, first introduced by Planinc (1998). The finite element formulation is based on the principle of virtual work. The following finite element derivation is based on the work of Planinc (1998) and also by Čas et al. (2004); Schnabl (2007) and Kroflič (2012), modifying the application for multilayer composite beams. The basic formulation of the principle of virtual work essentially defines that the work of the internal forces is equal to the work of the external loading to achieve infinitesimally small virtual deformations and displacements (Washizu, 1994; Saje et al., 1997; Planinc, 1998). When the glued laminated beam consists of multiple laminations, the principle of virtual work of the beam is equal to the sum of the principles of virtual work for all the laminations:

$$\begin{aligned}\delta W = \sum_{i=1}^{N} \delta W = \sum_{i=1}^{N} \Big(& \int_0^L N^i \delta\varepsilon^i dx + \int_0^L Q^i \delta\gamma^i dx + \int_0^L M^i \delta\kappa^i dx - \\ & - \int_0^L (p_X^i + p_{c,X}^i)\delta u^i - \int_0^L (p_Z^i + p_{c,Z}^i)\delta w^i - \\ & - \int_0^L (m_Y^i + m_{c,Y}^i)\delta\varphi^i - \sum_{k=1}^{6} S_k^i\, \delta U_k^i \Big)\end{aligned} \tag{2.107}$$

The quantities δu^i, δw^i, and $\delta\varphi^i$ are virtual perturbations of the horizontal and vertical displacements and rotations of the reference axis x^i, and $\delta\varepsilon^i$, $\delta\gamma^i$, and $\delta\kappa^i$ are virtual perturbations of the axial and shear deformations and curvature of the lamination i. The S_k^j are generalized nodal loads and δU_k^j are virtual perturbations of generalized nodal kinematic quantities:

$$\begin{aligned} \delta U_1^i &= \delta u^i(0), & \delta U_4^i &= \delta u^i(L), \\ \delta U_2^i &= \delta w^i(0), & \delta U_5^i &= \delta w^i(L), \\ \delta U_3^i &= \delta\varphi^i(0), & \delta U_6^i &= \delta\varphi^i(L). \end{aligned} \tag{2.108}$$

Since it is assumed that the constitutive equations, Eqs. (2.29) – (2.31), are identically satisfied, the equilibrium forces and bending moments can be replaced by constitutive forces and bending moments.

$$\begin{aligned}\delta W = \sum_{i=1}^{N} \delta W = \sum_{i=1}^{N} \Big(& \int_0^L N_C^i \delta\varepsilon^i dx + \int_0^L Q_C^i \delta\gamma^i dx + \int_0^L M_C^i \delta\kappa^i dx - \\ & - \int_0^L (p_X^i + p_{c,X}^i)\delta u^i - \int_0^L (p_Z^i + p_{c,Z}^i)\delta w^i - \\ & - \int_0^L (m_Y^i + m_{c,Y}^i)\delta\varphi^i - \sum_{k=1}^{6} S_k^i\, \delta U_k^i \Big)\end{aligned} \tag{2.109}$$

According to the kinematic equations, Eqs. (2.11) – (2.13), there are only three independent variables between u^i, w^i, φ^i, ε^i, γ, and κ^i. It has been shown that the finite element formulation using the kinematic quantities u^i, w^i, φ^i can exhibit locking problem and is not as robust as the formulation using the deformation variables ε^i, γ, and κ^i as unknowns. For this reason, the finite element formulation used is referred to as the locking free strain-based finite element formulation (Planinc, 1998). The problem is considered as a constrained variational calculus problem and the kinematic equations are the constraints. To introduce them into the principle of virtual work in Eq. (2.109), the kinematic equations, Eqs. (2.11)–(2.13), are multiplied by the Lagrangian multipliers R_1^i, R_2^i and R_3^i. The multipliers can be chosen arbitrarily, but must be differentiable, i.e., continuous on $x^i \in [0, L^i]$. The products are then integrated over the length of the element L. As we proceed, the expressions are varied with respect to the unknowns u^i, w^i, φ^i, ε^i, γ^i, κ^i, R_1^i, R_2^i, R_3^i. We thus obtain:

$$\delta E_1 = \sum_{i=1}^{N} \int_0^L \Big((u^{i\prime} - \varepsilon^i)\, \delta R_1^i + (\delta u^{i\prime} - \delta \varepsilon^i)\, R_1^i \Big) dx, \tag{2.110}$$

$$\delta E_2 = \sum_{i=1}^{N} \int_0^L \Big((w^{i\prime} + \varphi^i - \gamma^i)\, \delta R_2^i + (\delta w^{i\prime} + \delta\varphi^i - \delta \gamma^i)\, R_2^i \Big) dx, \tag{2.111}$$

$$\delta E_3 = \sum_{i=1}^{N} \int_0^L \Big((\varphi^{i\prime} - \kappa^i)\, \delta R_3^i + (\delta \varphi^{i\prime} - \delta \kappa^i) \Big) dx. \tag{2.112}$$

When the Eqs. (2.110) – (2.112) are added to the principle of virtual work in Eq. (2.109), the expression for the modified principal of virtual work $\delta W^\star$ is obtained. After rearranging it is written as follows:

$$\begin{aligned}
\delta W^\star &= \delta W + \delta E_1 + \delta E_2 + \delta E_3 = \\
&= \sum_{i=1}^{N} \Big\{ \int_0^L \Big((N_C^i - R_1^i)\, \delta\varepsilon^i + (Q_C^i - R_2^i)\, \delta\gamma^i + (M_C^i - R_3^i)\, \kappa^i \Big) dx - \\
&- \int_0^L \Big((p_X^i + p_{c,X}^i + R_1^{i\prime})\, \delta u^i + (p_Z^i + p_{c,Z}^i + R_2^{i\prime})\, \delta w^i \Big)\, dx - \\
&- \int_0^L \Big(m_Y^i + m_{c,Y}^i - R_2^i + R_3^{i\prime})\, \delta\varphi^i \Big) dx + \\
&+ \int_0^L \Big((u^{i\prime} - \varepsilon^i)\, \delta R_1^i + (w^{i\prime} + \varphi^i - \gamma^i)\, \delta R_2^i + (\varphi^{i\prime} - \kappa^i)\, \delta R_3^i \Big) dx - \\
&- (R_1^i(0) + S_1^i)\, \delta u^i(0) - (R_2^i(0) + S_2^i)\, \delta w^i(0) - (R_3^i(0) + S_3^i)\, \delta\varphi^i(0) + \\
&+ (R_1^i(L) - S_4^i)\, \delta u^i(L) + (R_2^i(L) - S_5^i)\, \delta w^i(L) + (R_3^i(L) - S_6^i)\, \delta\varphi^i(L) \Big\} = 0
\end{aligned} \tag{2.113}$$

The variations $\delta\varepsilon^i$, $\delta\gamma^i$, $\delta\kappa^i$, δu^i, δw^i, $\delta\varphi^i$, δR_1^i, δR_2^i, and δR_3^i are arbitrary functions of x^i. The coefficients $\delta u^i(0)$, $\delta w^i(0)$, $\delta\varphi^i(0)$, $\delta u^i(L)$, $\delta w^i(L)$, and $\delta\varphi^i(L)$ are also arbitrary independent discrete values of the displacements and rotations at the edges of the element. Using the calculus of variations, for Eq. (2.113) to be identically satisfied, the coefficients of any arbitrary independent variations must equal 0. Thus, the Euler-Lagrange equations of the laminated beam are obtained. For $i = (1, 2, ...N), j = (1, 2, ...N-1), x \in [0, L]$:

Constitutive equations

$$f_i = N_C^i - R_1^i = 0, \tag{2.114}$$
$$f_{N+i} = Q_C^i - R_2^i = 0, \tag{2.115}$$
$$f_{2N+i} = M_C^i - R_3^i = 0. \tag{2.116}$$

Kinematic equations

$$f_{3N+i} = u^{i\prime} - \varepsilon^i = 0, \tag{2.117}$$
$$f_{4N+i} = w^{i\prime} + \varphi^i - \gamma^i = 0, \tag{2.118}$$
$$f_{5N+i} = \varphi^{i\prime} - \kappa^i = 0. \tag{2.119}$$

Equilibrium equations

$$f_{6N+i} = R_1^{i\prime} + p_X^i + p_{c,X}^i = 0, \tag{2.120}$$
$$f_{7N+i} = R_2^{i\prime} + p_Z^i + p_{c,Z}^i = 0, \tag{2.121}$$
$$f_{8N+i} = R_3^{i\prime} - R_2^i + m_Y^i + m_{c,Y}^i = 0. \tag{2.122}$$

Kinematic and equilibrium boundary conditions
$x = 0:$

$$\begin{aligned} U_1^i - u^i(0) = 0 \quad &\text{or} \quad S_1^i + R_1^i(0) = 0, \\ U_2^i - w^i(0) = 0 \quad &\text{or} \quad S_2^i + R_2^i(0) = 0, \\ U_3^i - \varphi^i(0) = 0 \quad &\text{or} \quad S_3^i + R_3^i(0) = 0. \end{aligned} \tag{2.123}$$

$x = L:$

$$\begin{aligned} U_4^i - u^i(L) = 0 \quad &\text{or} \quad S_4^i - R_1^i(L) = 0, \\ U_5^i - w^i(L) = 0 \quad &\text{or} \quad S_5^i - R_2^i(L) = 0, \\ U_6^i - \varphi^i(L) = 0 \quad &\text{or} \quad S_6^i - R_3^i(L) = 0. \end{aligned} \tag{2.124}$$

Beside the Euler-Lagrange equations, Eqs. (2.114) – (2.124), the additional equations must be stated, which define the interaction between the laminations:

$$\Delta_X^j = u^{i+1} - u^i + z^j\left(\varphi^{i+1} - \varphi^i\right), \tag{2.125}$$
$$\Delta_Z^j = w^i - w^{i+1} = 0, \tag{2.126}$$
$$p_{c,X}^{i,j}(x) = K_{\mathrm{X}}^j \Delta_X^j, \tag{2.127}$$

for $x \in [0, L]$.

2.4.1.1 Euler-Lagrange equations of the Timoshenko-Ehrenfest laminated beam

As for the analytical model for the Timoshenko-Ehrenfest laminated beam, similar assumptions are considered for the numerical model:

$$w^i = w^{i+1} = w, \tag{2.128}$$

$$\gamma^i = \gamma^{i+1} = \gamma, \tag{2.129}$$

$$\varphi^i = \varphi^{i+1} = \varphi, \tag{2.130}$$

$$\kappa^i = \kappa^{i+1} = \kappa. \tag{2.131}$$

With these assumptions, the expression for modified principle of virtual work $\delta W^\star$ in Eq. (2.113) is simplified. Considering Eqs. (2.59),(2.60), and (2.54) the system of Euler-Lagrange equations can be rewritten as follows:
For $i = j = (1, 2, ...N)$, $x \in [0, L]$:
Constitutive equations

$$f_i = N_C^i - R_1^i = 0, \tag{2.132}$$

$$f_{N+1} = Q_C - R_2 = 0, \tag{2.133}$$

$$f_{N+2} = M_C - R_3 = 0. \tag{2.134}$$

Kinematic equations

$$f_{N+2+i} = u^{i\prime} - \varepsilon^i = 0, \tag{2.135}$$

$$f_{2N+3} = w' + \varphi - \gamma = 0, \tag{2.136}$$

$$f_{2N+4} = \varphi' - \kappa = 0. \tag{2.137}$$

Equilibrium equations

$$f_{2N+4+i} = R_1^{i\prime} + p_X^i + p_{c,X}^i = 0, \tag{2.138}$$

$$f_{3N+5} = R_2{}' + \sum_{i=1}^{N} p_Z^i = 0, \tag{2.139}$$

$$f_{3N+6} = R_3{}' - R_2 + \sum_{i=1}^{N} m_Y^i = 0. \tag{2.140}$$

Kinematic and equilibrium boundary conditions
$x = 0:$

$$\begin{aligned} U_1^i - u^i(0) &= 0 \quad \text{or} \quad S_1^i + R_1^i(0) = 0, \\ U_2 - w(0) &= 0 \quad \text{or} \quad S_2 + R_2(0) = 0, \\ U_3 - \varphi(0) &= 0 \quad \text{or} \quad S_3 + R_3(0) = 0. \end{aligned} \tag{2.141}$$

$x = L:$

$$\begin{aligned} U_4^i - u^i(L) &= 0 \quad \text{or} \quad S_4^i - R_1^i(L) = 0, \\ U_5 - w(L) &= 0 \quad \text{or} \quad S_5 - R_2(L) = 0, \\ U_6 - \varphi(L) &= 0 \quad \text{or} \quad S_6 - R_3(L) = 0. \end{aligned} \tag{2.142}$$

Beside the Euler-Lagrange equations, Eqs. (2.132) – (2.142), the additional, constraining equations must be defined:

$$\Delta_X^j = u^{i+1} - u^i, \tag{2.143}$$
$$\Delta_Z^j = w^{i+1} - w^i = 0, \tag{2.144}$$
$$p_{c,X}^{i,j}(x) = K_{\mathrm{X}}^{i,j}\Delta_X^j, \tag{2.145}$$

where $i = (1, 2, ...N)$, $j = (1, 2, ..., N-1)$ and $x \in [0, L]$. The kinematic equations, Eqs. (2.135)–(2.135), can be integrated over the length of the element $x \in [0, L]$, so the kinematic unknowns u^i, w, and φ are expressed by strain quantities:

$$u^i(L) = u^i(0) + \int_0^L \varepsilon^i \, dx, \tag{2.146}$$
$$w(L) = w(0) + \int_0^L (\gamma - \varphi) \, dx, \tag{2.147}$$
$$\varphi(L) = \varphi(0) + \int_0^L \kappa \, dx \tag{2.148}$$

The equilibrium quantities are also integrated over the length of the element $x \in [0, L]$ and thus defined with known boundary forces:

$$R_1^i(L) - R_1^i(0) + \int_0^L (p_X^i + p_{c,X}^{i,j} - p_{c,X}^{i,j-1})dx = 0, \tag{2.149}$$
$$R_2(L) - R_2(0) + \int_0^L \sum_{i=1}^N p_Z^i dx = 0, \tag{2.150}$$
$$R_3(L) - R_3(0) - \int_0^L (R_2 - \sum_{i=1}^N m_Y^i)dx = \tag{2.151}$$

With Eqs. (2.149) – (2.151), the elements of Eq. (2.113) associated with the variations of the displacements δu^i, δw^i, and the rotation of the cross-section $\delta\varphi^i$ are identically satisfied. This formulation express the modified principle of virtual work with only $N + 2$ unknown functions $\varepsilon^i(x)$, $\gamma(x)$, and $\kappa(x)$. All other variables are now represented only by the boundary values $R_1^i(0)$, $R_2(0)$, $R_3(0)$, $R_1^i(L)$, $R_2(L)$, and $R_3(L)$, which are known and defined by the position of the element in the glued laminated beam. The final form of the modified principle of virtual work δW^{**} for a laminated Timoshenko-Ehrenfest beam with interlayer slips is now as follows:

$$\begin{aligned}
\delta W^{**} = \sum_{i=1}^N \Bigg\{ & \int_0^L \Big((N_C^i - R_1^i)\,\delta\varepsilon^i + (Q_C - R_2)\,\delta\gamma + (M_C - R_3)\,\delta\kappa \Big) dx + \\
& + \Big(u^i(L) - u^i(0) - \int_0^L \varepsilon^i dx \Big)\,\delta R_1^i + \Big(w(L) - w(0) - \int_0^L (\gamma - \varphi) dx \Big)\,\delta R_2 + \\
& + \Big(\varphi(L) - \varphi(0) - \int_0^L \kappa dx \Big)\,\delta R_3 - \\
& - \big(R_1^i(0) + S_1^i\big)\,\delta u^i(0) - \big(R_2(0) + S_2\big)\,\delta w(0) - \big(R_3(0) + S_3\big)\,\delta\varphi(0) \Bigg\} + \\
& + \big(R_1^i(L) - S_4^i\big)\,\delta u^i(L) + \big(R_2(L) - S_5\big)\,\delta w(L) + \big(R_3(L) - S_6\big)\,\delta\varphi(L) = 0.
\end{aligned} \tag{2.152}$$

2.4.2 Discretization of Euler-Lagrange equations of laminated Timoshenko-Ehrenfest beam

The basic equations are nonlinear and in general form cannot be solved uniquely, so we must use an inexact method with approximation of the unknowns. The Petrov-Galerkin method is used to translate the complex continuous functions into smaller discrete functions that are easier to solve. At this point, it is important to note that the same assumptions in Eqs. (2.128) – (2.131) are used as in the derivation of the initial Euler-Lagrange equations for the Timoshenko-Ehrenfest beam.

The element is divided into $N^* - 1$ smaller sections with N^* nodes, where $*$ stands for ε, γ, and κ. In general, the number of nodes need not be equal, so $N^{\varepsilon,i} \neq N^{\gamma,i} \neq N^{\kappa,i}$. We assume that all laminations have the same number of nodes, i.e., $N^{\varepsilon,i} = N^{\varepsilon,i+1} = N^{\varepsilon}$, $N^{\gamma,i} = N^{\gamma,i+1} = N^{\gamma}$, and $N^{\kappa,i} = N^{\kappa,i+1} = N^{\kappa}$. Lagrange polynomial interpolation is used to approximate the unknown functions $\varepsilon^i(x)$, $\gamma(x)$, and $\kappa(x)$. The number of nodes N^* along the length of the element L defines the degree of the Lagrange interpolation polynomials $L_n(x)$ for functions $\varepsilon^i(x)$, $\gamma(x)$ and $\kappa(x)$. The interpolation takes the form:

$$\varepsilon^i(x) \approx \sum_{n=1}^{N^{\varepsilon}} L_n(x)\, \varepsilon_n^i, \tag{2.153}$$

$$\gamma(x) \approx \sum_{n=1}^{N^{\gamma}} L_n(x)\, \gamma_n, \tag{2.154}$$

$$\kappa(x) \approx \sum_{n=1}^{N^{\kappa}} L_n(x)\, \kappa_n, \tag{2.155}$$

where the ε_n^i, γ_n, and κ_n are the discrete values of the axial, transverse and rotational strains determined at the nodes of the element. In a similar way, the variations of the strain quantities $\delta\varepsilon^i$, $\delta\gamma$, and $\delta\kappa$ are interpolated, see Eqs. (2.156) – (2.158), using the discrete nodal values $\delta\varepsilon_n^i$, $\delta\gamma_n$, and $\delta\kappa_n$. The collocation points for the variation are chosen to coincide with the nodal points.

$$\delta\varepsilon^i(x) \approx \sum_{n=1}^{N^{\varepsilon}} L_n(x)\, \delta\varepsilon_n^i, \tag{2.156}$$

$$\delta\gamma(x) \approx \sum_{n=1}^{N^{\gamma}} L_n(x)\, \delta\gamma_n, \tag{2.157}$$

$$\delta\kappa(x) \approx \sum_{n=1}^{N^{\kappa}} L_n(x)\, \delta\kappa_n. \tag{2.158}$$

The interpolations in Eqs. (2.153) – (2.158) are now introduced into the functional in Eq. (2.152). The fundamental lemma of the calculus of variation states that all coefficients associated with the independent variations in the functional must equal 0. In this way, the system of discrete generalized equilibrium equations of the laminated beam is obtained as follows:

$$f_{(i-1)N^{\varepsilon}+n} = \int_0^L (N_C^i - R_1^i)\, L_n(\xi)\, d\xi = 0; \qquad n = (1, 2, ..., N^{\varepsilon}), \tag{2.159}$$

$$f_{N \cdot N^{\varepsilon}+n} = \int_0^L (Q_C - R_2)\, L_n(\xi)\, d\xi = 0; \qquad n = (1, 2, ..., N^{\gamma}), \tag{2.160}$$

$$f_{N \cdot N^{\varepsilon}+N^{\gamma}+n} = \int_0^L (M_C - R_3)\, L_n(\xi)\, d\xi = 0; \qquad n = (1,2,...,N^{\kappa}), \tag{2.161}$$

$$f_{N \cdot N^{\varepsilon}+N^{\gamma}+N^{\kappa}+i} = u^i(L) - u^i(0) - \sum_{i=1}^{N^{\varepsilon}} L_n^*(x)\, \varepsilon_n^i dx = 0, \tag{2.162}$$

$$f_{N \cdot (N^{\varepsilon}+1)+N^{\gamma}+N^{\kappa}+1} = w(L) - w(0) + \varphi(0)\, L - \sum_{n=1}^{N^{\gamma}} L_n^*\, \gamma_n + \sum_{n=1}^{N^{\kappa}} L_n^{**}\, \kappa_n = 0, \tag{2.163}$$

$$f_{N \cdot (N^{\varepsilon}+1)+N^{\gamma}+N^{\kappa}+2} = \varphi(L) - \varphi(0) - \sum_{i=1}^{N^{\kappa}} L_n^*(x)\, \kappa_n^i dx = 0, \tag{2.164}$$

$$f_{N \cdot (N^{\varepsilon}+1)+N^{\gamma}+N^{\kappa}+2+i} = S_1^i + R_1^i(0) = 0, \tag{2.165}$$

$$f_{N \cdot (N^{\varepsilon}+2)+N^{\gamma}+N^{\kappa}+3} = S_2 + R_2(0) = 0, \tag{2.166}$$

$$f_{N \cdot (N^{\varepsilon}+2)+N^{\gamma}+N^{\kappa}+4} = S_3 + R_3(0) = 0, \tag{2.167}$$

$$f_{N \cdot (N^{\varepsilon}+2)+N^{\gamma}+N^{\kappa}+4+i} = S_4^i - R_1^i(0) - \int_0^L \left(p_X^i + p_{c,X}^{i,j} - p_{c,X}^{i,j-1}\right) dx = 0, \tag{2.168}$$

$$f_{N \cdot (N^{\varepsilon}+3)+N^{\gamma}+N^{\kappa}+5} = S_5 - R_2(0) - \sum_{i=1}^{N} \int_0^L p_Z^i dx = 0, \tag{2.169}$$

$$f_{N \cdot (N^{\varepsilon}+3)+N^{\gamma}+N^{\kappa}+6} = S_6 - R_3(0) - \int_0^L \left(R_2 - \sum_{i=1}^{N} m_Y^i\right) dx = 0, \tag{2.170}$$

where $i = (1,2,...,N), j = (1,2,...,N-1)$ The integrals of the Lagrangian polynomials are denoted by $L_n^*(x)$ and $L_n^{**}(x)$ and are:

$$L_n^*(x) = \int_0^x L_n(\xi) d\xi, \tag{2.171}$$

$$L_n^{**}(x) = \int_0^x \left(\int_0^{\eta} L_n(\xi) d\xi \right) d\eta, \tag{2.172}$$

for $x \in [0, L]$.

2.4.2.1 Solution of the generalized discrete equilibrium equations of glued laminated beam

The system of generalized equilibrium equations of a laminated beam, Eqs. (2.159) – (2.170) consists of $n_g = N\, N^{\varepsilon} + N^{\gamma} + N^{\kappa} + 3\, N + 6$ algebraic equations for the same number of unknowns, of which there are $2\, N + 4$ of external degrees of freedom, i.e. $u^i(0)$, $w(0)$, $\varphi(0)$, $u^i(L)$, $w(L)$, and $\varphi(L)$, and $N\, N^{\varepsilon} + N^{\gamma} + N^{\kappa} + N + 2$ internal degrees of freedom, i.e., ε^i, γ, κ, $R_1(0)$, $R_2(0)$, and $R_3(0)$. The integrals in the Eqs. (2.159) – (2.161) were evaluated using Gaussian numerical integration, but other methods of numerical integration can be used as well. The internal unknowns are then eliminated using static condensation for each element individually. The condensed global tangent stiffness matrix and the condensed residual force vector are then assembled in a classical manner (Schnabl et al., 2007; Zienkiewich and Taylor, 1991).

The solution is obtained by the following procedure:

$$\mathbf{g}(\mathbf{u}) - \lambda\, \mathbf{p} = 0, \tag{2.173}$$

where $\mathbf{u}$ is the vector of unknown components of nodal displacements and rotations, i.e., external degrees of freedom, and $\mathbf{p}$ is the vector of external load with load factor λ. The system of generalized discrete equations, defined in Eq. (2.173), can be solved by various algorithms, but for our model the standard iterative Newton-Raphson method was used. In this method, the equations must be linearized with consistent linearization (Hughes and Pister, 1978; Bonet and Wood, 1997), Eq. (2.9), and thus the full tangential stiffness matrix $\mathbf{K_T}$ is obtained:

$$\mathbf{K_T} = \begin{bmatrix} K_{11} & K_{12} & \cdots & K_{1\,n_g} \\ K_{21} & K_{22} & \cdots & K_{2\,n_g} \\ \vdots & \vdots & \ddots & \vdots \\ K_{n_g\,1} & K_{n_g\,2} & \cdots & K_{n_g\,n_g} \end{bmatrix}. \tag{2.174}$$

The coefficients K_{kl}, where $k = (1, 2, \cdots, n_g)$ and $l = (1, 2, \cdots, n_g)$, are the components of the tangential stiffness matrix and are obtained by partial derivative of $\mathbf{g}(\mathbf{u})$ with respect to the external and internal degrees of freedom. When N is the number of laminations and $i = (1, 2, ..., N)$, the elements of $\mathbf{K_T}$ are as follows:
For $k = (i-1)N^\varepsilon + n$:

$$K_{k,k} = \frac{\partial f_k}{\partial \varepsilon_n^i} = C_{11}^i\, L_n - \int_0^L (K_{\mathrm{X}}^i + K_{\mathrm{X}}^{i-1})\, L_n^* dx, \quad n = (1, 2, ..., N^\varepsilon),\ K_{\mathrm{X}}^0 = 0 \tag{2.175}$$

$$K_{k,iN^\varepsilon+n} = \frac{\partial f_k}{\partial \varepsilon_n^{i+1}} = \int_0^L K_{\mathrm{X}}^i\, L_n^* dx, \qquad n = (1, 2, ..., N^\varepsilon), \text{ for } i < N \tag{2.176}$$

$$K_{k,(i-2)N^\varepsilon+n} = \frac{\partial f_k}{\partial \varepsilon_n^{i-1}} = \int_0^L K_{\mathrm{X}}^{i-1}\, L_n^* dx, \qquad n = (1, 2, ..., N^\varepsilon), \text{ for } i > 1 \tag{2.177}$$

$$K_{k,NN^\varepsilon+N^\gamma+n} = \frac{\partial f_k}{\partial \kappa_n} = C_{13}^i\, L_n \qquad n = (1, 2, ..., N^\kappa) \tag{2.178}$$

$$K_{k,NN^\varepsilon+N^\gamma+N^\kappa+i} = \frac{\partial f_k}{\partial R_1^i(0)} = -1, \tag{2.179}$$

$$K_{k,N(N^\varepsilon+1)+N^\gamma+N^\kappa+2+(i-1)} = \frac{\partial f_k}{\partial u^{i-1}(0)} = \int_0^L K_{\mathrm{X}}^{i-1}\, dx, \qquad \text{for } i > 2 \tag{2.180}$$

$$K_{k,N(N^\varepsilon+1)+N^\gamma+N^\kappa+2+i} = \frac{\partial f_k}{\partial u^{i}(0)} = -\int_0^L (K_{\mathrm{X}}^i + K_{\mathrm{X}}^{i-1})\, dx, \quad K_{\mathrm{X}}^0 = 0 \tag{2.181}$$

$$K_{k,N(N^\varepsilon+1)+N^\gamma+N^\kappa+2+(i+1)} = \frac{\partial f_k}{\partial u^{i+1}(0)} = \int_0^L K_{\mathrm{X}}^{i}\, dx, \qquad \text{for } i < N. \tag{2.182}$$

For $k = NN^\varepsilon + n$:

$$K_{k,k} = \frac{\partial f_k}{\partial \gamma} = \sum_i C_{22}^i\, L_n, \qquad n = (1, 2, ..., N^\gamma) \tag{2.183}$$

$$K_{k,N(N^\varepsilon+1)+N^\gamma+N^\kappa+1} = \frac{\partial f_k}{\partial R_2(0)} = -1. \tag{2.184}$$

For $k = NN^\varepsilon + N^\gamma + n$:

$$K_{k,(i-1)N^\varepsilon+n} = \frac{\partial f_k}{\partial \varepsilon_n^i} = C_{13}^i, \qquad n = (1, 2, ..., N^\varepsilon) \tag{2.185}$$

$$K_{k,k} = \frac{\partial f_k}{\partial \kappa} = \sum_i^N C_{33}^i\, L_n, \qquad n = (1, 2, ..., N^\kappa) \tag{2.186}$$

$$K_{k,N(N^\varepsilon+1)+N^\gamma+N^\kappa+1} = \frac{\partial f_k}{\partial R_2(0)} = -x_n, \quad n = (1,2,...,N^\kappa) \tag{2.187}$$

$$K_{k,N(N^\varepsilon+1)+N^\gamma+N^\kappa+2} = \frac{\partial f_k}{\partial R_3(0)} = -1, \quad n = (1,2,...,N^\kappa). \tag{2.188}$$

For $k = NN^\varepsilon + N^\gamma + N^\kappa + i$:

$$K_{k,(i-1)N^\varepsilon+n} = \frac{\partial f_k}{\partial \varepsilon_n^i} = -L_n^*(L), \quad n = (1,2,...,N^\varepsilon) \tag{2.189}$$

$$K_{k,N(N^\varepsilon+1)+N^\gamma+N^\kappa+2+i} = \frac{\partial f_k}{\partial u^i(0)} = -1, \tag{2.190}$$

$$K_{k,N(N^\varepsilon+2)+N^\gamma+N^\kappa+4+i} = \frac{\partial f_k}{\partial u^i(L)} = 1. \tag{2.191}$$

For $k = N(N^\varepsilon + 1) + N^\gamma + N^\kappa + 1$:

$$K_{k,NN^\varepsilon+n} = \frac{\partial f_k}{\partial \gamma} = -L_n^*(L), \quad n = (1,2,...,N^\gamma) \tag{2.192}$$

$$K_{k,NN^\varepsilon+N^\gamma+n} = \frac{\partial f_k}{\partial \kappa} = L_n^{**}(L), \quad n = (1,2,...,N^\kappa) \tag{2.193}$$

$$K_{k,N(N^\varepsilon+2)+N^\gamma+N^\kappa+3} = \frac{\partial f_k}{\partial w(0)} = -1, \tag{2.194}$$

$$K_{k,N(N^\varepsilon+2)+N^\gamma+N^\kappa+4} = \frac{\partial f_k}{\partial \varphi(0)} = L, \tag{2.195}$$

$$K_{k,N(N^\varepsilon+3)+N^\gamma+N^\kappa+5} = \frac{\partial f_k}{\partial w(L)} = 1. \tag{2.196}$$

For $k = N(N^\varepsilon + 1) + N^\gamma + N^\kappa + 2$:

$$K_{k,NN^\varepsilon+N^\gamma+n} = \frac{\partial f_k}{\partial \kappa} = -L_n^*(L), \quad n = (1,2,...,N^\kappa), \tag{2.197}$$

$$K_{k,N(N^\varepsilon+2)+N^\gamma+N^\kappa+4} = \frac{\partial f_k}{\partial \varphi(0)} = 1, \tag{2.198}$$

$$K_{k,N(N^\varepsilon+3)+N^\gamma+N^\kappa+6} = \frac{\partial f_k}{\partial \varphi(L)} = 1,. \tag{2.199}$$

For $k = N(N^\varepsilon + 1) + N^\gamma + N^\kappa + 2 + i$:

$$K_{k,NN^\varepsilon+N^\gamma+N^\kappa+i} = \frac{\partial f_k}{\partial R_1^i(0)} = 1. \tag{2.200}$$

For $k = N(N^\varepsilon + 2) + N^\gamma + N^\kappa + 3$:

$$K_{k,N(N^\varepsilon+1)+N^\gamma+N^\kappa+1} = \frac{\partial f_k}{\partial R_2(0)} = 1. \tag{2.201}$$

For $k = N(N^\varepsilon + 2) + N^\gamma + N^\kappa + 4$:

$$K_{k,N(N^\varepsilon+1)+N^\gamma+N^\kappa+2} = \frac{\partial f_k}{\partial R_3(0)} = 1. \tag{2.202}$$

For $k = N(N^\varepsilon + 2) + N^\gamma + N^\kappa + 4 + i$:

$$K_{k,(i-1)N^\varepsilon+n} = \frac{\partial f_k}{\partial \varepsilon_n^i} = -\int_0^L (K_\mathrm{X}^i + K_\mathrm{X}^{i-1})\, L_n^*\, dx, \quad n = (1,2,...,N^\varepsilon),\ K_\mathrm{X}^0 = 0 \tag{2.203}$$

$$K_{k,iN^\varepsilon+n} = \frac{\partial f_k}{\partial \varepsilon_n^{i+1}} = \int_0^L K_\mathrm{X}^i\, L_n^*\, dx, \quad n = (1,2,...,N^\varepsilon), \text{ for } i < N \tag{2.204}$$

$$K_{k,(i-2)\,N^\varepsilon+n} = \frac{\partial f_k}{\partial \varepsilon_n^{i-1}} = \int_0^L K_\mathrm{X}^{i-1}\, L_n^*\, dx, \quad n = (1,2,...,N^\varepsilon), \text{ for } i > 1 \tag{2.205}$$

$$K_{k,NN^\varepsilon+N^\gamma+N^\kappa+i} = \frac{\partial f_k}{\partial R_1^i(0)} = -1, \tag{2.206}$$

$$K_{k,N(N^\varepsilon+1)+N^\gamma+N^\kappa+2+i} = \frac{\partial f_k}{\partial u^i(0)} = -\int_0^L (K_\mathrm{X}^i + K_\mathrm{X}^{i-1})\, dx, \quad K_\mathrm{X}^0 = 0 \tag{2.207}$$

$$K_{k,N(N^\varepsilon+1)+N^\gamma+N^\kappa+2+(i+1)} = \frac{\partial f_k}{\partial u^{i+1}(0)} = \int_0^L K_\mathrm{X}^i\, dx, \quad \text{for } i < N \tag{2.208}$$

$$K_{k,N(N^\varepsilon+1)+N^\gamma+N^\kappa+2+(i-1)} = \frac{\partial f_k}{\partial u^{i-1}(0)} = \int_0^L K_\mathrm{X}^{i-1}\, dx, \quad \text{for } i > 1 \tag{2.209}$$

For $k = N(N^\varepsilon + 3) + N^\gamma + N^\kappa + 5$:

$$K_{k,N(N^\varepsilon+1)+N^\gamma+N^\kappa+1} = \frac{\partial f_k}{\partial R_2(0)} = -1. \tag{2.210}$$

For $k = N(N^\varepsilon + 3) + N^\gamma + N^\kappa + 6$:

$$K_{k,N(N^\varepsilon+1)+N^\gamma+N^\kappa+1} = \frac{\partial f_k}{\partial R_2(0)} = -L, \tag{2.211}$$

$$K_{k,N(N^\varepsilon+1)+N^\gamma+N^\kappa+2} = \frac{\partial f_k}{\partial R_3(0)} = -1. \tag{2.212}$$

The x_n are the interpolation nodes, which generally depend on the selection of interpolation method for each lamination, and L is the length of the element. The rest of the components K_{kl}, $k, l = (1, 2, ...n_g)$ are equal to 0.

Finally, the finger joint had to be implemented in the tangential stiffness matrix. Finger joints represent the connection between the adjacent elements and therefore cannot be defined only at the level of a single element, but are implemented subsequently when the tangent matrix of the whole model is assembled. Finger joints were accounted for by an additional ”dummy” degree of freedom added to the tangent stiffness matrix of the element in which the finger joint is positioned. It should be noted that the corresponding matrix component also contains the information of axial displacement at the end of the previous element ($u_{e_\mathrm{FJ}-1}(L_{e_\mathrm{FJ}-1})$), where e_FJ denotes the number of element where finger joint is positioned. Eq. (2.213) shows the additional discrete equation, that must be added to the system of Eqs. (2.159) – (2.170).

$$f_{N(N^\varepsilon+3)+N^\gamma+N^\kappa+6+i} = u_{e_\mathrm{FJ}}^i(0) - u_{e_\mathrm{FJ}-1}^i(L_{e_\mathrm{FJ}-1}) - \frac{R_{1,e_\mathrm{FJ}}^i(0)}{K_\mathrm{FJ}}, \tag{2.213}$$

where $e_\mathrm{FJ} \in \{1, 2, ..., N_{el}\}$ is the number of the element in which the finger joint is assumed and $i \in \{1, 2, ..., N\}$ is the number of the lamination where the finger joint is assumed. The N and N_{el} are the total numbers of laminations and of elements, respectively. In this way, the continuity of the kinematic field is satisfied. The final dimension of the stiffness matrix was $n_g + n_{\mathrm{FJ}}$, where n_{FJ} is the total number of finger joints in the element. Each lamination of the element can have one finger joint, so in general, it is true that $n_{\mathrm{FJ}} \leq N$, N being the number of laminations. According to this formulation, the finger joints define the meshing of the model along the length of the beam. The tangential stiffness matrix of the element (2.174) is then extended and now written as:

$$\mathbf{K_{T,FJ}} = \begin{bmatrix} K_{1,1} & K_{1,2} & \cdots & K_{1,n_g} & K_{1,n_g+1} & \cdots & K_{1,n_g+n_{\mathrm{FJ}}} \\ K_{2,1} & K_{2,2} & \cdots & K_{2,n_g} & K_{2,n_g+1} & \cdots & K_{2,n_g+n_{\mathrm{FJ}}} \\ \vdots & \vdots & \ddots & \vdots & \vdots & \vdots & \vdots \\ K_{n_g,1} & K_{n_g,2} & \cdots & K_{n_g,n_g} & K_{n_g,n_g+1} & \cdots & K_{n_g,n_g+n_{\mathrm{FJ}}} \\ K_{n_g+1,1} & K_{n_g+1,2} & \cdots & K_{n_g+1,n_g} & K_{n_g+1,n_g+1} & \cdots & K_{n_g+1,n_g+n_{\mathrm{FJ}}} \\ \vdots & \vdots & \ddots & \vdots & \vdots & \cdots & \vdots \\ K_{n_g+n_{\mathrm{FJ}},1} & K_{n_g+n_{\mathrm{FJ}},2} & \cdots & K_{n_g+n_{\mathrm{FJ}},n_g} & K_{n_g+n_{\mathrm{FJ}},n_g+1} & \cdots & K_{n_g+n_{\mathrm{FJ}},n_g+n_{\mathrm{FJ}}} \end{bmatrix}. \tag{2.214}$$

To calculate the additional components of the new tangential stiffness matrix also the Eq. (2.213) must be linearized i.e. it must be partially derived with respect to all variables.

For $k = N(N^{\varepsilon} + 3) + N^{\gamma} + N^{\kappa} + 6 + i$:

$$K_{k,k} = \frac{\partial f_k}{\partial u^i_{e_{\mathrm{FJ}}-1}(L_{e_{\mathrm{FJ}}-1})} = -1, \tag{2.215}$$

$$K_{k,N(N^{\varepsilon}+1)+N^{\gamma}+N^{\kappa}+2+i} = \frac{\partial f_k}{\partial u^i_{e_{\mathrm{FJ}}}(0)} = +1, \tag{2.216}$$

$$K_{k,NN^{\varepsilon}+N^{\gamma}+N^{\kappa}+i} = \frac{\partial f_k}{\partial R^i_{1,e_{\mathrm{FJ}}}(0)} = -\frac{1}{K_{\mathrm{FJ}}}. \tag{2.217}$$

Other components of the tangential stiffness matrix are equal to 0. After the condensation of the matrix, the additional degree of freedom is considered as external degree of freedom.

2.5 Finger joints

Finger joints are used for longitudinal connection of laminations, which are further used in glued structural timber products. Their mechanical properties are crucial for the strength characteristics properties and behaviour of the structural members (Aicher and Klöck, 2001; Tran et al., 2014; Franke et al., 2014). Finger joints were primarily developed for use in softwood bonding and to date there is no European standard regulation for the manufacture of glued structural elements made of hardwoods. A draft standard is in progress, but the process is not yet complete, so the standard has not yet been published. Some European companies have started production using European Technical Approval (ETA), so there are some such documents, but they are not yet widely available. For example, there is Z-9.1-679 (DIBt, 2019), which refers to European beech wood and was obtained by the German company BS-Holz with requirements for the production of homogeneous, combined or hybrid glued laminated beams up to strength class GL48. Finger joints are considered the weakest link in glued structural timber in general and can be the dominant factor in the load bearing capacity of structural members (Aicher and Klöck, 1991).

However, some efficient finger joints are commonly used by manufacturers in the production of glued softwood lumber. The most commonly used finger joint length (20 mm) may not be optimal in terms of strength for softwoods (Aicher and Klöck, 1991) and hardwoods (Tran et al., 2014; Franke et al., 2014), although in the case of softwoods it still provides the strength values required for structural members. In addition, the standard EN 14080 (CEN, 2013e), which regulates the production of glued laminated timber and glued solid wood from softwoods and poplar, recommends 20 mm finger joints. Since hardwoods generally have higher mechanical properties than softwoods, the finger joint currently used could pose a problem for the jointing of beech and the strength of the glued element. This has been observed by several researchers, e.g., Ehrhart et al. (2018b); Franke et al. (2014); Frese and Blass (2006). However, finger joint length is only one of several parameters that affect the final strength properties. Essentially, the strength of a finger joint is determined by three factors. In addition to the profile of the finger joint, the strength of the joined boards and the quality of production also play an important role. The type and amount of adhesive, the type of adhesive application, the clamping pressure, the time between planing and glue application, and the pressing time are also parameters that need to be considered in the production of a finger joint (Konnerth et al., 2006; Franke et al., 2014; Lehmann, 2019). In the past, several studies have been conducted on the mechanical behaviour of finger joints. Most of them are numerical studies based on different formulations of finite elements (Aicher and Klöck, 1991; Milner and Yeoh, 1991; Serrano). Adhesive joints with simpler geometries have more often been analysed in closed form, starting with lap joints with flat adherends, step joints, or slotted joints (Erdogan and Ratwani, 1971; Aicher, 2003; Crocombe and Ashcroft, 2008; da Silva et al., 2009). The stress distribution in the bonded joint is nonlinear and exhibits stress peaks at the ends of the bonded area. The irregularities in the stress distribution may increase if the geometry of the finger joint is more complex compared to the geometry of the simpler joints (lap joints, slotted joints) and therefore require more complex calculations. In these cases, finite element methods are usually used. In order to predict the strength of the connection, the stress distribution and a suitable failure criterion must be determined. The failure limit state can be determined within the framework of continuum mechanics with limit stresses or strains (Norris, 1962; Aicher and Klöck, 2001; Sandhaas, 2012; Danielsson, 2013) or in the context of fracture mechanics, where the limit state is defined with stress intensity factors or fracture energies (Patton-Mallory and Cramer, 1987; Aicher and Klöck, 1991; da Silva and Campilho, 2012). Most commercial finite element programmes, e.g., (Smith, 2009), have implemented cohesive elements that are used to model adhesives and can simulate the fracture behaviour of the adhesive. Determining the mechanical parameters needed to model the finger joint is not straightforward. It is critical to determine the parameters related to the bond line, which is composed of the adhesives, the adhesive, and the interface between them, as well as the parameters specific to each of these combinations. A comprehensive analysis of finger joints has been carried out by Serrano, focusing on the fracture properties of the adhesive joint. Several numerical models of finger joints have already been developed for application to beech wood, e.g., by Tran et al. (2014); Franke et al. (2014), where the maximum strengths of finger joints and the stress distribution along the finger joint were studied. Although the EN 14080 (CEN, 2013e) standard for glued softwood and poplar structural timber specifies the tensile and bending strength requirements for finger joints, they are often subjected to (almost) pure tensile stresses. This is especially true when thinner laminations are used in the glued lumber. Considering the low dimensional stability of beech wood and the fact that the yield of laminations suitable for glued laminated production is relatively low (Westermayr et al., 2018), the use of thinner laminations is quite reasonable. This part of the dissertation, in which finger joints are investigated, therefore focuses exclusively on the optimization of the geometry and the influence of the adhesive with respect to the tensile strength of the finger joint made of beech wood.

2.5.1 Preliminary research

After the literature review, a brief preliminary assessment of the tensile strength of the finger joint was made based on simple equilibrium equations for scarf joints. The geometry of the scarf joint is shown in Fig. 2.7. According to Aicher (2003), the scarf joints are known to be the most effective from engineering point of view and provide the highest strengths, but are very uneconomical due to the extensive timber loss. However, the geometry of the joint is very simple and the stresses can be easily evaluated:

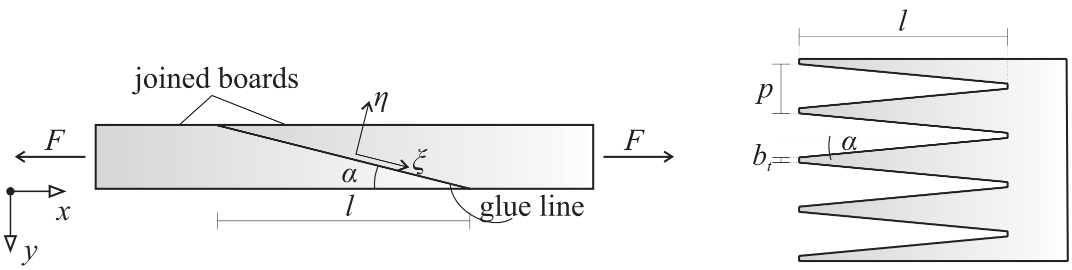

Figure 2.7: Geometry of a scarf joint (left) and geometry of a finger joint (right).
Slika 2.7: Geometrija poševnega spoja (levo) in geometrija zobatega spoja (desno).

$$\sigma_{\xi\eta} = \sigma_0 \sin\alpha \cos\alpha \quad \text{and} \quad \sigma_{\eta\eta} = \sigma_0 \sin^2\alpha. \tag{2.218}$$

The σ_0 is the normal stress in the longitudinal direction ($\sigma_0 = F/A$) and by definition represents the horizontal tensile strength of the scarf joint. Because of the analogous geometry of the finger joint shown in Fig. 2.7 (right), σ_0 is the object of our optimization. Here, F is the axial force and A is the area of the cross-section. It is important to note that the distribution of stresses along the glue line were assumed to be constant, which of course is not the case in reality. As mentioned in the previous literature review, the stress distribution along the glue line is nonlinear and exhibits pronounced stress peaks at the ends of the joints. However, for the purposes of the preliminary assessment, this assumption was considered sufficient. The shear strength τ_1 and the normal peel strength σ_u were calculated assuming the quadratic strength criteria according to the Eq. (2.219), which was presented by Aicher (2003). The ratio $\tau_1/\sigma_u = 6$ was assumed (Tran et al., 2015). With the determined strength properties of the glue line, the determined nominal tensile strength of the finger joint f_t was observed

$$\left(\frac{\sigma_{\xi\eta}}{\tau_1}\right)^2 + \left(\frac{\sigma_{\eta\eta}}{\sigma_u}\right)^2 = 1. \tag{2.219}$$

A reference shear strength of 8.8 N/mm^2 and a normal peel strength of 1.5 N/mm^2 were used for the calculation. Both were evaluated according to the quadratic strength criteria, Eq. (2.219), where for σ_0 the average tensile strength of the 20 mm finger joints was taken from the experimental test results. To estimate the tensile strength, a parametric study was performed for a number of different finger joint profiles. The calculations were performed for half of the finger joint, see Figure 2.8, where l is the length of the finger joint and t_l is the width of a slope and the tip width b_t is neglected within the effective glue line. The parameters were set in the range of: (i) $b_t = 1 - 2$ mm, (ii) $l = 10 - 50$ mm, and (iii) $\alpha = 2 - 5°$.

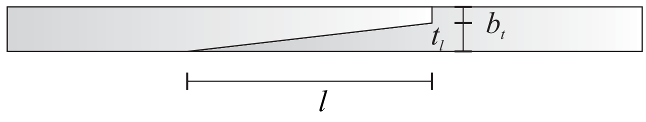

Figure 2.8: Geometry of a half of a finger joint for analytical model.
Slika 2.8: Geometrija polovice zobatega spoja za analitični model.

The results of the parametric study are shown in Figure 2.9. The pitch p is the width of the finger and is indirectly expressed by the angle α, which is defined as the slope of the finger, see Fig. 2.7.

$$\alpha = \arctan \frac{t_l}{l}. \tag{2.220}$$

The influence of all geometry parameters b_t, p, and l can be seen in the graphs in Fig. 2.9. It can be seen that the tensile strength is linearly correlated with the effective glue line area. Longer finger joints results in a higher tensile strength. The increase in strength can also be achieved by optimizing the angle α ($\alpha \approx 3.5$ %) and reducing the tip width b_t. To achieve higher strengths, for example, 80 N/mm^2, which is about 10 % above the average tensile strength of Slovenian beech wood (Fortuna et al., 2018a), it would be necessary to increase the length to at least 30 mm, and the angle α and tip width b_t should be rather small compared to the usual geometry profiles (Aicher, 2003).

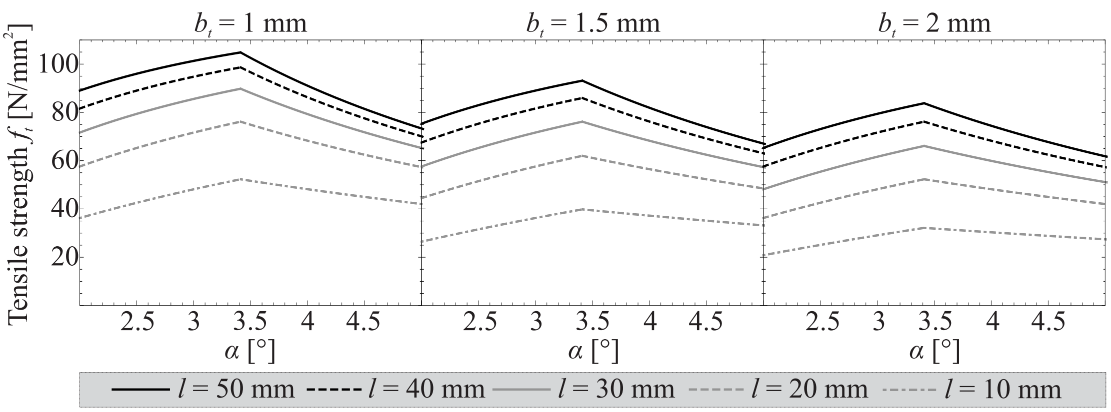

Figure 2.9: Influence of geometric parameters of the finger joint l, p, and b_t on the tensile strength of finger joints based on the analytical solution.
Slika 2.9: Vpliv geometrijskih parametrov zobatega spoja l, p, and b_t na natezno trdnost zobatih spojev po analitični rešitvi.

2.5.2 Numerical model of the finger joint

As part of the TIGR4smart project[1], the numerical model of a half of the finger joint was created with one of the partners[2]. The main objective of the parametric studies was to optimise finger joint geometry and adhesive properties for beech boards. The tensile test was simulated using a 2D numerical model in Abaqus (Smith, 2009). The model accounts for the symmetrical response along the longer axis of the lamination. Therefore, only a small section of the lamination was analysed with one half of the finger (Figure 2.10). The lamination was fixed at one end, while a displacement (u_x) was introduced at the other end until failure. The model is supported due to the symmetry in the transverse direction. Biquadratic quadrilateral elements with eight nodes (Smith, 2009) were used for the finite element model. The mesh is condensed in the local area adjacent to the cohesive elements and the cohesive surface. The maximum size of the element was approximately 0.5×0.5 mm. The model consisted of parts with

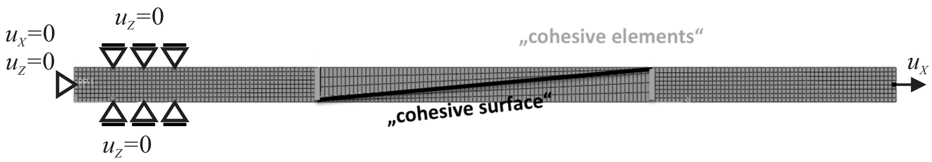

Figure 2.10: Numerical model of half of the finger joint with boundary conditions.
Slika 2.10: Numerični model polovice zobatega spoja z robnimi pogoji.

linear elastic and orthotropic behaviour for beech, with wood fibres oriented longitudinally. The mean values for the elastic behaviour of beech (Tab. 2.1) were assumed according to the literature (Desch and Dinwoodie, 2016; Sandhaas, 2012). Nonlinear behaviour was assumed in the adhesive layer (failure of the joint, modelled by a cohesive surface) and along the weakened area of the pitch (wood failure, modelled by cohesive elements). A cohesive zone model (CZM) was used to model the adhesive layer. The input parameters for shear and tensile strengths (Tab 2.2) for adhesive 1 were taken from the studies of Tran et al. (2014) and Khelifa et al. (2016), in which experiments were conducted for the melamine-urea-formaldehyde adhesive and beech wood. For the second adhesive, the initial strength parameters were increased by about 20 %, as described by Müller et al. (2009). Such an increase has also been confirmed in other studies (Serrano, 2001) and can be explained by the fact that the strength represents the local strength (at a material point) and, also to some extent, by the stress distribution at failure. Since no information on the fracture energy G_f of the glue line can be found in the literature, the input parameter remained unchanged for both adhesives. Moreover, the increase in glue line performance can be a consequence of various factors, such as the quality of the surface, environmental conditions, applied pressure, etc. Therefore, it was decided to use a value that lies between the relatively high values of Sterley and Gustafsson (2012) and the lower values of Müller et al. (2009). Finally, a fracture energy parameter of 0.5 N/mm was used in the model (Tab. 2.2). The damage initiation was assumed by a quadratic traction criterion and the evolution of the damage was considered according to the energy law.

Tabs. 2.1 and 2.2 show the material properties used in the model. The values E_1 and E_2 are the elastic moduli in the longitudinal and radial directions of the wood, ν_{12} is the Poisson's ratio, where the first index refers to the direction of applied stress and the second index to the direction of lateral deformation,

[1] National project, http://kc-tigr.si/projekti/tigr4smart/
[2] ZAG, dr. Azinovič Boris

Table 2.1: Mechanical properties of beech wood (mean values used for the Abaqus model).

Preglednica 2.1: Mehanske lastnosti bukovega lesa (srednje vrednosti količin uporabljenih v modelu v Abaqusu).

E_1[N/mm^2]	E_2[N/mm^2]	ν_{12}	G_{12}[N/mm^2]
13700	11400	0.51	1060

Table 2.2: Parameters used for the cohesive elements and cohesive surface in Abaqus model.

Preglednica 2.2: Parametri uporabljeni za kohezivne elemente in kohezivno površino za model v Abaqusu.

	σ_u [N/mm^2]	τ_1 [N/mm^2]	S_{nn} [N/mm^2/mm]	$S_{tt,1}$ [N/mm^2/mm]	G_f [N/mm]	η [-]
Timber adhesive bond-line (cohesive surface-adhesive 1)	1.6	9.6	default contact enforcement method		0.5	0.001
Timber adhesive bond-line (cohesive surface-adhesive 2)	3.0	15.0	default contact enforcement method		0.5	0.001
Beech along the glueline (cohesive elements)	70	100	13700	1610	10	$5{\cdot}10^{-6}$

and G_{12} is the shear modulus in the 12-plane. σ_u in Tab. 2.2 is the strength in normal direction, τ_1 is the shear strength, S_{nn} is the stiffness in normal direction, $S_{tt,1}$ is the stiffness in shear direction, G_f is the fracture energy (mode independent), and η is the coefficient of viscosity. As in the analytical approach presented in Section 2.5.1, the three parameters were varied, i.e., tip thickness (b_t), the length of the fingers (l), and the pitch (p). The parameters were varied in the following ranges: (i) $b_t = 1 - 2$ mm, (ii) $l = 10 - 50$ mm, and (iii) $\alpha = 2 - 6°$.

The results of the parametric study are shown for adhesive 1 and for adhesive 2 in Figure 2.11. For each curve in the plots (with constant b_t and l), an optimal pitch dimension p can be found. In the first part of the curve (low values of p), the load bearing capacity of the joint increases until the optimal p is reached. At smaller values of p (smaller angle of the fingers), the failure occurs in the cohesive elements and simulates the failure of wood. After reaching the optimal pitch p, the failure mode changes and the load-carrying capacity decreases with further increase of p, since the area of the glued surface decreases accordingly. The optimal angle of the fingers for the analysed numerical model with adhesive 1 (MUF) and the assumed failure mechanisms was found to be approximately $3-4°$. A comparison of the Figs. 2.9 and 2.11 shows that the results of numerical simulations for longer finger joints are lower than those of the analytical analysis. The opposite is true for the shorter finger joints, where the strengths of the analytical model are lower. This is due to the fact that the analytical model was fitted to the experiments where the length of the finger joint was 18 mm and the angle was $5.7°$. It is likely that the differences are mainly due to the stress distribution along the glue line which is assumed to be constant in the analytical model, which is not the case in reality, where the peaks of shear stress occur at the beginning and end of the glue line and represent the critical point of rupture. Therefore, the misestimation of the strengths

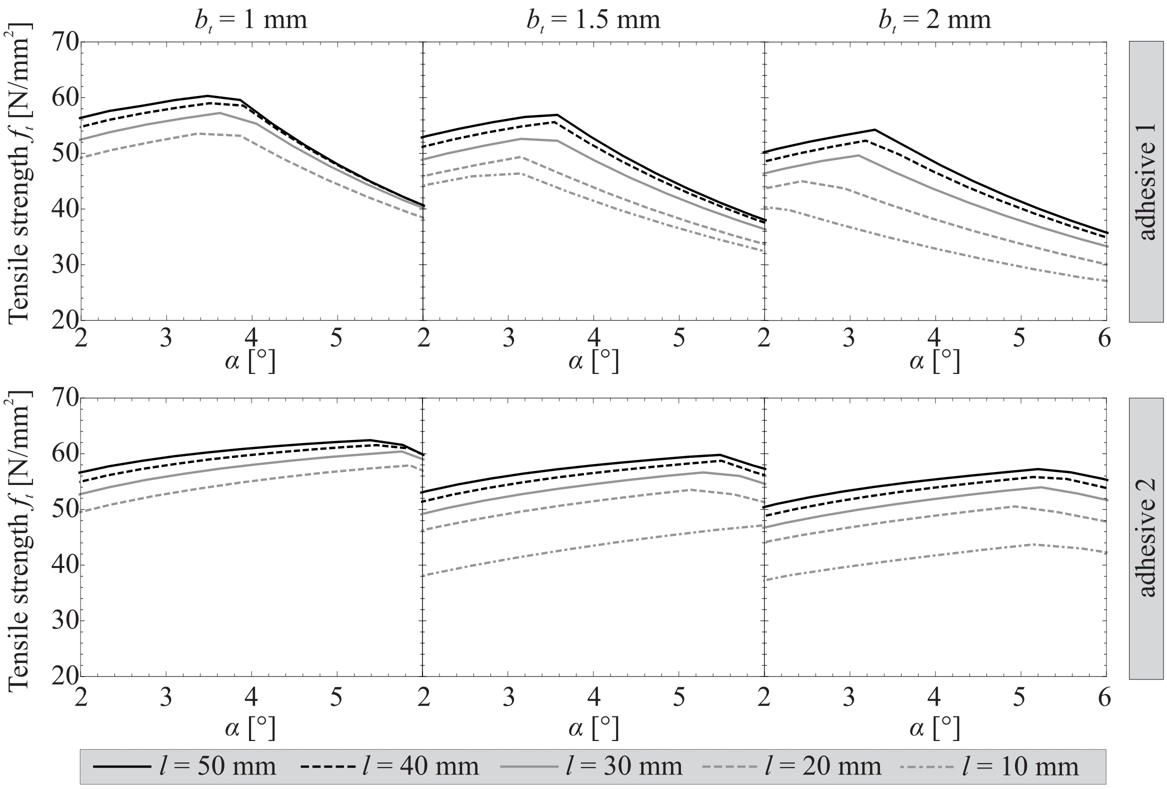

Figure 2.11: The influence of the geometric parameters α, b_t, and l on the tensile strength of finger joints based on numerical solution.
Slika 2.11: Vpliv geometrijskih parametrov α, b_t in l zobatega spoja glede na numerično rešitvev.

increases with the increase of the difference between the considered length and the reference length of 18 mm. The numerical model, on the other hand, determines the stress distribution along the glue line and therefore represents a better prediction of the behaviour of the finger joint.

The numerical simulation of the tensile test for adhesive 2 with higher strength properties showed that the influence of the adhesive decreases with length. This is because the failure in the longer finger joints is not governed by the rupture in the glue line, and therefore the glue has less influence on the final strength. For example, for tip width b_t = 2 mm, the difference between the maximum strengths achieved with the weaker adhesive 1 and the stronger adhesive 2 was 15 % for the 10 mm finger joints, while it decreased to 5 % for the 50 mm finger joint. This can be seen in Figure 2.12, which shows the differences between the maximum strengths obtained with adhesive 1 and adhesive 2 (y-axis) with the length of the finger joint (x-axis).

The influence of the geometric parameters on the analytical calculations of the load bearing capacities of the finger joint in tension was investigated. Adhesive properties were also included in the numerical model. The results are further validated with the results of the experimental tests presented in the following chapter 3. However, the models were created to determine the optimum geometry and adhesive used for the beech finger joints. It was expected that the length of the finger joint would play an important role in the strength of the joints. This was shown in the study by Franke et al. (2014), where

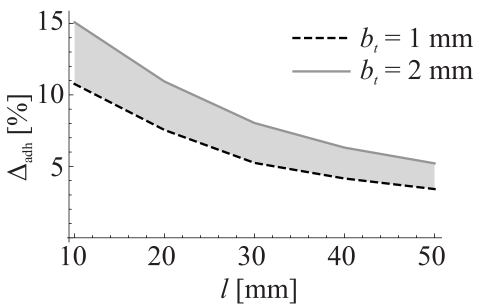

Figure 2.12: Differences of maximum tensile strengths, Δ_{adh}, between adhesive 1 and adhesive 2 for different lengths (for $b_t = 1$ mm and $b_t = 2$ mm)
Slika 2.12: Razlike med maksimalni natezni trdnosti, Δ_{adh}, doseženi z lepilom 1 ter lepilom 2 (za $b_t = 1$ mm in $b_t = 2$ mm).

longer (50 mm) finger joints resulted in higher flat-wise bending strength, and in the study by Tran et al. (2014), where maximum finger joint length and minimum pitch gave the best results in edge-wise bending tests of beech wood finger joints. Our investigation confirmed these results, but we also obtained some additional important information. The angle of the finger joint, i.e., the pitch and the width of the finger joint tip, also contribute significantly to the load bearing capacity of the finger joint in tension. To achieve a tensile strength of at least 80 N/mm^2, which is about 10 % higher than the mean value for Slovenian beech (Fortuna et al., 2018b,a), some suitable profiles would be $l = 30$ mm, $p = 5.8$ mm, and $b_t = 1$ mm; $l = 40$ mm, $p = 7.1$ mm, and $b_t = 1$ mm or $l = 50$ mm, $p = 8.4$ mm, and $b_t = 1$ mm. Another finger joint profile that could be used and was represented in the older version of EN 385:2001 as $l \times p \times b_t = 32 \times 6.2 \times 1.0$ mm ($\alpha = 3.8°$). According to the analytical model, a tensile strength of about 80 N/mm^2 would be expected, whereas the strength parameters obtained from experiments assume the quadratic strength criterion. The numerical model shows lower strengths (about 60 N/mm^2) than the analytical model. In Fig. 2.13 the comparison between the numerical and analytical model are shown on the example of the $b_t = 1.5$ mm. The results are similar for the $b_t = 1$ mm and $b_t = 2$ mm. It must be pointed out that the strength parameters are taken from the literature and are probably slightly underestimated. It was concluded that the use of finger joints capable of withstanding that withstand 55 to 60 N/mm^2 in tension would have a significant effect on the bending strength of the glued laminated beech beam.

2.5.3 Adhesives

Adhesives are essential for most wood elements and composites. Gluing wood allows us to use only the best parts of the wood, free of imperfections and local weakening anomalies, resulting in stronger and more reliable products. This led to an increased use of timber structural elements, which are now mostly used in the form of composites, replacing the use of structural elements made of sawn wood. The construction industry is one of the largest consumers of adhesives, as they are used in most structural and non-structural wood elements such as glued laminated beams, cross-laminated timber, fiberboard, OSB,

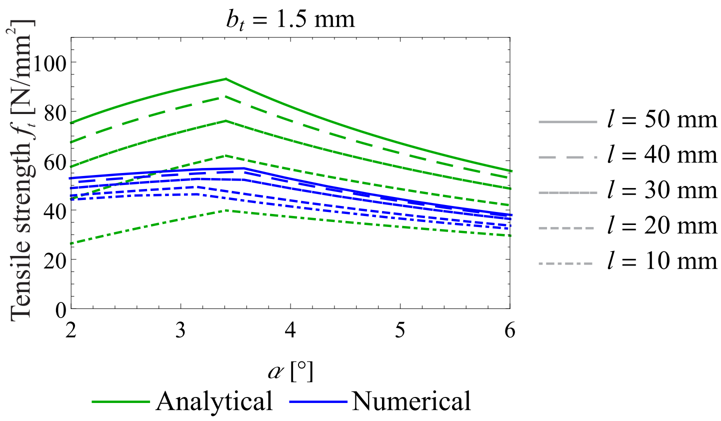

Figure 2.13: Comparison of calculated expected results of finger joints tension strengths f_t for different α, b_t, and l, obtained with analytical and numerical model (adhesive 1).
Slika 2.13: Primerjava izračunanih pričakovanih nateznih trdnosti zobatih spojev f_t za različne α, b_t in l, dobljenih z analitičnim in numeričnim modelom (lepilo 1).

etc., (Conner, 2001). The load bearing capacity of such structural elements is increasing and adhesives are one of the main factors that allow us today to design multi-story buildings with a wooden structure. Low-quality wood can also be used in the production of these elements, reducing the amount of wood waste, which is, of course, a great advantage for manufacturers (Conner, 2001).
The mechanical properties of wood increase with its density (Konnerth et al., 2016) and this was confirmed by the study of the projects EU HARDWOODS [3] and GRADEWOOD[4] also for structural sized timber (Fortuna et al., 2018a). The mechanical properties of spruce, beech, and oak were measured on representative sample with structural dimensions. Oak has more than twice the tensile strength of spruce, while beech has three times the tensile strength. This makes beech wood very interesting for use in load bearing elements, since the high load bearing capacity could significantly reduce the dimensions of the cross-sections. However, compared to other wood species, beech wood is much more sensitive to changes in moisture content, which can lead to significant deformation due to swelling and shrinkage. Beech is therefore potentially useful primarily in the form of thinner laminations in glued beams which however, results in higher costs (Westermayr et al., 2018).

In Slovenia and in Europe in general, structural wood composites are mostly made of softwood, mainly spruce and fir (*Picea abies and Abies alba*), and have been used in glulam elements for more than 100 years. Their behaviour is already well known and existing technical standards are based on the known properties of conifers. Existing adhesives are largely adapted to the properties of these species. However, the desire to use hardwoods in glued laminated structures is relatively new and there are still many unknowns in this area that need to be researched and suitable solutions found. This section provides a brief overview of the adhesives that can be used in structural elements and the standards that address this area. The parameters that influence the quality of bonding are presented, with emphasis on the properties of hardwood, with the emphasis on the beech wood.

[3] http://km.fgg.uni-lj.si/hardwood/index.html, part of the Wood Wisdom.Net programme
[4] part of the Wood Wisdom.Net programme

The strength of the adhesive and its durability, i.e., the ability of the adhesive to maintain the specified strength properties over time and under different and varying environmental conditions, are the result of a number of factors that determine the selection of the adhesive. The most important factors are the chemical composition, the structure of the adhesive, the curing method or mechanism, the compatibility with the wood to be bonded, the surface preparation of the wood and the hardness of the environment in which the bond will be used, etc. (Kellar, 2010).

2.5.3.1 Classification of the adhesives

In terms of their chemical structure, wood adhesives can generally be divided into natural and synthetic adhesives. Due to the high requirements for structural adhesives, i.e. high strength properties and long durability, the synthetic adhesives are the most suitable for structural use. They are further subdivided according to the type of polymers they are composed of. Oligomeric adhesives are cured by what is known as in-situ polymerization, usually by the addition of catalysts that accelerate the cross-linking of the adhesive. Solvents are used to facilitate the application of synthetic polymers (water is a common solvent). The curing of polymer adhesives is usually directly related to the cooling and/or evaporation or adsorption of water (Conner, 2001). For structural purposes, thermosetting adhesives are mainly used. They are characterised by being non-deformable, non-melting and insoluble after curing. Aminoplastic adhesives are among the most commonly used adhesives in the wood industry, with urea-formaldehyde adhesives (UF) and melamine-formaldehyde adhesives (MF) being the most common. UF adhesives are characterised by good water solubility, high strength properties and fire resistance, but unfortunately do not provide adequate water resistance. Melamine adhesives, on the other hand, are characterised out precisely by their good water-resistant properties. Because of the optimal combination of strength, durability, and also because of the relatively low price, melamine-urea-formaldehyde (MUF) adhesives are widely used in practise (Ugovšek and Šernek, 2012).
Adhesives based on phenolic resins were widely used in the past, but these adhesives are toxic and therefore often undesirable and even banned from use in structures. Moreover, they are dark coloured and often unsuitable for aesthetic reasons alone (Šernek, 2018). Nevertheless, they are among the typical structural adhesives. When resorcinol resins are added to phenolic adhesives, the so-called phenol-resorcinol-formaldehyde adhesives (PRF) are obtained. Resorcinol greatly accelerates the curing time, even at room temperature, and is used in applications where rapid curing at room temperature is required or where the geometry of the composite prevents the transfer of high temperatures to the bonding interface within the composite to cure the adhesive. Such a problem often occurs in the manufacture of laminated beams. Such adhesives form a good bond with the wood of different moisture contents (2-20 %), and the adhesive joints are resistant to moisture, high temperatures, chemicals and pests. However, the price of resorcinol is much higher than that of phenol and it also has a darker colour (Conner, 2001; Šernek, 2018).

A slightly different classification of adhesives is presented by Frihart (2009) and is based on the ability of the adhesive to interact with the wood. This classification has been shown to be consistent with the morphology of the polymers in the adhesive and the response of the surface to changes in the moisture content of the wood. The latter is one of the main factors affecting durability. Depending on their chemical and structural properties, adhesives are divided into prepolymerized and in-situ polymerized adhesives. Most wood adhesives belong to the group of in-situ polymerized adhesives. They are characterised by rapid penetration into cell walls before curing and limited creep. They consist of relatively rigid polymers and are densely cross-linked after curing. The polymer chains are composed of oligomers and/or monomers. The chains are formed after the adhesive is applied to the wood surface. This group includes melamine and urea resins, which are linked to the formaldehydes by a condensation or polycondensation process (Šernek and Kutnar, 2009). These adhesives are very rigid and have limited ability to adapt to wood deformation, usually caused by swelling or shrinkage due to moisture changes. Nevertheless, these adhesives form strong and resistant joints. Phenolic adhesives, methylene diphenyl isocyanate adhesives and epoxy adhesives also belong to this group. Epoxy adhesives are characterised by high stiffness but have lower durability, while phenolic and phenol-resorcinol adhesives have much better moisture resistance because they penetrate cell walls and reduce their swelling capacity, resulting in higher durability (Frihart, 2009). The second group of adhesives are the so-called prepolymerization adhesives, which include polyvinyl acetates, polyurethanes and emulsion polymer isocyanates. They can also be used as structural adhesives. Their molecular structure prevents penetration into the cell walls and they can penetrate into the cell lumens. They are characterised by a more elastic behaviour and are able to transfer deformations of the wood across the interface into the adhesive itself (Frihart, 2009).

To give a brief overview of standardisation in this field, only a few important documents are mentioned here. The classifications and requirements for the phenolic and aminoplastic polycondensation adhesives are contained in SIST EN 301 (CEN, 2006), while the one-component polyurethanes (PUR) are covered in SIST EN 15425 (CEN, 2017). The EN 302 series of standards (CEN, 2013b,c,d) defines the various environmental conditions to which adhesives are exposed. Requirements include shear tests, delamination tests, tests for damage to wood fibres by acid (due to cyclic exposure to temperature and humidity), tests for shrinkage intensity of adhesives after the joints have been exposed to certain environmental conditions (temperature and humidity), etc.

Standardisation distinguishes between two types of adhesives in terms of environmental conditions, defined by temperature and relative humidity. Type I adhesives are suitable for more demanding conditions of use, where they are exposed to high temperatures ($> 50°$C) and high humidity (RH > 85 %), while the Type II is intended for the use under normal conditions (T $\approx 20°$C and RH < 85 %). The methodology for determining these tests is defined in the first four parts of EN 302 (CEN, 2013b). The other three parts deal with the physical properties of the adhesives, i.e. viscosity and alkalinity, and the use of the adhesives (application method, maximum assembly time and minimum curing time, etc.).

2.5.3.2 Formation of the adhesive bond of wood

In general, two main mechanisms are involved in the formation of an adhesive bond, namely cohesion and adhesion (Fig. 2.14). Cohesion is the phenomenon in which forces are created between the basic building components of a material. In mechanics, this is referred to as the mechanical strength of the material. Adhesion, on the other hand, is a surface phenomenon in which bonding between two surfaces occurs based on three mechanisms (Šernek, 2018):

- A mechanical bond is a bond at the macroscopic level. It is created by the penetration of the liquid adhesive. When the adhesive is cured, anchors are formed in the material that create a mechanical bond with the adhesive. The porosity of the material allows the adhesive to penetrate and is thus a necessity for the mechanical bond.

- The physical bond is based on the force attraction between molecules. The formation and strength of the physical forces depend on the wetting of the wood cell walls with the adhesive and their adsorption in the wood. The physical bond is a secondary bond. These bonds are weak compared to the primary bonds, but make up the majority of adhesive bonds in wood bonding.
- The chemical bond between the glue and wood molecules, called the primary bond, is formed when cross-linking adhesives are used. Ionic and covalent bonds are known as primary bonds in adhesives. The covalent bonds are chemical bonds between the atoms of the material and the ionic bonds are bonds between oppositely charged ions. In general, the ionic bonds have the greatest amount of stored energy, but are not usually formed in wood bonding. The covalent bonds are the most effective of the two types of bonds when it comes to bonding wood.

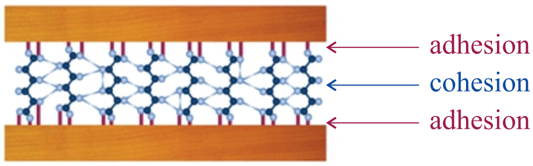

Figure 2.14: A schematic of adhesion and cohesion in the glueline. Adopted after Ülker (2016).
Slika 2.14: Shematski prikaz adhezije in kohezije v lepljenem spoju. Povzeto po Ülker (2016).

Ultimate strength of the adhesive joint therefore depends on the cohesive forces in the adhesive and in the base material, i.e., adherend, as well as on the adhesive bonds that form the interface between the adhesive and the adherend. Furthermore, three types of adhesive bond failure (Fig. 2.15) of the adhesive bond can be distinguished (Šernek, 2018; Deng et al., 2015):

- adhesive fracture,
- cohesive fracture in the adhesive and,
- cohesive fracture in the adherend.

As with the design process of the structure, we also strive to utilise the design process of the structural elements. Implicitly, this means that the joints have a higher load bearing capacity than the structural material. Such requirements are typical for all types of building materials. Therefore, the level of construction adhesives also takes into account the level of fracture in the wood compared to the interface (Šernek, 2018; CEN, 2013b). For gluing to work properly, the adhesive must be able to fill the gaps and small dents in the wood. The viscosity of the adhesive must be such that it can penetrate the pores. Otherwise, additional pressure is required to achieve adequate bonding of the joint. There are seven key factors that affect surface quality, (Davis, 1997):

- **Wettability** is the ability of the surface to absorb the liquid. It is influenced by the surface energy, chemical composition, and surface texture. Ideally, the adhesive should spread easily on the surface to achieve close contact with the wood molecules - lignin and cellulose.
- **Surface contamination** can cause a weak layer inside the joint. Common contaminants that usually appear on the wood surface are oils and dust particles from wood processing. In addition, the

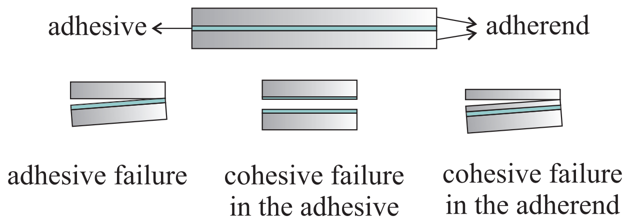

Figure 2.15: A schematic of typical failure modes of glued joints. Adopted after (Deng et al., 2015).
Slika 2.15: Shematski prikaz tipičnih porušitev v lepljenem spoju. Povzeto po (Deng et al., 2015).

so-called extractives, which are formed during the growth of the tree, can also contaminate the surface. They appear on the surface as plugs in the cell lumina and can move freely on the wood. The number of extractives on the surface is usually small, but they contribute significantly to the colour, odour, and biological durability of the wood (Kos, 2013). They can be removed with a variety of solvents. Extractives consist of a variety of groups of chemical components (tannins, anthocyanins, flavones, and others). Extractives that are not chemically or physically bonded (oils, waxes, fats, and sugars) can remain on the surface for a long time after surface treatment. It is strongly recommended that the adhesive be applied immediately after the wood has been treated. Adhesives are able to absorb and thus tolerate a limited amount of contaminants, but their presence should be taken into account and the surface should be cleaned as thoroughly as possible. In general, hardwoods contain more extractives than softwoods (Davis, 1997).

- **Roughness and porosity** are determined by the cell structure and are critical for the molecules of the adhesive to form adequate adhesion. The adhesive also strengthens the cells that were damaged during the processing of the wood and contributes to a more uniform stress distribution at the interface of the joint.
- **Smoothness of the surface** is closely related to roughness (Davis, 1997). The surface must be smooth and free from material residues that easily adhere to the wood surface. It depends on the technology of surface preparation.
- **Surface uniformity** depends on how the surface was processed. Generally, three processing methods are used: Sawing, grinding and cutting (Davis, 1997). In practise, sawn wood is not suitable for bonding without further treatment and processing. Cutting is the most commonly used method and includes planing and milling. Surface uniformity is also affected by irregularities in the wood, such as the presence of knots and local fibre deflection (Davis, 1997).
- **Compatibility with adhesives**. This aspect mainly refers to the chemical structure of the bond between the adhesive and the adherend. Wood may contain chemicals that adversely affect the bond (surface contamination). The water content of the wood also plays a role. Therefore, the moisture content of the wood is also very important when bonding. A moisture content of 8-12 % is optimal (Davis, 1997).
- **The control of environmental conditions**. It is important to control climatic conditions during production. Wood reacts differently to changes in humidity than the adhesive, which usually has a negative effect on the strength of the bond.

To achieve the proper bonding properties, the wood must be properly dried. The contact surfaces must fit together perfectly and the wood must not warp (Davis, 1997).

To ensure the quality of the adhesive, the user must follow the manufacturer's recommendations for its application. The recommendations usually take into account the storage conditions of the adhesive, the preparation of the surface, the moisture content of the wood, the environmental conditions in terms of air temperature and relative humidity, the mixing ratio, if applicable, the amount of adhesive application, the pot life, and the assembly time. The pot life is the period of time during which the mixture of adhesive and hardener can be used after mixing the components, while the assembly time is divided into an open assembly time (OAT) and a closed assembly time (CAT). The OAT is the time between the application of the adhesive and the assembly of the parts to be bonded. The CAT is the time between the assembly of the parts to be bonded and the onset of the pressure in the press (AkzoNobel, 2017). The storage time, pot life and assembly time depend on the environmental conditions.

Ensuring adequate strength properties of finger joints and glued laminated beech wood joints is a major challenge. The structure of the wood as a substrate is critical to the strength and durability of the joints. Hardwoods, including beech, have high density and mechanical properties, so adhesives must withstand higher loads. However, the properties of hardwoods often have a negative effect on the curing process and the final strength of the adhesives and, therefore, the joints. Hardwoods, including beech, have low acidity and fewer hydroxyl groups, which are necessary for the formation of stable bonds (in the case of urea resin adhesives). The surface of hardwoods is much more saturated with impurities and precipitates, which are still released after the wood has been treated and, in turn, have a negative effect on strength. In addition to the faster and more intensive water absorption of beech wood compared to spruce wood, the high density of beech wood means that fibres are less damaged during processing (planing), makes it more difficult to create a suitable contact surface between the glue and the substrate. Such structural differences in the wood are ultimately reflected in the altered behaviour of the adhesives, resulting in inadequate strength properties of the adhesive joints compared to the raw material. Although standard shear tests for adhesives show encouraging results for hardwoods, such tests are performed on smaller samples of pure wood without major anomalies, which are unfortunately unavoidable in the manufacture of structural elements.

The strength of adhesives or adhesive joints is influenced by a variety of factors. It is difficult to choose the optimum adhesive in every respect. In general, duromer adhesives would be the most suitable, as they can usually achieve high strengths and, with the appropriate chemical composition, can also achieve adequate water resistance and thus better durability. According to the literature review (Ammann et al., 2016; Konnerth et al., 2016; Aicher and Reinhardt, 2006; Knorz et al., 2015; Franke et al., 2014), PRF and PUR would be the most suitable adhesives for use in combination with beech wood, but the results of delamination tests also show a good behaviour of MUF. However, under mild climatic conditions and with appropriate surface preparation, the requirements of the standard can also be achieved with EPI adhesives.

The adhesives predominantly used for structural joints (phenolic and aminoplast adhesives) exhibit very brittle behaviour, while polyurethanes show ductile behaviour. The most commonly used adhesive for wooden components, especially in Slovenia, is melamine-urea-formaldehyde (MUF). This is because of the combination of MUF adhesive and softwood results in strong and durable glue lines that are resistant to temperature and humidity variations in the environment. However, in the past, phenol-resorcinol-formaldehyde was a commonly used wood adhesive for structural purposes (Serrano) and is considered one of the most stable and moisture resistant adhesive types (Frihart, 2009). Due to its dark brown colour and the fact that it contains a phenolic component, the use of PRF is declining (depending on the service class). Polyurethane adhesives (PU) are also increasingly used for structural purposes, but their poorer resistance to changes in moisture content has proven to be their weakness (Knorz et al., 2015; Konnerth et al., 2016). For the above reasons, the decision was made to use the MUF and PRF adhesives for the experimental tests in this dissertation.

3 EXPERIMENTAL INVESTIGATION

The experimental part of the dissertation is divided into two subsections. In the first, the experimental testing of finger joints in tension is presented. Three different profile configurations were tested and three types of adhesives were used. In the first part of the study, the two shorter finger joint profiles were tested in tension. The first batch of finger joints consisted of 53 specimens of 10 mm finger joints. MUF and PRF adhesives were used to evaluate the effect of adhesive type on tensile strength. The second batch consisted of 79 specimens of 18 mm finger joints, for which MUF and PRF adhesives were also used. However, the variable of pressure applied during assembly of the finger joints was also included. Therefore, the group of finger joints bonded with MUF adhesive was further divided into two groups. The first group of finger joints was pressed at a pressure of 5 N/mm^2, while the second group was pressed at a pressure of 10 N/mm^2. The specimens of the 10 mm and 18 mm finger joints were then tested in tension. Based on the results presented in the following sections, it became clear that stronger finger joints were required for installation in the glued laminated beech beams and that the use of PRF adhesive did not provide any benefits for longer finger joints. For this reason, the new cutting head was designed with a longer and more slimmer profile. A final series of test specimens with 40 mm finger joints was also made with two types of adhesive, except that in this case another melamin-urea-formaldehyde type of adhesive, denoted as GP (GripPro), was used instead of PRF. The test program for the tensile testing of the finger joints is shown in Tab. 3.1.

The glued laminated beams were produced in two batches from Slovenian beech wood. In the first one, 10 glued laminated beams with 18 mm finger joints were produced in the production line, and in the second one, 4 glued laminated glued laminated beams with 40 mm finger joints were produced. The laminations of these 4 beams were joined longitudinally manually while the laminations were stacked and pressed together in the production line. More details can be found later in this chapter (Section 3.2). The glued laminated beams of both batches consisted of 10 laminations with a thickness of 18 mm and the nominal cross-section of all 14 beams was 10×18 cm. Both batches were glued with the MUF adhesive.

Table 3.1: The number of test specimens for individual length of finger joints and used adhesive.
Preglednica 3.1: Število preizkušancev za posamezno dolžino zobatega spoja in uporabljeno lepilo.

Length of finger joints [mm] / Adhesive type	MUF	PRF	GP
10	28	25	-
18	27 (5 N/mm^2)* + 26 (10 N/mm^2)*	26	-
40	22	-	25

*the MUF test specimens were pressed at two pressure levels

3.1 Material and test configuration

The material for all experiments came from a larger batch of wood prepared for a comprehensive study of the mechanical properties of European beech (*Fagus Sylvatica*) from Slovenia. The study was part of the international project EU HARDWOODS and the national project TIGR4smart. The beech wood was collected in the southeastern part of Slovenia. The beech logs were provided by the Gozdno Gospodarstvo (GG) Novo mesto, d.d. sawmill. Each board was plain sawn from a different log, air dried, and then sawn and planed to nominal cross-sections of 120×24 mm, 120×32 mm, 140×20 mm, and 200×16 mm. Moisture content was measured using a Brookhuis FME resistance moisture meter and after destructive testing in accordance with the standard EN 13183-1 (CEN, 2003) using the oven dry method.

For the finger joint test, each board was carefully cut into one or two shorter boards so that the board was as clean as possible at the end where the finger joint was provided. This means that there was minimal slope of grain, no red heart and, as required by the standard, there was at least $3 \times d$ distance between the cut and the knots, where d is the knot diameter. Since beech has fairly large knots, our general guideline was that the board must be knot-free at least 300 mm from the cut. Pairs of boards were randomly selected for gluing the finger joints.

Before discussing the results of the finger joint tensile tests, we refer the reader to the studies by Plos et al. (2022) and Plos et al. (2018a), which present the tensile strength results for Slovenian beech from the wood lot. Tensile strength values of all boards ranged from 5.8 to 164.1 N/mm^2 with a mean tensile strength of 72.5 N/mm^2 and a standard deviation of 31.5 N/mm^2 with fairly large coefficient of variation (43 %). The characteristic value (5$^{\text{th}}$ percentile) of the tensile strengths was 21.5 N/mm^2. The mean static modulus of elasticity and density were 16300 N/mm^2 and 710 kg/m^3, respectively. All properties were measured according to the standards EN 408 CEN (2010) and EN 384 (CEN, 2016c). The density of the boards was determined by measuring the weight and actual dimensions of each board. The statistical distributions of tensile strength and modulus of elasticity in tension of all boards are shown in Fig. 3.1. The tensile tests were performed in a tensile test construction as shown in Fig. 3.2. The boards were clamped with 1 m clamps on each side of the specimen. The load was applied with two hydraulic pistons. The load was controlled with displacements. The free length of the specimens was between 500 and 1000 mm.

3.1.1 10 mm finger joints

Finger joints were made of boards with an initial cross-section of 120×24 mm, but the width of the boards was later reduced to 70 mm due to machine limitations. The length of the boards before gluing was 1.2 m. The finger joints were manufactured by MSora d.d., a Slovenian window manufacturer, d.d. The requirements for longitudinal joints of wood for non-structural purposes differ from the requirements of the standard (CEN, 2001, 2013e). The profile is smooth without sharp fingers (Fig. 3.3) and no self-interlocking is required, as is the case with structural finger joints. For this reason, the sole purpose of this series of finger joints was to evaluate the effects of the type of adhesive on the tensile strength, as shown by the results of the preliminary numerical study of the finger joints in Section 2.5.2. The pitch $p = 6$ mm and the tip width $b = 2$ mm. The application of the adhesive and the joining of the

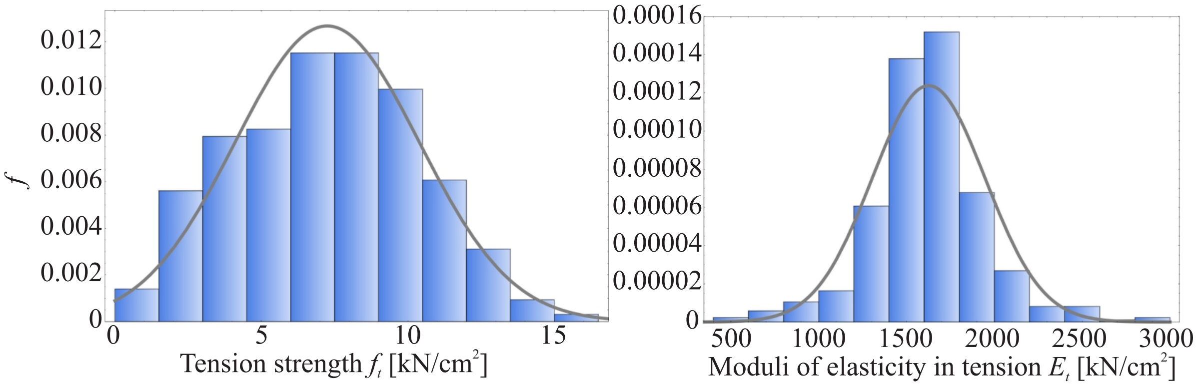

Figure 3.1: Histogram and probability density function of tensile strength f_t and modulus of elasticity in tension E_t of beech boards (Plos et al., 2022).

Slika 3.1: Histogram in gostota porazdelitve nateznih trdnosti f_t in nateznih modulov elastičnosti E_t desk iz bukovine, (Plos et al., 2022).

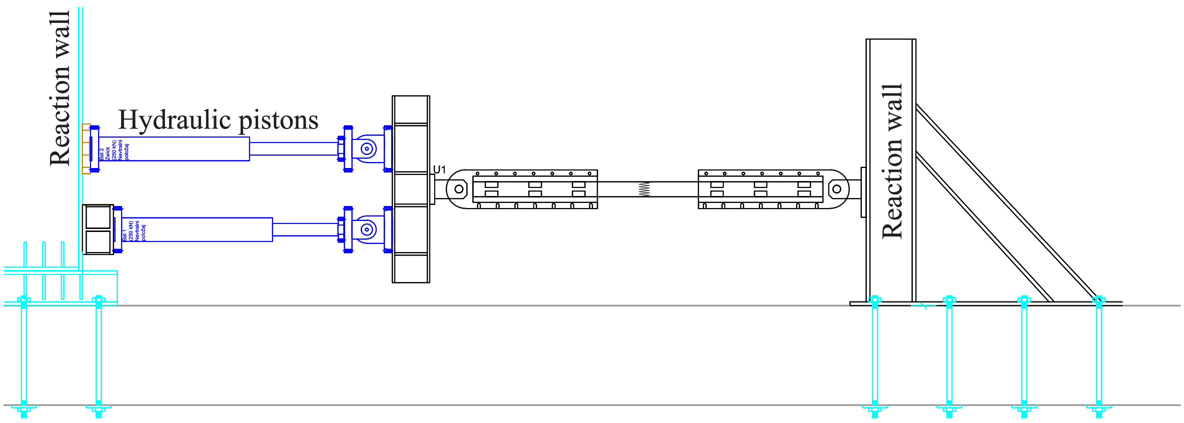

Figure 3.2: A schematic of construction for tensile tests.

Slika 3.2: Shematski prikaz konstrukcije za izvedbo nateznih testov.

boards was done manually. The joined boards were then placed in a press for 24 hours to cure (see Fig. 3.4). It can also be seen in the figure that two different adhesives were used. The first is the two-component adhesive MUF, which is manufactured by CASCO AkzoNobel for the production of load bearing timber structures and finger joints. The first component is melamine-urea adhesive 1247 and the second component is hardener 2526. This adhesive was used for 28 test specimens. The second adhesive was the two-component adhesive PRF Cascosinol Phenol Resorcinol 1711 with hardener 2520 from the same manufacturer CASCO AkzoNobel. The adhesive is approved for use in the manufacture of load bearing wood structures, but can also be used in the manufacture of doors and finger joints, as well as to other wood applications (AkzoNobel, 2017).

The specimens were then tested in tension. The tensile strengths obtained were low, but this was to be expected since the profile of the finger joints did not allow interlocking of the finger joints and the

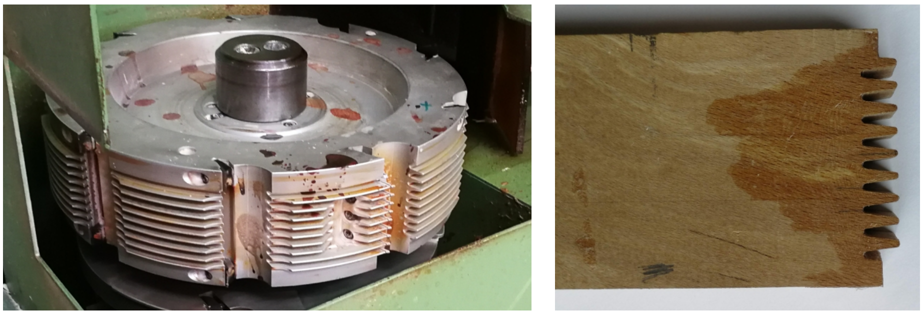

Figure 3.3: The cutting head for the 10 mm finger joint (left) and the board with the 10 mm finger joint (right).

Slika 3.3: Rezkalna glava za 10 mm dolg zobati spoj (levo) in deska z 10 mm dolgim zobatim spojem (desno).

Figure 3.4: Pressing and curing of the 10 mm finger joint.

Slika 3.4: Stiskanje in utrjevanje 10 mm dolgih zobatih spojev.

length of the finger joints was short. The maximum tensile strength achieved was 9 N/mm^2 for the MUF adhesive and 20 N/mm^2 for the PRF adhesive. Fig. 3.5 shows the results graphically. On the left side, the results are shown in a box-and-whiskers diagram, while on the right side, the values are sorted according to the tensile strength values. It can be seen that there is a significant difference between the tensile strengths of the adhesives compared. The PRF as the strongest adhesive confirms our expectations. On average, the ratio between the adhesives was about 1:2.3. Joint failure occurred regularly in the glue line (see Fig. 3.6), except for a few specimens with the adhesive PRF, which failed in the wood. However, the wood failures were entirely due to the poor quality of the wood. For example, the specimen in Fig. 3.6 (right) had a tensile strength of 19 N/mm^2, which is the second highest strength achieved, but when the value is compared with the histogram in Fig. 3.1, it is clear that the strength is very low, i.e., the quality of the wood is low.

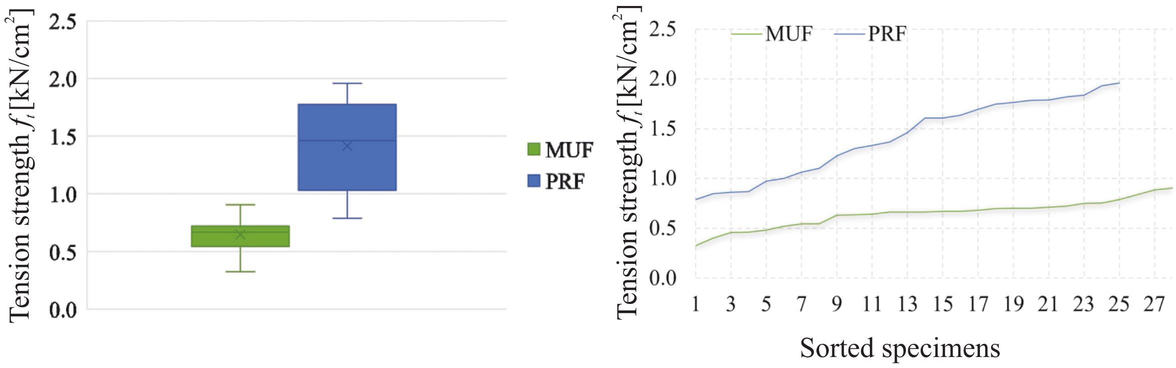

Figure 3.5: Results of tensile testing of 10 mm finger joints.
Slika 3.5: Rezultati nateznih testov 10 mm dolgih zobatih spojev.

Figure 3.6: Failure in glue line (MUF adhesive, left) and wood failure (PRF adhesive, right).
Slika 3.6: Porušitev v lepljenem spoju (lepilo MUF, levo) in porušitev v lesu (PRF, desno).

3.1.2 18 mm finger joints

The 18 mm finger joints were made on boards with a cross-section of 120 $\times$ 24 mm. The specimens were made in the Slovenian glued laminated timber factory Hoja d.d., where glued laminated beams are mainly made of spruce and fir. The finger joints were made with cutting knives otherwise used for longitudinal joining of conifers, which are characterised by lower strengths. The configuration is standard for structural finger joints, i.e., self-interlocking. The cutting head is shown in Fig. 3.7. The pitch was $p = 6$ mm and the tip width $b_t = 1$ mm. Cutting and pressing were performed automatically. Again, the same adhesive MUF 1247 with hardener 2526 and the adhesive PRF 1711 in combination with hardener 2520, both from CASCO AzkoNobel, were used. Since the company uses the MUF adhesive regularly, it was applied automatically in the production line, while the PRF adhesive was applied manually with a special brush adapted to the profile of the finger joint. Two pressure levels were used when pressing the finger joints glued with MUF adhesive: 5 N/mm^2 and 10 N/mm^2. The length of the boards before gluing was 1.5 m.
Before cutting, the boards were non-destructively tested. The dynamic modulus of elasticity E_{dyn} from the longitudinal vibrations was determined using the strength grading machine STIG from the Slovenian company ILKON d.o.o., which was developed in cooperation with our group at the University of Ljubljana, Faculty of Civil and Geodetic Engineering, and accredited for Slovenian spruce. The measurements were performed with a microphone that recorded the sound oscillations from a hammer impact

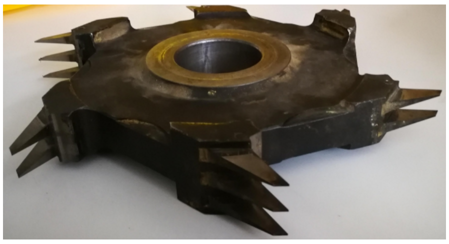

Figure 3.7: The cutting head for the 18 mm finger joint (left) and the board with the 18 mm finger joint.
Slika 3.7: Rezkalna glava za 18 mm dolg zobati spoj (levo) in deska z 18 mm dolgim zobatim spojem.

on the end of the board. In the study on the mechanical properties of Slovenian beech wood (Fortuna et al., 2018a), the correlations of the machine measurements with the STIG and the strength determining properties were reported. To assess the influence of jointing on nondestructive testing, measurements of E_{dyn} were repeated after cutting and gluing. The correlations between the measured dynamic modulus of elasticity E_{dyn} and tensile strength f_t and static modulus of elasticity E_t were $R = 0.47$ and 0.66, respectively. To evaluate the effect of joining on nondestructive testing, the measurements of E_{dyn} were repeated on the entire lamination after cutting and bonding. Strength classes were assigned according to the proposal of Fortuna et al. (2018a). The limiting values for the measured property E_{dyn} can be found in Tab. 3.2 along with the strength class assignment according to EN 338:2016 (CEN, 2016b). The limiting values can be considered as a settings for machine strength grading of Slovenian beech wood, but they have not yet been certified by the corresponding technical committee.

The glued specimens were then tested for tensile strength and static modulus of elasticity. The test length without restraint, was 1.20 m and the finger joint was positioned midway, between the clamps. The deformations of the glue line are quite difficult to measure because it is difficult to exclude the deformation of the wood within the measured length and special testing equipment is required (Serrano). Therefore, it was decided to measure the deformations in the same way as is commonly used for tensile tests on whole boards, i.e., with linear variable displacement transformers (LVDTs) and at a reference length l_0 equal to $5 \times b$, where b is the board width, i.e., l_0 = 600 mm (Fig. 3.8). Due to the reference length, most of the deformation was the result of the deformation of the wood and only a small part of the deformation was caused by the glue. It was not possible to determine the actual contributions of each component. Since the deformation obtained is a combination of glue and wood deformation, the quality of the whole joint and the area around the joint was evaluated. When working in the laboratory, higher accuracy the elastic modulus E_t measurements was observed when the loading cycle was repeated three times (Fig. 3.9). It was decided to follow this approach and use the data from the second and third loading cycles for further analysis. To avoid damaging the specimens, they were loaded up to 30 kN. The last displacement measurement was taken into account when calculating the elastic modulus. Before further loading, the LVDTs were removed and the specimens were tested to failure. The position of the clamping system remained unchanged.

The results of the tensile tests on 18 mm finger joints are shown in Tab. 3.3. The average tensile strength value for all specimens was 43.4 N/mm^2 and the 5th percentile was 15.0 N/mm^2. More than 40 % of the MUF specimens and more than 65 % of the PRF specimens failed in the wood. 17 of 22 MUF specimens

Table 3.2: Strength class assignment for Slovenian beech wood according to previous study (Fortuna et al., 2018a)

Preglednica 3.2: Razvrstitev lesa slovenskega bukovega lesa v trdnostne razrede v skladu s predhodnimi raziskavami (Fortuna et al., 2018a).

EN 338 strength class	Settings (minimal requirements) for E_{dyn} [N/mm^2]
D60	18666
D50	16496
D35	11539

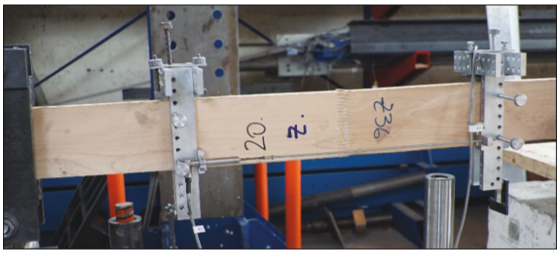

Figure 3.8: Experimental measurements of elastic modulus in tension of 18 mm finger joint with MUF adhesive.

Slika 3.8: Eksperimentalne meritve nateznega modula elastičnosti 18 mm dolgega zobatega spoja z lepilom MUF.

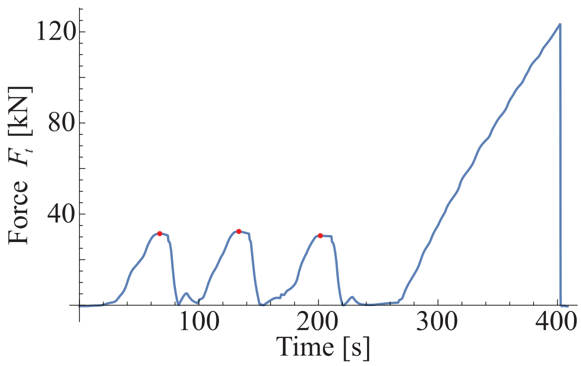

Figure 3.9: Diagram of the tension loading of the board for the determination of the static modulus of elasticiy in tension E_t.

Slika 3.9: Diagram obremenjevanja deske v nategu za določitev statičnega modula elastičnosti v nategu E_t.

failed outside the joint area (mid 600 mm) due to fibre orientation. The tensile strength of the wood fibres was reached in 2 specimens meaning that the tensile strength of finger joints was higher than of wood. At PRF adhesive, 14 of 17 specimens failed due to the slope of grain outside the finger joint area, 2 failed inside the finger joint area, and 1 cracked due to wood fibre failure. The strengths of the finger

Table 3.3: Statistical values for tensile strength, modulus of elasticity in tension and dynamic modulus of elasticity for specimens divided into six groups by the type of adhesive, assembling pressure and type of failure for 18 mm finger joints.

Preglednica 3.3: Statistične vrednosti nateznih trdnosti, nateznega modula elastičnosti in dinamičnega modula elastičnosti preizkušancev razdeljenih v šest skupin glede na tip lepila, pritiska pri stiskanju in načina porušitve za 18 mm dolge zobate spoje.

	Wood failure			Joint failure		
f_t[N/mm^2]	MUF (5 N/mm^2)	MUF (10 N/mm^2)	PRF (10 N/mm^2)	MUF (5 N/mm^2)	MUF (10 N/mm^2)	PRF (10 N/mm^2)
5th percentile	23.0	15.3	11.2	23.0	36.7	42.4
Mean	42.0	35.5	32.7	47.6	50.5	54.1
St. deviation	12.3	14.9	16.8	16.5	8.3	10.2
N	13	9	17	14	17	9
Mean E_t[N/mm^2]	17500	16600	16500	17900	18300	17800
Mean E_{dyn}[N/mm^2]	15900	14500	15300	16900	16300	16900

joints are relatively low, especially when compared to the study presented by Aicher et al. (2001), in which 20 mm finger joints were tested on beech wood with a melamine adhesive and a weighted average tensile strength of 62 N/mm^2 was obtained. One of the reasons for the difference could be the difference in manufacturing precision and pressure applied. In the present study, quite a number of the specimens cracked in the joint area during the gluing and pressing process. This could be due to dull cutting finger joint knives. Although the boards were not graded according to the standard for visual strength grading of hardwoods, some slope of grain and discoloration were observed, which could be the reason for lower strength values in Tab. 3.4. It is suspected that the most important reason for the lower strengths is the test arrangement. The tests were conducted in accordance with EN 408 CEN (2010), with a test span of $9 \times h$ for the determination of elastic modulus in tension and tensile strength. With such a long test span, it is more likely that fracture will occur in the wood because more weak points of the wood are included. This was the case in this study, where quite a few wood failures occurred outside the joint area, i.e., 300 mm from the glue line. In the study by Aicher et al. (2001), the distance between the clamps was only $4 \times h$, which could have an influence on the higher strengths obtained. However, the mean value of all specimens is in the range of tensile strengths reported by other researchers (Aicher and Klöck, 2001; Blaß et al., 2005; Franke et al., 2014).

When comparing the two adhesive types, it is noticeable that the specimens bonded with PRF (Fig. 3.10, left) have slightly higher values, but the ANOVA (for $\alpha = 0.05$) showed that the null hypothesis, which states that the adhesive type has no influence on the tensile strength, cannot be rejected with a p-value being 0.11. In the case of the adhesive PRF, a high percentage of wood failure was observed. This means that the measured strengths represent the tensile strength of the wood. Previous studies indicate that higher strength properties can be expected for European beech wood (Ehrhart et al., 2018a; Fortuna et al., 2018a). In the Fig. 3.10 (right) the results of the dynamic modulus of elasticity with the tensile strength of individual boards are shown for all specimens that failed in wood and in finger joint separately. The correlation coefficient of those who failed in finger joint is practically 0, while the correlation of those

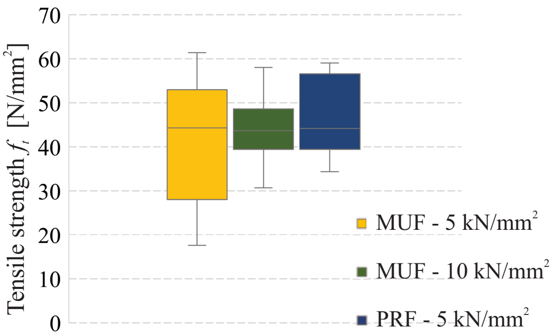

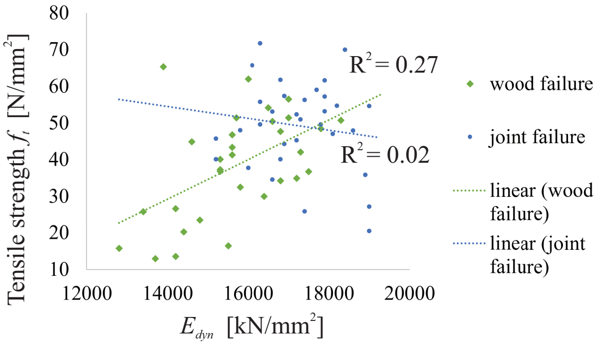

E_{dyn}/-	Wood failure	Joint failure	All
f_t	0.52	-0.14	0.40
E_t	0.44	0.32	0.48

Figure 3.10: Box and whiskers plots of tensile strengths for three groups of finger joints that failed in the glue line (left) and correlation of dynamic modulus of elasticity measured on joined boards and tensile strength of the finger joint specimens (right).
Slika 3.10: Škatlasti diagram nateznih trdnosti za tri skupine zobatih spojev, s porušitvijo v stiku (levo) in korelacija med dinamičnim modulom elastičnosti zlepljenih desk in natezno trdnostjo zobatega spoja (desno).

who failed in wood is better as expected. Tab. 3.3 lists the strengths for the specimens that failed in the glue joint separately by glue and pressure used. The results are consistent with the numerical simulation results, where the influence of the adhesive type decreased as the length of the finger joints increased, and the selected finger joint profile became the influential parameter for increasing the strength (Fig. 2.11). The difference between the strengths of specimens with different clamping pressure was not observed.

The dynamic modulus of elasticity measurements were performed on individual boards just before gluing and then repeated on the glued boards. The results of the grading based on the dynamic elastic modulus measurements, are shown in Tab. 3.4. No measurements were performed for 16 specimens, so they were not included in further analysis. According to the settings presented in presented in Tab. 3.2 (Fortuna et al., 2018a), the majority of the individual boards were graded as D50 and D35. Approximately 15 % of the boards were graded as D60 and less than 4 % were rejected. The grading results of the individual boards are shown in Tab. 3.4.
Figure 3.11 (left) shows the comparison between the dynamic modulus of elasticity of the glued boards and the average value of the dynamic moduli of elasticity of the two individual boards measured before gluing. In most cases, the average value of two boards was smaller than the measured value of the joined boards. The correlation coefficient R was 0.72. The grading results of the joined boards changed compared to the individual boards. The yield increased in the upper strength classes and there were no rejected boards. Figure 3.11 (right) shows the relationship between the measured dynamic modulus of elasticity and the tensile strength of all joined boards (wood and joint failure) for each strength class. The correlation between the measured E_{dyn} and the tensile strength was analysed. Including all specimens (wood and joint failure), the correlation R was 0.40 for tensile strength f_t and 0.48 for the static modulus of elasticity E_t and is similar to what can be expected for beech wood (Fortuna et al., 2018a). When analysing specimens grouped by type of failure, these correlations changed significantly. In the

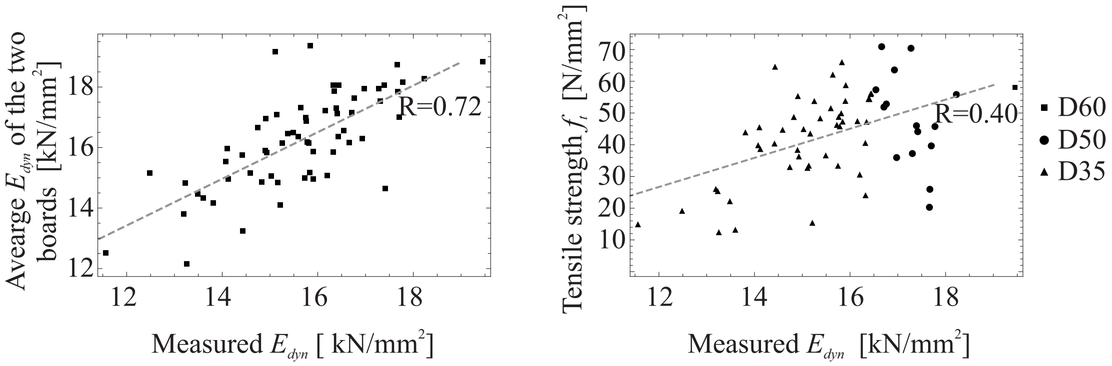

Figure 3.11: Correlation between the dynamic modulus of elasticity on boards (average of the two single boards) before gluing and dynamic modulus of elasticity on glued boards (left) and grading results, based on dynamic modulus of elasticity on glued boards and associated tensile strength (right).
Slika 3.11: Korelacija med dinamičnim modulom elastičnosti desk (povprečje dveh posameznih desk) pred lepljenjem in dinamičnim modulom elastičnosti zlepljenih desk (levo) in rezultati razvrščanja na osnovi dinamičnega modula elastičnosti na zlepljenih deskah in pripadajoča natezna trdnost.

Table 3.4: Strength class assignment for separate boards on the basis of settings from Tab. 3.2 (tensile strength of the corresponding finger joint).
Preglednica 3.4: Razvrstitev v trdnostne razrede posameznih desk glede na nastavitve iz Tab. 3.2 (natezne trdnosti pripadajočega zobatega spoja).

	board 1		board 2		joined boards	
EN 338 strength class	N	Mean f_t [N/mm^2]	N	Mean f_t [N/mm^2]	N	Mean f_t [N/mm^2]
D60	12	43.1	7	48.1	17	57.9
D50	23	48.0	22	42.7	31	47.3
D35	26	40.0	31	45.1	15	42.5
Reject	2	36.4	3	19.5	0	-

case of the group with joint failure (Fig. 3.12), the correlation was negative (Figure 3.10, right) and not statistically significant. It can be concluded that the dynamic modulus of elasticity cannot be used as an indicator of the tensile strength of the finger joints. However, in the case of wood failure, the correlation was $R = 0.52$, which is a relatively high correlation for a non-destructively measured property that can be easily and quickly determined and potentially incorporated into glued laminated beams production as part of the structural element manufacturing process and used as an indicator of the overall lamination quality.

The results of the experimental testing of the 18 mm finger joints confirmed the trend that had been indicated in by the preliminary research, that the influence of the adhesive decreases with increasing length of the finger joints. The strengths obtained were rather low and strongly influenced by the specimens failing in wood. However, higher stresses (also in wood) were to be expected.

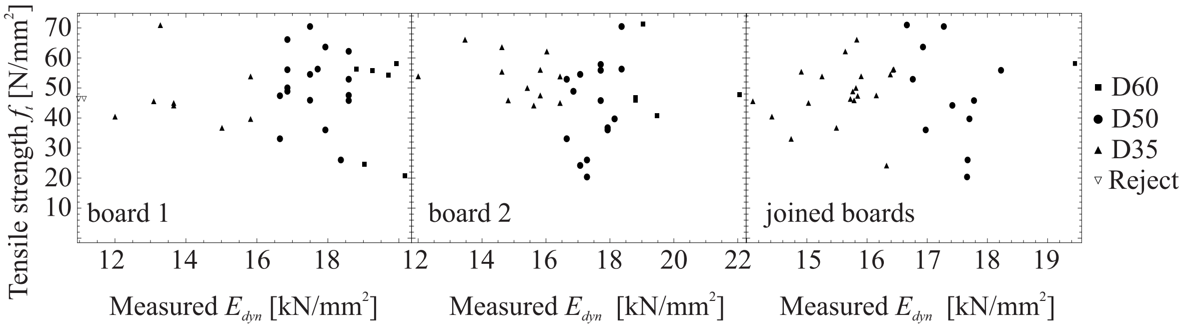

Figure 3.12: Results of the grading based on the measurements of dynamic modulus of elasticity for single boards before gluing and dynamic modulus of elasticity on joined boards with associated tensile strength (specimens failed in finger joint).

Slika 3.12: Rezultati razvrščanja na osnovi dinamičnega modula elastičnosti posameznih desk pred lepljenjem in na osnovi dinamičnega modula elastičnosti zlepljenih desk s pripadajočo natezno trdnostjo (preizkušanci s porušitvijo v zobatem spoju).

3.1.3 40 mm finger joints

As shown in the previous sections, stronger finger joints are required to join beech wood. The new profile of the fingers was designed based on the preliminary theoretical investigations (see Fig. 3.13). The influence of the type of adhesive on the final tensile strength was tested to obtain the actual tensile strength. The goal was to obtain strengths between 55 and 60 N/mm^2, as indicated by the numerical model of the finger joints, see Section 2.2.3.

The production of the proposed slender profiles requires the manufacture of suitable cutting heads. This has its own limitations and proved to be somewhat of a challenge. After discussions with cutting head manufacturers and adjustments to the geometry, the final finger joint profile was selected as follows: $l = 40$ mm, $p = 8$ mm, and $b_t = 1.5$ mm. The profile is shown in Fig. 3.13. Originally, we intended to install the cutting head in the finger jointing line of the Slovenian glulam manufacturer Hoja d.d., where finger joints with the standard geometry and a length of 18 mm were produced for the purpose of this study (see Chapter 3). Unfortunately, the machinery was not suitable for cutting heads for longer finger joints. Therefore, the cutting head was installed in the computer numerical controlled machine, better known as CNC machine, in the Slovenian carpentry company Tesarstvo in krovstvo Štebe d.o.o. More details about the production can be found in Chapter 3. The boards for the finger joints were from the same batch as the two shorter finger joint profiles. The cross-section of the boards was 100×18 mm and they were 1.5 m long. The mean density was 692 kg/m^3 with a standard deviation of 41 kg/m^3. There were 50 specimens in total. The finger joints were glued with two types of adhesives. The first was MUF adhesive 1247 with hardener 2526 (the same as used for the 10 mm and 18 mm finger joints). The second was also the MUF adhesive and from the same manufacturer, CASCO AkzoNOBEL, but with a different chemical composition. It consists of a liquid melamine resin adhesive A002 and a liquid hardener H002 with the trade name GripPro (GP). It has been specially developed for gluing hardwoods such as oak, chestnut, birch, and beech. It is designed to be more flexible and to have high water and weather resistance. The production of finger joints was not automated. The finger joints were cut using

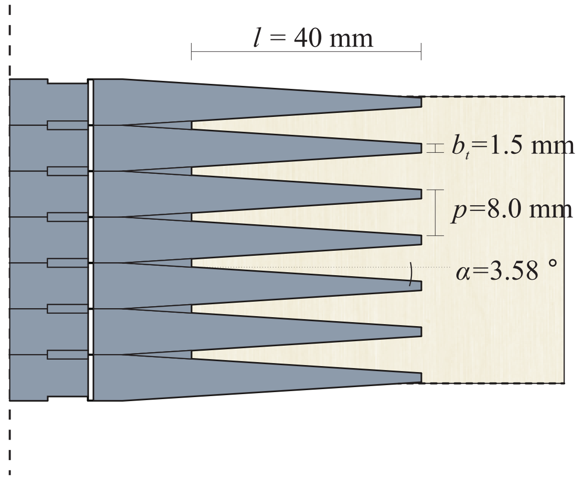

Figure 3.13: The geometry of the chosen profile of the finger joint (cutting head).
Slika 3.13: Geometrija izbranega profila zobatega spoja (rezkalna glava).

a CNC machine equipped with a specially designed cutting head Fig. 3.14. Beech is a relatively brittle and hard wood and there was some difficulty in obtaining clean cuts. It would seem that reducing the cutting speed would help, but this was not possible with the machine used. The problems were solved by cutting the finger joints in small batches of 4 boards at a time. The adhesive was applied within a few seconds after cutting using a special 3D-printed brush with suitable geometry. The specified open assembly times of the adhesives were not exceeded. This was 5 minutes for the MUF adhesive and 20 minutes for the GP adhesive. After application of the adhesive, the finger joints were pressed together with a minimum pressure of 5 N/mm^2 for the MUF adhesive and 1.4 N/mm^2 for the GP adhesive. The pressure was applied manually with a special pressing device, Fig. 3.15, and the pressure was recorded with a force sensor. The finger joints were then stored under controlled conditions and cured for about two months before the tensile test. Glued 40 mm finger joint is shown in Fig. 3.16.
For the 40 mm finger joints, the test configuration of the 18 mm finger joint was slightly modified. The free span between the clamps was reduced to 500 mm, so that the tests were more restricted to the finger joint area. The test configuration is shown in Fig. 3.17. Tensile strength and static modulus of elasticity under tension were determined.
The deformations were measured using a 3D optical measurement software called GOM. The plates were sprayed with a stochastic pattern over the 40 mm finger joints. The GOM software provides an option with a continuous displacement field over the surface so that the deformation of the entire specimen is recorded. The application of the load was monitored every second throughout the test. Photographs were taken with two Nikon D850 cameras in image format DX, i.e., 5408×3600 pixel resolution. The cameras were positioned 600 mm away from the specimens.

The static modulus of elasticity in tension was calculated based on the relative deformation of the distance between two selected points. A total of 30 points were systematically selected on the surface around the finger joint, so that we obtained measurements for 15 distances with an initial length of 40 mm. The distances were positioned at the top, center, and bottom of the board. Groups of the three distances across the width of the board were positioned on the left side of the finger joint, above the finger joint, and on the right side of the board, as shown in Fig. 3.18. To evaluate the accuracy of the measurement system, the middle column of distances was repeated two more times in close proximity. Fig. 3.19 shows the

Figure 3.14: The cutting head for the 40 mm finger joint mounted on a CNC machine.
Slika 3.14: Rezkalna glava za 40 mm dolg zobati spoj nameščena na CNC stroj.

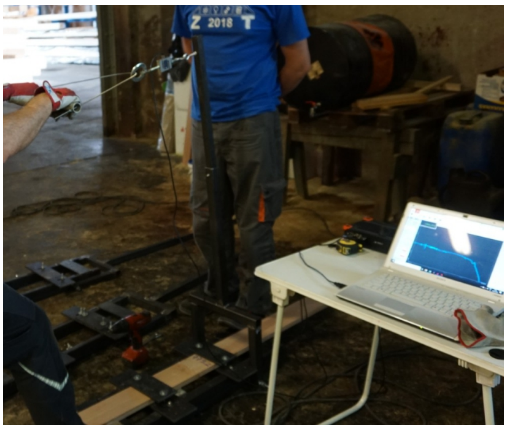

Figure 3.15: Pressing device for pressing the finger joints with controlled pressure application, prototype on the left picture and final version on the right picture.
Slika 3.15: Naprava za stiskanje zobatih spojev pod kotroliranim nanosom pritiska, prototip na levi sliki in končna izvedba na desni sliki.

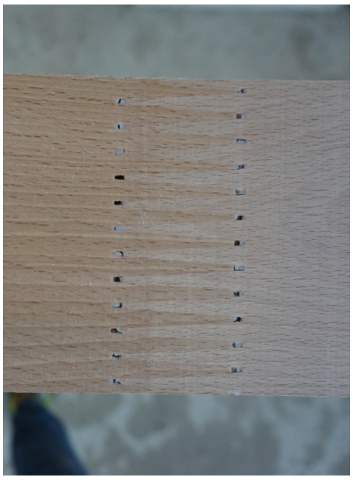

Figure 3.16: Glued 40 mm finger joint.
Slika 3.16: Zlepljen 40 mm dolg zobati spoj.

Figure 3.17: Test configurations and specimen after failure in tension.
Slika 3.17: Postavitev testa in preizkušanec po natezni porušitvi.

maximum differences between the moduli of elasticity in tension measured at the same location (gray triangles) and between modulus over the width of the boards (dark green dots). It can be seen that the majority of the gray triangles are quite low and the differences between the elastic moduli across the width of the board are relatively high. Therefore, the moduli of elasticity in tension were calculated as the average of all 15 measurements, excluding outliers. The mean values of the moduli of elasticity in tension for the finger joint specimens, which were divided into four groups depending on the type of failure and adhesive, are shown in Tab. 3.5. Three specimens were excluded due to poor displacement measurements. Fig. 3.23 shows the measured moduli of elasticity in tension for all finger joints. The measurements are lognormally distributed. This was also confirmed by the Kolmogorov-Smirnov test with an assumed confidence value $\alpha = 0.05$.

The axial deformations around a finger joint is shown in Fig. 3.20. They are shown at a time before the fracture and immediately after the fracture. The GOM software detected some deformations formed around the fingertips, but no clear deformations were seen along the glue line of the fingers.
The statistical values for the tensile strength of the 40 mm finger joints are shown in Tab. 3.5. The mean tensile strength for all finger joints was 55.8 N/mm^2, which is in line with the expectations of the preliminary study. The average tensile strength for all 18 mm finger joints was 37.7 N/mm^2. This means that we able to increase the average tensile strength by almost 50 % just by increasing the length of the finger joints. It should be noted that only the MUF type of adhesive was used for 40 mm finger joints, while for the 18 mm finger joints, we also used the PRF adhesive, for which according to the literature (Knorz et al., 2015; Konnerth et al., 2016), higher strengths can be expected. This was proven also by the experimental results since most of the highest values for tensile strength of the 18 mm finger joints were obtained with the PRF adhesive.
The comparison of the finger joints between the two adhesives types, MUF and GP, is shown in Fig. 3.21. It can be seen that there is no significant difference between the two groups of finger joints, which was confirmed by the ANOVA test, where the p-value was 0.64. Such results were expected mainly for two reasons. The first reason was the preliminary study and experimental test result for 18 mm finger joints. The second reason is that the MUF adhesive modified for hardwood, i.e. GP, was not declared as a

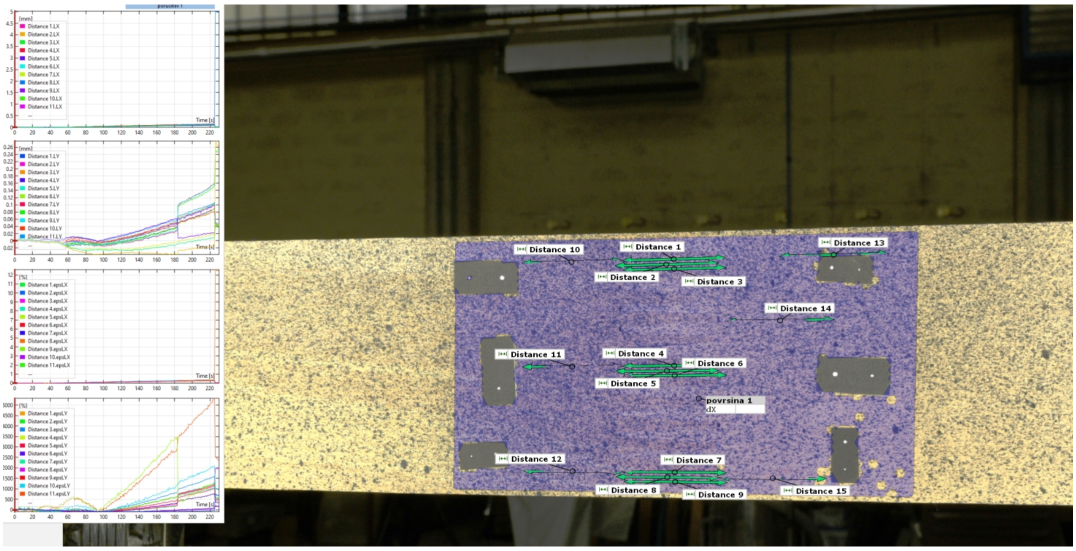

Figure 3.18: An example of a specimen in GOM 2018 Professional software with tagged distances for the determination of the static modulus of elasticity in tension.

Slika 3.18: Primer vzorca v programu GOM 2018 Professional z označenimi razdaljami za določitev statičnega modula elastičnosti v nategu.

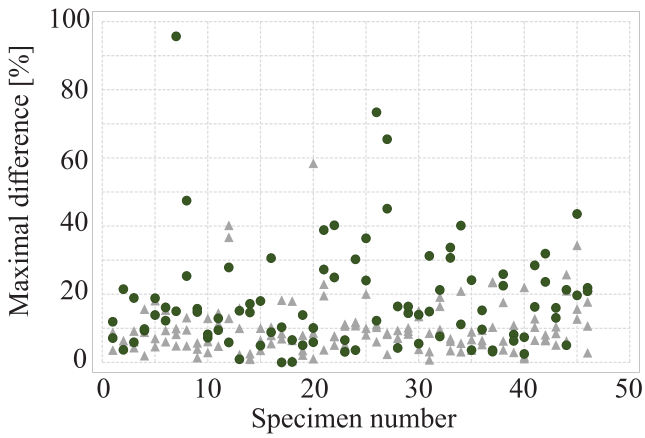

Figure 3.19: Maximal differences of moduli of elasticity within measurements in the same position (gray triangles) and between measurements over the width of the boards(green dots) in percent.

Slika 3.19: Največja odstopanja modulov elastičnosti znotraj meritev na istem mestu (sivi trikotniki) in znotraj meritev po širini desk (temno zelene pike) v odstotkih.

stronger adhesive but as a more durable and resistant adhesive. Since there is no statistically significant difference between the tensions strength obtained with one adhesive or the other, it would be recommended to use the adhesive GP to obtain more durable and stable joints.

Considering the type of failure, the GP group showed better results, as more than 90 % of the specimens failed in wood, while for the MUF group only approximately 64 % of the finger joint failed in wood, but this could also be due to the relatively small number of specimens. The two failure modes of 40 mm finger joints are shown in Fig. 3.22. The mean modulus of elasticity of the finger joints of all the tested 40 mm finger joints was 12100 N/mm^2. The minimum, maximum and mean values for groups of

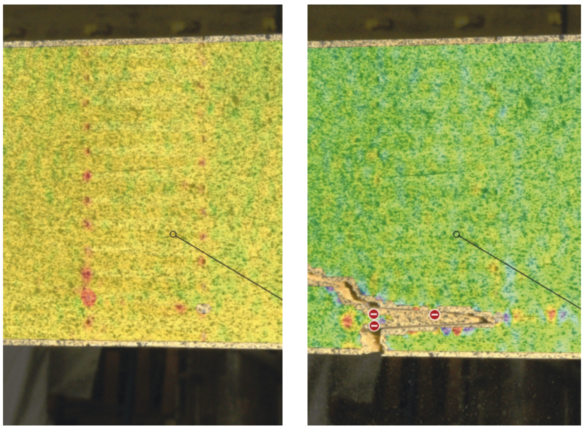

Figure 3.20: The longitudinal deformation ε_X of finger joint area a moment before a failure (left) and right after the rupture (right) from GOM software.

Slika 3.20: Osna deformacija ε_X območja zobatega spoja trenutek pred porušitvijo (levo) in takoj po porušitvi (desno) iz programa GOM.

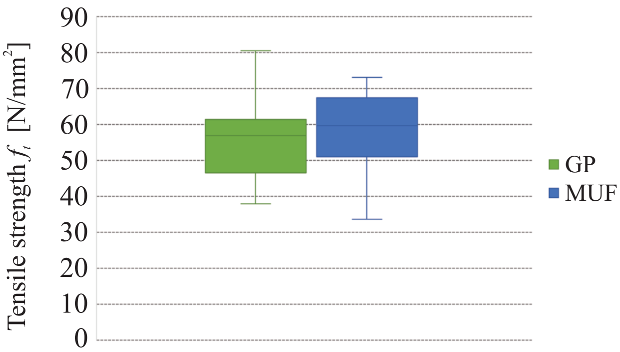

Figure 3.21: Box and Whiskers plots of tensile strengths for four groups of 40 mm finger joints divided by type of adhesive.

Slika 3.21: Škatlasti diagram nateznih trdnosti za štiri skupine 40 mm dolgih zobatih spojev razdeljenih glede na vrsto lepila.

Figure 3.22: Failure of the 40 mm finger joint in the joint (left) and failure in wood (right).

Slika 3.22: Porušitev 40 mm dolgega zobatega spoja po stiku (levo) in porušitev po lesu (desno).

Table 3.5: Statistical values for tensile strength and modulus of elasticity in tension for 40 mm finger joints, divided into four groups by the type of adhesive and type of failure.
Preglednica 3.5: Statistične vrednosti o natezni trdnosti in statičnih modululov elastičnosti 40 mm dolgih zobatih spojev, razdeljenih v štiri skupine glede na vrsto lepila in tip porušitve.

	Wood failure		Joint Failure	
f_t [N/mm^2]	GP	MUF	GP	MUF
Min	14.8	25.9	59.1	51.9
Max	80.6	73.2	69.1	72.0
Mean	54.2	53.3	64.1	63.0
5$^{\text{th}}$ percentile	38.2	31.0	59.6	52.3
E_t [N/mm^2]				
Min	8790	9450	12900	9490
Max	15500	14300	13000	13800
Mean	12400	11500	12900	12300
N	23	14	2	8

joints divided by type of failure and type of adhesive are shown in Tab. 3.5. In Fig. 3.23 the histogram of the measured modulus of elasticity are shown with the probability density function of the log normal distribution.

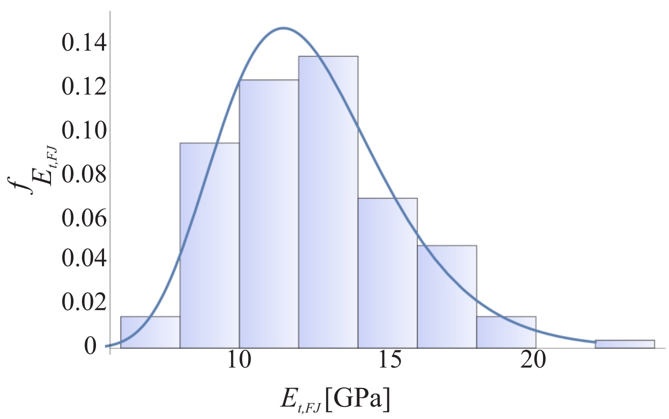

Figure 3.23: Probability density function for lognormal distribution and histogram of measured moduli of elasticity $E_{t,\mathrm{FJ}}$ of the 40 mm finger joints.
Slika 3.23: Gostota porazdelitve po logaritemsko normalni porazdelitvi ter histogram izmerjenih modulov elastičnosti $E_{t,\mathrm{FJ}}$ 40 mm dolgih zobatih spojev.

3.2 Bending tests of the laminated beams made of beech wood

The four-point bending tests were performed in accordance with the standard EN 408 (CEN, 2010). The test configuration is shown in Fig. 3.24. To determine the local and global modulus of elasticity in bending, E_l and E_g, respectively, the vertical displacements were measured in three positions. For the

E_g, the displacements were measured at the midspan between the two supports. For the local modulus of elasticity E_l, two additional measurements must be made at the mid-span at a distance of $5 \times h$, where h denotes the height of the beam. The displacement was measured with the LVDTs. The load was applied symmetrically at two points at a distance of $6 \times h$. The cross-section of the beam was 180×100 mm^2.

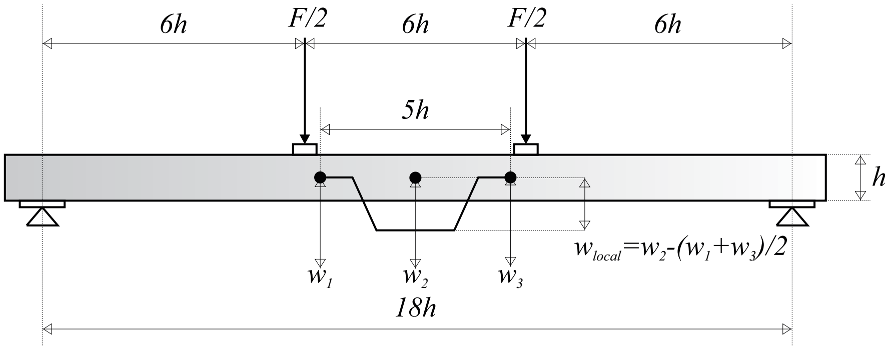

Figure 3.24: Test configuration for determination of the local and global modulus of elasticity. Adopted after EN 408(CEN, 2010).
Slika 3.24: Testna postavitev za določitev lokalnega in globalnega modula lastičnosti. Povzeto po EN 408(CEN, 2010).

The beams were divided into two groups, according to the two different finger joint profiles used in the production of the laminations. The first group of 10 laminated beams was made with 18 mm finger joints. The second group of 4 laminated beams was made with 40 mm finger joints. In order to achieve the highest possible strength, we tried to select the best boards from the batch for the laminations of these beams. The boards were selected based on the most obvious visual parameters such as knots, curvature, and slope of the grain (although the latter is very difficult to determine for beech wood).
The adhesive used was MUF adhesive 1247 with hardener 2526 and was the same for both groups. The main reason for the choice of adhesive was the fact that the company where the beams were made used this adhesive regularly, so the application of the adhesive was automated. However, the production of the beams with longer finger joints was not fully automated. As explained in Section 3.1.3, the cutting of 40 mm finger joints could not be done within the production line. Therefore, the laminations for this group of beams were joined longitudinally manually at the Tesarstvo in krovstvo Štebe facilities, where the cutting head for the 40 mm finger joints was mounted. Gluing was performed under the same conditions as in Section 3.1.3. The laminations were then transported to the facilities of Hoja, d.d., the manufacturer of the glued laminated beams. The laminations were planed to the final thickness of 18 mm and then immediately compressed into glued laminated beams on the production line (Fig. 3.25). All beams had 10 laminations.

3.2.1 Laminated beams with 18 mm finger joints

The bending strength for the first group with standard finger joint profile is shown in Tab. 3.6. The first column contains the values calculated directly from the test results. In the second column, the strengths are adjusted with a height factor, as required by the standard EN 384 (CEN, 2016c). The height factor is used to adjust and normalize the values to the height of the beam $h = 150$ mm. The mean value

Figure 3.25: Gluing of the glued laminated beams with 18 mm finger joints.
Slika 3.25: Lepljenje lameliranih nosilcev z 18 mm dolgimi zobatimi spoji.

of the adjusted bending strengths for the 10 laminated beams made with a standard finger joint profile and beech wood was 64.4 N/mm^2 with a standard deviation of 13.3 N/mm^2. Since the sample size is quite small, the 5th percentile cannot be determined very reliably. The characteristic value was calculated assuming that the bending strengths are lognormally distributed. Such an assumption is made also in the standard for calculation and verification of characteristic values of timber structures EN 14358 (CEN, 2016a). If we were to strength grade this batch of timber only on the bending strength, it would be graded as GL40. The GL stands for the strength class designation for glued laminated timber. For information, currently the certified Slovenian producers can produce glued laminated beams with the highest strength class GL28 (ZAG).

Table 3.6: Statistical values for the experimentally measured bending strength and bending strength adjusted with k_h factor (CEN, 2013e), of the glued laminated beech beams with standard finger joint geometry.
Preglednica 3.6: Statistične vrednosti o eksperimentalno izmerjenih upogibnih trdnostih ter trdnostih z upoštevanjem k_h faktorja (CEN, 2013e), lameliranih lepljenih nosilcev s standardno geometrijo zobatih spojev.

	f_b [N/mm^2]	f_b/k_h [N/mm^2]
Min	43.3	44.9
Max	84.1	87.4
Mean	62.1	64.4
5th percentile* (Lognormal distribution estimate)	39.4	41.2
St. Deviation	12.8	13.3
N	10	

*k_s factor for small samples considered in the calculation (CEN, 2016a).

All the beams failed in the area of maximum moment load, i.e., in the middle part of the span, and most of them failed in the finger joints. Fig. 3.26 shows the loaded beams just before (left image) and just after the failure of the finger joint in the middle of the span (right image). The failure of the finger joint is clearly visible and the lower lamination has separated from the beam. In Fig. 3.27, the lamination with the finger joint can be seen. The finger joint profile is nearly intact and it was determined that the failure originated here. As can be seen in the image Fig. 3.26, the rupture then continued through the lamination towards the upper laminations.

Figure 3.26: Beam with 18 mm finger joints before failure (left) and after failure (right).
Slika 3.26: Nosilec z 18 mm dolgimi zobatimi spoji pred porušitvijo (levo) in po poruštivi (desno).

Figure 3.27: Failure of the 18 mm finger joint in the lower lamination of the beam.
Slika 3.27: Porušitev 18 mm dolgega zobatega spoja v spodnji lameli nosilca.

As mentioned earlier, the local and global modulus of elasticity in bending were determined during the bending tests. The results are shown in Tab. 3.7. In most cases, the local modulus of elasticity, E_{local}, had a smaller value than the global modulus of elasticity, E_{global}, with the exception of one beam that had an extremely high value (15900 N/mm^2). If we exclude this measurement as an outlier, some correlation between the local and global moduli could be observed (Fig. 3.28). When a linear regression is performed on the data, a linear function can be written:

$$E_{\text{local}} = 1.417\, E_{\text{global}} - 8370. \tag{3.1}$$

The standard EN 384 (CEN, 2016c) provides an equation for the relationship between the local and global modulus of elasticity is given for softwood, along with the statement that special equations should be provided for hardwood. Eq. (3.1) could be used for Slovenian beech wood, but the sample size in our study is too small to reliably define a new equation.

Table 3.7: Statistical values for the of the global and local modulus of elasticity in bending of the laminated beams with standard finger joint geometry.
Preglednica 3.7: Statistične vrednosti o globalnem in lokalnem upogibnem modulu elastičnosti lameliranih nosilcev s standardno geometrijo zobatih spojev.

	E_{global} [N/mm^2]	E_{local} [N/mm^2]
Min	13300	9400
Max	16000	15900
Mean	14900	13200
N	10	

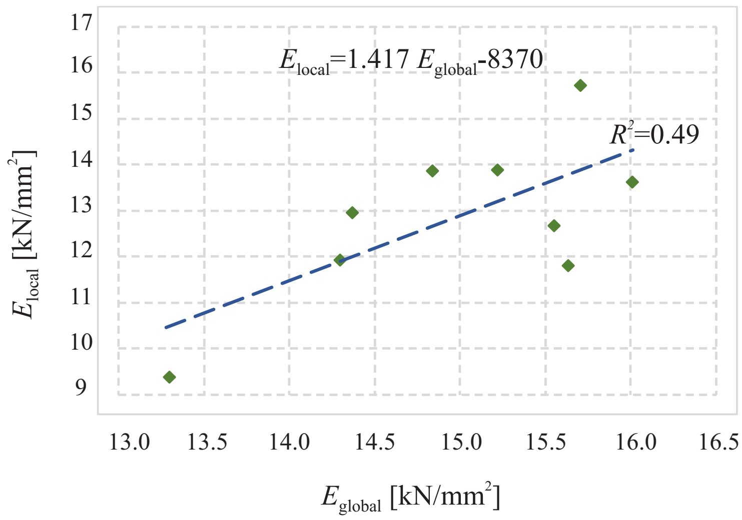

Figure 3.28: Correlation of the local and global moduli of elasticity in bending.
Slika 3.28: Korelacija med lokalnimi in globalnimi upogibnimi moduli elastičnosti.

3.2.2 Laminated beams with 40 mm finger joints

The laminations for the beams with 40 mm finger joints were thoroughly measured. A total of 88 boards were used to make the 4 glued laminated beams. The weight of each board was measured to determine the density. The mean density of the boards was 725 kg/m^3, which is slightly higher than the mean density of Slovenian beech (Fortuna et al., 2018a). Before gluing, the dynamic modulus of elasticity was also measured using the STIG strength grading machine. When strength grading was performed based on the E_{dyn} settings from Tab. 3.2, the 15 boards are graded as D60, 26 boards as D50, 42 boards as D35, and 5 boards as rejects. When gluing the laminations, we tried to place the best boards in the lower laminations, knowing that their quality would be crucial for the final bending strength of the beams. However, we had to work within the limits of the board lengths. Three beams had finger joints at mid-span, while one beam had no finger joints at mid-span. The bending test configuration for the glued laminated beams with 40 mm finger joints is shown in Fig. 3.29.

The bending strength of the laminated beams with 40 mm finger joints is shown in Tab. 3.8. Since the sample size is small, the strengths are given for all glued laminated beams with 40 mm finger joints. The mean value for all four beams was nearly 93 N/mm^2, which is a significant increase (44 %) compared to the glued laminated beams with 18 mm finger joints. The characteristic values are also given, but since the sample is small, they must be considered with caution.

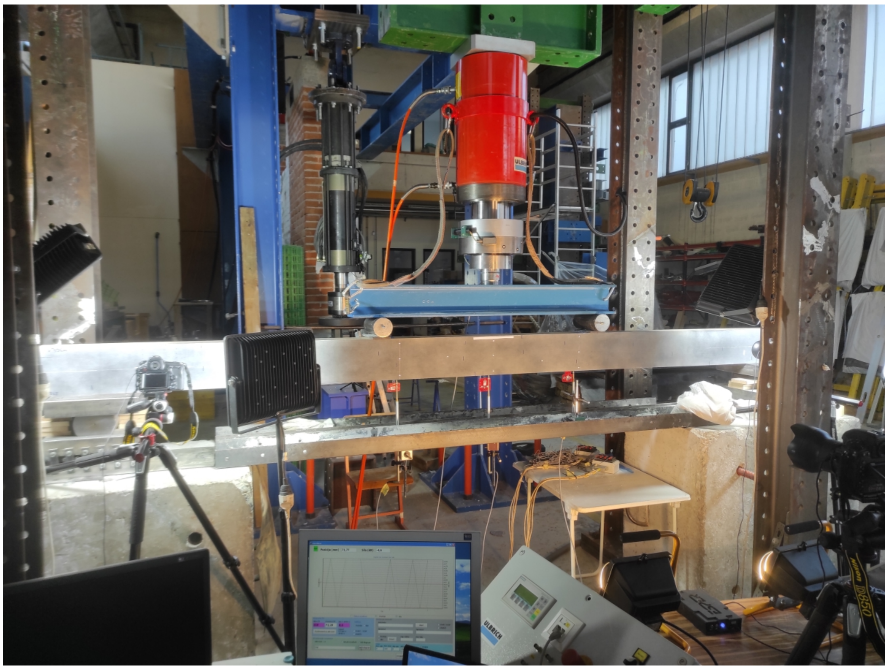

Figure 3.29: Bending test configuration for the beams with 40 mm finger joints.
Slika 3.29: Postavitev upogibnega testa za nosilce z 40 mm dolgimi zobatimi spoji.

The failures of all four beams are shown in Fig. 3.30. The first beam with the highest bending strength had a very explosive failure. There were no finger joints in the lowest lamination of this glued laminated beam. The failure was due to tensile failure of the second lamination. The stresses were extremely high and the failure was very brittle. Beam 2 failed in a mixed mode, where a smaller portion of the lower lamination failed in the finger joint and the rest of the lamination failed in the wood. Similarly, for the Beam 4, the portion that failed in the finger joint was even smaller: the crack was significantly affected by the slope of the grain. Bending strength was also lowest in this beam, so it was assumed that the material properties were somewhat weaker. Beam 3 exhibited a very noticeable finger joint failure at mid-span in the lowest lamination. As would be expected with wood, the beam failures occurred very suddenly and were brittle.

The bending tests of the laminated beams with 40 mm finger joints were also monitored using the GOM system for optical measurements. The standard EN 408 (CEN, 2010) requires that the vertical displacement of the beam should be measured at the centre of the beam height. This was not possible with LVDTs, but with the GOM system such measurements are feasible. The beams were sprayed with a stochastic pattern. Three hanging targets were placed on the back of the beam at the centre of the beam height and one at the centre of the beam span with a mutual spacing of $2.5 \times h$. Thus, the vertical displacement was measured at 6 positions. The results obtained with the GOM software are shown in

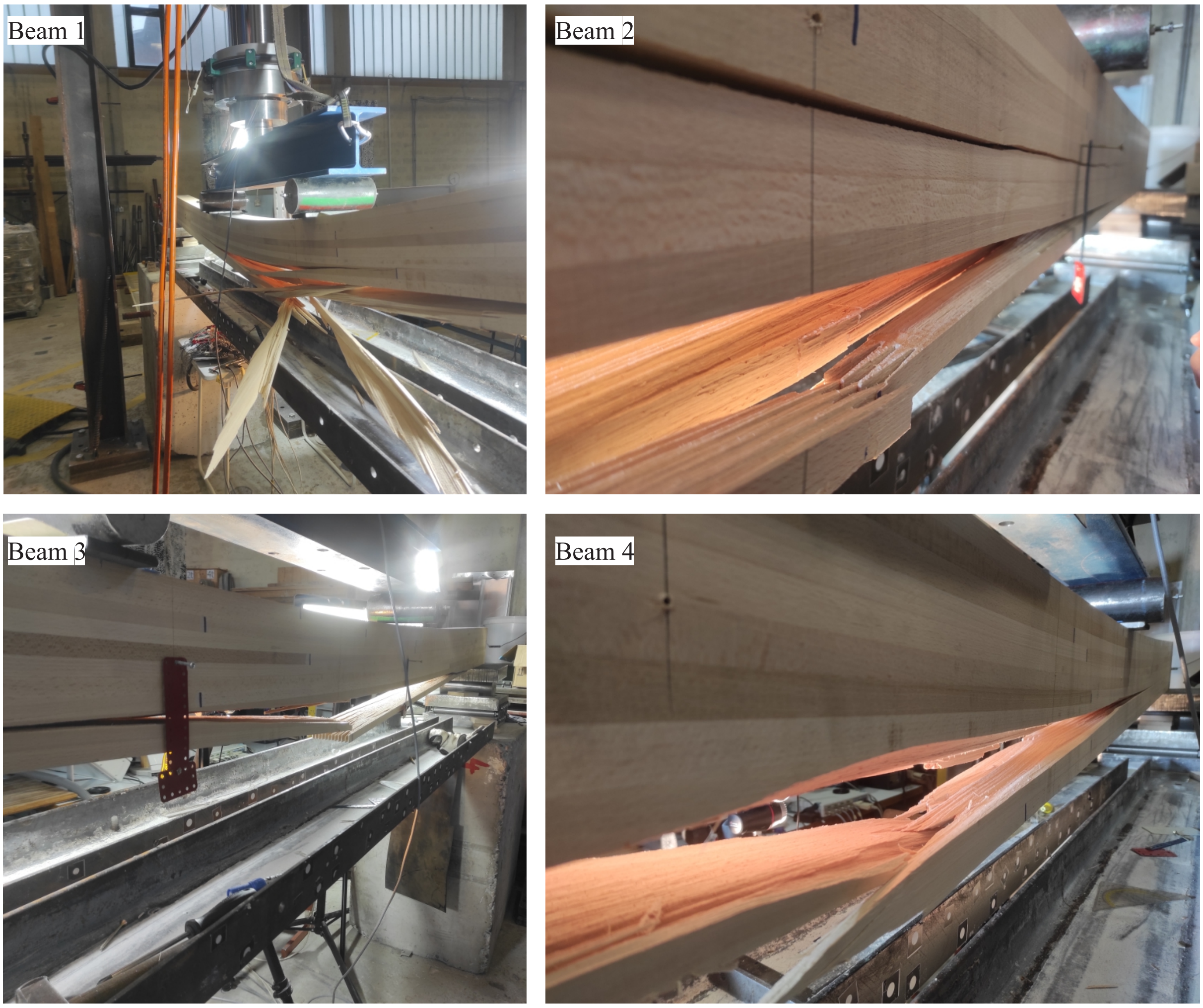

Figure 3.30: Failures of all four beams with 40 mm finger joints.
Slika 3.30: Porušitve vseh štirih nosilcev z 40 mm dolgimi zobatimi spoji.

Tab. 3.9. The relationship between force and displacement is linear, as can be seen in Fig. 3.31, where the vertical displacement for the three targets (front of the beam) is shown for the Beam 2. The results of the measured vertical displacement at the midspan for all four beams are shown in Fig. 3.32.

The moduli were calculated based on the section of the section of the load vs. displacement diagram between $0.1 \times F_{\mathrm{max}}$ and $0.4 \times F_{\mathrm{max}}$, where F_{max} is the maximum load reached. The results are listed separately for the back and front targets in Tab. 3.9. It can be seen that the elastic moduli can be very different on each side of the beam. The values of elastic moduli in bending are quite high. The average local modulus of elasticity is 19000 N/mm^2, which is more than 30 % higher than the highest required value of the modulus of elasticity for the glued laminated beams strength class GL32h (14200 N/mm^2), which is specified in the standard EN 14080 (CEN, 2013e).

There is little information in the literature on the shear modulus of beams, especially for beams made of beech wood. Similarly, there is a lack of information on the slip modulus for the glue line between the laminations (K_{X}, defined in Section 2.2). Therefore, we attempted to measure the shear deformation and shear slip between the laminates using the GOM system.
The cameras were positioned at each end of the beam where the maximum shear stresses were expected

Table 3.8: Bending strengths measured with experimental testing and bending strengths adjusted with k_h factor (CEN, 2013e), of the glued laminated beech beams with 40 mm finger joints.

Preglednica 3.8: Upogibne trdnosti izmerjene z eksperimentalnimi testi ter trdnost z upoštevanim k_h faktorjem (CEN, 2013e), lameliranih lepljenih nosilcev s 40 mm dolgimi zobatimi spoji.

Specimen name	f_b [N/mm^2]	f_b/k_h [N/mm^2]
Beam 1	112.5	116.7
Beam 2	82.9	85.9
Beam 3	81.2	84.2
Beam 4	77.5	80.3
Mean	89.6	92.9
5th percentile* (Lognormal distribution estimate)	55.5	57.6
St. Deviation	14.0	14.5

*k_h factor for small samples considered in the calculation (CEN, 2016a).

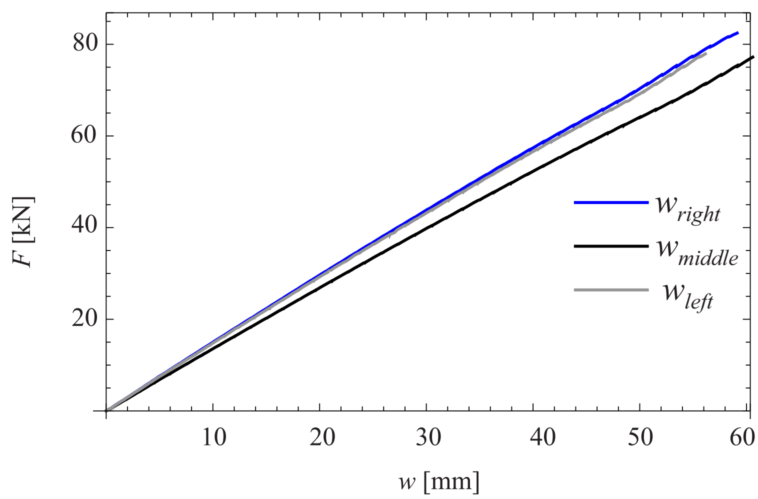

Figure 3.31: Comparison of the load/vertical displacements curves measured at three points in the middle of Beam 2 with 40 mm finger joints (targets on the front side of the beam).

Slika 3.31: Primerjava krivulj obtežba/navpični pomik izmerjenih v treh točkah na sredini Nosilca 2 s 40 mm dolgimi zobatimi spoji (tarč na sprednji strani nosilca).

to occur. The shear moduli were determined assuming a plane strain condition. As shown in Fig. 3.33, the axial deformations of "Distance 1"($\varepsilon_{\eta\eta}$) and "Distance 2"($\varepsilon_{\xi\xi}$) were measured. The two distances define a square with side length "Distance 4"(ε_{yy}) or "Distance 5"(ε_{xx}). Based on the Eq. 3.2, the shear deformation ε_{xy} was calculated. It is assumed that the shear deformation is approximately equal to half the change in the right angle between the x and y directions (Eq. 3.3). A linear regression was performed between the shear stress τ_{xy} and the shear strain $\Delta\gamma_{xy}$ was performed, and the shear modulus was calculated as $G = \tau_{xy}/\Delta\gamma_{xy}$. The results are shown in Tab. 3.10 for all beams on both sides. For the Beam 1, the results for the right end of the beam could not be determined due to poor surface quality in the GOM software. However, all measured shear moduli were within the expected values for hardwoods. The minimum measured value of shear moduli was 460 N/mm^2 and the maximum value was 1310. Comparing these values with the range of mean shear moduli for the hardwood strength classes (CEN,

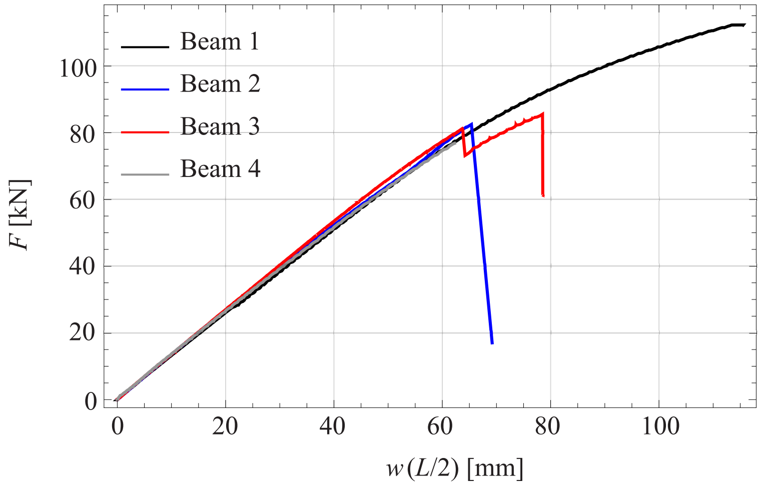

Figure 3.32: Measured load/displacement curve for vertical displacement at the mid-span of the beams.
Slika 3.32: Izmerjena krivulja obtežba/navpični pomik na sredini razpona za vse štiri nosilce.

Table 3.9: Global and local elastic moduli in bending for the laminated beams with 40 mm finger joints.
Preglednica 3.9: Globalni in lokalni elastičbi upogibni moduli lameliranih nosilcev s 40 mm dolgimi zobatimi spoji.

Specimen name	Target position	$E_{\text{global,GOM}}$ [N/mm^2]	$E_{\text{local,GOM}}$ [N/mm^2]
Beam 1	front	22300	17000
	back	24100	18500
Beam 2	front	22300	19800
	back	23600	18900
Beam 3	front	23500	20700
	back	not measured	
Beam 4	front	22900	18600
	back	22000	19700
Mean value	all targets	22000	19000

2016b), the minimum value is smaller than the required mean shear modulus for the lowest strength class, D18. The scatter of values is quite large, but the mean value of shear moduli G is 820 N/mm^2, which corresponds to strength class D40 (for sawn hardwood).

$$\varepsilon_{xy} = -\frac{1}{2\,\sin\alpha\,\cos\alpha}\left(\varepsilon_{\eta\eta} + \varepsilon_{xx}\,\sin^2\alpha - \varepsilon_{yy}\,\cos^2\alpha\right), \tag{3.2}$$

where $\alpha = \frac{\pi}{4}$ and

$$\Delta\gamma_{xy} \approx 2\,\varepsilon_{xy}. \tag{3.3}$$

The slip modulus was determined from the difference between the horizontal displacements of the two points were very close to each other, but on different laminations. For Beam 4, these were Point 41 and Point 42 (Fig. 3.33). The rotation of the entire beam was eliminated with a control length ("Distance 4"). The slip between the two points was determined only on the left side of the glued laminated beam. The results are shown in Tab. 3.11 along with the corresponding shear stress. The slip moduli were assumed to be linear and calculated as the slope of the curve $\tau_{xy}(\gamma_{xy})$.

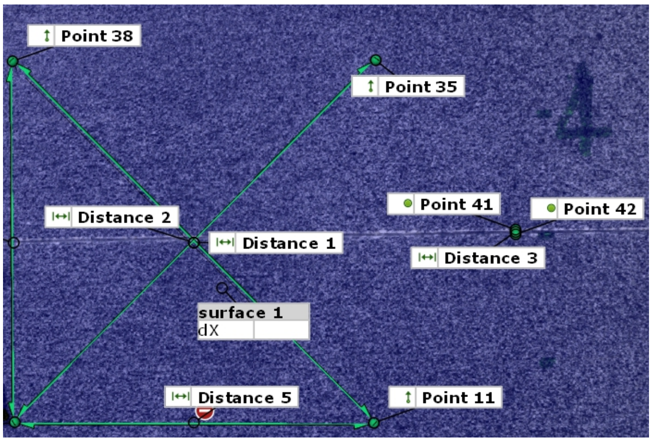

Figure 3.33: A surface model of deformations of the beam at support for determination of the shear modulus.

Slika 3.33: Model deformirane površine nosilca pri podporah v programu GOM, za določitev strižnega modula.

Table 3.10: Shear moduli for the laminated beams with 40 mm finger joints at both supports.

Preglednica 3.10: Strižni moduli lameliranih nosilcev s 40 mm dolgimi zobatimi spoji pri obeh podporah.

Specimen name	Measurement position	G [N/mm^2]
Beam 1	Right end of the beam	not measured
	Left end of the beam	640
Beam 2	Right end of the beam	780
	Left end of the beam	460
Beam 3	Right end of the beam	1090
	Left end of the beam	790
Beam 4	Right end of the beam	1310
	Left end of the beam	640
Mean value		820

Table 3.11: Measured slip between the middle laminations and corresponding shear stress of the laminated beams with 40 mm finger joints at both supports.

Preglednica 3.11: Izmerjen zdrs med sredinskima lamelama in pripadajoča strižna napetost v lameliranem nosilcu s 40 mm dolgimi zobatimi spoji.

Specimen name	γ_{xy} [rad]	τ_{xy} [kN/cm^2]	K_{X} [kN/cm^2]
Beam 1	0.0029	0.469	161.7
Beam 2	0.0022	0.345	156.8
Beam 3	0.0015	0.357	238.0
Beam 4	0.0021	0.322	153.3

4 ILLUSTRATIVE EXAMPLES

In this chapter, some illustrative examples of different configurations of laminated beams with finger joints and interlayer slip are presented. The analytical and numerical models are used to calculate the examples and the results are compared. The parametric calculations with both models for different parameters are also included in this chapter. At the end, a short stochastic analysis is shown.

4.1 Analytical model

4.1.1 Simply supported two-layer Euler-Bernoulli beam with two finger joints-analytical model

A simply supported two-layer beam is analysed using the solution derived in Section 2.3. For this example, Bernoulli theory is used, i.e., shear deformations are neglected. The bottom lamination of the beam consists of three boards connected longitudinally with two finger joints. The boards in the lamination have the same material properties and are connected with finger joints with known material properties and both finger joints have the same stiffness. The properties of the laminations are from the experimental tests of Fortuna et al. (2018a) for the bottom lamination a (mean static modulus of elasticity for beech wood) and from EN 338 (CEN, 2016b) for softwoods, which corresponds to the strength class C24 assumed for the upper lamination b. In the middle part of the lower lamination, a fully debonded interlayer connection (K_{X} = 0) is assumed. In the calculation, it is considered to be equal to zero (no connection, e.g. due to a lack of adhesive application). For the rest of the interlayer connection, the stiffness K_{X} = 81 kN/cm^2 is assumed, which corresponds to the mean shear modulus of strength class D40 of hardwood (CEN, 2016b). The beam is loaded with a vertical uniformly distributed load. The load is applied to each lamination separately. In general, the load should be distributed among the laminations in proportion to the stiffness properties of each lamination, as done in (Ko et al., 1972). However, in this example, the lower lamination a is loaded more compared to the ratio of the stiffness properties between the laminations, see Fig. 4.1, therefore delamination between the laminations occurs in the part without interlayer connection. Finger joints are assumed at the two connection points and the hybrid continuity conditions are used. Eqs. (4.1) show the boundary conditions for a simply supported two-layer beam with two segments with partial debonding on the outside of the beam.

$$
\begin{aligned}
X = 0: \quad & u^a(0) = 0, & \qquad X = L: \quad & N^a(L) = 0,\\
& N^b(0) = 0, & & N^b(L) = 0,\\
& w(0) = 0, & & w(L) = 0,\\
& M(0) = 0. & & M(L) = 0.
\end{aligned}
\tag{4.1}
$$

The equilibrium and kinematic quantities are evaluated for the case without the debonded segment and two, rather extreme, lengths of the fully debonded segment L_{FDS} = 1 and 150 cm to assess the influence of the fully debonded segment (FDS) on the behaviour of the beam. The results are presented in the

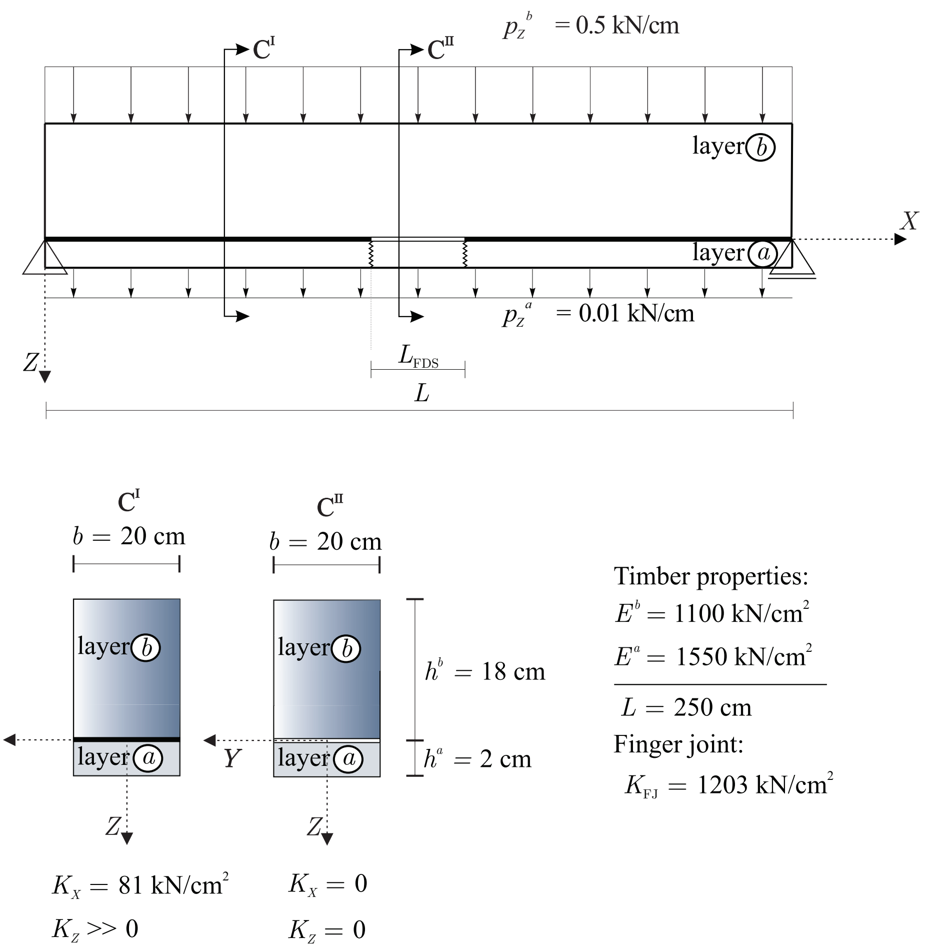

Figure 4.1: Geometric and material data of a two-layer beam with two finger joints and fully debonded interlayer.
Slika 4.1: Geometrijski in materialni podatki za dvoslojni nosilec z dvema zobatima spojema in popolno razslojenim stikom.

Tabs. 4.1-4.2. In Figs. 4.2–4.3, the results are shown graphically only for the two cases with FDS, since the results of the case without FDS would overlap with the result of the case with L_{FDS} = 1 cm. It should be noted again that all quantities are evaluated with respect to the global reference axis, which coincides with the contact area between the laminations. The results in Tabs. 4.1-4.2 are shown for 5 positions along the beam length. Note that the fully debonded segment is always placed in the centre of the beam so that the finger joints are symmetrically placed in the centre of the beam. Although the beam is loaded only vertically, the interlayer slip between the laminations causes the axial longitudinal forces to occur in laminations N^a and N^b and to be equal in magnitude but opposite in direction.

The presence of the fully debonded segment is evident for all quantities. In general, the kinematic quantities increase with the length of the fully debonded segment, as expected. For both lengths, the fully debonded segment causes a decrease in the axial deformations of the lower lamination ε^a and an increase in the upper lamination ε^b. However, it should be mentioned that the axial deformation ε^b in the middle of the span is slightly lower in the case of longer FDS. This results from the redistribution of axial stresses along the fully debonded segment, where the axial forces have a constant value.

The influence of the finger joint is shown in Figs. 4.2 and 4.3. The influence is more evident in the case of longer FDS, where significant peaks appear in the graphs due to the change in stiffness properties.

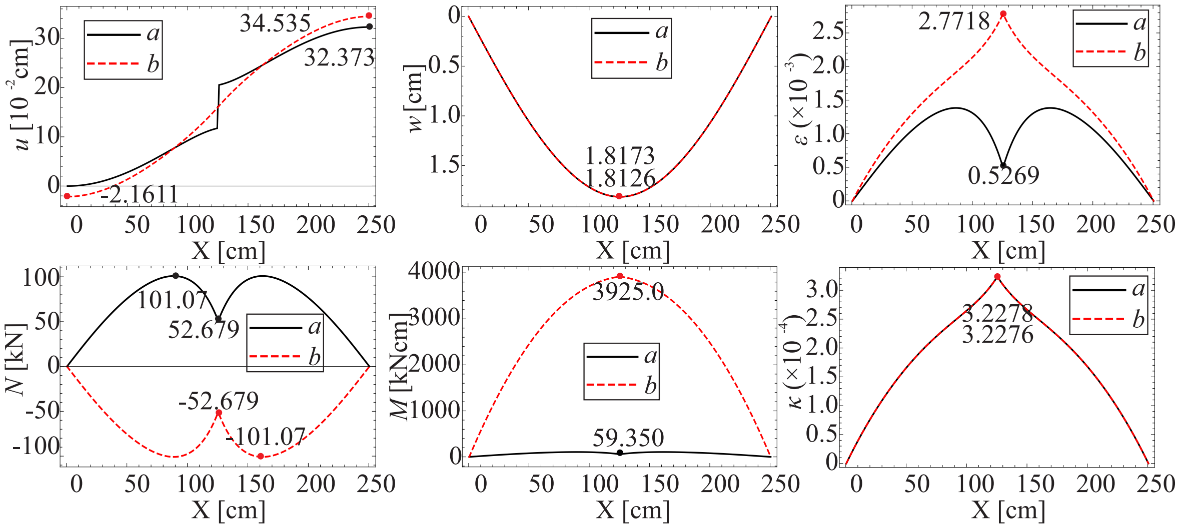

Figure 4.2: Equilibrium and kinematic quantities of a two-layer beam with two finger joints and fully debonded segment with L_{FDS} = 1 cm, shown for both laminations.

Slika 4.2: Ravnotežne in kinematične količine dvoslojnega nosilca z dvema zobatima spojema in popolno razslojenim delom z L_{FDS} = 1 cm, prikazane za oba sloja.

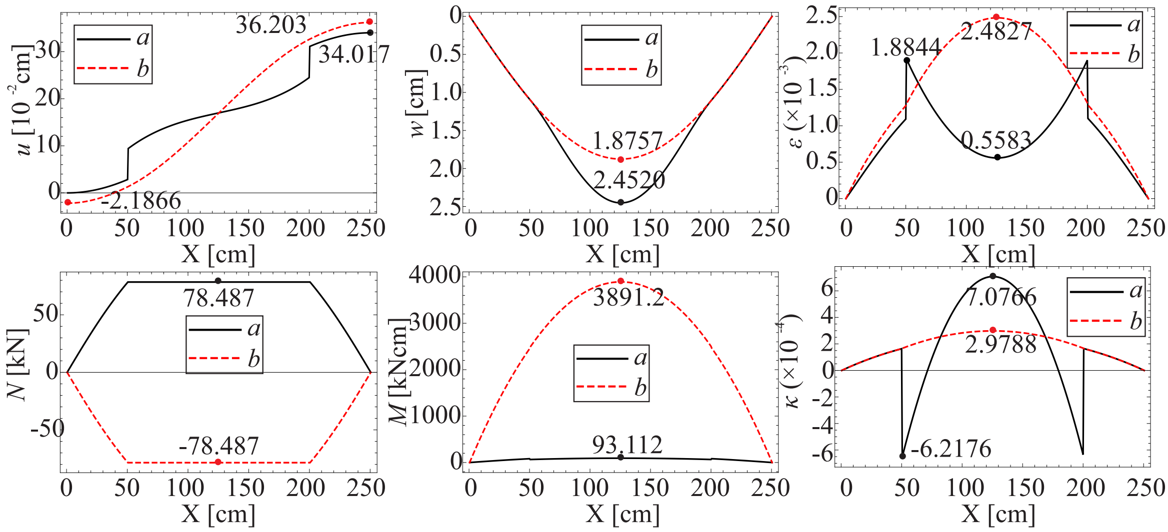

Figure 4.3: Equilibrium and kinematic quantities of a two-layer beam with two finger joints and fully debonded segment with L_{FDS} = 150 cm, shown for both laminations.

Slika 4.3: Ravnotežne in kinematične količine dvoslojnega nosilca z dvema zobatima spojema in popolno razslojenim delom z L_{FDS} = 150 cm, prikazane za oba sloja.

Table 4.1: Kinematic quantities of two-layer Euler-Bernoulli beam with finger joints evaluated with analytical model at five points along the span for $L_{\mathrm{FDS}} = 0$ cm.

Preglednica 4.1: Kinematične količine dvoslojnega Euler-Bernoullijevega nosilca z zobatima spojema izračunane z analitičnim modelom v petih točkah vzdolž nosilca za $L_{\mathrm{FDS}} = 0$ cm.

	$L_{\mathrm{FDS}} = 0$ cm				
	x = 0	x = L/4	x = L/2	x = 3L/4	x = L
u^a [10^{-2} cm]	0.0000	4.2701	16.163	28.056	32.327
u^b [10^{-2} cm]	-2.1614	3.2010	16.163	29.126	34.449
w^a [cm]	0.0000	1.2764	1.8153	1.2764	0.0000
w^b [cm]	0.0000	1.2764	1.8153	1.2764	0.0000
ε^a [10^{-3}]	0.0000	1.2363	0.5146	1.2363	0.0000
ε^b [10^{-3}]	0.0000	1.5402	2.7796	1.5402	0.0000
φ^a [10^{-2} rad]	-2.2818	-1.5999	0.0000	1.5999	2.2818
φ^b [10^{-2} rad]	-2.2818	-1.5999	0.0000	1.5999	2.2818
κ^a [10^{-4} rad/cm]	0.0000	1.9605	3.2343	1.9605	0.0000
κ^b [10^{-4} rad/cm]	0.0000	1.9605	3.2343	1.9605	0.0000
Δ_X [10^{-2} cm]	-2.1614	-1.0692	0.0000	1.0692	2.1614
N^a [kN]	0.0000	88.808	51.963	88.808	0.0000
N^b [kN]	0.0000	-88.808	-51.963	-88.808	0.0000
M^a [kNcm]	0.0000	92.859	58.647	92.859	0.0000
M^b [kNcm]	0.0000	2895.4	3925.7	2895.4	0.0000
$p^a_{c,X} = -p^b_{c,X}$ [kN/cm]	-1.7507	-0.8661	0.0000	0.8661	1.7507

4.1.2 Parametric study on two-layer simply supported Euler-Bernoulli beam

4.1.2.1 Parametric study on two-layer Euler-Bernoulli beam with one finger joint

The first parametric calculation was performed for a similar simply supported two-layer beam as presented in the previous section 4.1.1, but with only one finger joint and without a fully debonded segment. Therefore, the influence of finger joints is isolated and more evident. The geometry and material properties are shown in Fig. 4.4. Moreover, the effect of x_{FJ} on $w(L/2)$, N^a, and N^b for various K and K_{FJ} is investigated and shown in Figs. 4.5–4.6. In Fig. 4.5, $w(L/2)$ is plotted against x_{FJ} for various K_{FJ} while $K = 1/10$ kN/cm^2. However, it is clear that $w(L/2)$ is largest for $x_{\mathrm{FJ}} = 125$ cm, that is, when the finger joint is positioned at mid-span for all values of K_{FJ}. For example, for $x_{\mathrm{FJ}} = 125$ cm, the mid-span deflection is $w(L/2)[K_{\mathrm{FJ}} = 1/100] = 6.5179$ cm; $w(L/2)[K_{\mathrm{FJ}} = 1] = 6.5120$ cm; $w(L/2)[K_{\mathrm{FJ}} = 5] = 6.4989$ cm; $w(L/2)[K_{\mathrm{FJ}} = 10] = 6.4917$ cm; $w(L/2)[K_{\mathrm{FJ}} = 1000] = 6.4758$ cm. Interestingly, the effect of x_{FJ} on $w(L/2)$ is insignificant in this case and is less than 1 % regardless of K_{FJ}. Moreover, $w(L/2)$ is also independent of x_{FJ} for $K_{\mathrm{FJ}} \lesssim 1000$ kN/cm^2, namely for very stiff finger joints.

The effect of x_{FJ} on N^a for various K_{FJ} is also investigated and shown in Fig. 4.5 for $K = 1/100$ kN/cm^2.

Again, it is clear that N^a is affected by the x_{FJ} and K_{FJ}. For example, when $x_{\mathrm{FJ}} = 125$ cm, the N^a is for different K_{FJ} as follows: $N^a[K_{\mathrm{FJ}} = 0] = 0.000$ kN; $N^a[K_{\mathrm{FJ}} = 1/10] = 0.0900$ kN; $N^a[K_{\mathrm{FJ}} = 1/2] = 0.290$ kN; $N^a[K_{\mathrm{FJ}} = 2] = 0.497$ kN; $N^a[K_{\mathrm{FJ}} = \infty] = 0.647$ kN. Again, it is clear that the effect of x_{FJ} on the magnitude and distribution of N^a can be considerable. More information on

Table 4.2: Kinematic quantities of two-layer Euler-Bernoulli beam with finger joints evaluated with analytical model at five points along the span for $L_{\rm FDS} = 1$ and 150 cm.

Preglednica 4.2: Kinematične količine dvoslojnega Euler-Bernoullijevega nosilca z zobatima spojema izračunane z analitičnim modelom v petih točkah vzdolž nosilca za $L_{\rm FDS}$ = 0 cm.

	$L_{\rm FDS} = 1$ cm					$L_{\rm FDS} = 150$ cm				
	x = 0	x = L/4	x = L/2	x = 3L/4	x = L	x = 0	x = L/4	x = L/2	x = 3L/4	x = L
u^a [10^{-2} cm]	0.0000	4.2685	16.187	28.105	32.373	0.0000	11.550	17.008	22.466	34.017
u^b [10^{-2} cm]	-2.1611	3.2024	16.187	29.171	34.535	-2.1866	3.2043	17.008	30.813	36.203
w^a [cm]	0.0000	1.2777	1.8173	1.2777	0.0000	0.0000	1.3775	2.4520	1.3775	0.0000
w^b [cm]	0.0000	1.2744	1.8126	1.2744	0.0000	0.0000	1.3202	1.8757	1.3202	0.0000
ε^a [10^{-3}]	0.0000	1.2354	0.5269	1.2354	0.0000	0.0000	1.5033	0.5583	1.5033	0.0000
ε^b [10^{-3}]	0.0000	1.5408	2.7718	1.5408	0.0000	0.0000	1.6601	2.4827	1.6601	0.0000
φ^a [10^{-2} rad]	-2.2838	-1.6017	0.0000	1.6017	2.2838	-2.3561	-2.4540	0.0000	2.4540	2.3838
φ^b [10^{-2} rad]	-2.2838	-1.6017	0.0000	1.6017	2.2838	-2.3562	-1.6714	0.0000	1.6714	2.3562
κ^a [10^{-4} rad/cm]	0.0000	1.9610	3.2278	1.9610	0.0000	0.0000	-2.3740	7.0766	-2.3740	0.0000
κ^b [10^{-4} rad/cm]	0.0000	1.9610	3.2276	1.9610	0.0000	0.0000	2.0654	2.9788	2.0654	0.0000
Δ_X [10^{-2} cm]	-2.1611	-1.0661	0.0000	1.0661	2.1611	-2.1866	-8.3461	0.0000	8.3461	2.1866
N^a [kN]	0.0000	88.755	52.679	88.755	0.0000	0.0000	78.487	78.487	78.487	0.0000
N^b [kN]	0.0000	-88.755	-52.679	-88.755	0.0000	0.0000	-78.487	-78.487	-78.487	0.0000
M^a [kNcm]	0.0000	92.808	59.350	92.808	0.0000	0.0000	73.581	93.112	73.581	0.0000
M^b [kNcm]	0.0000	2895.5	3925.0	2895.5	0.0000	0.0000	2914.7	3891.3	2914.7	0.0000
$p^a_{c,X} = -p^b_{c,X}$ [kN/cm]	-1.7505	-0.8635	0.0000	0.8635	1.7505	-1.7711	0.0000	0.0000	0.0000	1.7711

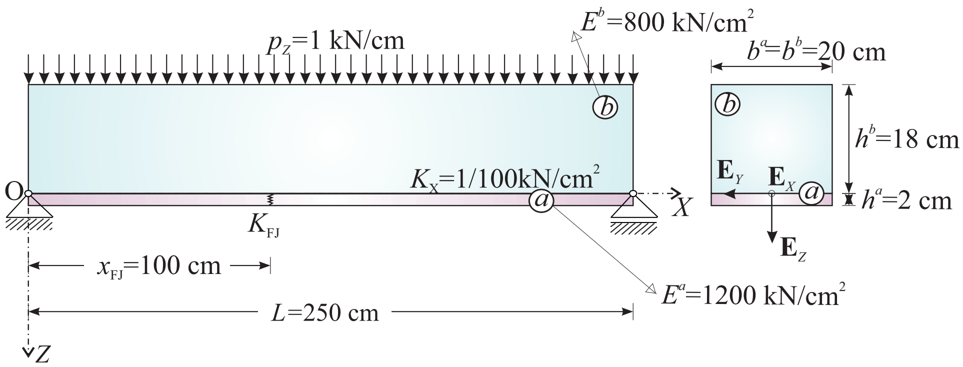

Figure 4.4: Geometric and material properties of the laminations, position and magnitude of the loading and the finger joint and material properties of the interlayer contact and the finger joint.

Slika 4.4: Geometrijske in materialne lastnosti slojev, pozicije in velikosti obtežbe in zobatega spoja ter materialne lastnosti stika med sloji in zobatega spoja.

the analysis of this example can be found in the work of Fortuna et al. (2021).

4.1.2.2 Stiffness properties of the interlayer connection K_X and finger joints $K_{\rm FJ}$

Based on the model in Section 4.1.1, a similar model is used for further parametric studies focusing on the stiffness properties of the finger joints $K_{\rm FJ}$ and the interlayer connection stiffness $K_{\rm X}$. The boundary conditions of the model remain the same, Eqs. (4.1), as well as the external loading ($p_Z = 0.51$ kN/cm^2). The material properties and geometry of the beam also remain unchanged, except for the length of the fully debonded segment, which is fixed at 50 cm and positioned at the center of the beam span. Two

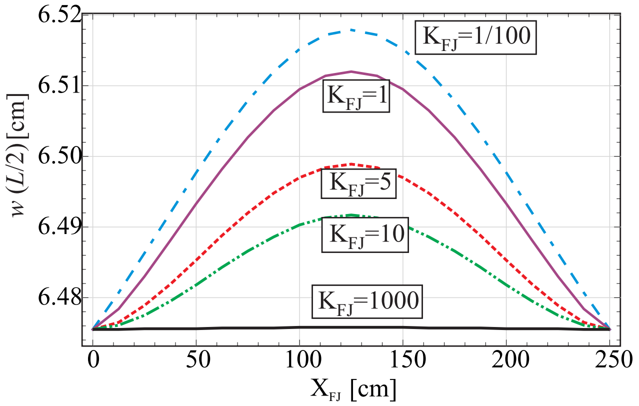

Figure 4.5: Vertical displacement in the middle of the span, $w(L/2)$, of glued laminated beam, as a function of different finger joint position and different finger joint stiffness, K_{FJ}.

Slika 4.5: Navpični pomik na sredini razpona, $w(L/2)$, lepljenega slojevitega nosilca z zobatim spojem, kot funkcija različnih pozicij zobatega spoja, x_{FJ}, in različnih togosti zobatega spoja, K_{FJ}.

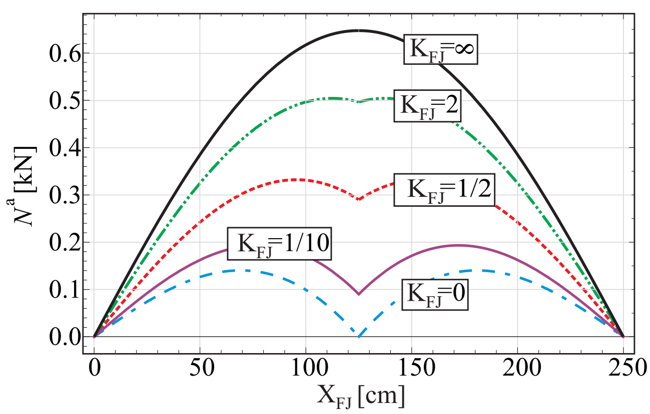

Figure 4.6: Axial stresses of lamination a (N^a) of finger jointed glued laminated beam, as a function of different finger joint position x_{FJ} and different finger joint stiffness K_{FJ}.

Slika 4.6: Osne napetosti v sloju a (N^a) lepljenega nosilca z zobatim spojem, kot funkcija različnih pozicij zobatega spoja x_{FJ} in različnih togosti zobatega spoja K_{FJ}.

finger joints are considered in the bottom lamination. The stiffness properties K_{X} and K_{FJ} are varied between $1 - 10^6$ N/cm^2 for the contact between the layers and the finger joints. To validate the model, an additional calculation is performed with a very high stiffness $K_{\mathrm{FJ}} = 10^{10}$ N/cm^2. The results are compared with those obtained with the analytical model of Schnabl et. al. (Schnabl, 2007). The basic equilibrium quantities N^i, M^i, and the kinematic quantities u^i and w^i are determined at midspan of the beam (Tab. 4.3 and 4.4). Fig. 4.7 shows a graphical representation of the influence of stiffness on the horizontal and vertical displacements of the bottom lamination a.

The results in Tabs. 4.3–4.4 are presented in compact form because the horizontal displacement at mid-span is the same for both laminations and the axial forces of the laminations are symmetric about midspan and the values for the laminations are equal but opposite. The vertical displacements and bending moments are calculated for the mid-span only. Due to the full debonding of the laminations at mid-span of the beam, the vertical displacements of the bottom lamination w^a are slightly larger than the vertical displacements of the top lamination w^b. Tabs. 4.3–4.4 show that there is no influence of the stiffness properties $K_{\rm X}$ and $K_{\rm FJ}$ on the difference of displacements, e.g. delamination. Nevertheless, Fig. 4.7 shows the influence of the stiffness properties $K_{\rm X}$ and $K_{\rm FJ}$ on w^a, where the influence of the latter is less pronounced. The bending moments of the laminations are interdependent due to the contact properties between the laminations, i.e., a decrease in one increases the other. An important influence of the stiffness K_X is shown in the bending moments. Since the sum of moments remains the same for both laminations, K_X increases the bending moments in the lower lamination. The influence of the stiffness (of the interlayer surface and also of the finger joints) becomes evident for larger values of the stiffness (Fig. 4.8). The values of kinematic and equilibrium quantities for the case with finger joints with very high stiffness $K_{\rm FJ} = 10^{10}$ N/cm^2 are almost identical to those of Schnabl et. al.(Schnabl, 2007).

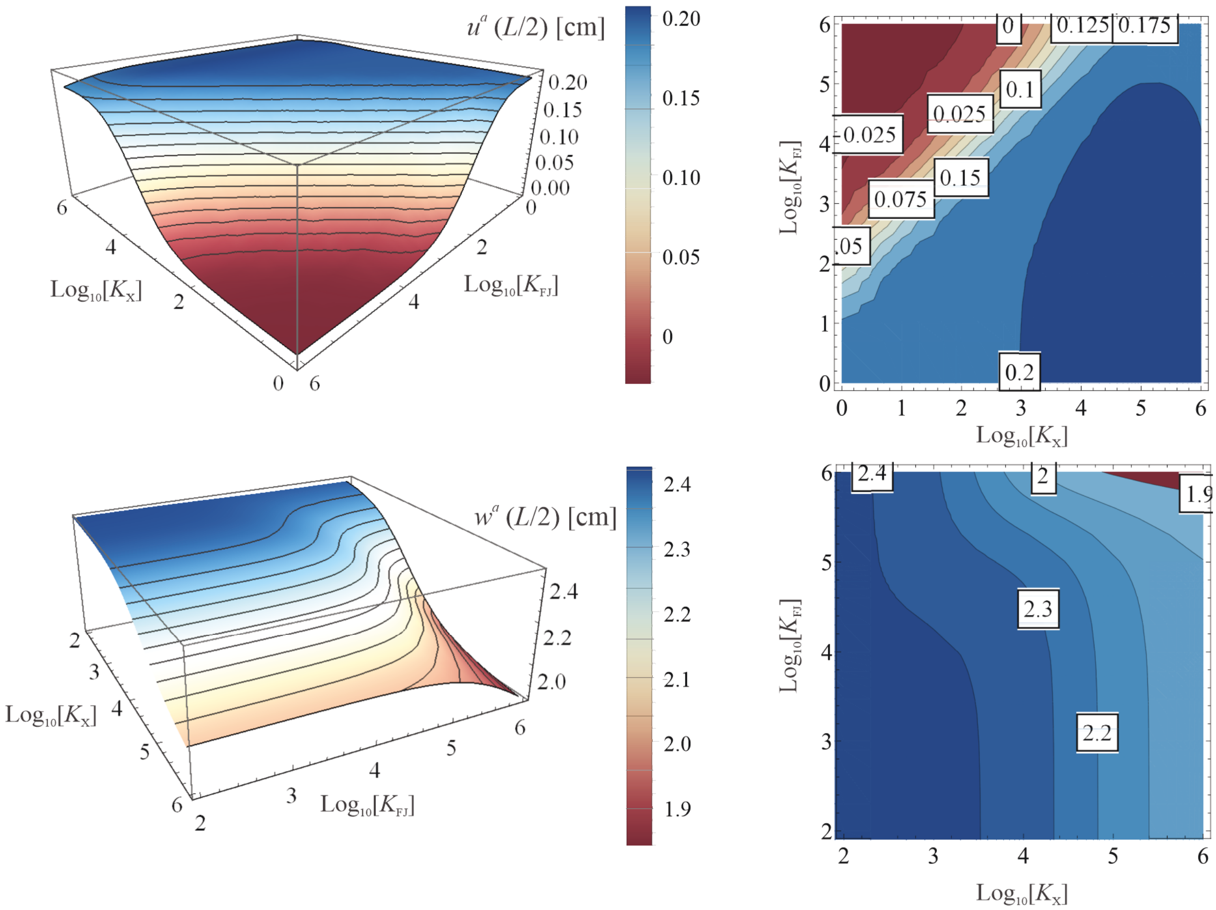

Figure 4.7: Horizontal and vertical displacement u^a and w^a at the mid-span of the beam as a function of the stiffness of the finger joint $K_{\rm FJ}$ and longitudinal stiffness of the interlayer contact K_X.
Slika 4.7: Vodoravni in navpični pomik u^a in w^a na sredini razpona nosilca kot funkcija togosti zobatega spoja $K_{\rm FJ}$ in vzdolžne togosti stika K_X.

4.1.2.3 Position and length of the fully debonded segment

The model of the beam was also parameterized in terms of the position $x_{\rm FDS}$ and the length $L_{\rm FDS}$ of the fully debonded segment. The material and geometry parameters for this study are the same as for the illustrative example (Fig. 4.1), but the FDS is no longer located in the mid-span of the beam. The

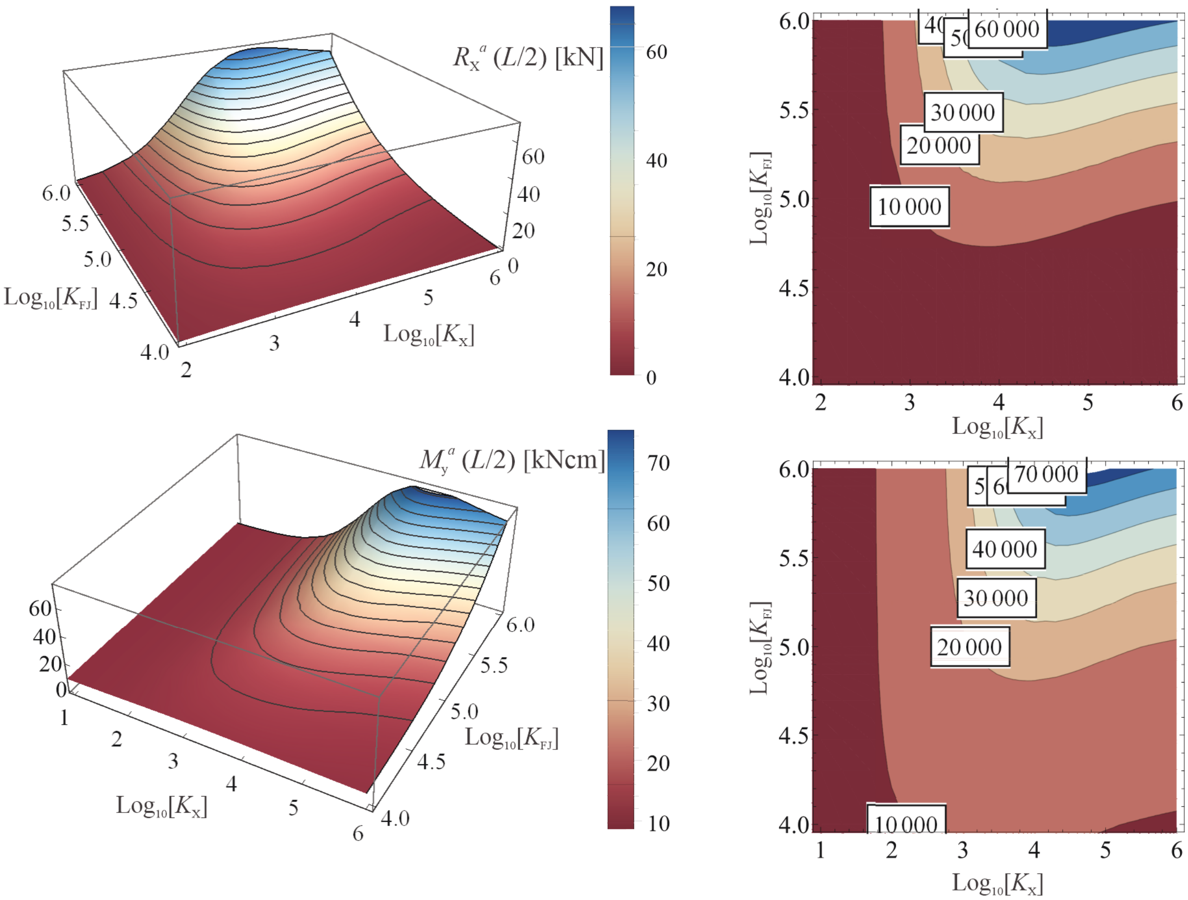

Figure 4.8: Internal axial force N^a and bending moment M^a at the mid-span of the beam as a function of the stiffness of the finger joint K_{FJ} and stiffness of the interlayer contact K_{X}.
Slika 4.8: Notranje osne sile N^a in upogibni moment M^a na sredini razpona dvoslojnega nosilca kot funkcija togosti zobatega spoja K_{FJ} in togosti stika med lamelami K_{X}.

position of the fully debonded segment x_{FDS} defines the starting point of the FDS. The position is varied from 5 to 145 cm, and the lengths L_{FDS} are: 10, 50 and 100 cm. In Fig. 4.9, the horizontal and vertical displacements with axial force and bending moment are shown for the bottom lamination, which are evaluated at the midspan of the beam. For the horizontal displacements, the influence of FDS is not significant. The maximum values of $u^a(L/2)$ are in the same range for all L_{FDS}. Also, the axial force and bending moment give approximately the same maximum values for L_{FDS} = 10 and 50 cm, while the 100 cm FDS results in smaller values for axial force and bending moment. Of course, the decrease in values also depends on the x_{FDS}. The vertical displacement increases when the FDS coincides with the midspan.

4.1.3 Continuous two-layer Euler-Bernoulli beam with finger joints in the two spans

The analytical model was used to determine the kinematic and equilibrium unknowns of the continuous two-layer timber beam with two spans. In both spans, the finger joints are included in the lower lamination. The analytical model provides solutions for arbitrary lengths between the supports and finger joints.

Table 4.3: Selected kinematic and equilibrium quantities of two-layer beam with finger joints evaluated with numerical model for different K_X and K_{FJ} at different locations for $L_{\mathrm{FDS}} = 50$ cm and comparison with results of analytical model by Schnabl (2007)

Preglednica 4.3: Izbrane kinematične in ravnotežne količine dvoslojnega nosilca z zobatima spojema izvrednotene z analitičnim modelom pri različnih K_X in K_{FJ} in različnih pozicijah $L_{\mathrm{FDS}} = 50$ cm in primerjava rezultatov z rezultati analitičnega modela po (Schnabl, 2007).

	$K_{\mathrm{X}} = 1$ N/cm^2					
$L_{\mathrm{FDS}} = 50$ cm	$K_{\mathrm{FJ}} = 1$	$K_{\mathrm{FJ}} = 10^2$	$K_{\mathrm{FJ}} = 10^4$	$K_{\mathrm{FJ}} = 10^6$	$K_{\mathrm{FJ}} = 10^{10}$	Schnabl (2007)
u^a(L/2) =u^b(L/2) [10^{-2} cm]	19.732	8.4312	-2.8679	-3.0938	-3.0962	-3.0962
u^a(L/4) [10^{-2} cm]	-0.9684	-0.9680	-0.9676	-0.9676	-0.9676	-0.9676
u^a(3L/4) [10^{-2} cm]	40.432	17.830	-4.7682	-5.2201	-5.2247	-5.2247
w^a(L/2) [cm]	2.4285	2.4285	2.4284	2.4284	2.4284	2.4284
w^b(L/2) [cm]	2.4214	2.4213	2.4213	2.4213	2.4213	2.4213
N^a(L/2) = $-N^b$(L/2) [kN]	0.0002	0.0115	0.0228	0.0231	0.0231	0.0231
N^a(L/4) = N^b(3L/4) [kN]	0.0030	0.0100	0.0171	0.0172	0.0172	0.0172
M^a(L/2) [kNcm]	8.6260	8.6371	8.6481	8.6484	8.6484	8.6484
M^b(L/2) [kNcm]	3975.8	3975.7	3975.7	3975.7	3975.7	3975.7

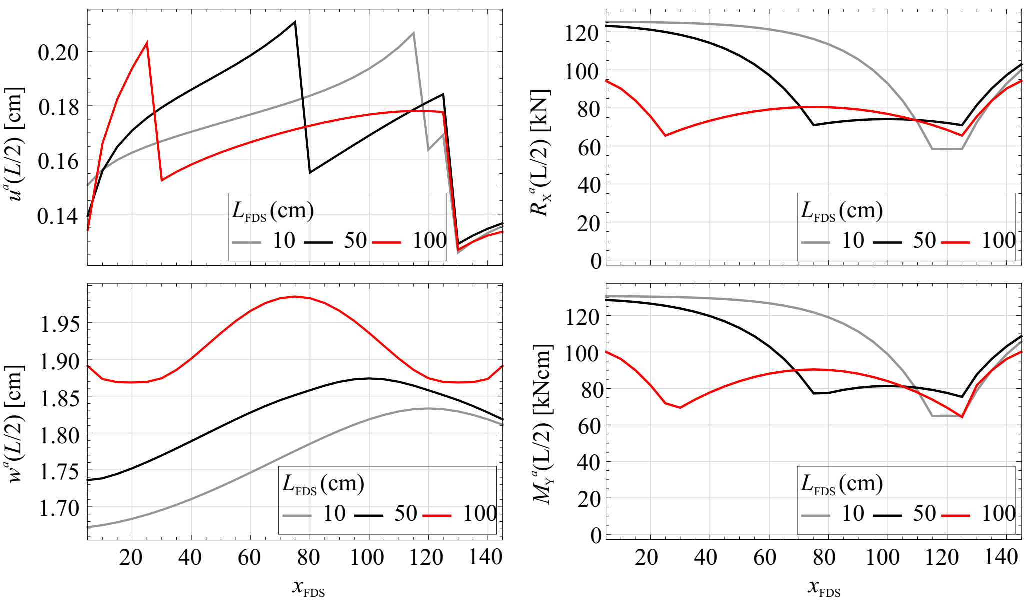

Figure 4.9: Selected kinematic and equilibrium quantities as a function of the position of the fully debonded segment x_{FDS} for the three lengths of fully debonded segment L_{FDS} = 10, 50 and 100 cm.

Slika 4.9: Izbrane kinematične količne kot funkcija pozicije popolnoma razslojenega dela x_{FDS} za tri dolžine popolnoma razslojenega dela L_{FDS} = 10, 50 and 100 cm.

Thus, for the illustrative example, the asymmetric continuous beam is as shown in Fig. 4.10. The width of the beam is $b = 20$ cm. The material data are the same as for the example of the simply supported beam from Section 4.1.1. The beam is loaded with a vertical distributed load of 0.1 kN/cm. The boundary conditions are similar to those for the simply supported beam (Eqs. 4.1) with an additional condition

Table 4.4: Selected kinematic and equilibrium quantities of two-layer beam with finger joints evaluated with numerical model for different K_X and K_{FJ} at different locations for $L_{\mathrm{FDS}} = 50$ cm and comparison with results of analytical model by Schnabl (2007)

Preglednica 4.4: Izbrane kinematične in ravnotežne količine dvoslojnega nosilca z zobatima spojema izvrednotene z analitičnim modelom pri različnih K_X in K_{FJ} in različnih pozicijah $L_{\mathrm{FDS}} = 50$ cm in primerjava rezultatov z rezultati analitičnega modela po Schnabl (2007).

	$K_X = 10^6$ N/cm^2					
$L_{\mathrm{FDS}} = 50$ cm	$K_{\mathrm{FJ}} = 1$	$K_{\mathrm{FJ}} = 10^2$	$K_{\mathrm{FJ}} = 10^4$	$K_{\mathrm{FJ}} = 10^6$	$K_{\mathrm{FJ}} = 10^{10}$	Schnabl (2007)
u^a(L/2) =u^b(L/2) [10^{-2} cm]	20.066	20.065	20.028	18.025	15.672	15.672
u^a(L/4) [10^{-2} cm]	4.8749	4.8749	4.8749	4.8761	4.8774	4.8774
u^a(3L/4) [10^{-2} cm]	35.257	35.256	35.181	31.174	26.467	26.466
w^a(L/2) [cm]	2.0349	2.0348	2.0313	1.8449	1.6260	1.6259
w^b(L/2) [cm]	2.0277	2.0277	2.0242	1.8378	1.6188	1.6188
N^a(L/2) = $-N^b$(L/2) [kN]	0.0001	0.0113	1.1160	60.288	129.81	129.82
N^a(L/4) = N^b(3L/4) [kN]	98.816	98.816	98.819	98.930	99.061	99.061
M^a(L/2) [kNcm]	8.6260	8.6368	9.7201	67.750	135.93	135.94
M^b(L/2) [kNcm]	3975.8	3975.7	3974.7	3916.6	3848.4	3848.4

at the middle support:

$$
\begin{aligned}
&X = 0: && X = L_1 + L_2: && X = L: \\
&u^a(0) = 0, && w(L_1 + L_2) = 0, && N^a(L) = 0, \\
&N^b(0) = 0, && && N^b(L) = 0, \\
&w(0) = 0, && && w(L) = 0, \\
&M(0) = 0. && && M(L) = 0.
\end{aligned} \tag{4.2}
$$

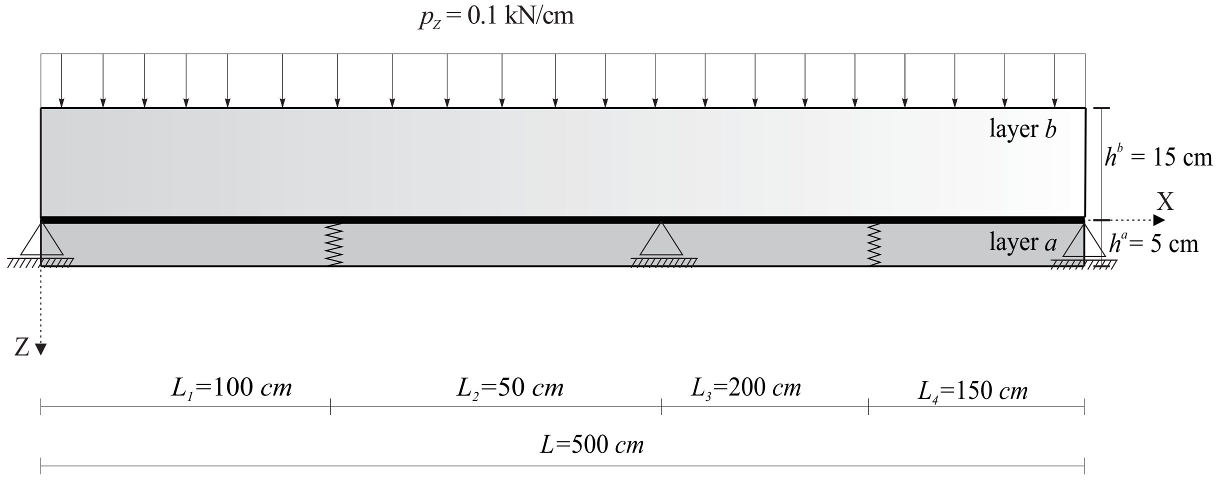

Figure 4.10: Geometric data for the continuous two-layer beam with two spans and two finger joints.
Slika 4.10: Geometrijski podatki za dvoslojni nosilec z dvema razponoma in dvema zobatima spojema.

The kinematic and equilibrium quantities of the continuous beam are evaluated. In Figs. 4.11 and 4.12

the equilibrium and kinematic quantities are shown along the length of the beam. The axial force N and the shear force Q for both laminations are plotted together, while the internal bending moment is plotted separately for each lamination to make their shapes clearer and more distinct. The shape of the diagrams indicates the position of the supports and finger joints. For example, in the case of the axial force, the position of the finger joint is clear in the left span due to the significant decrease. However, in the right span of the beam, the value 0 of the internal axial force has nothing to do with the presence of the finger joint, but the geometry of the beam implies such a distribution of axial forces. The situation is similar with the internal shear force Q. The finger joint in the left span is more distinct than the one in the middle of the right span although the stiffness properties of both finger joints are identical. Again, there is a relationship with the distribution of the internal bending moment, with values close to 0 at the position of the finger joint on the right side.

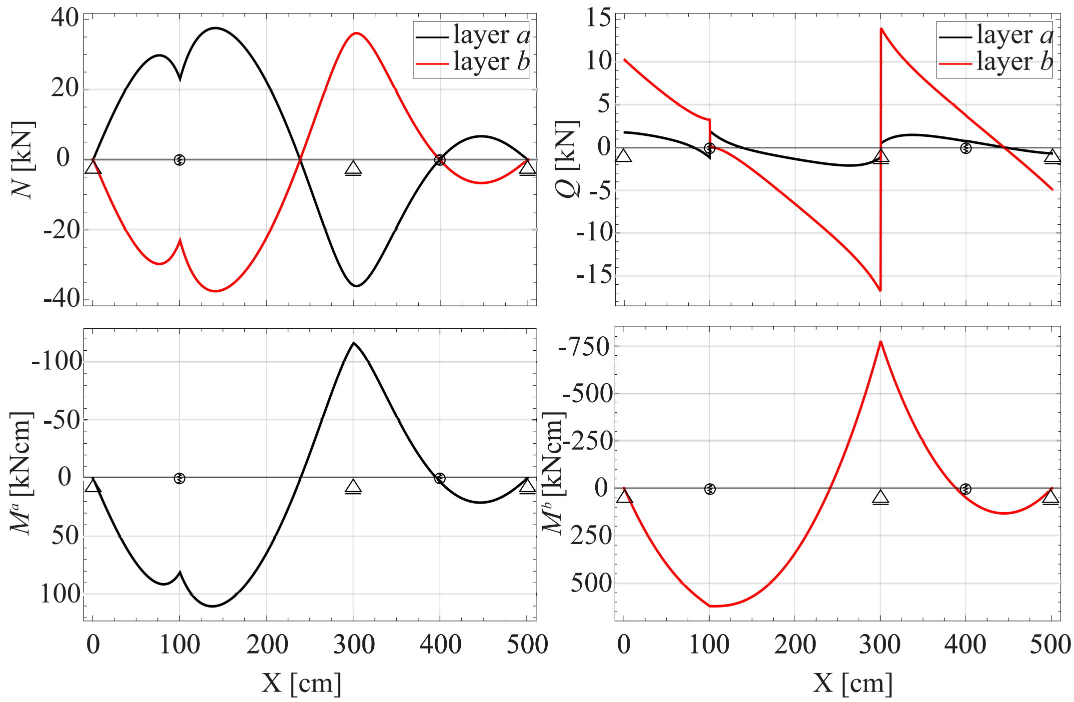

Figure 4.11: Equilibrium quantities of two-layer continuous beam with two finger joints calculated with analytical model.

Slika 4.11: Ravnotežne količine dvoslojnega kontinuirnega nosilca z dvema zobatima spojema izračunane z analitičnim modelom.

The vertical displacements w and the specific curvature κ are the same for both laminations, while are different between the laminations. The $(\cdot)^*$ stands for A and B, respectively. The position of the supports and finger joints is again very transparent. The results for all sizes are also presented in numerical form.

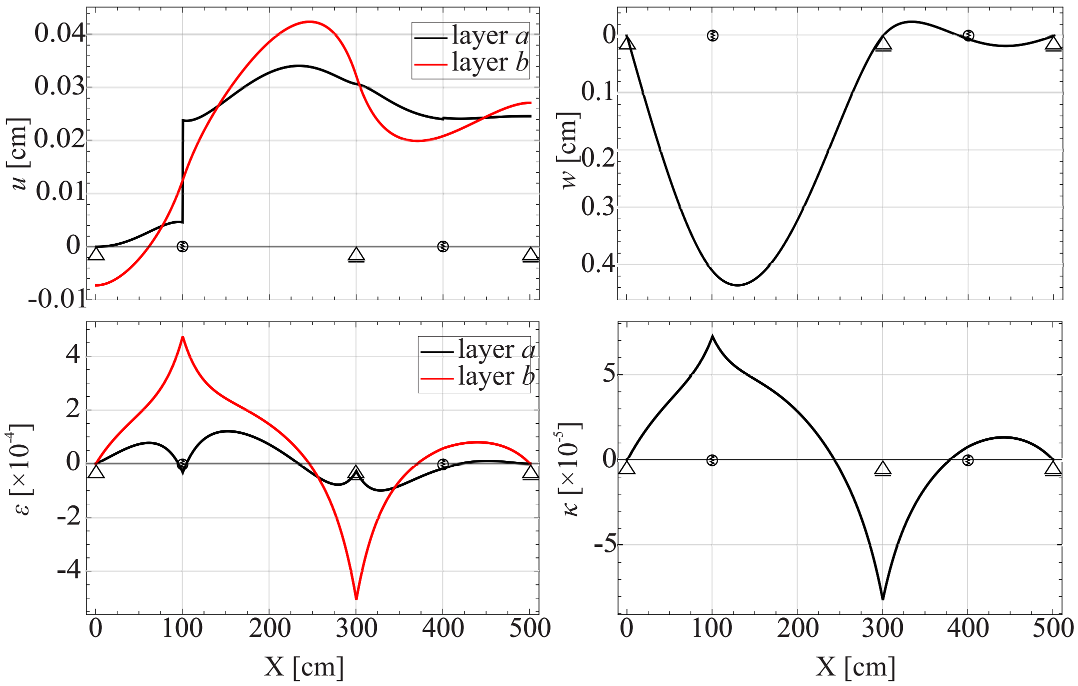

Figure 4.12: Kinematic quantities of two-layer continuous beam with two finger joints calculated with analytical model.

Slika 4.12: Kinematične količine dvoslojnega kontinuirnega nosilca z dvema zobatima spojema izračunane z analitičnim modelom.

4.1.4 Parametric study on continuous two-layer Euler-Bernoulli beam with finger joints in the two spans

A parametric study was conducted to evaluate the effects of joint stiffness on the kinematic and equilibrium variables. The geometry and material properties were the same as in the illustrative example of the continuous beam. In the first study, the interlayer contact stiffness parameter was varied from $K_{\mathrm{X}} = 10$ kN/cm^2 to $K_{\mathrm{X}} = 10^5$ kN/cm^2 at a fixed value of finger joint stiffness $K_{\mathrm{FJ}} = 1200$ kN/cm^2. The kinematic and equilibrium quantities are presented in Tab. 4.5 for the lowest and the highest interlayer contact stiffness. In the case of the lowest interlayer stiffness, the finger joint point has no effect on the internal forces and bending moment, as can be seen in Fig. 4.13. The $K_{\mathrm{X}} = 10$ kN/cm^2 cannot be clearly distinguished. Since the interlayer contact traction is the only horizontal load, the internal axial forces in the laminations depend on the interlayer stiffness. Therefore, it is expected that higher contact stiffness between the laminations will result in higher internal axial forces in both laminations. In addition, the presence of finger joints becomes more evident as the contact stiffness increases.

Fig. 4.14 shows the axial deformations, vertical displacement, and interlayer slip. In general, the maximum vertical displacement occurs in the middle of the largest (left) span and is smallest (w = 0.4265 cm) when the stiffness is highest and largest (w = 0.8763 cm) when the stiffness is lowest. In the second part of the parametric study, the influence of finger joint stiffness is investigated. The stiffness varied from $K_{\mathrm{FJ}} = 10$ kN/cm^2 to $K_{\mathrm{FJ}} = 10^6$ kN/cm^2 and the contact stiffness was $K_X = 81$ kN/cm^2. As can be seen from Fig. 4.15, where the vertical displacement and interlayer slip are shown, the finger with the lower stiffness values does not have a strong effect on the behaviour of the beam. The blue line indica-

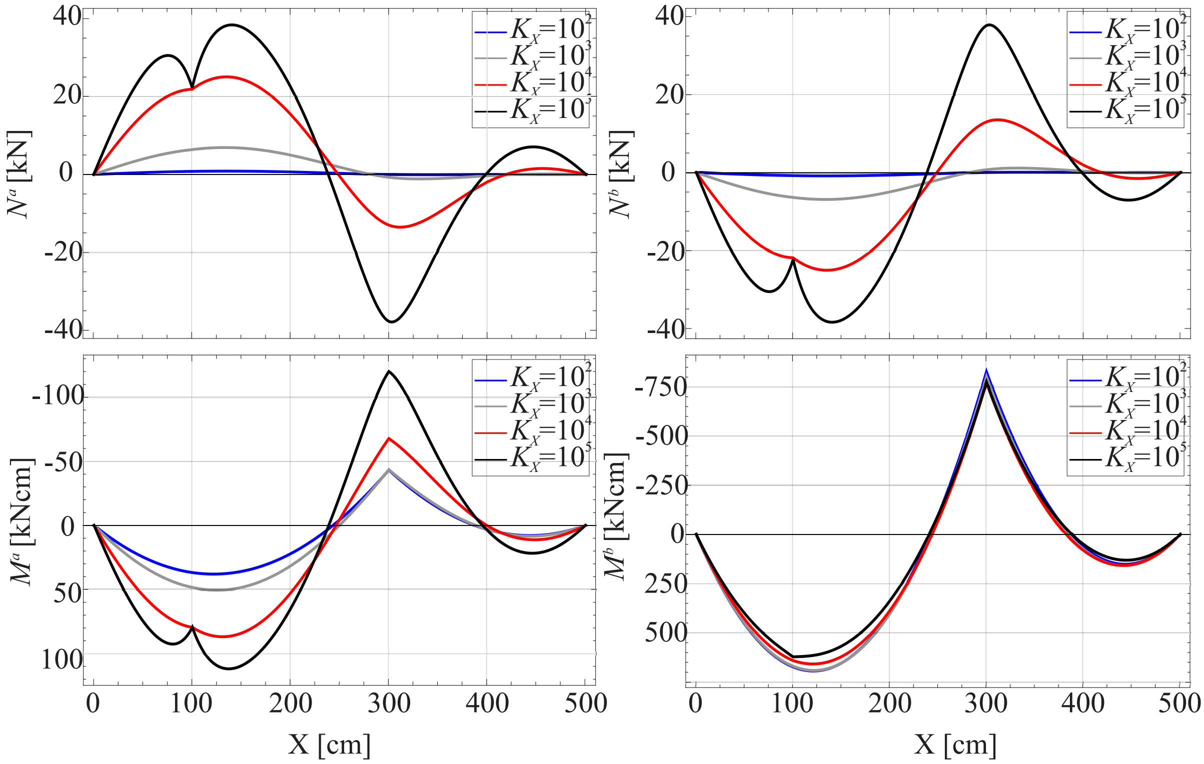

Figure 4.13: Equilibrium quantities in the laminations along the length of the two-layer beam for different interlayer contact stiffness K_{X}, calculated with analytical model.

Slika 4.13: Ravnotežne količine v slojih vzdolž dvoslojnega kontinuirnega nosilca za različne togosti stika K_{X}, izračunani z analitičnim modelom.

ting the lowest stiffness is completely aligned with the grey line indicating the second lowest stiffness value. The high stiffness of the finger joints (when their value approaches the mechanical properties of the material) begins to have a greater effect on the size of the displacements. The distributions of the internal forces along the beam are not shown, but they show similar results.

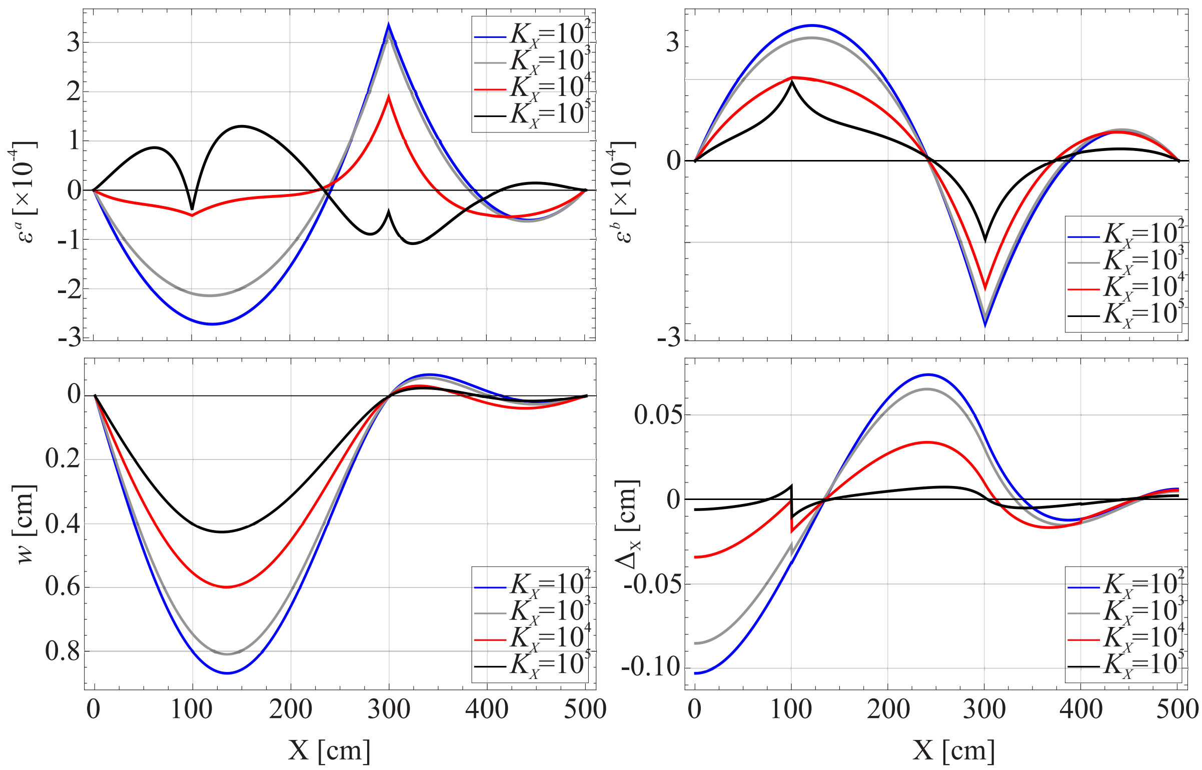

Figure 4.14: Kinematic quantities in the laminations along the length of the two-layer beam for different interlayer contact stiffness K_{X}, calculated with analytical model.

Slika 4.14: Kinematične količine v slojih vzdolž dvoslojnega kontinuirnega nosilca za različne togosti stika K_{X}, izračunani z analitičnim modelom.

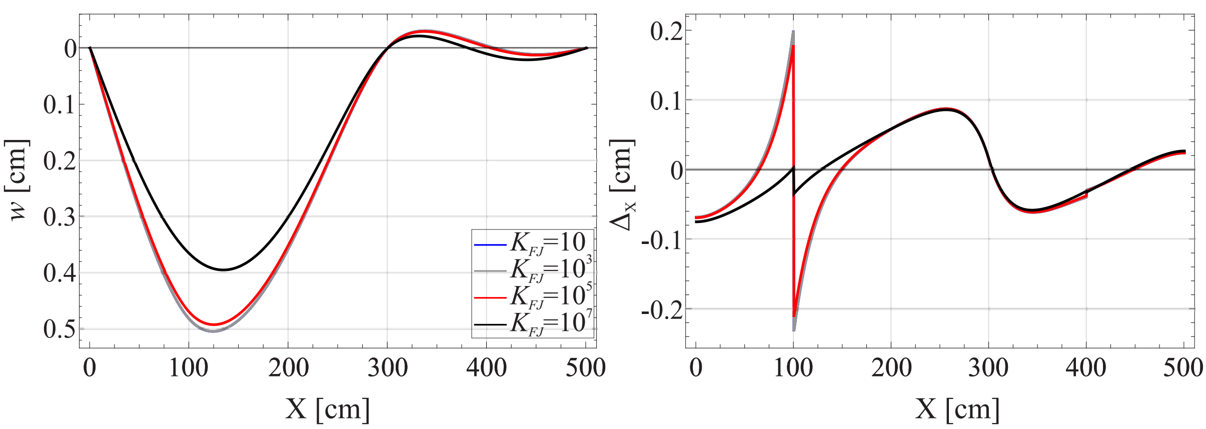

Figure 4.15: Vertical displacement w and interlayer slip Δ_{X} along the beam for different finger joint stiffness K_{FJ}, calculated with analytical model.

Slika 4.15: Navpični pomiki w in zdrs med slojema Δ_{X} vzdolž nosilca za različne togosti zobatega spoja K_{FJ}, izračunani z analitičnim modelom.

Table 4.5: Kinematic and equilibrium quantities of two-layer continuous beam with finger joints evaluated with analytical model for different K_X and at different locations along the beam.

Preglednica 4.5: Kinematične in ravnotežne količine dvoslojnega kontinuirnega nosilca z zobatima spojema izvrednotene z analitičnim modelom pri različnih K_X in pri različnih lokacijah vzdolž nosilca.

	K_{X}	x = 0 cm	x = 100 cm	x = 150 cm	x = 300 cm	x = 500 cm
$N^a = -N^b$ [kN]	10^2	0	0.0808	0.0862	-0.0001	0
	10^5	0	22279	37856	-37729	0
M^a [kNcm]	10^2	0	35302	34283	-43379	0
	10^5	0	79440	109.45	-120.03	0
M^b [kNcm]	10^2	0	673.17	653.43	-831.19	0
	10^5	0	622.04	567.77	-775.52	0
Q^a [kN]	10^2	601.51	104.17	-144.93	712.13	-279.23
	10^5	1810.6	2208.2	-363.05	500.62	-709.19
Q^b[kN]	10^2	11483	1981	-2770.3	13661	-5347.9
	10^5	10204	-193	-2622.1	13977	-4813.1
u^a [cm]	10^2	0	-0.0167	-0.0304	-0.0358	-0.0278
	10^5	0	0.0237	0.0278	0.0308	0.0248
u^b [cm]	10^2	-0.1053	-0.055	-0.0137	0.0025	-0.0214
	10^5	-0.0061	0.0132	0.0289	0.0319	0.027
w [cm]	10^2	0	0.8099	0.8632	0	0
	10^5	0	0.4021	0.4155	0	0
φ [$\times10^{-3}$]	10^2	-10.550	-3.8363	1.6785	3.8351	0.6423
	10^5	-5.1882	-1.7711	10.275	1.7172	0.4676
κ [$\times10^{-5}$]	10^2	0	10.870	10.550	-13.433	0
	10^5	0	7.3528	4.5874	-7.9604	0
ε^a [$\times10^{-5}$]	10^2	0	-27.122	-26.320	33.584	0
	10^5	0	-4.0086	12.955	-4.4405	0
ε^b [$\times10^{-5}$]	10^2	0	81.499	79.099	-100.75	0
	10^5	0	48.395	22.934	-48.270	0
Δ_{X} [cm]	10^2	-0.1053	-0.0383	0.0168	0.0383	0.0064
	10^5	-0.0061	-0.0105	0.0011	0.0011	0.0022

4.2 Numerical model

4.2.1 Verification of numerical model

Before showing the results of the numerical model with an arbitrary number of laminations and finger joints, the numerical model is verified. The verification is performed on the example of a four-layer beam without finger joints. The results are compared with those of Kroflič (2012) and Sousa Jr and Silva (2010). The beam is simply supported, but only the lower lamination is supported. The length of the beam is $L = 400$ cm and the beam is loaded with the distributed load $p_Z = 0.1$ kN/cm. The height of the laminations varies from 4 to 10 cm, as shown in Fig. 4.16, and the width of the beam is $b = 10$ cm. All the laminations have the same modulus of elasticity $E = 5000$ kN/cm^2. The shear moduli of the laminations are assumed to be $G = 10^5$ kN/cm^2. The stiffness of the interlayer contact is equal to $K_\mathrm{X} = 0.5$ kN/cm^2 for all interlayers.
In Fig. 4.17 the comparison of the results for the interlayer slips Δ_X^j, for $j = \{1, 2, 3\}$ is shown. It can be seen that the results of all three models agree well. There was a small deviation in the slip values, which could be due to the lack of information about the shear moduli of the laminations in the case of Sousa Jr and Silva (2010) or to the fact that delamination is neglected in our model, while Kroflič (2012) considers a very high stiffness of the interlayer contact in the transverse direction. In our numerical model, a high shear modulus $G = 10^5$ kN/cm^2 is considered, as it was done by Kroflič (2012). The results are also presented in numerical form in Tab. 4.6 for all three models, where the vertical displacement at the centre of the beam span is also given. The differences between the vertical displacements are slightly larger, but still not excessive. Our model agrees best with the model of Sousa Jr and Silva (2010). In addition, the four-layer beam was also analysed using our analytical model. As expected, the agreement with the exact solution of Sousa Jr and Silva (2010) but also our numerical model shows almost identical results (except for the vertical displacement, where the difference appears only at the 5$^{\text{th}}$ significant digit. The comparison between the analytical and numerical models from this dissertation is validated using the calculated errors. It can be seen that the errors are very small. Therefore, we can conclude that the numerical (and analytical) model gives correct and reliable results.

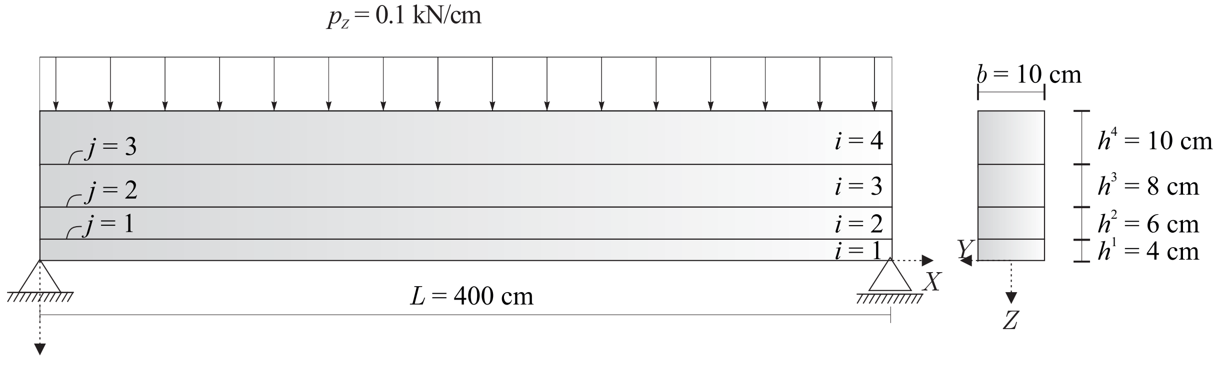

Figure 4.16: Four-layer laminated beam used for the verification of numerical model.
Slika 4.16: Štirislojni lamelirani nosilec uporabljen za verifikacijo numeričnega modela.

Table 4.6: Interlayer slips Δ_X^j at the beginning of the four-layer beam and vertical displacement w at the middle of the beam span calculated with the proposed analytical and numerical model and comparison with the results from the literature (Sousa Jr and Silva, 2010; Kroflič, 2012).
Preglednica 4.6: Zdrsi med sloji Δ_X^j na začetku štirislojnega nosilca in navpični pomik w na sredini razpona nosilca izračunani z izdelanim analitičnim in numeričnim modelom ter primerjava z rezultati iz literature (Sousa Jr and Silva, 2010; Kroflič, 2012).

	$\Delta_X^{j=1}$ (0) [cm]	$\Delta_X^{j=2}$ (0) [cm]	$\Delta_X^{j=3}$ (0) [cm]	w (L/2) [cm]
Sousa, 2010	0.149301	0.214333	0.270896	3.82794
Kroflič, 2012	0.158872	0.215143	0.269841	3.83519
Numerical model, $N_{el} = 6$ (Timoshenko-Ehrenfest)	0.149301	0.214330	0.270896	3.82801
Analytical model (Euler-Bernoulli)	0.149301	0.214333	0.270896	3.82793
Error (Numerical vs. Analytical model) [%]	2.7 10^{-4}	1.4 10^{-3}	1.8 10^{-4}	-2.2 10^{-4}

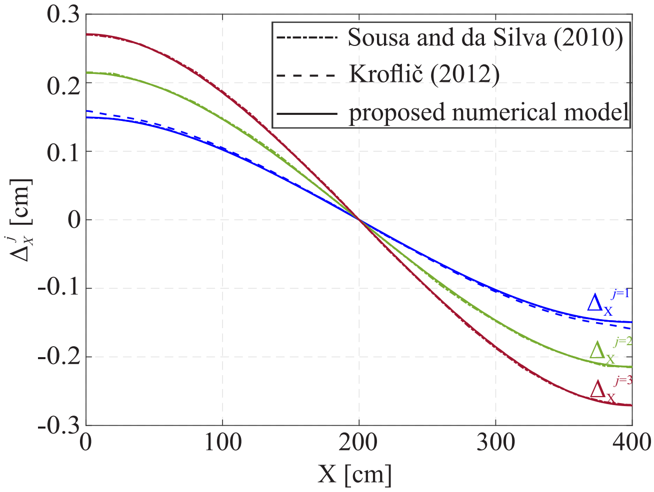

Figure 4.17: Comparisson of slips in four-layer beam calculated with numerical model with the data from the literature (Kroflič, 2012; Sousa Jr and Silva, 2010).
Slika 4.17: Primerjava zdrsov štirislojnega nosilca, izračunanih z numeričnim modelom s podatki iz literature (Kroflič, 2012; Sousa Jr and Silva, 2010).

4.2.2 Validation of the numerical model

As mentioned in Section 3.2.2, the glued laminated beech beams made with 40 mm finger joints were thoroughly measured. The beech boards and laminations were nondestructively tested before the beams were fabricated so that the dynamic moduli of elasticity E_{dyn} were determined. Information on the shear and slip moduli was also determined during bending tests of the glued laminated beech beams. Thus, all input data for the numerical model were obtained. Based on the measurements, the model of the Beam 2 is presented as an example. Fig. 4.18 shows schematically the position of each board and finger joint, and Tab. 4.7 lists the beech boards in each lamination of the Beam 2 along with the length of the boards and the corresponding dynamic elastic moduli, which were determined nondestructively before gluing. To calculate the stiffness of the finger joints, the mean of the measured static moduli of elasticity in tension of all 40 mm finger joints $E_{t,\mathrm{FJ}} = 1242.0$ kN/cm^2 (presented in Section 3.1.3) is used for this model. The numerical model requires the axial stiffness K_{FJ} as input data. Therefore, the moduli of elasticity in tension for the finger joints obtained from experiments must be converted to the corresponding cross-section and length of the finger joint ($l_{\mathrm{FJ}} = 4$ cm), see Eq. (4.3). The shear modulus of the beam was taken from Tab. 3.10 as the average value of the measurement on the left and right sides of the beam, $G = 62.0$ kN/cm^2, and the slip modulus was taken from Tab. 3.11, $K_{\mathrm{X}} = 157$ kN/cm^2.

$$K_{\mathrm{FJ}} = \frac{b^i \, h^i}{l_{\mathrm{FJ}} \, E_{t,\mathrm{FJ}}} \tag{4.3}$$

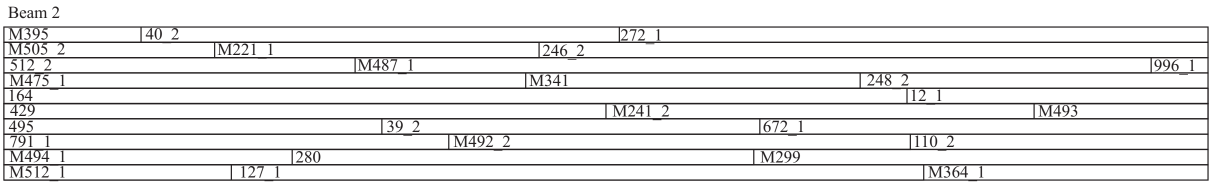

Figure 4.18: Schematic presentation of positions of the non-destructively measured beech boards and positions of the finger joints in the ten-layer Beam 2, prepared for the numerical modelling.
Slika 4.18: Shematski prikaz položajev bukovih desk in položajev zobatih spojev v deset slojnem Nosilcu 2, pripravljen za numerično modeliranje.

Table 4.7: List of boards, their lengths and dynamic moduli of elasticity in laminations of Beam 2 used in numerical model of Beam 2.
Preglednica 4.7: Seznam desk, njihovih dolžin in dinamičnih modulov v lamelah Nosilca 2 uporabljenih v numeričnem modelu Nosilca 2.

Lamination	Board number			Lenghts of the board [cm]			E_{dyn} [kN/cm^2]		
10	M395	40_2	272_1	41	143	174	1480	1940	1820
9	M505_2	M221_1	246_2	63	97	198	1690	1110	1690
8	512_2	M487_1	996_1	105	38	15	1900	1720	1220
7	M475_1	M341	248_2	156	100	102	1590	1580	1480
6	164	12_1		270	88		1420	1690	
5	429	M241_2	M493	180	128	50	1550	1490	1380
4	495	39_2	672_1	113	113	133	1690	2370	1430
3	791_1	M492_2	110_2	133	138	88	1590	1260	1990
2	M494_1	280	M299	87	138	135	1180	1620	1690
1	512_1	127_1	M364_1	68	207	84	1970	1820	1980

These input were used to build the numerical model. Since the mechanical properties of the bottom laminations have the greatest influence on the behaviour of the beam, the model was initially somewhat simplified. Only the three lower laminations were defined precisely, while the average value of the modulus of elasticity was assumed for the upper laminations and the finger joints in these laminations were neglected. Then, the simulation of the loading of the beam model was performed. As in the experimental bending test, the load was applied symmetrically at two points. At the load $P = 82.86$ kN, the maximum load in the experiment, the vertical displacement at the midspan was 7.87 cm, which is much larger than the experimentally measured displacement $w(L/2) = 6.54$ cm. The loading curve with vertical displacement is shown in Fig. 4.19 for the experiment and the numerical model. The error is about 20 %, which could be an acceptable result since the input data itself cannot be considered completely accurate.

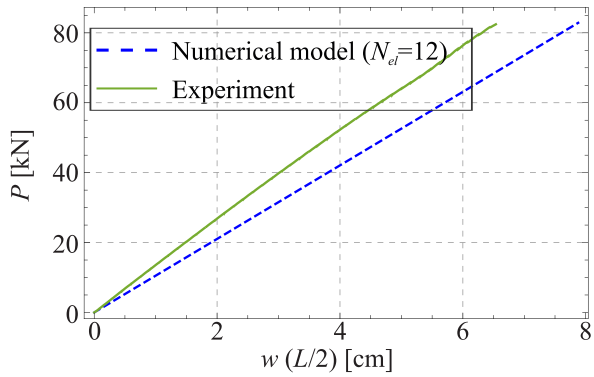

Figure 4.19: Comparison of the measured and calculated load/vertical displacement curve for Beam 2 with finger joints, modelled only in the lower three laminations with averaged modulus of elasticity of upper seven laminations.

Slika 4.19: Primerjava med izmerjeno in izračunano krivuljo obtežbo/navpični pomik za Nosilec 2, z upoštevanjem zobatih spojev samo v spodnjih treh slojih ter povprečnim modulom elastičnosti zgornjih sedmih slojev.

Before stacking and gluing the lamination (boards connected longitudinally), the dynamic moduli of elasticity were also determined for whole individual lamination. The measured moduli of elasticity of the whole laminations were significantly higher which can be seen from comparing the Tab. 4.7 and Tab. 4.8. Another calculation was performed for the same model, but instead of the dynamic moduli of elasticity of the individual boards in the laminations, the measurements of dynamic moduli of elasticity of the whole laminations were inserted in the model. The stiffness of the finger joints remained the same $E_t = 1242$ kN/cm^2 for all finger joint as did the input data for shear modulus and slip modulus (the same for all laminations, elements, and interlayers). The load-displacement curve for this calculation is shown in the left diagram in Fig. 4.20. The maximum vertical displacement was $w(L/2) = 6.98$ cm, which is a much better fit compared to the previous numerical calculation. Since the curves for other equilibrium and kinematic quantities were very similar to the previous calculation, their plots are not shown here.

Another calculation was performed for Beam 2. In this case, all finger joints of all laminations were implemented into the model. The number of elements along the beam thus increased from 12 to 24 elements. All other parameters remained the same. After loading, the maximum deflection of the beam at mid-span was calculated to be $w(L/2) = 6.64$ cm, which is an even better approximation of the experiment, and the error was only 1.5 %. Thus, from these observations, we can conclude that the best approach to modelling the experiments is to use the E_{dyn} of the whole laminations (measuring on boards already longitudinally connected) and to include all finger joints in the model. Since the material properties of the finger joints could not be measured, the average value of the tensile testing of the 40 mm finger joints is considered and the result does not seem to be significantly affected by this simplification. The

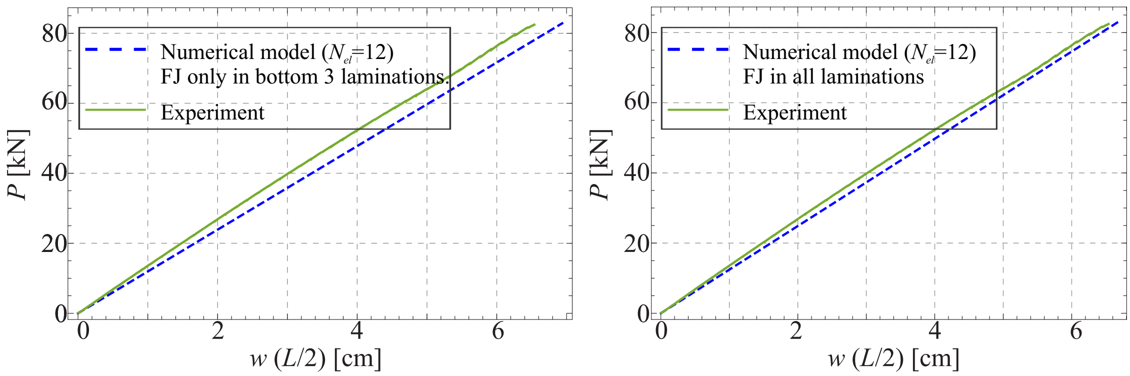

Figure 4.20: Comparison between the measured and calculated load/vertical displacement curve (same E_{dyn} for whole lamination). Left diagram is for the model with finger joint only in the lower three laminations and the right diagram is for the model with finger joints in all the laminations.
Slika 4.20: Primerjava med izmerjeno in izračunano krivuljo obtežba/navpični pomik (enak E_{dyn} za celotni sloj). Levi diagram velja za model z zobatimi spoji samo v spodnjih treh slojih in desni diagram velja za model z zobatimi spoji v vseh desetih slojih.

other beams tested experimentally were then modelled using the same assumptions. The shear moduli G and the contact stiffness K_{X} between the laminations were taken from the measurements of each beam, and the moduli of elasticity of the laminations were used as given in Tab. 4.8. The modelled beams were loaded at two points with a concentrated force equal to the maximum load determined experimentally. The comparison between the numerical model results and the experimentally measured vertical displacements is shown in Fig. 4.21 for the other three beams. Beam 1 was modelled with 17 elements, Beam 3 with 22 elements, and Beam 4 with 24 elements. The maximum vertical displacements in the centre of the beams are shown in Tab. 4.9, which were determined by the numerical model and measured in the experiment. In general, the results agree well, except for the Beam 1, where there were no finger joints in the area of maximum bending moments in the lower lamination. The experimental bending strength was very high and it can be seen that the behaviour of the beam cannot be described as linear, as it was assumed. However, up to a bending stress of about 8 kN/cm^2 (corresponding to a force of 80 kN for this geometry), the curve is linear. The stress of about 8 kN/cm^2 appears to be some sort of limit stress for these beams, indicating either failure or the onset of nonlinear behaviour. For 3 of 4 beams (except Beam 1), the average bending stress was 8.2 kN/cm^2. The experimental data for Beam 3 indicate a partial failure likely caused by failure of one of the internal laminations or finger joints, which we were unable to model from the measured data. Therefore, the errors for Beam 1 and Beam 3 are slightly larger.

As can be seen from Fig. 4.21, Beam 1 shows a nonlinear response to loading. This change in behaviour from a (nearly) linear to a linear response could be due to several reasons. One of them could be instability such as warping of the beam or buckling. Fig. 4.22 shows the measurement of the maximum vertical displacement in front of and behind the beam. It should be noted that the vertical displacement at the back of the beam was not measured throughout the test, so the end of the blue curve does not indicate failure of the beam. At the force of just over 100 kN, the centre inspection point moved out of range of the camera and we could no longer determine the displacement (although failure had not yet occurred). However, it can be seen that the response of the beam is asymmetric, as the displacement measured at

Table 4.8: List of measured dynamic moduli of elasticity of the laminations in four beams (input data in the numerical models).

Preglednica 4.8: Seznam izmerjenih dinamičnih modulov elastičnosti laminacij v štirih nosilcih (vhodni podatki za numerične modele).

Lamination	Beam 1	Beam 2	Beam 3	Beam 4
10	18500	20800	17500	17100
9	18000	17800	20200	17000
8	18800	20300	19400	18500
7	14400	17300	20300	18900
6	19300	16600	19000	22100
5	16300	17600	14900	21200
4	19200	20300	18100	17900
3	19700	15200	20200	18700
2	20600	18100	20000	18100
1	21000	21100	20700	20700

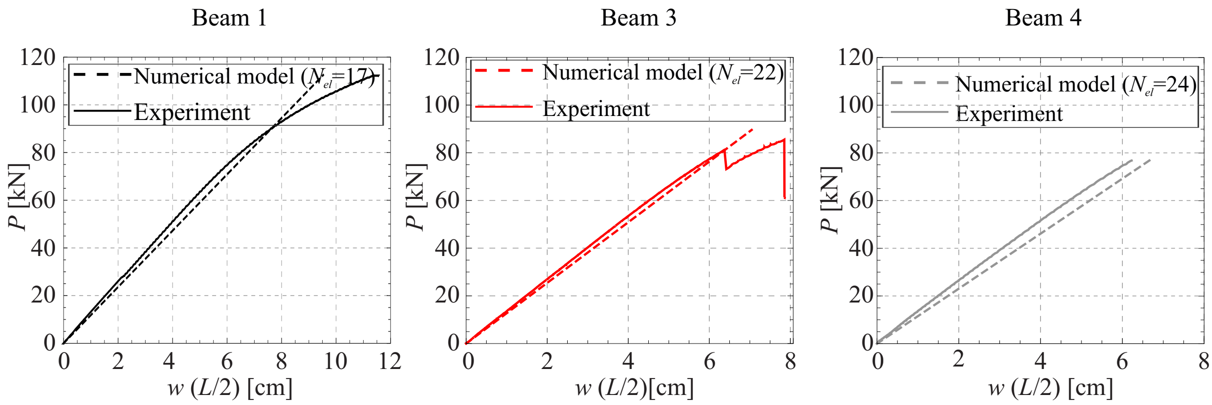

Figure 4.21: Comparison between the measured and calculated load/vertical displacement curve for Beam 1, Beam 3, and Beam 4.

Slika 4.21: Primerjava med izmerjeno in izračunano krivuljo obtežba/navpični pomik za Nosilec 1, Nosilec 3 in Nosilec 4.

the rear is slightly smaller than that measured at the front. This occurred only with this beam, while with the other three beams, were virtually identical. The difference in displacements can be considered as an indication of instability. Since our numerical model was based on first-order theory, which does not accounts for the large displacements and deformations, the instability cannot be modeled. Another reason for the nonlinear behaviour could be the nonlinearity of the material, although the previously performed experiments proved that this is not the case for beech wood. Nevertheless, it was decided to simulate the behaviour of the beam using the nonlinear material of the laminations and the interlayer contact. The constitutive laws are shown in Figs. 4.23 for the interlayer contact and for the laminations (wood) and were used to simulate the behaviour of the Beam 1. The shear modulus and finger joint stiffness remained linear in this model.

Table 4.9: Values of measured and calculated maximum vertical displacements of the glued laminated beams with 40 mm finger joints.
Preglednica 4.9: Vrednosti izmerjenih in izračunanih največjih pomikov lepljenih lameliranih nosilcev s 40 mm dolgimi zobatimi spoji.

Specimen name	N_{el}	Numerical $w(L/2)$ [cm]	Measured $w(L/2)$ [cm]	Error [%]
Beam 1	17	9.53	11.55	17.5
Beam 2	24	6.96	6.92	-0.6
Beam 3	22	7.05	7.85	10.2
Beam 4	24	6.72	6.23	-7.9

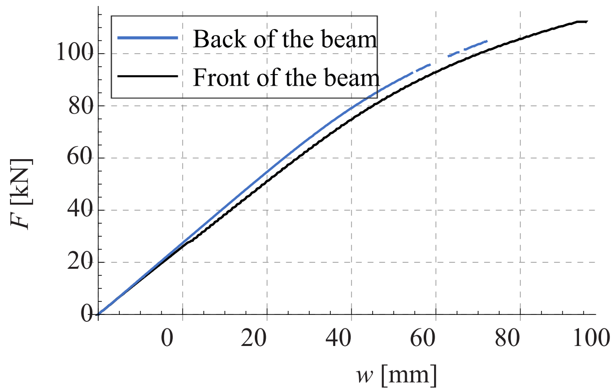

Figure 4.22: Measured vertical displacement in the middle of the span, in front and on the back of the Beam 1.
Slika 4.22: Izmerjen navpični pomik Nosilca 1 na sredini razpona na sprednji in zadnji strani.

The nonlinear model of Beam 1 shows good agreement with the results of the experiment (Fig. 4.24). In the numerical model with nonlinear material laws, the failure occurred at the load $P_{\max} = 110.8$ kN with the maximum vertical displacement $w(L/2) = 11.1$ cm which is very close to the results of the experiment. The comparison of the values is shown in Tab. 4.10.

4.2.3 Verification of the influence of the finger joint

The verification presented in Section 4.2.2 was performed for a multilayer example without finger joint. What remains is to validate the influence of the finger joints. This is performed on a simply supported two-layer beam with multiple finger joints and the results are compared to the analytical model. The analytical model has one finger joint with an axial stiffness $K_{\mathrm{FJ}} = 100$ kN/cm^2, while the numerical model has one finger joint with the same axial stiffness $K_{\mathrm{FJ}} = 100$ kN/cm^2 and three other finger joints with a very high stiffness $K_{\mathrm{FJ}} = 10^{12}$ kN/cm^2, so their influence on the behaviour should not be noticeable. The finger joints with $K_{\mathrm{FJ}} = 100$ kN/cm^2 are located at $5/6\,L$ along the beam in both the analytical and numerical models. The modulus of elasticity of both layers was $E_t = 1200$ kN/cm^2. The

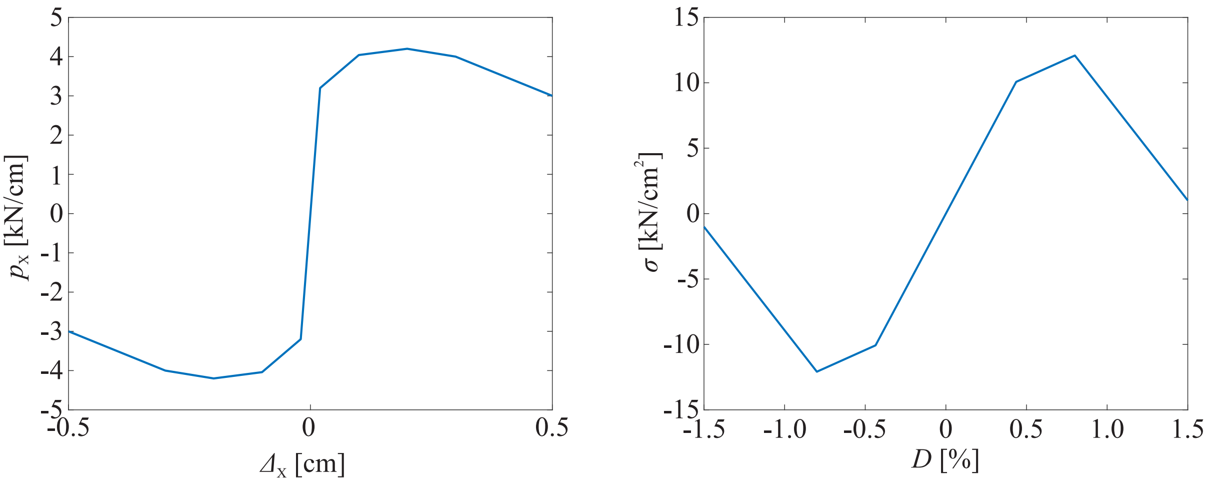

Figure 4.23: Nonlinear constitutive law for interlayer contact (left) and nonlinear constitutive law for the laminations (right), input data for nonlinear numerical model of Beam 1.
Slika 4.23: Nelinearni konstitutivni zakon stika med sloji (levo) in nelinearni konstitutivni zakon lamel (desno), vhodni podatki za nelinearni numerični model Nosilca 1.

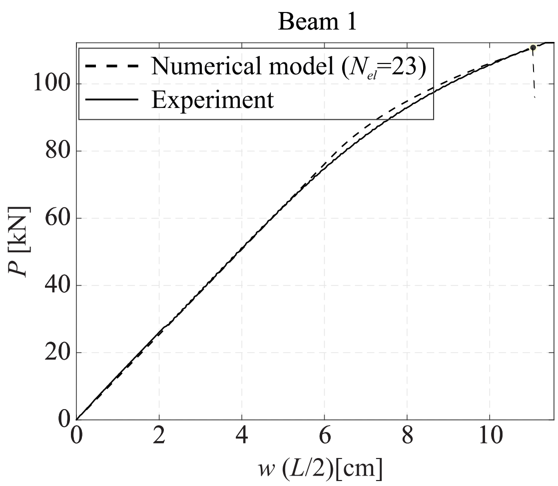

Figure 4.24: Measured and calculated load/vertical displacement curve with nonlinear numerical model at the mid-span of Beam 1.
Slika 4.24: Izmerjen in izračunana krivulja obtežba/navpični pomik z nelinearnim numeričnim modelom na sredini razpona Nosilca 1.

length of the beam was $L = 250$ cm and the beam width was $b = 30$ cm. The bottom lamination with the finger joint had a thickness of $h^a = 10$ cm and the top lamination had a thickness of $h^b = 10$ cm. The beam was loaded with a uniformly distributed load $p_Z = 0.1$ kN/cm^2. The contact stiffness was $K_X = 0.243$ kN/cm^2.

The equilibrium and kinematic quantities were compared and very good agreement was found between the two models. This was expected since the models are based on the same exact equations and the implemented material is linear. In Fig. 4.25 the slip and vertical displacement of the two-layer beam with finger joint in the lower lamination are shown. The curves obtained with both models agree with each other.

Table 4.10: Values of measured and calculated maximum load and vertical displacements of the Beam 1 with nonlinear material model.
Preglednica 4.10: Vrednosti izmerjene in izračune maksimalne sile in pomika Nosilca 1 z nelinearnim materialnim modelom.

		Numerical		Measured	
Specimen name	N_{el}	$w(L/2)$ [cm]	$P_{\max}$ [kN]	$w(L/2)$ [cm]	$P_{\max}$ [kN]
Beam 1 (nonlinear)	25	11.1	110.8	11.6	112.5

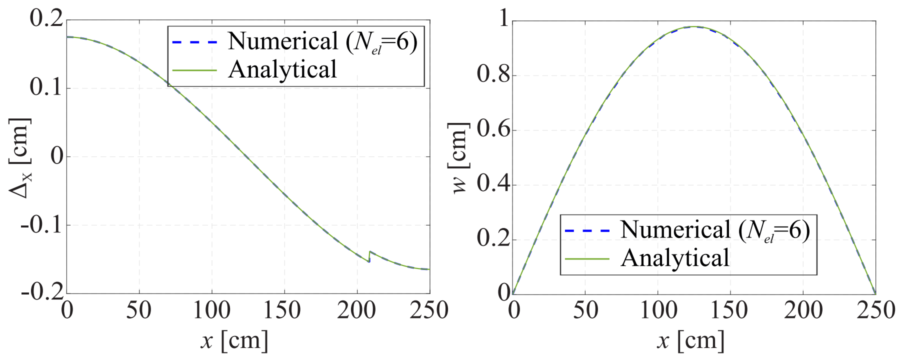

Figure 4.25: Slip Δ_{X} and vertical displacement w of two-layer beam with finger joint at $x_{\mathrm{FJ}} = 5/6L$ with finger joint stiffness $K_{\mathrm{FJ}} = 100$ kN/cm^2 (analytical and numerical model).
Slika 4.25: Zdrs Δ_{X} in navpični pomik w dvoslojnega nosilca z zobatim spojem pri $x_{\mathrm{FJ}} = 5/6L$ s togostjo zobatega spoja $K_{\mathrm{FJ}} = 100$ kN/cm^2 (analitični in numerični model).

In the second example, the length of the beam, the size of the cross-section, and the material properties of the laminations remained the same. Only the position of the finger joint and its stiffness were changed. The finger joint was placed in the middle of the span and the stiffness was lowered to $K_{\mathrm{FJ}} = 50$ kN/cm^2. The slip and vertical displacement are shown in Fig. 4.26. The position and stiffness of the finger joint had no significant effect on the vertical displacement, but the slip at the ends of the beam was reduced by about 8 %.

4.2.4 The robustness of the numerical model

The convergence of the numerical model was unproblematic, which is to be expected for materials with linear elastic behaviour, which is in the case of beech wood true for the first part of the curves, as confirmed by an experimental study. However, numerical models in general can be very sensitive to the number of elements or to the type and order of interpolation and integration along the finite element and across the cross-section. These parameters were evaluated using the example of the 400 cm long simply supported beam with a cross-section of $b \times h = 20 \times 30$ cm^2 with two laminations of equal height. In Fig. 4.27 the interlayer slip and the maximum vertical displacement are shown as a function of the number of elements. It can be seen that both quantities converge rapidly towards the final value. With 5 finite elements, reliable results can be expected. The influence of integration and interpolation method on the results of the model has already been studied by Schnabl (2007) for this type of finite elements. For

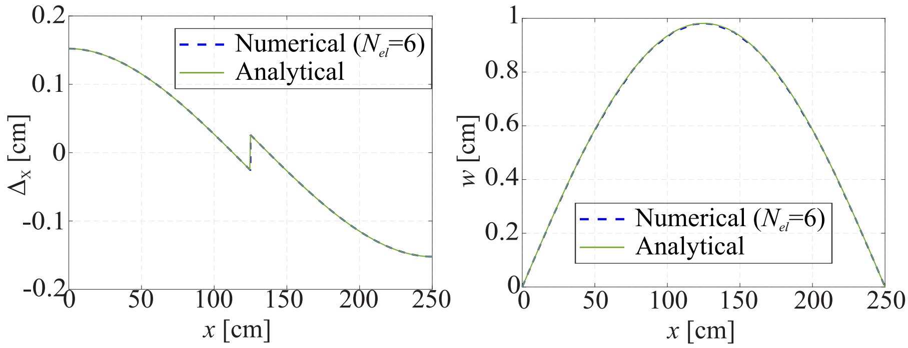

Figure 4.26: Slip Δ_{X} and vertical displacement w of two-layer beam with finger joint at $x_{\mathrm{FJ}} = L/2$ with finger joint stiffness $K_{\mathrm{FJ}} = 50$ kN/cm^2 (analytical and numerical model).
Slika 4.26: Zdrs Δ_{X} in navpični pomik w dvoslojnega nosilca z zobatim spojem pri $x_{\mathrm{FJ}} = L/2$ s togostjo zobatega spoja $K_{\mathrm{FJ}} = 50$ kN/cm^2 (analitični in numerični model).

our model, two integration methods were used for integration along the finite element, namely Gaussian integration method and Lobatto integration method (Golum, 1973). The results showed that the type of integration method is not as influential as the order of integration or the degree of interpolation chosen. However, when the order of integration was greater than 5, the results converged to the final value for both methods. For our calculation, a d.o.i. of 9 was chosen. The number of collocation points (greater than 2) for the interpolation polynomials also did not significantly affect the results. The interpolation order chosen for our further calculation was 4. The material constants were numerically integrated over the cross-section using the trapezoidal rule. Since the number of integration points over the cross-section did not significantly increase the computation time, the cross-section was divided by 1000 points.

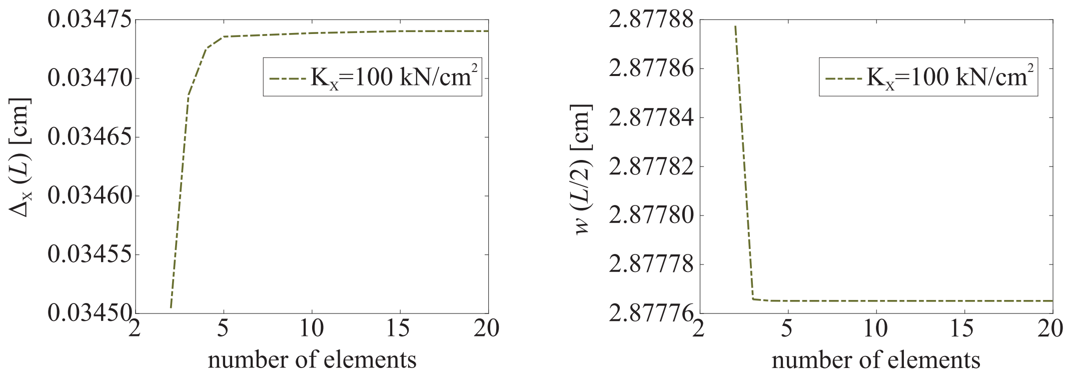

Figure 4.27: Dependence of the interlayer slip at the end of the beam (left) and vertical displacement in the middle of the span of the beam (right) on the number of finite elements.
Slika 4.27: Odvisnost zdrsa med slojema na koncu nosilca (levo) in navpičnega pomika na sredini razpona nosilca (desno) od števila končnih elementov.

As mentioned above, the best results of the numerical model are obtained when the dynamic moduli of elasticity, E^i_{dyn}, measured on whole laminations i are used as input data. Additional improvement of the model was achieved by implementing all finger joints in all laminations. To illustrate the results that can be obtained with the numerical model, the results for the example of Beam 2 are shown in

Figs. 4.28–4.29. The presence of the finger joints is most clearly seen on the graph of interlayer slips where pronounced jumps in the slips j can be seen. The axial force N^i of the layers also shows some irregularities, but they are less pronounced. All internal forces and deformations of all laminations can be determined and analysed.

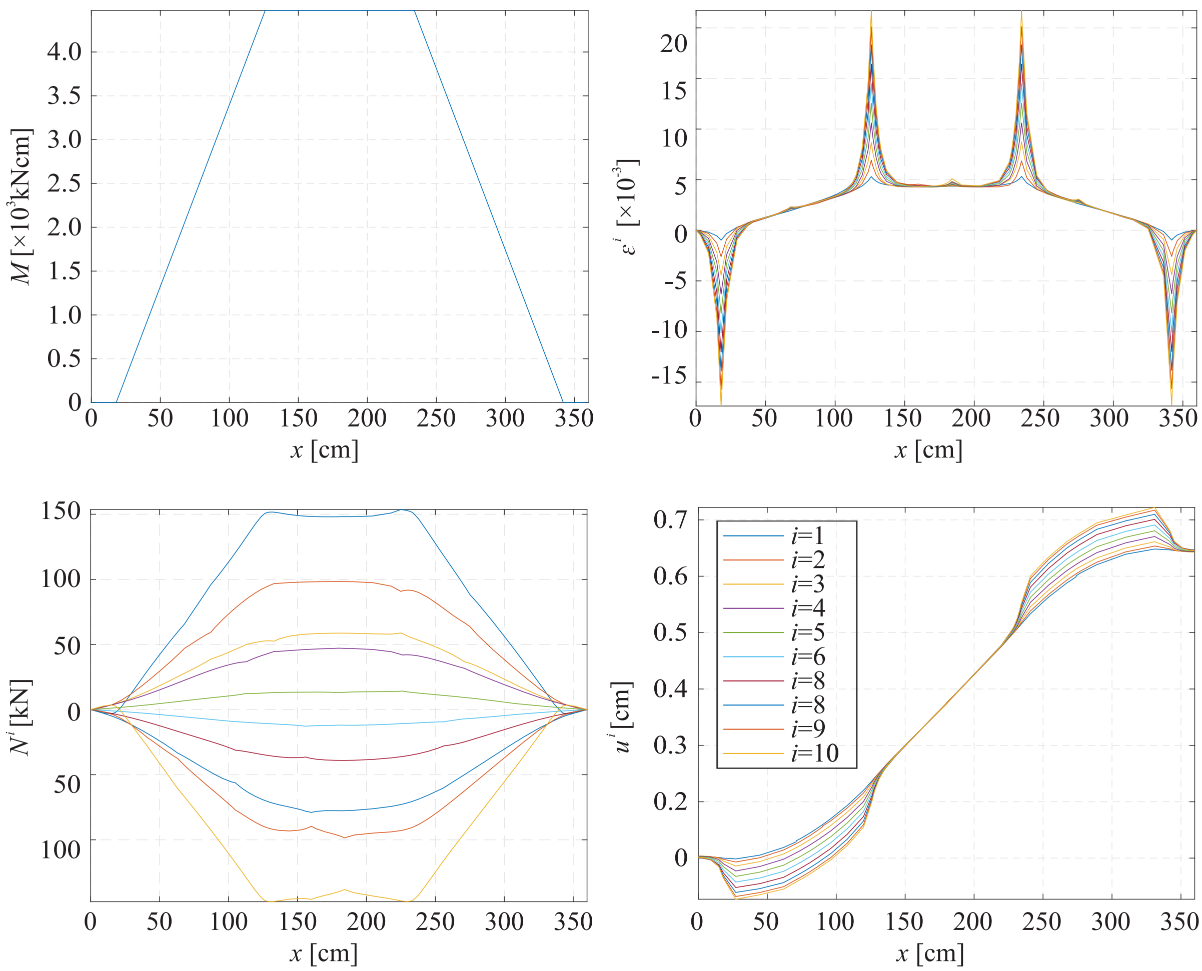

Figure 4.28: Internal moment in the beam and internal axial forces in the laminations (left), axial deformations (upper right) and horizontal displacements of the laminations (bottom right).
Slika 4.28: Notranji moment v nosilcu in notranja osna sila v posameznih slojih (levo), osne deformacije (desno zgoraj) in vodoravni pomik slojev (desno spodaj).

4.2.5 Parametric study on multi-layer simply supported Timoshenko-Ehrenfest beam

4.2.5.1 Influence of number of laminations

Based on the similar beam model as presented in Section 4.2.1, the number of laminations was analysed as a variable parameter and the vertical displacement at midspan was observed. The cross-section $b \times h = 20\ \mathrm{cm} \times 30\ \mathrm{cm}$ was divided into 2-10 laminations of equal thickness and the slip of the lowest interlayer contact at the end of the beam (Fig. 4.30) was observed for different interlayer stiffnesses K_X. The interlayer slip decreases with the number of laminations and with higher interlayer stiffness, which was expected. In the graph, the values $K_\mathrm{X} = 50, 100, 150$ kN/cm^2 are shown together because they give

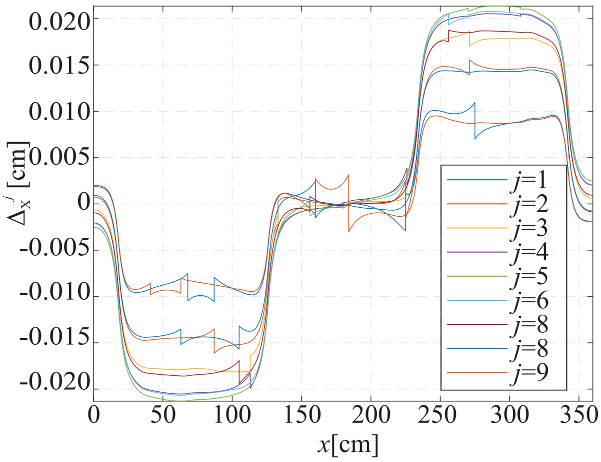

Figure 4.29: Calculated slips between the individual laminations of the Beam 2.
Slika 4.29: Izračunani zdrsi med posameznimi sloji Nosilca 2.

similar results.

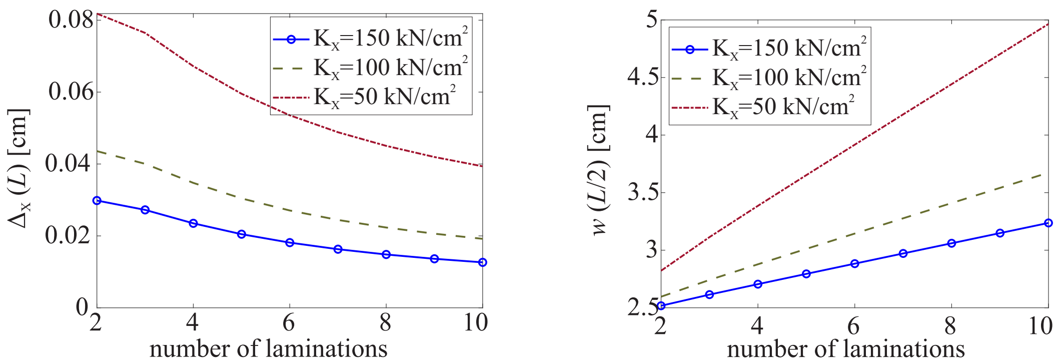

Figure 4.30: Dependence of the interlayer slip at the end of the beam (left) and vertical displacement in the middle of the span of the beam (right) on the number of laminations.
Slika 4.30: Odvisnost zdrsa med slojema na koncu nosilca (levo) in navpičnega pomika na sredini razpona nosilca (desno) od števila slojev.

When the stiffness of the interlayer is reduced to $K_\mathrm{X} = 10$ kN/cm^2, the slip of the lower interlayer increases almost by a factor of 4 compared to $K_\mathrm{X} = 50$ kN/cm^2 and is therefore shown separately in Fig. 4.31. It shows a small peak when the beam is divided into three laminations. In general, we can observe that the vertical displacement in the centre of the beam increases linearly with the number of laminations of the beam and decreases with the interlayer stiffness.

4.2.5.2 Parametric study on ten-layer simply supported Timoshenko-Ehrenfest beam

To evaluate the influence of each parameter on the behaviour of the glued laminated Timoshenko-Ehrenfest beam with finger joints, several parametric studies are presented in this section. The parametric studies were performed based on the geometry and material properties of the example of Beam 2.
The geometry of the beam remained the same, as did the location of the finger joints in the bottom three laminations. The shear and slip moduli were unchanged, $G = 62$ kN/cm^2 and $K_\mathrm{X} = 157$ kN/cm^2. For

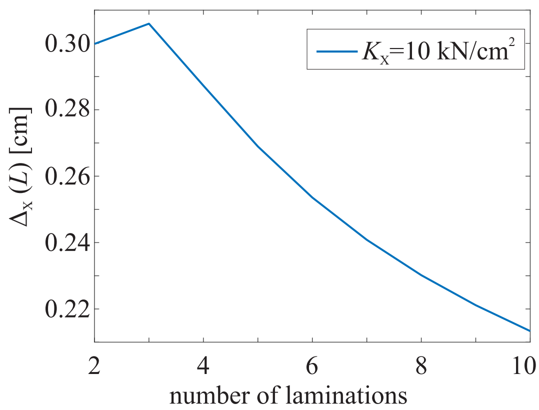

Figure 4.31: Dependence of the interlayer slip at the end of the beam on the number of laminations for $K_\mathrm{X} = 10$ kN/cm^2.
Slika 4.31: Odvisnost zdrsa med slojema na koncu nosilca od števila slojev za $K_\mathrm{X} = 10$ kN/cm^2.

the first parameters, the moduli of elasticity in tension of the laminations and finger joints were chosen, E_t and $E_{t,\mathrm{FJ}}$, respectively. The moduli were varied between 100 and 10000 kN/cm^2 for E_t and between 10 and 10000 kN/cm^2 for $E_{t,\mathrm{FJ}}$. All the laminations and all finger joints had the same equal mechanical properties.

The results showed that the stiffness of the finger joints $E_{t,\mathrm{FJ}}$ had a much smaller effect on the midspan vertical displacements than the stiffness of the laminations E_t. The difference between the displacements with the highest and lowest moduli of elasticity of the finger joints was almost 1 to 6 %, while the moduli of elasticity of the boards had a significant influence, as shown in Fig. 4.32. In the range of moduli of elasticity that are normally expected for beech wood, the stiffness of the finger joint can increase or decrease the vertical displacement between 4 and 5 %.

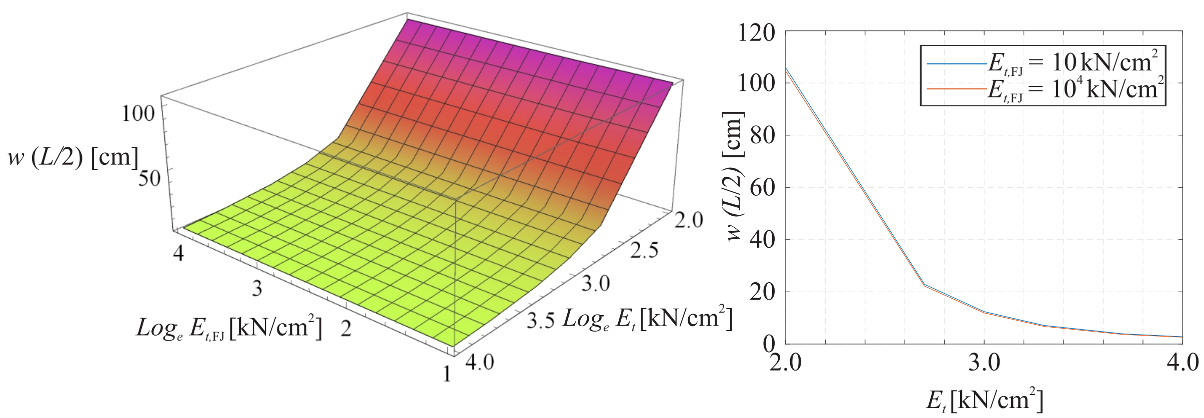

Figure 4.32: Influence of the moduli of elasticity in tension of the laminations E_t and of the finger joints $E_{t,\mathrm{FJ}}$ on the vertical displacement at the mid-span of the glued laminated beam $w(L/2)$.
Slika 4.32: Vpliv nateznih modulov elastičnosti slojev E_t in zobatih spojev $E_{t,\mathrm{FJ}}$ na navpični pomik na sredini lameliranega lepljenega nosilca $w(L/2)$.

The second parameter to be varied was the shear modulus G. The other material parameters remained the same as in the example of Beam 2, as did the geometry of the beam. The influence of the shear modulus of the laminations G and the interlayer contact stiffness K_{X} was investigated and the results are shown in Fig. 4.33. The shear modulus of the laminations is influential when the values are smaller than $G = 100$ kN/cm^2. Such results are to be expected since the beam becomes stiff in the transverse direction beyond a certain point and increasing the stiffness has no effect. Of course, the point at which this happens also depends on the geometry of the beam and other material parameters of the beam (moduli of elasticity of the boards and finger joints). In the standard EN 338 (CEN, 2016b), which lists strength classes for hardwood, the expected shear moduli range from $G = 59$ to 150 kN/cm^2.

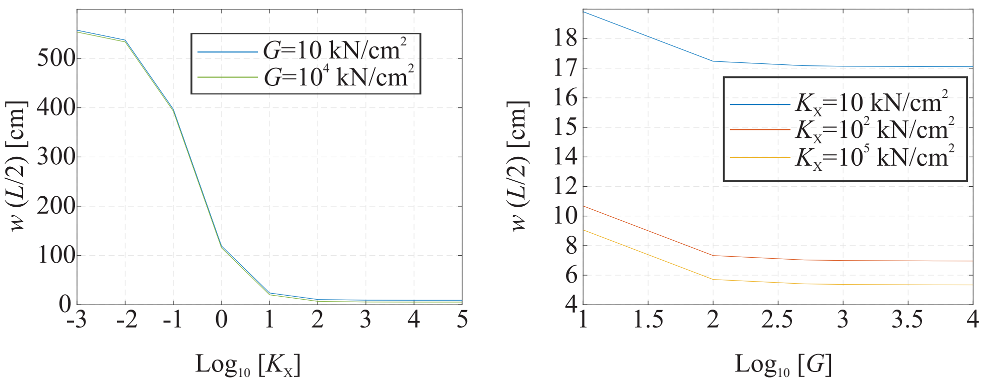

Figure 4.33: Influence of the shear modulus G and interlayer stiffness K_{X} on the vertical displacement in the middle of the span of the glued laminated Timoshenko-Ehrenfest beam.
Slika 4.33: Vpliv strižnega modula G in togostjo vzdolžnega stika K_{X} na navpični pomik na sredini lameliranega lepljenega Timoshenko-Ehrenfestovega nosilca.

The contact stiffness between laminations has a slightly larger effect on the vertical displacement. When the contact stiffness between laminations is increased from $K_{\mathrm{X}} = 10$ to 10^5 kN/cm^2, the vertical displacement at midspan is reduced by a factor of approximately 2.

4.3 Stochastic approach to modelling the laminated beams with finger joints

All results shown so far were obtained using a deterministic approach. All data had a definite deterministic value. However, in reality we do not know the material properties and can only evaluate the input data. The scatter of the material properties must be taken into account. The scatter is even more pronounced when beech wood is involved and existing (simple) methods for evaluating wood properties have limited accuracy. Therefore, it is reasonable to adopt a stochastic approach to modelling glued laminated beams. In this part of the dissertation, a brief study of the influence of scatter, which is typical of the mechanical properties of the beech wood, was carried out.

4.3.1 Simulations on two-layer simply supported Euler-Bernoulli beam with one finger joint

The study was initially conducted using the analytical model of a two-layer, simply supported beam with a finger joint within the span. The beam is based on the illustrative example in Section 4.1.1. The geometry is shown in Fig. 4.34. All geometric and material input parameters were considered stochastically, as in Tab. 4.11, where an assumed distribution with associated means μ_{X} and standard deviations σ_{X} for all stochastic variables X are given. All variables were assumed to be independent and normally distributed, except for the modulus of elasticity of the laminations, for which a lognormal distribution was assumed. The mean value of the length of the beam was $\mu_L = 250$ cm, and the thickness of the lower and upper laminations were $\mu_{h^a} = 2$ cm and $\mu_{h^b} = 18$ cm, and the mean width of the beam was $\mu_b = 20$ cm. A coefficient of variation of 1 % was assumed for all geometric parameters, 5 % for finger joint stiffness K_{FJ} and interlayer contact stiffness K_{X}, and 15 % for moduli of elasticity of both laminations. Simulation of loading of the beam with uniformly distributed load p_Z along the beam was repeated 100 times. The load was also considered to be stochastic and normally distributed with a mean value $\mu_{p_Z} = 0.10$ kN/cm^2.

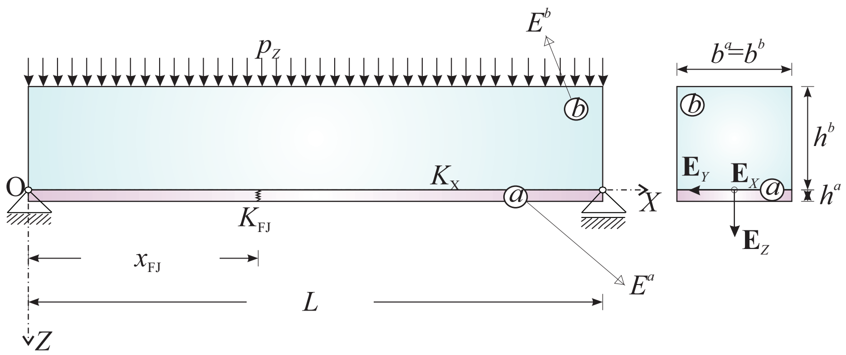

Figure 4.34: Two-layer glued laminated beam with one finger joint for stochastic analysis.
Slika 4.34: Dvoslojni lepljeni nosilec z enim zobatim spojem za stohastično analizo z analitičnim modelom.

Table 4.11: Statistical values and distribution type of variables, used for stochastic analysis of two-layer beam with finger joint for different values of K_{X} with analytical model.
Preglednica 4.11: Statistične vrednosti in tip porazdelitve spremenljivk uporabljenih za stohastično analizo dvoslojnega nosilca z zobatim spojem za različne srednje vrednosti K_{X} z analitičnim modelom.

Variable X	Distribution type	Mean value μ_{X}	Coefficient of variation
$K_{\mathrm{X}1}$[kN/cm]	Normal	10^{-5}	0.05
$K_{\mathrm{X}2}$[kN/cm]	Normal	10	0.05
$K_{\mathrm{X}3}$[kN/cm]	Normal	10^5	0.05
E_t^a [kN/cm^2]	Lognormal	1200	0.15
E_t^b [kN/cm^2]	Lognormal	800	0.15
K_{FJ}[kN/cm^2]	Normal	0.10	0.05
h^a [cm]	Normal	2	0.01
h^b [cm]	Normal	18	0.01
b [cm]	Normal	20	0.01
x_{FJ} [cm]	Normal	100	0.01
L [cm]	Normal	250	0.01
p_Z[kN/cm]	Normal	0.10	0.01

The simulations were repeated for three different mean values of the interlayer contact stiffness: $\mu_{K_{\mathrm{X}1}}$,

$\mu_{K_{\mathrm{X2}}}$ and $\mu_{K_{\mathrm{X3}}}$. In Fig. 4.35 the results of the vertical displacement at mid-span are illustrated. The cumulative distribution functions are shown in the left plot and the probability density function is shown in the right plot. As expected, the mid-span vertical displacements are smaller when the contact stiffness is larger. For the input data presented, the displacements range from 0 to 1.5 cm with mean values of 0.65, 0.61, and 0.45 cm for simulations with $\mu_{K_{\mathrm{X1}}}$, $\mu_{K_{\mathrm{X2}}}$, and $\mu_{K_{\mathrm{X3}}}$, respectively (see Tab. 4.13). The shape of the probability density function of the vertical displacement mid-span resembles a lognormal distribution, so the Pearson χ^2 distribution fit test was performed for all three cases with MATHEMATICA. The p-values were 0.38, 0.30, and 0.23 for $\mu_{K_{\mathrm{X1}}}$, $\mu_{K_{\mathrm{X2}}}$, and $\mu_{K_{\mathrm{X3}}}$, respectively. If we consider the confidence level of $\alpha = 0.05$, the null hypothesis that the vertical displacement is distributed according to the lognormal distribution cannot be rejected for all the cases with $\mu_{K_{\mathrm{X1}}} = 10^{-5}, 10$, and 10^5. Therefore, we will assume, that the vertical displacements are lognormally distributed regardless to the interlayer contact stiffness. The cumulative distribution functions for the three cases with input parameters, presented in Tab. 4.11, can be expressed with the parameters m and s of lognormal distribution, presented in Tab. 4.12 for $\mu_{K_{\mathrm{X1}}}$, $\mu_{K_{\mathrm{X2}}}$, and $\mu_{K_{\mathrm{X3}}}$. In engineering, it is common to limit the maximum

Table 4.12: Parameters m and s for the evaluation of probability that vertical displacement at mid-span of the beam reaches a certain value $w_{L/2}$, determined under the assumption that the mid-span vertical displacement is lognormally distributed, for three mean values K_{X}.
Preglednica 4.12: Parametra m in s, za izvrednotenje verjetnosti, da navpični pomik na sredini nosilca doseže izbrano vrednost $w_{L/2}$, določeni ob predpostavki, da je navpični pomik na sredini nosilce porazdeljen po lognormalni porazdelitvi, za tri srednje vrednosti $\mu_{K_{\mathrm{X}}}$.

	$\mu_{K_{\mathrm{X1}}}$	$\mu_{K_{\mathrm{X2}}}$	$\mu_{K_{\mathrm{X3}}}$
m [cm]	-0.44286	-0.51328	-0.81541
s [cm]	0.19340	0.17205	0.17550

displacements of the load bearing elements using the serviceability limit state method. Let us assume the condition:

$$\max(w_{L/2}) \leq L/250. \tag{4.4}$$

In our case, this means that maximum allowable vertical displacement is 1 cm. If we use parameters m and s for the lognormal distribution presented in Tab. 4.12, we can say that the probability of beam reaching the serviceability limit state, with m contact stiffness of $\mu_{K_{\mathrm{Xl}}}$, where $l = 1, 2, 3$ is:

$$p_{F_1}(w_{L/2}) = 1 - F_{1,W_{L/2}}(w_{L/2} = 1) = 1.1\,\% \tag{4.5}$$

$$p_{F_2}(w_{L/2}) = 1 - F_{1,W_{L/2}}(w_{L/2} = 1) = 0.14\,\% \tag{4.6}$$

$$p_{F_3}(w_{L/2}) = 1 - F_{1,W_{L/2}}(w_{L/2} = 1) = 0.00017\,\%. \tag{4.7}$$

In the second calculation, the mean value of the finger joint stiffness was varied between $\mu_{K_{\mathrm{FJ1}}} = 10^{-5}, 10^2$, and 10^5 kN/cm^2 with a coefficient of variation of 0.05 with a fixed mean value of contact stiffness $K_{\mathrm{X}} = 1$ kN/cm^2. Again, the number of simulations was 100. All other parameters remained unchanged, as shown in Tab. 4.14. The results of the simulations can be seen in Fig. 4.36, where again

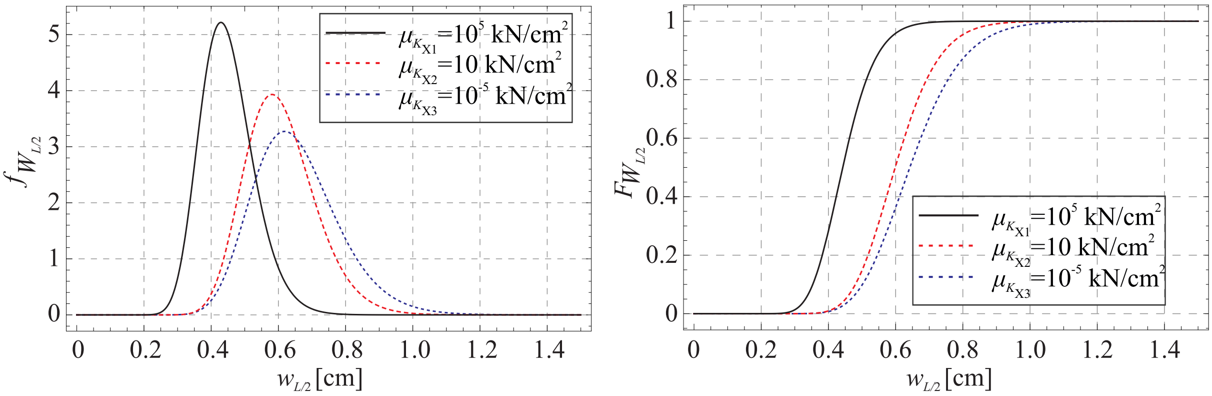

Figure 4.35: Probability density function (left) and cumulative distribution function (right) of the vertical displacement at mid-span of two-layer beam for 100 simulations for three different mean values of K_{X}.
Slika 4.35: Gostota verjetnosti (levo) in porazdelitvena funkcija (desno) za navpični pomik na sredini dvoslojnega nosilca za 100 simulacij pri treh različnih srednjih vrednostih K_{X}.

Table 4.13: Mean values and standard deviations from the results of stochastic analysis of two-layer beam with analytical model, where $\mu_{K_{\mathrm{X}}}$ was varied.
Preglednica 4.13: Srednje vrednosti in standardne deviacije iz rezultatov stohastične analize dvoslojnega nosilca z analitičnim modelom pri spreminjanju $\mu_{K_{\mathrm{X}}}$.

	$\mu_{K_{\mathrm{X1}}}$	$\mu_{K_{\mathrm{X2}}}$	$\mu_{K_{\mathrm{X3}}}$
$\mu_{w_{L/2}}$ [cm]	0.654	0.608	0.449
$\sigma_{w_{L/2}}$ [cm]	0.129	0.108	0.081

the probability density function and the cumulative distribution functions of the vertical displacement at mid-span are plotted for three different mean values of K_{FJ}. The differences between the curves are somewhat smaller than in the case where the contact stiffness was varied. The calculated mid-span vertical displacements varied in the range from 0.36 to 1.13 cm. The mean values of the three curves are very similar, see Tab. 4.15. However, it can be seen that the displacements $w_{L/2}$ are smaller when a larger mean value of finger joint stiffness is considered ($\mu_{K_{\mathrm{FJ}}} = 10^5$ kN/cm^2). For this calculations, also the interlayer slip between the two laminations was observed for the simulations with different mean values of K_{FJ}. In Fig. 4.37 the calculated interlayer slips Δ_L at the end of the beam are shown for the three different mean values of finger joint stiffness $\mu_{K_{\mathrm{FJ}}}$. Compared to the vertical displacement in the mid-span of the beam the influence of finger joints stiffness on the interlayer slips is more pronounced. The mean values of the interlayer slips were 0.039, 0.059, and 0.068 cm, for $\mu_{K_{\mathrm{FJ}}} = 10^{-5}$, $\mu_{K_{\mathrm{FJ}}} = 10^2$, and $\mu_{K_{\mathrm{FJ}}} = 10^5$, respectively (see Tab. 4.15). When the test of distribution fit was performed with MATHEMATICA (Wolfram Research), the results showed that p-values for simulations with all three K_{FJ} are above the 0.05 so the null hypothesis cannot be rejected. Therefore, we assume that the interlayer slips are distributed lognormally for all mean values of K_{FJ}. When the same analysis was performed for the vertical displacement at mid-span of the two-layer beam, the same results were obtained, e.g., also the vertical displacement is assumed to be lognormally distributed or all mean values of K_{FJ}.

Table 4.14: Statistical values and distribution type of variables, used for stochastic analysis of two-layer beam with finger joint with analytical model for different values of K_{FJ}.
Preglednica 4.14: Statistične vrednosti in tip porazdelitve spremenljivk uporabljenih za stohastično analizo dvoslojnega nosilca z zobatim spojem z analitičnim modelom za različne srednje vrednosti K_{FJ}.

Variable X	Distribution type	Mean value μ_{X}	Coefficient of variation
K_{FJ1}[kN/cm^2]	Normal	10^{-5}	0.05
K_{FJ2}[kN/cm^2]	Normal	10^{2}	0.05
K_{FJ3}[kN/cm^2]	Normal	10^{5}	0.05
E_t^a [kN/cm^2]	Log-Normal	1200	0.15
E_t^b [kN/cm^2]	Log-Normal	800	0.15
K_{X}[kN/cm^2]	Normal	1	0.05
h^a [cm]	Normal	2	0.01
h^b [cm]	Normal	18	0.01
b [cm]	Normal	20	0.01
x_{FJ} [cm]	Normal	100	0.01
L [cm]	Normal	250	0.01
p_Z[kN/cm]	Normal	0.10	0.01

Table 4.15: Mean values and standard deviations from the results of stochastic analysis of two-layer beam with analytical model, where $\mu_{K_{\mathrm{FJ}}}$ was varied.
Preglednica 4.15: Srednje vrednosti in standardne deviacije iz rezultatov stohastične analize dvoslojnega nosilca z analitičnim modelom pri spreminjanju $\mu_{K_{\mathrm{FJ}}}$.

	$\mu_{K_{\mathrm{FJ1}}}$	$\mu_{K_{\mathrm{FJ2}}}$	$\mu_{K_{\mathrm{FJ3}}}$
$\mu_{w_{L/2}}$ [cm]	0.645	0.629	0.617
$\sigma_{w_{L/2}}$ [cm]	0.124	0.105	0.097
μ_{Δ_L} [cm]	0.039	0.059	0.068
σ_{Δ_L} [cm]	0.007	0.010	0.011

4.3.2 Simulations on ten-layer simply supported beam with finger joints

The simulations were also performed for the ten-layer beam. The geometry was modelled after Beam 2. The beam consisted of 20 finger joints, two in each lamination. For each simulation, the input data were taken as random values according to the assumed distribution. For the modulus of elasticity of the boards, the values were assumed to be normally distributed, as was the case in the experiments (see Fig. 3.1), with mean value of 1878.5 kN/cm^2 and standard deviation of 182.0 kN/cm^2. The modulus of elasticity for the finger joints was considered distributed according to the log normal distribution, with mean value of 1242 kN/cm^2 and a standard deviation 286 kN/cm^2. The shear modulus was also considered to be randomly taken from the normal distribution (mean 81.6 kN/cm^2 and standard deviation 29.1 kN/cm^2), as was the stiffness of the interlayer contact K_{X} with a mean 179.3 kN/cm^2 and a standard deviation of 43.1 kN/cm^2.

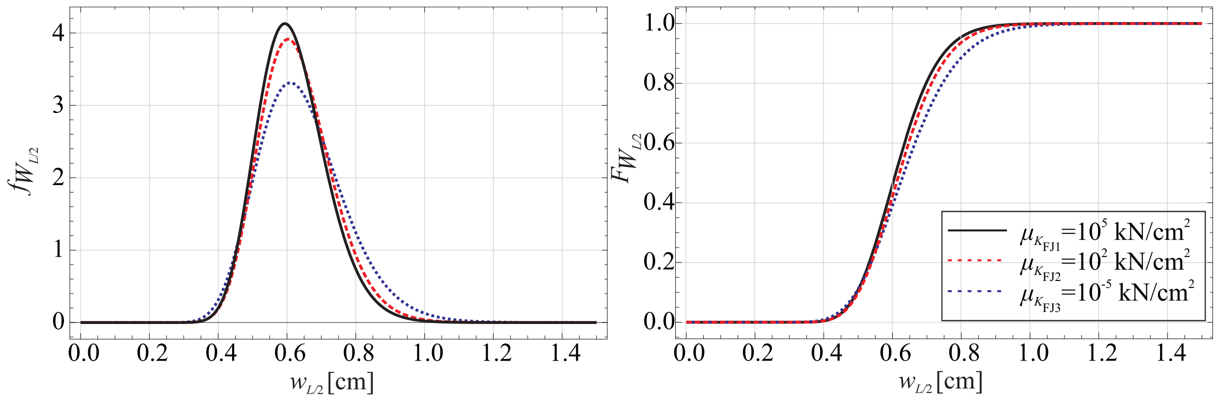

Figure 4.36: Probability density function (left) and cumulative distribution function (right) of the vertical displacement in the middle of two-layer beam for 100 simulations for three different mean values of K_{FJ}.
Slika 4.36: Gostota verjetnosti (levo) in porazdelitvena funkcija (desno) za navpični pomik na sredini dvoslojnega nosilca za 100 simulacij pri treh različnih srednjih vrednostih K_{FJ}.

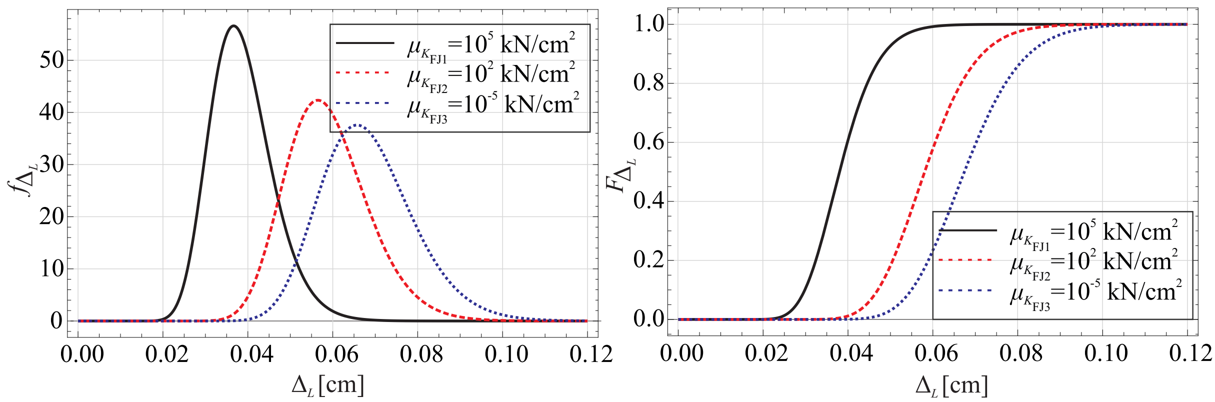

Figure 4.37: Probability density function (left) and cumulative distribution function (right) of the interlayer slip at the end of two-layer beam for 100 simulations for three different mean values of K_{FJ}.
Slika 4.37: Gostota verjetnosti (levo) in porazdelitvena funkcija (desno) za zdrs med slojema na koncu dvoslojnega nosilca za 100 simulacij pri treh različnih srednjih vrednostih K_{FJ}.

4.3.2.1 Linear material

The results of the simulations, in which all material properties were assumed to be linearly elastic, are presented in this section. Information on the input data and the assumed distributions are summarised in Tab. 4.16. Vertical displacement at midspan was observed for the given load. The load was applied at two points (see Fig. 3.24) with the sum of the two forces $P = 100$ kN. The results are shown in Fig. 4.38, where the cumulative distribution function and the probability density functions can be seen. It can be seen that the vertical displacement in the mid-span is distributed according to the normal distribution. The range of values is between 8.2 cm and 8.9 cm, which is considered rather small. The mean value of the vertical displacement was 8.51 cm with a standard deviation of 0.097 cm. The median value was 8.51 cm and the 5$^{\text{th}}$ percentile of vertical displacement at $P = 100$ kN is 8.36 cm.

As can be seen from the parametric study, the interlayer stiffness has a significant influence on the vertical displacement of the beam. Similar to what was shown in Section 4.3.1 for two-layer beam, a

Table 4.16: Statistical values and distribution type of variables, used for stochastic analysis of ten-layer beam with finger joint with numerical model.

Preglednica 4.16: Statistične vrednosti in tip porazdelitve spremenljivk uporabljenih za stohastično analizo desetslojnega nosilca z zobatim spojem z numeričnim modelom.

Variable X	Distribution type	Mean value μ_{X}	Coefficient of variation
E_t	Normal	1878.5	0.10
$E_{t,\mathrm{FJ}}$	Log-Normal	1242	0.23
K_{X}	Normal	179.3	0.24
G	Normal	81.6	0.36

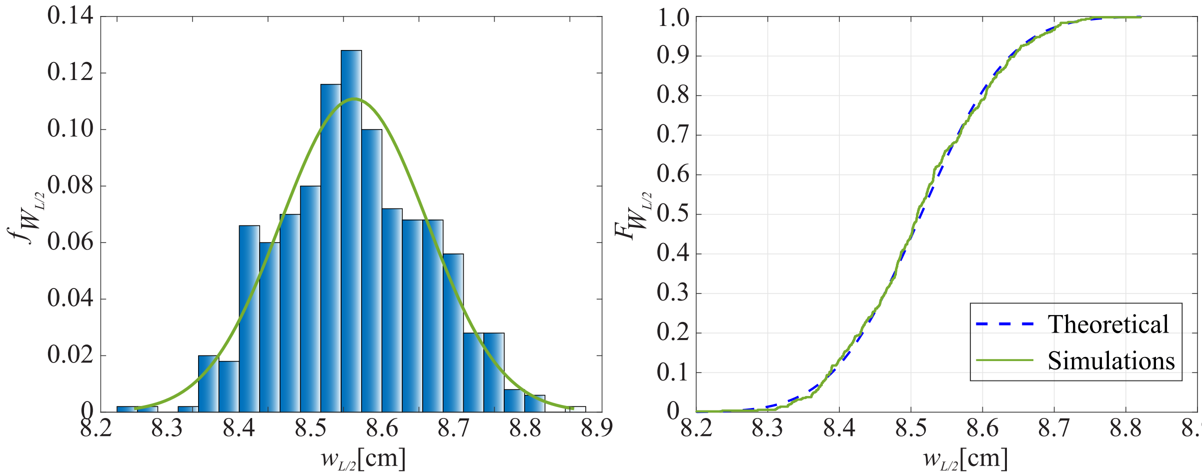

Figure 4.38: Probability density function with histogram (left) and cumulative distribution function (right) of the vertical displacement at given load for 500 simulations.

Slika 4.38: Gostota verjetnosti s histogramom (levo) in porazdelitvena funkcija (desno) za navpični pomik pri dani obtežbi za 500 simulacij.

comparison of simulations for three different mean values of contact stiffness $\mu_{K_{\mathrm{X1}}} = 100$ kN/cm^2, $\mu_{K_{\mathrm{X1}}} = 150$ kN/cm^2, and $\mu_{K_{\mathrm{X1}}} = 200$ kN/cm^2 is presented here for the numerical model of a ten-layer simply supported beam. The other parameters remained unchanged (see Tab. 4.17). For this example, the width and thickness b^i and h^i of each of the $i = (1, 2, ..., 10)$ laminations were also considered as normally distributed. For each $\mu_{K_{\mathrm{X1}}}$, 50 simulations were performed. All material parameters were considered to be linear elastic. The simulated beams were subjected to a symmetric point loading of $P = 100$ kN. The results are shown in Fig. 4.39 where the probability density functions and cumulative distribution functions are plotted for the vertical displacement at mid-span of the glued laminated beams. The mean values and standard deviations are given in Tab. 4.18. We see that the influence of the interlayer contact is much more pronounced here, with 10 laminations, than in the example of the two-layer beam, where the mean values $\mu_{K_{\mathrm{X1}}}$ were varied over a much wider range of values.

Furthermore, an additional 50 simulations were performed based on the data from the three beams, which exhibit what it is considered to be linear behaviour. Based on the scatter of the measured data for the moduli of elasticity of the boards and of the finger joints, the shear moduli, and the interlayer contact stiffness, the calculations were performed 50 times. The applied two-point load was $P = 82$ kN, which

Table 4.17: Statistical values and distribution type of variables, used for stochastic analysis of ten-layer beam with finger joint with numerical model for different values of μ_{K_X}.
Preglednica 4.17: Statistične vrednosti in tip porazdelitve spremenljivk uporabljenih za stohastično analizo desetslojnega nosilca z zobatim spojem z numeričnim modelom za različne srednje vrednosti μ_{K_X}.

Variable X	Distribution type	Mean value μ_X	Coefficient of variation
E_t [kN/cm^2]	Normal	1878.5	0.10
$E_{t,\mathrm{FJ}}$ [kN/cm^2]	Log-Normal	1242	0.23
G [kN/cm^2]	Normal	81.6	0.36
$K_{\mathrm{X}1}$ [kN/cm^2]	Normal	100	0.15
$K_{\mathrm{X}2}$ [kN/cm^2]	Normal	150	0.15
$K_{\mathrm{X}3}$ [kN/cm^2]	Normal	200	0.15
h^i [cm]	Normal	10.0	0.05
b^i [cm]	Normal	1.8	0.05

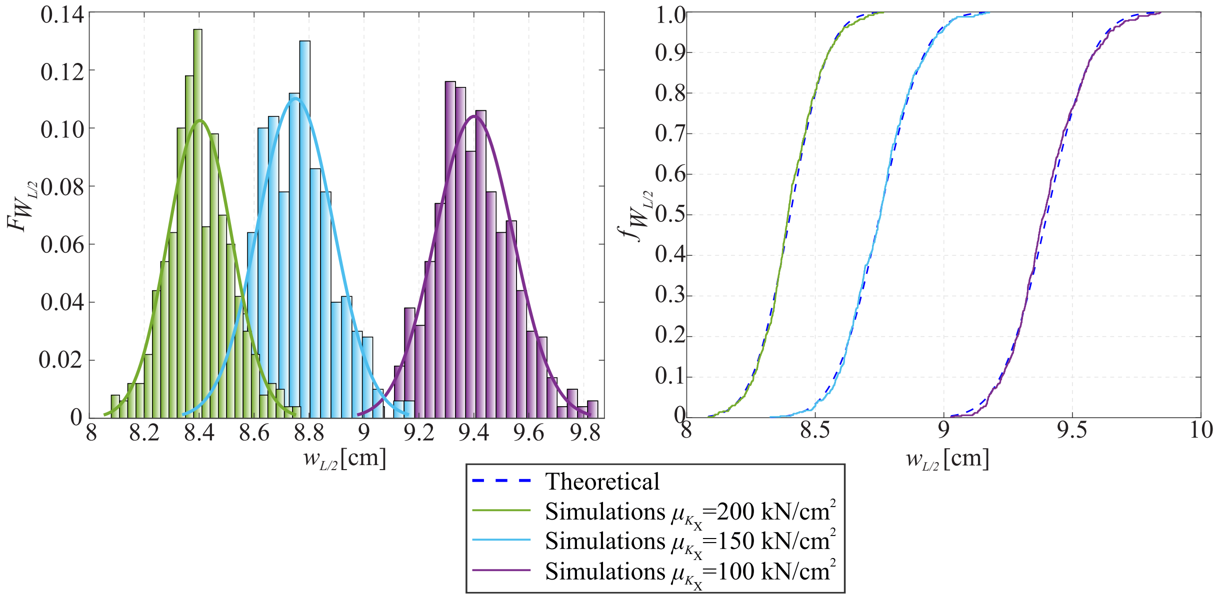

Figure 4.39: Probability density function with histogram (left) and cumulative distribution function (right) of the vertical displacement at mid-span of Beam 2 for three different mean values of K_X.
Slika 4.39: Gostota verjetnosti s histogramom (levo) in porazdelitvena funkcija (desno) za navpični pomik na sredini Nosilca 2 pri treh različnih srednjih vrednostih K_X.

corresponds to the average limit load of the three tested beams that exhibited linear behaviour. The results are shown in Fig. 4.40 along with the deterministically calculated response of the three beams on the left and the experimentally measured response on the right. As expected, the deterministically calculated lines lie between the stochastically determined lines. However, the scatter of the data is quite small, so the range of expected results is quite narrow. When we plot the actual load/deflection curve, we find that the measured data basically underestimate the bending stiffness of the glued beam and the measured values are not within the simulated scatter. The reason for this is probably the incorrectly estimated material parameters from the experiments as input parameters for the model.

Table 4.18: Mean values and standard deviations from the results of stochastic analysis of ten-layer beam with numerical, where $\mu_{K_{\mathrm{XJ}}}$ was varied.
Preglednica 4.18: Srednje vrednosti in standardne deviacije iz rezultatov stohastične analize desetslojnega nosilca z numeričnim modelom pri spreminjanju $\mu_{K_{\mathrm{X}}}$.

	$\mu_{K_{\mathrm{X1}}}$	$\mu_{K_{\mathrm{X2}}}$	$\mu_{K_{\mathrm{X3}}}$
$\mu_{w_{L/2}}$ [cm]	9.401	8.751	8.403
$\sigma_{w_{L/2}}$ [cm]	0.141	0.138	0.117

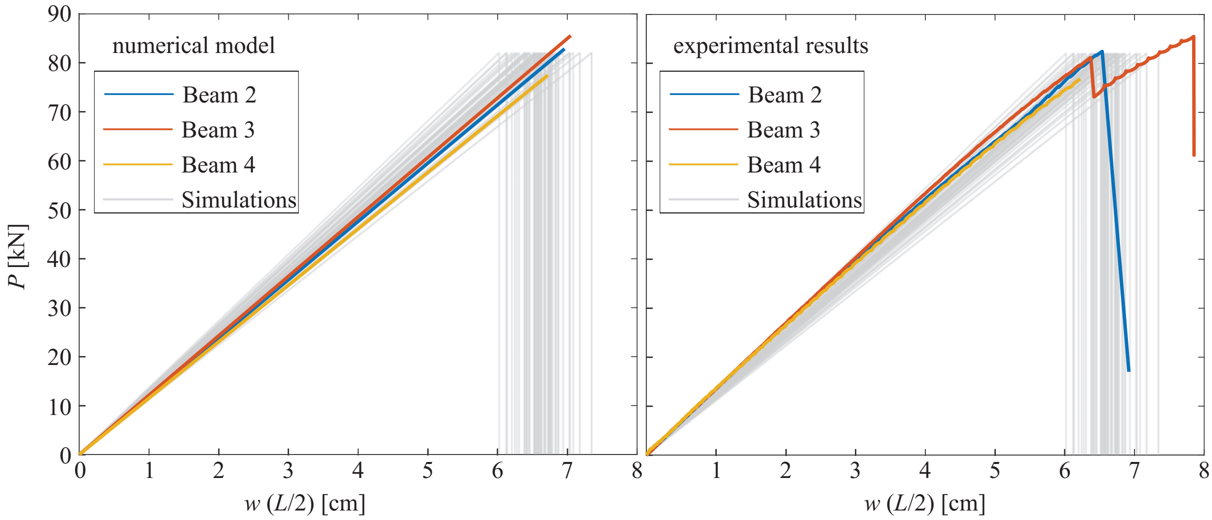

Figure 4.40: Load/vertical displacement curves (50 simulations) and deterministically calculated (left) and measured (right) vertical displacement of three beams at given load.
Slika 4.40: Krivulje obtežba/navpični pomik (50 simulacij) in deterministično izračunan (levo) in izmerjeni (desno) navpični pomik za tri nosilce pri dani obtežbi.

4.3.2.2 Nonlinear material

Simulations can also be performed with nonlinear material parameters. To illustrate this, it was decided to run simulations with similar assumptions to the linear model. In the simulations, each lamination and finite element of the model was stochastically assigned certain material properties according to the assumed distribution, as in Tab. 4.19. The shape of the constitutive law was defined as shown in the left plot in Fig. 4.41, while the exact definition of the curve was stochastic. The load was applied in increments of 5 kN. The width of the lamination was now considered deterministic, since in reality the beams are planed to the final width and thus all the laminations of the beam have the same width. However, in general, the width of the laminations could also be considered stochastic, since this is not the constraint of the model. All other parameters were the same as in the previous examples.
In this case, the number of simulations was increased to 150. The vertical displacement at mid-span was observed and the maximum load, i.e., the load bearing capacity of the simulated beams.

On the right side of Fig. 4.41, the load /vertical displacement curves of the simulations are plotted together with the measured curves for the three beams tested in bending. It can be seen that the experimental tests are approximately in the middle of the simulated results. Fig. 4.42 shows the cumulative distribu-

Table 4.19: Statistical values and distribution type of variables, used for stochastic analysis of ten-layer beam with finger joints with numerical model and nonlinear material model.
Preglednica 4.19: Statistične vrednosti in tip porazdelitve spremenljivk uporabljenih za stohastično analizo desetslojnega nosilca z zobatimi spoji z numeričnim modelom in nelinearnim materialnim modelom.

Variable X	Distribution type	Mean value μ_X	Coefficient of variation
E_t	Normal	1878.5	0.10
$E_{t,\mathrm{FJ}}$	Log-Normal	1242	0.23
G	Log-Normal	81.6	0.36
K_X	Normal	179.3	0.24
h^i [cm]	Normal	10.0	0.05

tion function and the probability density functions for the calculated maximum vertical displacement at mid-span. The mean value was 6.24 cm with a standard deviation of 0.70 cm. The mean is slightly lower than the average of the maximum vertical displacements of the three beams, which was 6.51 cm. We assume that this is due to the fact that the material properties of the individual lamination of each finite element were generated completely independently, so there is a possibility that the same board can have extremely high and extremely low material properties within a few centimetres. In reality, of course, this is very unlikely to happen.

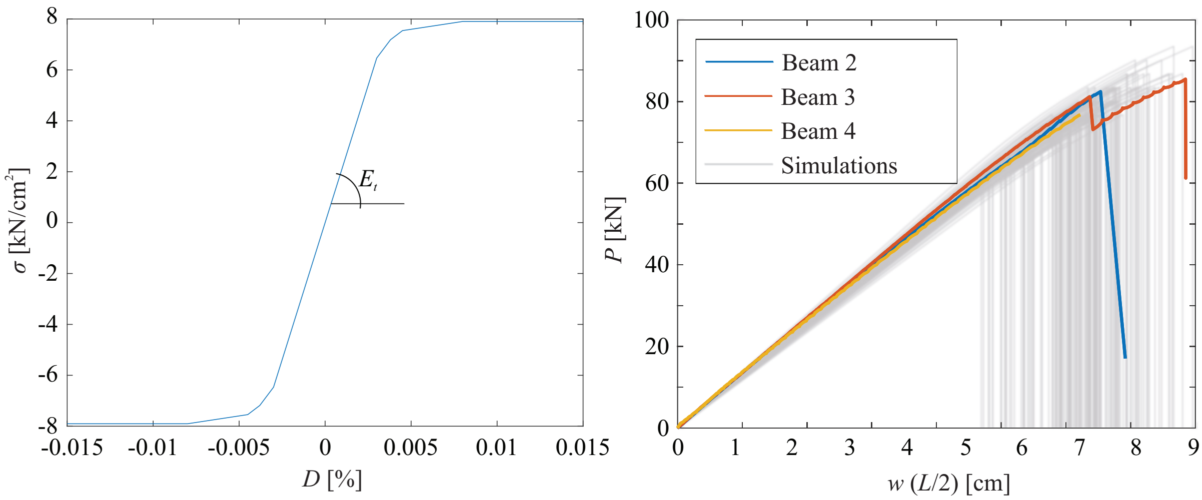

Figure 4.41: Example of constitutive law of one lamination in finite element (left) load/vertical displacement curve for 150 simulations together with measured beams (right).
Slika 4.41: Primer konstitucijskega zakona posamezne laminacije končnega elementa (levo) in krivulja obtežba/pomik za 150 simulacij skupaj z izmerjenimi nosilci (desno).

In Fig. 4.43, the cumulative distribution function and the probability density function are also shown for the maximum achieved load f_{lim} of the simulated beams, i.e., strength of the beams. The mean value of the strength was 7.67 kN/cm^2, with a standard deviation of 0.71 kN/cm^2. The mean value of the strength of the three beams was 8.05 kN/cm^2, which is about 5 % higher than the simulated results.

Using the cumulative distribution function for a load bearing capacity, we can calculate the probability

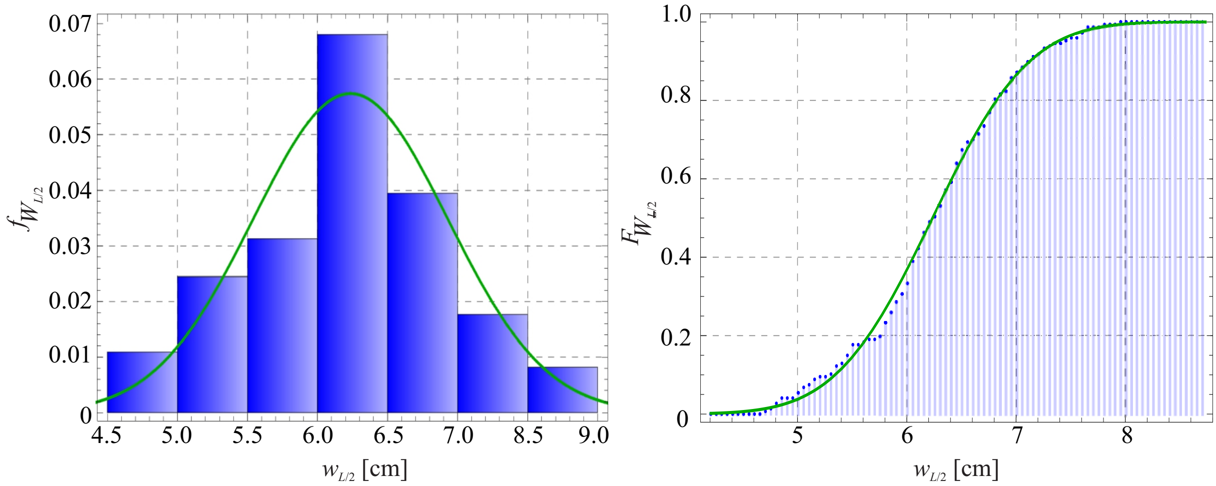

Figure 4.42: Probability density function with histogram (left) and cumulative distribution function (right) of the vertical displacement in the middle of the span of the beams for 150 simulations with nonlinear material.

Slika 4.42: Gostota verjetnosti s histogramom (levo) in porazdelitvena funkcija (desno) navpičnih pomikov na sredini nosilcev za 150 simulacij z nelinearnim materialom.

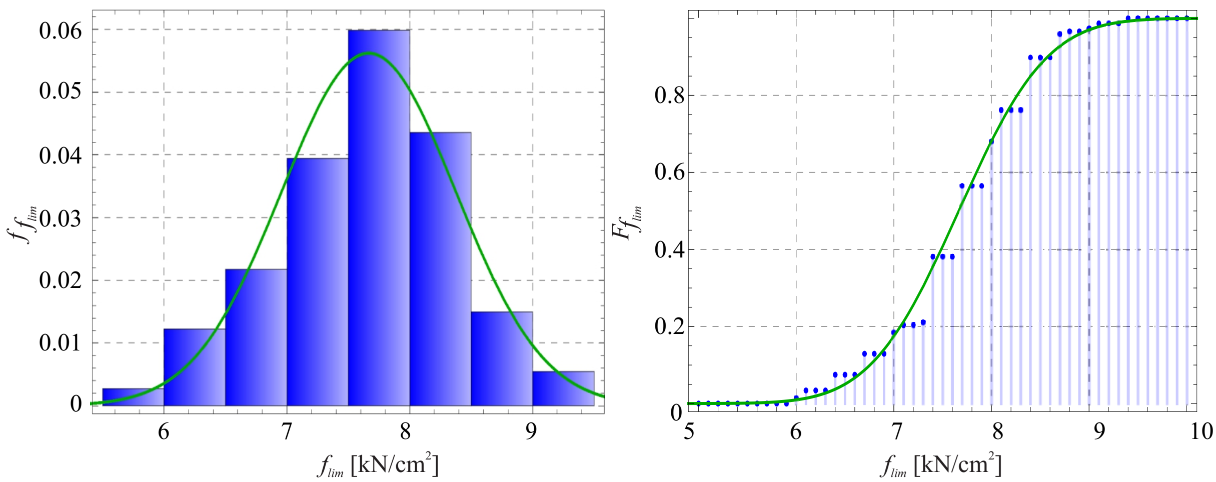

Figure 4.43: Probability density function with histogram (left) and cumulative distribution function (right) of final load bearing capacity for 150 simulations with nonlinear material.

Slika 4.43: Gostota verjetnosti s histogramom (levo) in porazdelitvena funkcija (desno) končne trdnosti nosilcev za 150 simulacij z nelinearnim modelom.

of failure of the beam at a given load. For this reason, again, the hypothesis tests of goodness-of-fit were performed (Wolfram Research) for normal and lognormal distribution. The obtained p-values were very small and we had to reject the hypothesis for both distributions. In Tab. 4.20, probabilities of glued laminated beam failure for 4 loads are shown. They were calculated for two different estimates for the distributions, the normal distribution and the empirical distribution defined with MATHEMATICA (Wolfram Research).

The stochastic analysis with analytical model of two-layer and numerical model of ten-layer glued beam

Table 4.20: Probability of failure of ten-layer beam with finger joints for given load, determined based on stochastic analysis with numerical model and nonlinear material model, for the normal distribution and empirical distribution estimate.

Preglednica 4.20: Verjetnost porušitve desetslojnega nosilca z zobatimi spoji, pri dani obtežbi določena na osnovi stohastične analize z numeričnim modelom in nelinearnim materialnim modelom ob predpostavki normalne porazdelitve in empirične porazdelitve porušitve nosilca.

Load P [kN]	Probability of failure (Normal distribution estimate)	Probability of failure (Empirical distribution estimate)
60	0.9 %	1.4 %
70	17.3 %	13.6 %
82.5*	79.4 %	76.2 %
90	97.0 %	98.6 %

*mean value of strengths for the three measured beams

with properties of beech wood was performed for the illustration of the possible applications of the model. Comparing the simulated results of some kinematic quantities and load bearing capacities showed, that the model can be used for stochastic analysis of glued laminated beams and that results are sensible. As can be seen from these comparisons, the test results are well within the results obtained by the model. Even more, the test results are in the middle of the calculated values and not at one or the other edge of the results of the simulations on the model. This is true for both the vertical displacement and even for the load bearing capacity making the model a useful computational tool for specifying both quantities. However, it must be pointed out that the input data for the model is very important for the results of the simulations. In the future, it would be sensible to pay attention also to this aspect of modelling, so different distributions of the input data would be considered. Another important improvement of the stochastic modelling would be the implementation of dependant variables. In this work, all the input parameters were generated as independent variable, which is not the case in reality. Thus, the result of the simulations on the numerical model would be more realistic.

5 CONCLUSIONS

Due to its high mechanical properties, beech wood is a very interesting species for use as a building material. The composition of beech wood makes the material very susceptible to large deformations due to environmental changes, such as warping and cracking. Therefore, the most sensible way to use beech wood is to use glued structural elements such as glued laminated beams. In order to take full advantage of the high mechanical properties of beech wood in glued laminated beams, the finger joints must also be able to withstand high loads.

Finger joints are used to longitudinally connect individual boards into laminations and are an important element of the glued laminated beams that can determine the load bearing capacity of the glued laminated beams. When beech wood is used in glulam beams, finger joints are even more influential, so special attention must be paid to them, especially to their strength under tensile loading. Our research has shown that the standard finger joint profile used in glued softwood glued laminated beams does not have sufficient tensile strength. The average tensile strength measured on the standard finger joint profiles (all 18 mm finger joints) was 37.7 MPa, which is about 50 % lower than the tensile strength of Slovenian beech wood. The results of experimental testing of finger joints in tension are strongly influenced by the specimens that failed in the wood, and somewhat higher tensile strengths had been expected. Nevertheless, it was obvious that the new finger joint configuration must be investigated. After the analytical and numerical study of the main geometrical parameters, finger joint length l, pitch p and, tip width b_t, the geometry of finger joint was optimised for higher tensile strength of the finger joints and the geometry was set to $l = 40$ mm, $p = 8$ mm, and $b_t = 1.5$ mm. Some other geometries such as $l = 40$ mm, $p = 7.1$ mm, and $b_t = 1$ mm or $l = 50$ mm, $p = 8.4$ mm, and $b_t = 1$ mm would be suitable in terms of the expected tensile strength of the finger joints, but were not chosen because of the technical difficulties in manufacturing the cutting head and installing it in the production line.

The configuration of the finger joints also depends on the adhesives used in the finger joints. In general, the properties of the structural adhesives are very versatile and a suitable combination of the adhesive with the adhered, i.e., beech wood, is crucial to achieve sufficient and durable tensile load bearing capacity of the finger joints. According to the experimental test results of the 18 mm finger joint as well as the 40 mm finger joints, where different adhesive types were used, the influence of the adhesive type decreased with longer and slimmer finger joint profiles. This confirmed the results of the preliminary study on the tensile strength of the finger joints. The average tensile strength of the optimised finger joint profile (all 40 mm finger joint test specimens) obtained from experimental tensile tests was 55.8 MPa, which is a significant improvement of almost 50 %. This is the average value for all specimens, regardless of the type of adhesive and the type of failure. It was concluded that the properties of the existing types of structural adhesives are suitable for longitudinal bonding of beech boards for glued laminated beams.

The insufficient tensile strength of the standard finger joint profile was also demonstrated by flexural experimental testing of the glued laminated beams. The mean flexural strength of 10 glued laminated beams with 18 mm finger joints was 64.4 MPa. In addition to tensile strength, the flexural modulus of elasticity was also determined during the tests. The mean global modulus of elasticity for 10 beams with 18 mm finger joints was 14900 MPa. Although all glued laminated beams failed in the finger joint in the bottom lamination, the obtained strength and modulus of elasticity confirm the high mechanical properties of beech wood compared to what can be expected for softwoods, see EN 14080 (CEN, 2013e). For comparison, 4 glued laminated beams were made from beech boards with 40 mm finger joints. Selection of the best boards was based on the visual assessment of the boards and also on machine strength grading. The glued laminated beams were then tested in bending. Mean flexural strength of 4 glued laminated beams with 40 mm finger joints was 92.9 MPa. The modulus of elasticity, shear modulus, and stiffness of the interlayer contact were also measured for this batch of beams. These mechanical properties of glued laminated beech beams are rarely found in the literature. When comparing the two batches of the glued laminated beech beams, the flexural strength was increased by 44 %, just by optimizing the finger joint profile. Glued laminated beech beams from both batches showed nearly linear elastic behaviour with sudden and brittle failure.

Analytical and numerical models were prepared for the analysis of the mechanical behaviour of the glued laminated beech beams were established in the study. For the first time, an exact analytical solution of the multilayer glued laminated beech beams with finger joints is presented. The models are based on the formulation of the Reissner planar beam (Reissner, 1972). The analytical model takes into account the slip between the layers and fully debonded parts of the laminated beams are also considered. The finger joints are implemented as linear springs. The derivation of the analytical solution was presented for Euler-Bernoulli beams and Timoshenko-Ehrenfest beams. The mathematical model can be used to evaluate the kinematic and equilibrium quantities in the glued laminated beams. A parametric study was conducted in which selected parameters were varied and their influence on the mechanical behaviour of the glued laminated beam was evaluated. The results showed that the finger joint stiffness K_{FJ} and the interlayer contact stiffness K_{X} have a significant influence on the kinematic and equilibrium quantities, especially on the vertical displacement at the mid-span of the beam $w(L/2)$ and on the interlayer slip Δ_{X}.

The complexity of the model is determined by the number of laminations and the number of finger joints. For example, if we model a glued laminated beam with 10 laminations and arbitrary position and number of finger joints, the analytical expressions become too complex to solve. For this reason, we derived a numerical model allows us to model more complex glued laminated beams, like the ones we used in experimental tests. The numerical model is based on the same theoretical foundation as it was the analytical model, i.e., a Reissner planar beam with the assumptions of the Timoshenko-Ehrenfest beam theory. First-order theory was taken into account so only small displacements and rotations are allowed. The number of laminations and finger joints is arbitrary, as are the constitutive laws of the layered material and of contact between layers, so that also nonlinear material properties can be used. The numerical model was verified with the result of the analytical model and also with the results obtained in the literature (Sousa Jr and Silva, 2010) and (Kroflič, 2012). The results showed a very good agreement. The numerical model was also validated with by comparing it with the experimental test results of the 4 beams with 40 mm finger joints. All four beams were modelled using the numerical model with the exact position of the finger joints and measured inputs for dynamic modulus of elasticity of the laminations, tensile modulus of elasticity of the finger joints, shear modulus and interlayer contact stiffness. The parameters of beech wood were first considered to be linearly elastic. Comparison of the vertical displacement at the mid-span of the beam between the numerical model and the experimental results showed agreement in the range of 5 %, except for one beam that exhibited nonlinear behaviour. This beam was additionally modelled with nonlinear material properties as an example. Both numerical and analytical models were used for the stochastic analysis of the glued laminated beams with linear and nonlinear material properties, and the failure load was also simulated. The experimental results agree with the results of the simulations. The difference between the measured and simulated mean failure loads was 10 %. A parametric study was performed with simulations varying the mean values of finger joint stiffness and contact stiffness, and it confirmed the important influence of these parameters on the vertical displacement in the mid-span of the glued laminated beech beam.

The original contributions of the present work are summarized as follows:

- The evaluation of the influence of the geometrical parameters of the finger joints and of influence of the type of adhesive used in the finger joints.
- Production of the new finger joint profile adapted to the high mechanical properties of beech wood.
- Experimental measurements of strength and stiffness properties of different finger joint geometries and different structural adhesives on test specimens made of Slovenian beech wood.
- Experimental testing of glued laminated beams made of Slovenian beech wood with different finger joint profiles.
- Production of glued laminated beams made of beech wood with the highest bending strength reported in the literature.
- First analytical solution for glued laminated beams with interlayer slip and finger joints.
- First numerical model for glued laminated beams with interlayer slip with arbitrary number of laminations and arbitrary number of finger joints.
- Stochastic analysis based on the analytical and numerical model of the glued laminated beams made from beech wood.
- Part of the research has already been published in the SCI indexed journals. The two papers can be found in the Appendices.

If we address the research hypotheses made at the beginning of the research and presented at the beginning of this work, we can conclude that:

- The load bearing capacity of glued finger joints made from beech wood can indeed be significantly increased by using longer and thinner finger joints. Since we could not achieve failure of the wood in all the finger jointed laminations, we cannot confirm, that the full utilization of the wood was achieved, but it was definitely increased.
- The calculations and experiments have confirmed that the influence of the type of adhesive decreases when the finger joint profile is optimised, so that no new type of adhesive is required for application to structural elements made of beech wood.
- The prepared numerical model of a glued laminated beam can simulate the actual flexural behaviour of beams made of beech wood. If the material properties are known, the deflections can be estimated very accurately using the numerical model.

The results presented above on the mechanical properties of finger joints and glued laminated beams made of Slovenian beech wood are a contribution to the currently not extensive database on the mechanical properties of glued elements made of beech wood. Due to the large scatter of mechanical properties of wood, the amount of data is of great importance. Thus, the results of the experimental tests could contribute to the preparation of the new regulations for the production of glued laminated structural elements made of beech wood. The mathematical models derived could be useful for the design of glued laminated beams and for the purposes of possible future studies in this field of research.

6 RAZŠIRJENI POVZETEK

6.1 Uvod

Les je zaradi zagotavljanja ugodnih bivanjskih pogojev in prijaznosti do okolja zelo zanimiv za uporabo v konstrukcijske namene. Sodobni konstrukcijski elementi so večinoma izdelani v obliki lepljenih nosilcev ali plošč pri tem pa se uporablja predvsem les iglavcev saj ga odlikuje hitra rast, enostavna obdelava in relativno dobra odpornost na zunanje vplive, kar podaljšuje njihovo življenjsko dobo. Vendar se tako v Sloveniji kot v Evropi zaloga lesa iglavcev v gozdovih vztrajno zmanjšuje. V Poročilu Zavoda za gozdove ZGS (2020) zasledimo, da se je zaloga iglavcev, tudi zaradi izrednih vremenskih pojavov, v zadnjih letih zmanjšala do te mere, da so zaloge iglavcev postale manjše od zalog listavcev. V iskanju možnih nadomestnih vrst lesa za uporabo v konstrukcijske namene je bukov les zelo logična izbira saj je v Jugovzhodni Evropi in posledično tudi v Sloveniji najbolj zastopana lesna vrsta ZGS (2020). Bukev je avtohtona vrsta, zato je bolj prilagojena na vremenske pogoje in manj občutljiva na morebitne izjemne pojave kot na primer žled. Je tudi manj izpostavljena napadom različnih insektov.
Bukov les je bil v preteklosti že uporabljen v konstrukcijske namene, (Peperko, 2006) vendar se je njena uporaba v moderni proizvodnji opustila predvsem zaradi težje obdelave. Ima namreč višjo gostoto, zato je posledično težji za obdelavo in tudi obraba obdelovalnih orodij je hitrejša, zato med proizvajalci lesnih konstrukcijskih elementov ni zaželena. Vendar pa bukov les odlikujejo visoke trdnostne in togostne lastnosti. Natezna trdnost je v povprečju kar trikrat višja od trdnosti smrekovega lesa (Ehrhart et al., 2016, 2018a; Fortuna et al., 2018a; Plos et al., 2018a), zato bi bil les lahko zelo uporaben za konstrukcijske elemente. Vendar je potrebno biti pri uporabi bukovega lesa nekoliko previdnejši, saj je neustrezno zaščiten les lahko izpostavljen velikim dimenzijskim spremembam in gnilobi (Aicher et al., 2001; Peperko, 2006). Kljub temu še vedno lahko najdemo konstrukcije iz bukovega lesa, ki so se ohranile vse od sredine 19. stoletja (Peperko, 2006). Bukov les ima torej potencial kot konstrukcijski material, vendar so njegove mehanske lastnosti še relativno neraziskane oziroma je količina podatkov o mehanskih lastnostih omejena. V trenutno veljavni evropski standardizaciji ni dokumenta, ki bi obravnaval uporabo bukov les v konstrukcijske namene v sodobni obliki slojevitih, lepljenih konstrukcijskih elementov (Franke et al., 2014).
Lepila so v lepljenih konstrukcijskih elementih pomemben dejavnik, ki ga je potrebno obravnavati v sklopu lesnih kompozitov. Lepljenje omogoča uporabo boljših kosov lesa, ki jih je nato mogoče sestaviti v močnejše in stabilnejše elemente. Lepilo ojača poškodovane celice in pripomore k enakomernejši porazdelitvi napetosti v stični ploskvi (Šernek et al., 1999). Lepilo lahko pripomore tudi k povečani trajnosti elementov. Pomembna je izbira primernega lepila, ki je odvisna od vrste lesa, zunanjih pogojev, katerim bo lepljen element izpostavljen in seveda zahtevanih mehanskih lastnosti, predvsem nosilnosti in modula elastičnosti konstrukcijskega elementa.
Med lesnimi kompoziti so v konstrukcijske namene najpogosteje uporabljeni lepljeni nosilci (GL) in križno lepljene plošče (CLT). Pri izdelavi obeh vrst elementov se uporabljajo vzdolžno lepljene deske. Vzdolžno spajanje se izvaja s t.i. zobatimi spoji, za katere so v standardu EN 14080 CEN (2013e) definirane zahteve za uporabo v konstrukcijske namene. Te zahteve so bile definirane v luči znanih mehanskih

lastnosti iglavcev, ki so, kot je bilo že omenjeno, znatno nižje. Ko govorimo o mehanskih lastnosti, se osredotočamo predvsem na natezno trdnost in elastični modul, saj imata ti dve lastnosti najpomembnejšo vlogo pri prevzemu upogibne obremenitve, kjer so spodnji sloji kompozitnih elementov obremenjeni natezno. Navpični pomik, ki je za inženirje eden pomembnejših dejavnikov pri zagotavljanju mejnega stanja uporabnosti, je neposredno odvisen od modula elastičnost. Nateznim obremenitvam so tako podvrženi tudi zobati spoji. Znano je, da zobati spoji običajno predstavljajo šibko točko (Aicher et al., 2001; Serrano, 2003; Franke et al., 2014; Tran et al., 2014), ki definira nosilnost elementa. Zato je pomembno posvetiti posebno pozornost njihovi natezni trdnosti, ki pa je odvisna od geometrije spoja, uporabljenega lepila in kvalitete izdelave ter seveda vrste lesa(Tran et al., 2014; Franke et al., 2014; Aicher and Radović, 1999; Collin and Ehlbeck, 1992; Konnerth et al., 2006).

Mehanske lastnosti lesa, zobatih spojev in lepil so bistveni vhodni podatki za računski model lepljenih nosilcev. Prvi računski modeli so bili enostavnejši z upoštevanjem tako geometrijske kot tudi materialne linearnost. Med modeli kompozitnih nosilcev z upoštevanjem delne povezanosti slojev je bila med prvimi uveljavljena Newmarkova teorija slojevitih nosilcev (Newmark, 1951). Kasneje je bilo predstavljenih še nekaj enostavnih računskih modelov, ki so upoštevali zdrs med sloji (Goodman and Popov, 1968; Ko et al., 1972). Adekola (1968) je predstavil nekoliko naprednejši model, kjer omejitve deformacij niso bile več potrebne. Motivacija Goodmanovega modela (Goodman and Popov, 1968) je bila ravno uporaba na lesenih kompozitih, vendar drugi materiali, kot npr. jeklo in beton, za natančnejšo analizo zahtevajo upoštevanje nelinearnega obnašanja materiala (Kroflič et al., 2011; Čas, 2004; Hozjan et al., 2013; Lolić et al., 2020; Adam and Furtmüller, 2019, 2020) ter stika (Xu and Wu, 2009; Wu et al., 2016a; Foschi and Bonac, 1977; Rassam et al., 1970; Galuppi and Royer-Carfagni, 2012; Siciliano et al., 2021) in modele, ki upoštevajo časovne vplive (Ranzi and Bradford, 2006; Wu et al., 2016a,b) ali temperaturne vplive (Schnabl, 2007). Nekateri modeli so zasnovani na enostavnejši Bernoullijevi teoriji nosilcev in zanemarijo vpliv strižnih deformacij slojev (Girhammar and Gopu, 1993; Xu and Wu, 2009; Adam and Furtmüller, 2019), drugi upoštevajo tudi strižne napetosti in deformacije (Wu et al., 2016a; Schnabl, 2007; Schnabl and Planinc, 2011; Xu and Wang, 2013; Ecsedi and Baksa, 2016; Siciliano et al., 2021). Poleg ravninskih modelov so v literaturi predstavljeni tudi tridimenzionalni modeli nosilcev in stebrov z zdrsi med sloji (Schnabl and Planinc, 2011; Challamel and Girhammar, 2012, 2013; Čas et al., 2018). Najdemo lahko tudi modele, ki upoštevajo tudi geometrijsko nelinearnost (Girhammar, 2009; Kroflič, 2012; Čas, 2004). Med numeričnimi modeli lepljenih lesenih nosilcev so najbolj znani modeli avtorjev Foschi and Barrett (1980); Ehlbeck et al. (1985b,a,c) in Serrano. Ti modeli upoštevajo tudi lokalne oslabitve, kot so grče in zobati spoji. Med najbolj naprednimi in širše uporabljenimi je t.i. model Karlsuhe (Ehlbeck et al., 1985b,a,c), ki pa ne upošteva porušitve v tlaku poleg tega pa so napetosti v posameznih slojih povprečene, s tem pa model izgubi na splošnosti uporabe. V literaturi tako nismo našli predstavljenega modela, ki bi s točnimi enačbami poleg poljubnega števila slojev in zdrsa med sloji upošteval tudi vpliv zobatih spojev.

V sklopu tega dela smo pripravili analitični in numerični model večslojnih lepljenih nosilcev iz bukovine. Modela sta zasnovana na enačbah ravninskega nosilca po Reissnerjevi teoriji (Reissner, 1972). Možna je uporaba nelinearnega materialnega modela lesa kot tudi stika med sloji bukovega lesa. V model so vključeni zobati spoji. Število zobatih spojev in njihova lega v posameznih slojih ni omejena. V raziskavi smo opravili tudi eksperimentalno testiranje zobatih spojev ter lepljenih nosilcev. V nategu smo testirali tri različne geometrije zobatih spojev, lepljenih s tremi različnimi vrstami lepila. Ena izmed preizkušanih geometrij je bila določena na osnovi preliminarne analize in ocene trdnosti zobatih spojev v odvisnosti od geometrijskih parametrov. Lepljeni nosilci so bili izdelani iz dveh različnih geometrij zobatih spojev. Izvedli smo upogibno testiranje lepljenih nosilcev. Z izmerjenimi podatki, tako med nateznimi testi kot med upogibnimi, smo pridobili vhodne podatke za pripravljen numerični model. Z rezultati upogibnih testov smo primerjali izračunane rezultate in tako preverili pravilnost numeričnega modela za lepljene lamelirane nosilce iz bukovega lesa.

6.2 Osnovne enačbe računskega modela lameliranega lepljenega nosilca z zobatimi spoji

Obravnavamo geometrijsko linearen, kompozitni nosilec s poljubnim številom slojev $i = (1, 2, ..., N)$. Stik med sloji ima zanemarljivo debelino in znane materialne lastnosti. Vsi sloji imajo enako začetno, nedeformirano dolžino, ki je enaka dolžini nosilca $L^i = L$. Nosilec je definiran v kartezijskem koordinatnem sistemu $\mathbb{R}^3 = \{X, Y, Z\}$ s fiksnimi ortonormiranimi baznimi vektorji $\mathbf{E}_X, \mathbf{E}_Y$ in $\mathbf{E}_Z$, kjer velja, da je $\mathbf{E}_Z = \mathbf{E}_X \times \mathbf{E}_Y$. Globalna referenčna os ravnega, nedeformiranega nosilca leži na spodnjem robu spodnjega sloja nosilca. Referenčne osi vseh slojev sovpadajo z globalno X osjo, ki ravno tako leži na spodjem robu spodnjega sloja nosilca. Prečni prerez sloja A^i v poljubni materialni koordinati (x^i, y^i, z^i) sloja i je prizmatične oblike z višino h^i in širino b^i v Y, Z ravnini. Prečni prerez sloja je homogen in se med deformacijo ne spreminja. Nosilec je obremenjen z zunanjo obtežbo $\mathcal{P}_{EX}$. Nedeformirana in deformirana oblika nosilca sta prikazani na Sliki 6.1. Sistem osnovnih algebrajsko diferencialnih enačb nosilca z zobatim spojem je sestavljen iz kinematičnih, ravnotežnih in konstitucijskih enačb. Za rešitev omenjenega sistema so potrebne še vezne enačbe in robni pogoji za posamezne sloje nosilca, saj deformacija slojev ni medsebojno neodvisna.

Pričakovane deformacije in pomiki nosilca so omejeni na majhne pomike zato lahko posplošene enačbe (Schnabl, 2007; Rodman, 2009; Kroflič, 2012), ki opisujejo deformiranje nosilca zapišemo v poenostavljeni, linearizirani obliki (Hughes and Pister, 1978; Bonet and Wood, 1997):

Kinematične enačbe

$$\frac{du^i(x^i)}{dx^i} - \varepsilon^i(x^i) = 0, \tag{6.1}$$

$$\frac{dw^i(x^i)}{dx^i} + \varphi^i(x^i) - \gamma^i(x^i) = 0, \tag{6.2}$$

$$\frac{d\varphi^i(x^i)}{dx^i} - \kappa^i(x^i) = 0, \tag{6.3}$$

kjer ε^i označuje osno deformacijo, γ^i strižno deformacijo in κ^i specifično ukrivljenost referenčne osi pri koordinati x^i. Vzdolžna deformacija $D^i(x^i, z^i)$ v poljubni točki nosilca pa je določena z enačbo:

$$D^i(x^i, z^i) = \varepsilon^i(x^i) + z^i\,\kappa^i(x^i), \tag{6.4}$$

kjer je $i = \{1, 2, ..., N\}$.
Ravnotežne enačbe

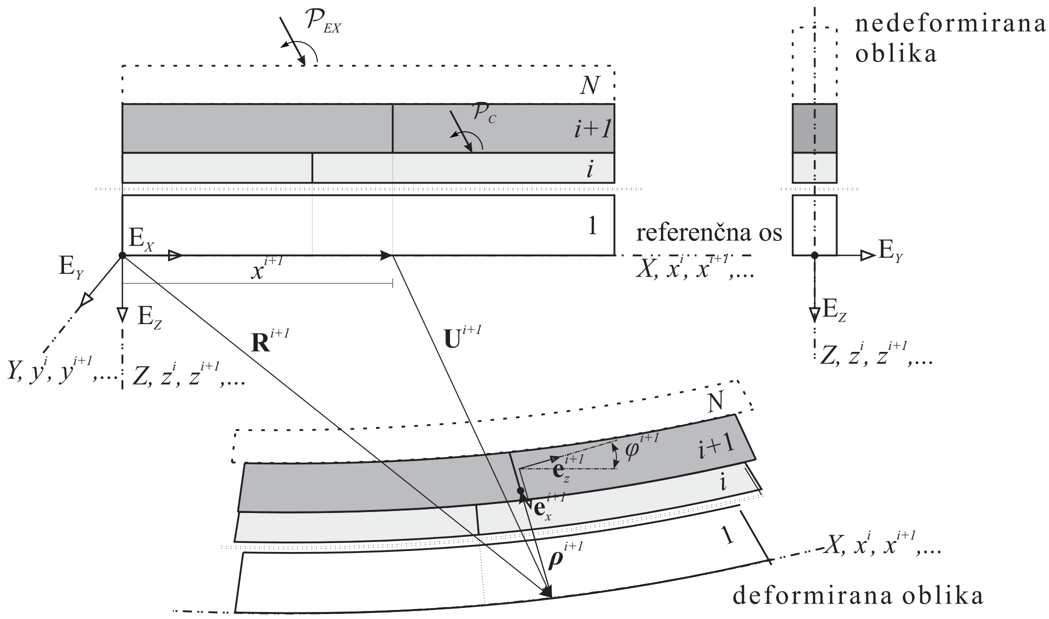

Figure 6.1: Undeformed and deformed configuration of laminated beam.
Slika 6.1: Nedeformirana in deformirana konfiguracija lameliranega nosilca.

Za posamezen sloj $i = (1, 2, ..., N)$ nosilca v splošnem velja, da je lahko izpostavljen trem komponentam zunanje obtežbe, p_X^i, p_Z^i in m_Y^i ter kontaktni obtežbi, $p_{c,X}^{i,j}$, $p_{c,X}^{i,j-1}$, $p_{c,Z}^{i,j}$ in $p_{c,Z}^{i,j-1}$. Z ravnotežnimi enačbami povežemo notranje sile N^i, Q^i in momente M^i z dano zunanjo obtežbo z naslednjimi izrazi:

$$\frac{dN^i(x^i)}{dx^i} + p_X^i(x^i) + p_{c,X}^{i,j}(x^i) - p_{c,X}^{i,j-1}(x^i) = 0, \tag{6.5}$$

$$\frac{dQ^i(x^i)}{dx^i} + p_Z^i(x^i) + p_{c,Z}^{i,j}(x^i) - p_{c,Z}^{i,j-1}(x^i) = 0, \tag{6.6}$$

$$\frac{dM^i(x^i)}{dx^i} - Q^i(x^i) + m_Y^i(x^i) + z^{j-1}\, p_{c,X}^{i,j-1}(x^i) - z^j\, p_{c,X}^{i,j}(x^i) = 0. \tag{6.7}$$

Konstitucijske enačbe

$$N^i(x^i) = N_C^i\big(\varepsilon^i(x^i), \kappa^i(x^i)\big) = C_{11}^i\, \varepsilon^i + C_{12}^i\, \kappa^i, \tag{6.8}$$

$$M^i(x^i) = M_C^i\big(\varepsilon^i(x^i), \kappa^i(x^i)\big) = C_{21}^i\, \varepsilon^i + C_{22}^i\, \kappa^i, \tag{6.9}$$

$$Q^i(x^i) = Q_C^i\big(\gamma^i(x^i)\big) = C_{33}^i\, \gamma^i, \tag{6.10}$$

kjer koeficienti C_{11}^i, C_{22}^i, $C_{12}^i = C_{21}^i$ in C_{33}^i predstavljajo komponente togostne matrike $\mathbf{C}^i$ v prečnem prerezu sloja i.

Posplošeni robni pogoji

$x = 0:$

$$\begin{aligned} &U_1^i - u^i(0) = 0 \quad \text{ali} \quad S_1^i + N^i(0) = 0, \\ &U_2^i - w^i(0) = 0 \quad \text{ali} \quad S_2^i + Q^i(0) = 0, \\ &U_3^i - \varphi^i(0) = 0 \quad \text{ali} \quad S_3^i + M_Y^i(0) = 0. \end{aligned} \tag{6.11}$$

$x = L:$

$$\begin{aligned} &U_4^i - u^i(L) = 0 \quad \text{ali} \quad S_4^i - N^i(L) = 0, \\ &U_5^i - w^i(L) = 0 \quad \text{ali} \quad S_5^i - Q^i(L) = 0, \\ &U_6^i - \varphi^i(L) = 0 \quad \text{ali} \quad S_6^i - M_Y^i(L) = 0. \end{aligned} \tag{6.12}$$

U_k^i so posplošeni robni pomiki za šest prostostnih stopenj $k = \{1, 2, ..., 6\}$ in definirajo kinematične robne pogoje sloja i. S_k^i so posplošene robne obtežbe s katerimi so definirani statični robni pogoji sloja i ravno tako za šest prostostnih stopenj $k = \{1, 2, ..., 6\}$.

Vezne enačbe

Vezne enačbe izhajajo iz razlike vektorjev pomika dveh poljubnih delcev sosednjih slojev i in $i + 1$, ki po deformaciji nosilca medsebojno sovpadata. Če razliko zapišemo v komponentni obliki enačbi za razliko pomikov v osni smeri in prečni smeri zapišemo kot:

$$\Delta_X^j(x^i) = u^{i+1}(x^{i+1}) - u^i(x^i) + z^j\,(\varphi^{i+1}(x^{i+1}) - \varphi^i(x^i)), \tag{6.13}$$

$$\Delta_Z^j(x^i) = w^{i+1}(x^{i+1}) - w^i(x^i) = 0. \tag{6.14}$$

V primeru, da upoštevamo, da je del stika med sloji popolnoma razslojen, torej da med sosednjima slojema ne obstaja nikakršna povezava, moramo vezne enačbe definirati nekoliko drugače. Enačba za vzdolžni zdrs med slojema ostane nespremenjena, medtem ko enačba za prečni razmik postane različna od 0, $\Delta_Z^j(x^i) = w^{i+1}(x^{i+1}) - w^i(x^i) \neq 0$. Iz tega izhaja naslednje poenostavitve, ki jih bomo upoštevali v nadaljevanju:

$$\gamma^i(x^i) = \gamma^{i+1}(x^{i+1}) = \gamma(x^i) \neq 0, \tag{6.15}$$

$$w^i(x^i) = w^{i+1}(x^{i+1}) = w(x^i), \tag{6.16}$$

$$\varphi^i(x^i) = \varphi^{i+1}(x^{i+1}) = \varphi(x^i), \tag{6.17}$$

$$\kappa^i(x^i) = \kappa^{i+1}(x^{i+1}) = \kappa(x^i). \tag{6.18}$$

Enačbi (6.13) in (6.14) sta neposredna posledica predpostavke, da je med sloji dovoljen samo zdrs, delaminacija v prečni smeri pa je preprečena. Za vsako deformacijo nosilca torej velja $w^i = w^{i+1}$. V osni smeri moramo tako definirati tudi kontaktno obtežbo $p_{c,X}^{i,j}(x^i)$ v poljubni koordinati x^i vzdolž sloja $i = (1, 2, ..., N)$, ki je odvisna tudi od zdrsa med sloji, $\Delta_X^j(x^i)$:

$$p_{c,X}^{i,j}(x^i) = \mathcal{S}_x^j\big(x^i, \Delta_X^j(x^i)\big), \tag{6.19}$$

kjer je $\mathcal{S}_x^i$ poljubna funkcija, ki predstavlja konstitutivni zakon stika med sloji. V skladu s tretjim Newtonovim zakonom, sosednji sloji drug na drugega vplivajo z nasprotno enakim vplivom:

$$p_{c,X}^{i,j}(x^i) + p_{c,X}^{i+1,j}(x^{i+1}) = 0. \tag{6.20}$$

Kontinuirni pogoji

Zobati spoji so v modelu upoštevni kot linearna vzmetv osni smeri, kot je prikazano na Sliki 6.2. Zaradi večje preglednosti, je na Sliki 6.2 prikazan primer s samo dvema slojema, s tem pa ne izgubimo na splošnosti. Osna sila $N_{\rm FJ}^k$ v zobatem spoju k je enaka sili v levem delu spoja $k-1$, N_{k-1}^a, in v desnem delu spoja $k+1$, N_{k-1}^a. Če togost zobatega spoja definiramo s koeficientom $K_{\rm FJ}^k$ potem lahko izračunamo raztezek zobatega spoja $\Delta_{\rm FJ}^k$. V skladu s to definicijo, zobati spoj definira delitev modela na dva dela, $k-1$ in $k+1$. Osnovne kinematične, ravnotežne in konsitutivne enačbe ostanejo nespremenjene, potrebno pa je zagotoviti kontinuirnost kinematičnih in ravnotežnih količin, čemur zadostimo z enačbami (6.21)–(6.26).

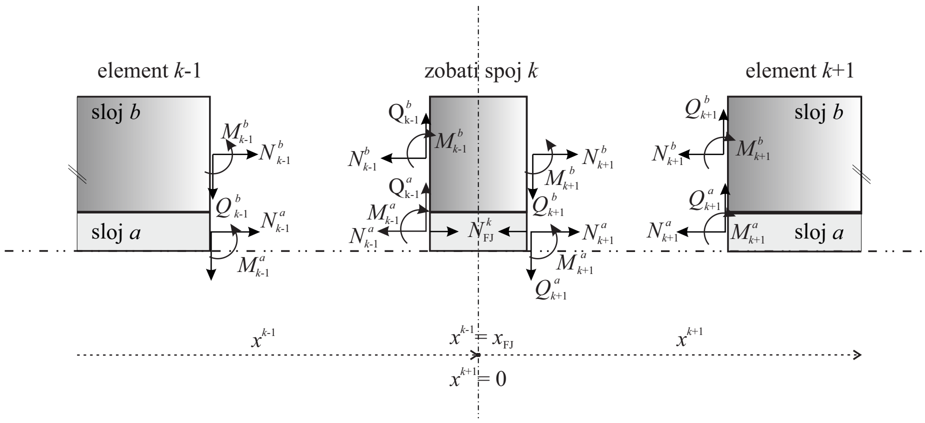

Figure 6.2: A schematic presentation of the internal forces due to the influence of finger joint k in layer a.
Slika 6.2: Shematski prikaz notranjih sil zaradi vpliv zobatega spoja k v sloju a.

$$u_{k-1}^a(x_{\rm FJ}) - u_{k+1}^a(0) - \Delta_{\rm FJ}^k = 0, \tag{6.21}$$
$$u_{k-1}^b(x_{\rm FJ}) - u_{k+1}^b(0) = 0, \tag{6.22}$$
$$w_{k-1}^a(x_{\rm FJ}) - w_{k+1}^a(0) = 0, \tag{6.23}$$
$$w_{k-1}^b(x_{\rm FJ}) - w_{k+1}^b(0) = 0, \tag{6.24}$$
$$\varphi_{k-1}^a(x_{\rm FJ}) - \varphi_{k+1}^a(0) = 0, \tag{6.25}$$
$$\varphi_{k-1}^b(x_{\rm FJ}) - \varphi_{k+1}^b(0) = 0. \tag{6.26}$$

kjer velja, da je $a = \{1, 2, ..., N\}$ in $b = \{1, 2, ..., N\}$. Pri tem velja:

$$\Delta_{\rm FJ}^k = N_{\rm FJ}^k / K_{\rm FJ}^k. \tag{6.27}$$

V doktorski disertaciji so predstavljene enačbe za enostavnejši, Euler-Bernoullijev model nosilca, kjer ni upoštevanih strižnih deformacij, podani pa so tudi izrazi za Timoshenko-Ehrenfestov nosilec, kjer strig ni zanemarjen.

6.2.1 Analitična rešitev lameliranega nosilca z zobatimi spoji

Pri izpeljavi analitične rešitve lameliranih nosilcev z zobatimi spoji je upoštevan ob predpostavki prizmatičnih in homogenih prerezih lamel nosilca. Prečni prerez je simetričen glede na z os in se med deformacijo ne spreminja. Vsi materialni parametri lamel, stika med lamelami in zobatih spojev so bili upoštevani kot linearno elastični. Zobati spoj je modeliran kot linearna vzmet v osni smeri. Debelina stika med lamelami je zanemarljiva, med lamelami pa je dovoljen samo zdrs, brez delaminacije v prečni smeri. Globalna ali lokalna nestabilnost se ne moreta pojaviti. Kot smo že omenili, so dovoljeni le majhni pomiki in deformacije, kar velja tudi za zdrs med sloji. Algoritem analitične rešitve je izpeljan na dejstvu, da vse neznanke problema lahko izrazimo z eno samo spremenljivko, to je zdrs med sloji, $\Delta_X^j(x^i)$:

$$\Delta_X^j(x^i) = u^{i+1}(x^i) - u^i(x^i). \tag{6.28}$$

Za izpeljavo potrebujemo še drugi odvod zdrsa vzdolž osi nosilca:

$$\frac{d^2\Delta_X^j(x^i)}{dx^{i2}} = \frac{d\varepsilon^{i+1}(x^i)}{dx^i} - \frac{d\varepsilon^i(x^i)}{dx^i}, \tag{6.29}$$

kjer velja, da je $i = (1, 2, ..., N)$ in $j = (1, 2, ..., N-1)$. V primeru upoštevanja strižnih deformacij slojev lameliranega nosilca lahko notranje sile in momente povežemo z notranjimi deformacijskimi količinami preko inverzne togostne matrike nosilca $\mathbf{C^{-1}}$:

$$\left\{\begin{matrix} \dfrac{d\varepsilon^i(x^i)}{dx^i} \\ \dfrac{d\kappa(x^i)}{dx^i} \\ \dfrac{d\gamma(x^i)}{dx^i} \end{matrix}\right\} = \mathbf{C}^{-1} \left\{\begin{matrix} \dfrac{N^i(x^i)}{dx^i} \\ \dfrac{M(x^i)}{dx^i} \\ \dfrac{Q(x^i)}{dx^i} \end{matrix}\right\}, \tag{6.30}$$

kjer je $i = (1, 2, ..., N)$.

Pri tem notranje sile in momente posameznih slojev določimo z integracijo vplivov na sloje p_X^i, $p_{c,X}^{i,j}$, $p_{c,X}^{i,j-1}$ in m_Y^i. V naslednjem koraku je potrebno odvajati izraz (6.28) vzdolž osi x^i s čimer izpeljemo navadno linearno diferencialno enačbo tretjega reda s konstantnimi koeficienti:

$$\Delta_X^{j\,'''} + A\Delta_X^{j\,'} - B\Delta_X^{j-1\,'} + C\Delta_X^{j+1\,'} + F = 0, \tag{6.31}$$

kjer so koeficienti A, B in C definirani kot geometrijske in materialne konstante sloja $i = (1, 2, ..., N)$, koeficient F pa vključuje zunanjo obtežbo na sloj i. Koeficiente določimo s členi inverzne togostne matrike $\mathbf{C^{-1}}$, $D_{i,i}$:

$$A = (D_{i+1,i} - D_{i,i} - D_{i+1,i+1} + D_{i,i+1})\, K_{\mathrm{X}}^j, \tag{6.32}$$

$$B = (D_{i+1,i} - D_{i,i})\, K_{\mathrm{X}}^{j-1}, \tag{6.33}$$

$$C = (D_{i+1,i+1} - D_{i,i+1})\, K_{\mathrm{X}}^{j+1} \tag{6.34}$$

in

$$\begin{aligned} F = {} & p_X^i\,(D_{i+1,i} - D_{i,i}) + p_X^{i+1}\,(D_{i+1,i+1} - D_{i,i+1}) + \\ & + \left(\sum_{i=1}^{N}(p_Z^i - m_Y^{i\,'})\right)(D_{i+1,N+1} - D_{i,N+1}) + \sum_{i=1}^{N} p_Z^{i\,''}\,(D_{i+2,N+2} - D_{i,N+2}). \end{aligned} \tag{6.35}$$

Sistem linearnih diferencialnih enačb (6.31) je enolično rešljiv samo, če je zadoščeno robnim pogojem zdrsa $\Delta_X^j(x^i = 0)$ in $\Delta_X^j(x^i = L)$, kjer velja, da je $i = (1, 2, ..., N)$ and $j = (1, 2, ..., N - 1)$. Sistem enačb (6.31) smo rešili z uporabo programa Wolfram MATHEMATICA (Wolfram Research). Z znanim zdrsom med slojema $\Delta_X^j(x^i)$ lahko dobimo analitične izraze za vse ostale, osnovne neznanke problema $\varepsilon^i(x^i)$, $\kappa(x^i)$, $u^i(x^i)$, $w(x^i)$, $\varphi(x^i)$, $N^i(x^i)$, $Q(x^i)$, $M(x^i)$ z enačbo konstrukcije:

$$\mathbf{K}\,\mathbf{U_0} = \mathbf{f}, \tag{6.36}$$

kjer je $\mathbf{U}_0$ vektor konstantnih vrednosti kinematičnih neznanih funkcij izvrednoten na konceh slojev i, $\mathbf{K}$ je tangentna togostna matrika nosilca in $\mathbf{f}$ je obtežni vektor. Analitični izrazi za neznanke so kompleksni, zato so predstavljeni v prilogah doktorske disertacije in sicer za primer dvoslojnega nosilca z dvema zobatima spojema in popolno razslojenim delom nosilca ter v (Fortuna et al., 2021).

6.2.2 Numerična rešitev lameliranega nosilca z zobatimi spoji

Splošna oblika osnovnih enačb (6.1)–(6.12) je zelo zahtevna za reševanje in analitično rešitev lahko dobimo samo v zelo enostavnih primerih lepljenih lameliranih nosilcev z omejenim številom slojev in zobatih spojev. Za bolj kompleksne modele se poslužujemo numeričnega reševanja enačb z uporabo končnih elementov. V predstavljenem modelu smo uporabili t.i. deformacijske končne elemente, ki jih je predstavil Planinc (1998), njihova učinkovitost pa je bila že večkrat dokazana, med drugim so jih uporabili Čas (2004); Schnabl (2007) in Kroflič (2012). Kot nakazuje že ime samo, so pri tovrstnih končnih elementih za osnovne neznanke izbrane deformacijske količine. Formulacija končnega elementa je osnovana na principu virtualnega dela, kjer velja, da je vsota virtualnega dela notranjih sil enaka virtualnemu delu zunanje obtežbe, ob predpostavki majhnih deformacij in pomikov (Washizu, 1994; Saje et al., 1997; Planinc, 1998). Pri izpeljavi je uporabljen t.i. modificiran princip virtualnega dela, kjer s poljubnimi a odvedljivimi funkcijami na območju $x^i \in [0, L^i]$, $R_1^i(x^i)$, $R_2^i(x^i)$ in $R_3^i(x^i)$ pomnožimo kinematične enačbe (6.1)–(6.3). Funkcije R_1^i, R_2^i in R_3^i se imenujejo Lagrangevi multiplikatorji. Produkte nato odvajamo vzdolž osi x^i in prištejemo osnovnemu izrazu principa o virtualnem delu.

V izrazu se pojavijo variacije $\delta\varepsilon^i$, $\delta\gamma^i$, $\delta\kappa^i$, δu^i, δw^i, $\delta\varphi^i$, δR_1^i, δR_2^i in δR_3^i, ki so poljubne funkcije x^i. Koeficienti $\delta u^i(0)$, $\delta w^i(0)$, $\delta\varphi^i(0)$, $\delta u^i(L)$, $\delta w^i(L)$ in $\delta\varphi^i(L)$ predstavljajo diskretne vrednosti pomikov in zasukov na konceh elementa. Problem je enolično rešljiv samo, če so koeficienti pri poljubnih neodvisnih variacijah enaki 0. Tako dobimo sistem kinematičnih, ravnotežnih in konstitutivnih enačb in robnimi pogoji. Opazimo, da z integracijo vzdolž osi x^i, enolično zadostimo koeficientom povezanih z variacijami pomikov in zasukov. Tako se izraz za princip virtualnega dela poenostavi in dobimo izraz, ki je odvisen samo od deformacij ter od robnih vrednosti pomikov in zasukov. Ob upoštevanju poenostavitev, ki izhajajo iz veznih enačb (6.15)–(6.18) zapišemo:

$$
\begin{aligned}
\delta W^{**} = \sum_{i=1}^{N} \Bigg\{ & \int_0^L \Big((N_C^i - R_1^i)\,\delta\varepsilon^i + (Q_C^i - R_2^i)\,\delta\gamma^i + (M_C^i - R_3^i)\,\kappa^i \Big) dx + \\
& + \left(u^i(L) - u^i(0) - \int_0^L \varepsilon^i dx \right) \delta R_1^i + \left(w(L) - w(0) - \int_0^L (\gamma - \varphi) dx \right) \delta R_2^i + \\
& + \left(\varphi(L) - \varphi(0) - \int_0^L \kappa dx \right) \delta R_3^i + \\
& + \big(R_1^i(L) - S_4^i \big)\, \delta u^i(L) + \big(R_2^i(L) - S_5^i \big)\, \delta w^i(L) + \big(R_3^i(L) - S_6^i \big)\, \delta\varphi^i(L) - \\
& - \big(R_1^i(0) + S_1^i \big)\, \delta u^i(0) - \big(R_2^i(0) + S_2^i \big)\, \delta w^i(0) - \big(R_3^i(0) + S_3^i \big)\, \delta\varphi^i(0) \Bigg\} = 0.
\end{aligned}
\tag{6.37}
$$

Osnovne enačbe so v splošni obliki nelinearne zato končnih analitičnih rešitev ne moremo dobiti. Uporabimo približno metodo reševanja enačb z Galerkinovo metodo končnih elementov, kjer zvezni problem prevedemo na diskretnega. Neznane funkcije ε^i, γ in κ aproksimiramo z Lagrangevimi interpolacijskimi polinomi. Posamezen element razdelimo na $N^* - 1$ delov, kjer * označuje količino, ki jo želimo aproksimirati torej $* \in \{\varepsilon, \gamma, \kappa\}$. Eksplicitne izraze za aproksimirane funkcije lahko med drugim najdemo v (Saje et al., 1997; Planinc, 1998; Schnabl, 2007; Kroflič, 2012). Aproksimirane funkcije uporabimo v izrazu za modificiran princip virtualnega dela. Tako dobimo sistem $N(N^\varepsilon + N^\gamma + N^\kappa) + 3N + 6$ algebrajskih enač, kjer je N število slojev. Neznanke problema razdelimo na $2N+4$ zunanjih prostostnih stopenj, kamor spadajo robne vrednosti pomikov in zasukov $u^i(0)$, $w(0)$, $\varphi(0)$, $u^i(L)$, $w(L)$ in $\varphi(L)$, ter $N\,(N^\varepsilon + N^\gamma + N^\kappa) + N + 2$ notranjih prostostnih stopenj kamor spadajo deformacijske količine ε^i, γ, κ ter robne obtežbe $R_1^i(0)$, $R_2(0)$ in $R_3(0)$. Integrale izvrednotimo s poljubno metodo numerične integracije. Notranje prostostne stopnje so nato izločene v postopku statične kondenzacije matrike posameznega elementa. Kondenzirana globalna togostna matrika in kondenziran obtežni vektor elementa sta nato ustrezno umeščena v matriko konstrukcije (Schnabl, 2007; Zienkiewich and Taylor, 1991). Rešitev dobimo s pomočjo enačbe konstrukcije:

$$
\mathbf{g}(\mathbf{u}) - \lambda\,\mathbf{p} = 0, \tag{6.38}
$$

kjer je $\mathbf{u}$ vektor neznanih vozliščnih pomikov in rotacij, $\mathbf{p}$ vektor zunanje obtežbe in λ obtežni faktor. V skladu z definicijo končnega elementa, zobati spoj predstavlja povezavo med dvema sosednjima končnima elementoma. V modelu je zobati spoj upoštevan kot dodatna prostostna stopnja v elementu, ki ima na začetku zobati spoj. Vpliv zobatega spoja upoštevamo z enačbo:

$$
f_{N(N^\varepsilon+3)+N^\gamma+N^\kappa+6+i} = u_{e_{\mathrm{FJ}}}^i(0) - u_{e_{\mathrm{FJ}}-1}^i(L_{e_{\mathrm{FJ}}-1}) - \frac{R_{1,e_{\mathrm{FJ}}}^i(0)}{K_{\mathrm{FJ}}}, \tag{6.39}
$$

kjer $e_{\mathrm{FJ}} \in \{1, 2, ..., N_{el}\}$ označuje element, kjer je prisoten zobati spoj. V splošnem velja, da je $i \in \{1, 2, ..., N\}$ označuje sloj z zobatim spojem. N je število slojev in N_{el} je število vseh elementov modela lepljenega lameliranega nosilce. Ker je enačba (6.39) odvisna tudi od elementa pred zobatim spojem, lahko vpliv zobatega spoja upoštevamo šele na nivoju konstrukcije.
Pri reševanju sistema posplošenih diskretnih enačb elementa smo uporabili Newton Raphsonovo iterativno metodo. Pri tej metodi se poslužimo konsistentne linearizacije (Hughes and Pister, 1978; Bonet and Wood, 1997) in izrazimo tangentno togostno matriko $\mathbf{K_T}$.

6.3 Zobati spoji

Zobati spoje se uporablja za vzdolžno spajanje posameznih desk, ki so kot lamele uporabljene pri proizvodnji lameliranih nosilcev. Mehanske lastnosti spojev so bistvenega pomena pri zagotavljanju trdnosti nosilnih elementov. Pri proizvodnji lameliranih nosilcev iz lesa iglavcev so uveljavljene dobro preverjene konfiguracije zobatih spojev. Najpogosteje se uporabljajo zobati spoji z dolžino zoba 20 mm, kar je tudi priproročilo zapisano v standardu EN 14080 (CEN, 2013e), ki obravnava proizvodnjo lameliranih lepljenih nosilcev iz lesa iglavcev in topola. Ker je les listavcev v splošnem trdnejši od lesa iglavcev, se izkaže, da tovrstni zobati spoji niso ustrezni (Aicher and Klöck, 1991; Tran et al., 2014; Ehrhart et al., 2018b; Franke et al., 2014; Frese and Blass, 2006). Dolžina oziroma oblika zobatega spoja pa ni edini parameter, ki vpliva na končno trdnost zobatega spoja, ampak je potrebno upoštevati tudi kvaliteto osnovnega materiala, kvaliteto proizvodnje (Aicher and Radović, 1999; Collin and Ehlbeck, 1992), vrsto in količino lepila, način njegovega nanosa, tlak pri stiskanju, čas med skobljanjem in aplikacijo lepila (Konnerth et al., 2006; Franke et al., 2014; Lehmann, 2019), itd. V sklopu doktorske disertacije smo opravili krajšo preliminarno raziskavo, s katero smo določili optimalno geometrijo zobatega spoja. Analizirali smo vpliv osnovnih geometrijskih parametrov spoja: dolžina spoja l, širino konice b_t in naklon α (Slika 6.3) ter vpliv mehanskih lastnosti lepila.

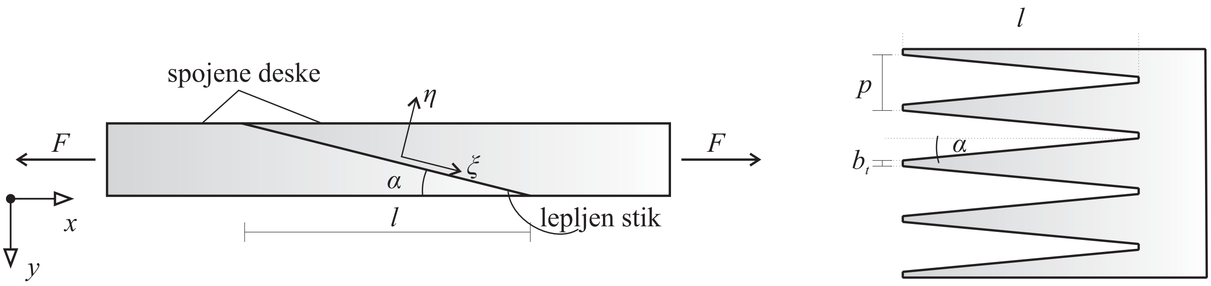

Figure 6.3: Geometry of a scarf joint (left) and geometry of a finger joint (right).
Slika 6.3: Geometrija poševnega spoja (levo) in geometrija zobatega spoja (desno).

Optimalno geometrijo zobatih spojev smo določili s poenostavljenim analitičnim modelom, kjer je upoštevan linearen potek tako strižnih kot normalnih napetosti vzdolž lepljenega spoja in numeričnim modelom v Abaqusu (Smith, 2009) z uporabo kohezivnih elementov. Pri primerjanju dveh vrst lepila smo ugotovili, da imajo mehanske lastnosti lepila vpliv na končno trdnost samo do določene geometrije zobatega spoja. Pri dovolj vitkih zobeh spoja, mehanske lastnosti osnovnega materiala postanejo merodajne za končno trdnost spoja in lepilo nima več tako očitnega vpliva, kot ga ima pri krajših in bolj topih zobatih spojih. Glede na rezultate izračunov in glede na dane možnosti izdelave nožev za izdelavo zobatih spojev se je za optimalno geometrijo zobatega spoja izkazala naslednja: $l = 40$ mm, $p = 8$ mm in $b_t = 1.5$ mm, ki je prikazana na Sliki 6.4. Glede na analitični model, bi s takšnim zobatim spojem lahko pričakovali trdnosti približno 80 MPa, medtem ko smo z numeričnim modelom dobili nižjo oceno trdnosti in sicer približno 55 MPa. Glede na to, da so v analitičnem modelu napetosti v spoju upoštevane poenostavljeno je pričakovana trdnost 80 MPa precenjena.

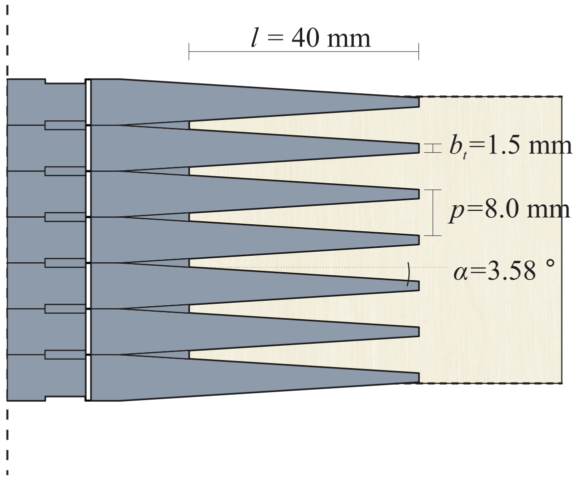

Figure 6.4: The geometry of the chosen profile of the finger joint.
Slika 6.4: Geometrija izbranega profila zobatega spoja.

6.4 Konstrukcijska lepila

Konstrukcijska lepila so bistvenega pomena v lesenih kompozitnih konstrukcijah. Z lepljenjem je omogočena uporaba le boljših kosov lesa, brez lokalnih oslabitev in posledično je s tem zagotovljena višja trdnost in kvaliteta lesenih konstrukcijskih elementov. To pripomore k vedno pogostejši uporabi lesenih konstrukcijskih elementov, ki nadomeščajo manj zanesljivejše elemente iz žaganega lesa. Conner (2001) poroča, da je gradbena industrija ena največjih uporabnikov lepil, saj se uporablja tako za nosilne kot tudi nenosilne elemente (lepljeni nosilci, križno lepljene plošče, vezane plošče, itd.). Na trdnost in trajnost lepljenih stikov vpliva vrsta faktorjev, ki določajo izbiro ustreznega lepila. Kellar (2010) kot najpomembnejše izpostavlja: kemijsko sestavo lepila, strukturo lepila, mehanizem utrjevanja, kompatibilnost z osnovnim materialom-lepljencem, pripravo površine lepljenca in klimatske pogoje okolja uporabe.
Glede na kemijsko sestavo, lepila za lepljenje lesa v splošnem razdelimo na naravna in sintetična lepila. Konstrukcijska lepila zahtevajo visoko trdnost in odpornost zato se za te namene uporabljajo predvsem slednja. Naprej se sintetična delijo na oligomerna ter duromerna lepila, ki so bolj primerna za rabo v konstrukcijskih elementih, saj so nedeformabilna in netopna (Conner, 2001). Aminoplastična lepila so med njimi najširše zastopana v lesni industriji. Glavna predstavnika te skupine lepil sta urea-formaldehid (UF) in melamin-formaldehidid (MF). Urea-formaldehidna lepila odlikujejo visoke mehanske lastnosti, požarna odpornost in dobra vodotopnost, kar pa je hkrati tudi slabost, saj v stiku ne zagotavljajo zadostne vodotesnosti in vodoodpornosti, kar negativno vpliva tudi na trajnost stika. Nasprotno imajo melaminska lepila visoko vodoodpornost zato je uporaba mešanice, melamin-urea-formaldehida (MUF), zelo uporabna v konstrukcijske namene (Ugovšek and Šernek, 2012). V preteklosti so bila pogosto uporabljena tudi lepila na osnovi fenolnih smol, vendar se je njihova uporaba zaradi škodljivih vplivov opustila in je v določenih primerih tudi prepovedana. Poleg tega so fenolne smole temno rjave barve in pri konstrukcijskih elementih pogosto ne pridejo v poštev že zaradi samih estetskih razlogov (Šernek, 2018). Z dodanim resorcinolom, ki pospeši proces utrjevanja, dobimo t.i. fenol-resorcinol-formaldehidna lepila (PRF), ki so tudi tipični predstavnik konstrukcijskih lepil z visokimi mehanskimi lastnostmi. Uporabljajo se predvsem tam, kjer je potrebno hitro utrjevanje pri normalnih temperaturah oziroma kjer segrevanje stika ni mogoče. To velja tudi za lepljene lamelirane nosilce (Conner, 2001; Šernek, 2018). Na osnovi

pregleda izsledkov raziskav v literaturi (Davis, 1997; Serrano; Aicher and Reinhardt, 2006; Frihart, 2009; Kos, 2013; Franke et al., 2014; Knorz et al., 2015; Deng et al., 2015; Ammann et al., 2016; Konnerth et al., 2016; Šernek, 2018) in po posvetovanju s proizvajalci lepil in njihovo literaturo (AkzoNobel, 2017), smo se za izvedbo laboratorijskih testov odločili za fenol-resorcinol-formaldehid (PRF) ter dve lepili tipa melamin-urea-formaldehid (MUF).

6.5 Laboratorijski testi

6.5.1 Natezno preizkušanje zobatih spojev

V eksperimentalnem delu disertacije smo opravili dve vrsti laboratorijskih testov. V prvem delu smo v nategu testirali tri različne geometrije zobatih spojev na deskah iz bukovega lesa. V drugem delu smo z uporabo dveh različnih zobatih spojev izdelali lamelirane lepljene nosilce iz bukovega lesa. Nosilce smo testirali s standardnim upogibnim testom (CEN, 2010). Les za preizkušance smo dobili iz jugovzhodnega dela Slovenije in sicer iz podjetja Gozdno gospodarstvo Novo mesto, d.d., kjer je bil les nažagan in skobljan na nominalne dimenzije: 120×24 mm, 120×32 mm, 140×20 mm in 200×16 mm. Pri lepljenju zobatih spojev in lepljenih nosilcev smo uporabili tri različna lepila. Prva dva sta iz skupine melamin-urea-formaldehidnih lepil in jih bomo v sklopu te disertacije poimenovali kot MUF (lepilo 1247 in utrjevalec 2526) in GP (lepilo A002 in utrjevalec H002) proizvajalca CASCO AkzoNOBEL. Lepilo MUF je lepilo, ki ga v redni proizvodnji uporablja slovenski proizvajalec lepljenih lameliranih nosilcev HOJA d.d., kjer smo izdelali večino preizkušancev. Drugo lepilo, GP, pa je bilo izbrano na osnovi priporočila proizvajalca lepila in naj bi bilo primernejše za lepljenje bukovega lesa. Tretje izbrano lepilo je bilo lepilo PRF Cascosinol, ravno tako dvokomponentno (lepilo 1711 in utrjevalec 2520) istega proizvajalca, CASCO AkzoNOBEL.

6.5.1.1 10 mm dolgi zobati spoji

Zobati spoji z dolžino 10 mm so bili izdelani v podjetju MSora, d.d. na deskah dimenzij 120×24 mm, ki so bile naknadno poskobljane na širino 70 mm. Izdelali smo 53 preizkušancev. Geometrija zobatega spoja po standardu EN 14080 (CEN, 2013e) ni zadoščala zahtevam konstrukcijskega spoja ($p = 6$ mm in $b_t = 2$ mm z zaobljeno konico), zato smo to serijo uporabili zgolj za validacijo numeričnega modela zobatega spoja, ki je pokazala, da je vpliv lepila največji pri krajših spojih. Uporabili smo dve vrsti lepila: MUF in PRF. Povprečna gostota uporabljenih lamel je bila 712 kg/m^3. Lepilo je bilo nanešeno ročno, stik pa se je utrjeval 24 ur. Preizkušanci so bili testirani z nateznim testom. Izmerjene trdnosti so bile po pričakovanjih nizke. Maksimalna dosežena trdnost z lepilom MUF je bila 9 MPa, z lepilom PRF pa 20 MPa. Pokazala se je očitna razlika med uporabljenima lepiloma. Razmerje povprečnih trdnosti je bilo 1:2.3. Vsi preizkušanci, z izjemo dveh z lepilom PRF, so se porušili po stiku.

6.5.1.2 18 mm dolgi zobati spoji

Zobati spoji so bili izdelani na deskah dimenzij 120×24 mm. Povprečna gostota desk je bila 684 kg/m^3 in vlažnost lesa 9.6 %. Izdelani so bili v podjetju Hoja, d.d. Geometrija spoja ($p = 6$ mm in $b_t = 1$ mm) je bila torej prilagojena njihovi običajni proizvodnji, ki sicer temelji na proizvodnji lepljenih nosilcev iz lesa smreke in jelke. Rezanje in stiskanje zobatih spojev je bilo avtomatizirano. Pri 26 preizkušancih smo ročno nanesli lepilo PRF, pri 53 pa je bil nanos lepila MUF avtomatiziran. V skupini MUF preizkušancev smo jih 27 stisnili pod tlakom 5 MPa in 26 pod tlakom 10 MPa.

Pred lepljenjem smo deske dolžine 1.5 m še neporušno testirali s prvo slovensko napravo za razvrščanje lesa STIG podjetja ILKON, d.o.o., ki je bila razvita v sodelovanju z našo skupino na Fakulteti za gradbeništvo in geodezijo. Naprava je sicer certificirana za uporabo na lesu smreke, vendar je bil na osnovi nateznih testov slovenskega bukovega lesa že pripravljen predlog za nastavitve in razrščanje tudi bukovega lesa (Fortuna et al., 2018a). Z napravo smo deskam izmerili dinamični elastični modul E_{dyn} in les razvrstili v trdnostne razrede. Meritve smo ponovili tudi na lepljenih preizkušancih in ugotovili, da obstaja relativno dobra korelacija med dinamičnim modulom elastičnosti posameznih desk in dinamičnim modulom elastičnosti zlepljenih preizkušancev, $R = 0.72$. V večini primerov je bil modul izmerjenega dinamičnega modula preizkušancev nekoliko višji od povprečja dinamičnih modulov pripadajočih desk. Posledično so bili tudi rezultati razvrščanja v trdnostne razrede boljši. Med posameznimi deskami smo jih v najvišji trdnostni razred D60, razvrstili 15 %, medtem ko smo v D60 razvrstili kar 27 % zlepljenih preizkušancev.

Z nateznimi testi smo izmerili natezne trdnosti zobatih spojev in statični modul elastičnosti v nategu v skladu s standardom EN 408 (CEN, 2010). Srednja vrednost trdnosti vseh preizkušancev je bila 43.4 MPa. Izkazalo se je, da izbira lepila nima statistično značilnega vpliva na trdnost zobatih spojev. Ravno tako ni bilo statistično značilne razlike med skupinama z različnim tlakom. Pri preizkušancih z MUF lepilom se jih je 40 % porušilo v lesu, medtem ko je bil v skupini PRF ta delež kar 65 %. Povprečna izmerjena trdnost je precej manjša od trdnosti, ki jih lahko najdemo v literaturi, kjer so z 20 mm dolgimi spoji na bukovem lesu izmerili povprečno trdnost 62 MPa (Aicher et al., 2001). Glede na visok odstotek porušitev v lesu, lahko sklepamo, da smo uporabili les nekoliko slabše kvalitete ali, da je bila proizvodnja zobatih spojev manj natančna in kvalitetna (obraba noža, tlak pri stiskanju, nečistoče, ipd.) Najverjetnejši razlog pa je v neprimerni postavitvi nateznih testov. Aicher et al. (2001) so uporabili krajši prosti razpon med klešČami ($4h$), kot je to priporočeno v standardu za natezno testiranje desk ($9h$), in ki smo ga upoštevali pri naši raziskavi (CEN, 2013e). S tem so imeli manjšo verjetnost porušitve izven samega območja zobatega spoja.

6.5.1.3 40 mm dolgi zobati spoji

Dokazali smo, da zobati spoji na bukovem lesu z običajno dolžino 18 mm ne dosegajo ustrezne trdnosti. Zato smo izdelali zobate spoje s prilagojeno geometrijo, ki naj bi bila primernejša za bukov les. Zobate spoje smo izdelali na deskah dimenzij 100×18 mm. Srednja vrednost gostote desk je bila 692 kg/m^3 s standardno deviacijo 41 kg/m^3. Povprečna vlažnost lesa je bila 11.2 %. Izdelali smo 47 preizkušancev. Pri lepljenju preizkušancev smo uporabili lepili MUF (22 preizkušancev) in GP (25 preizkušancev). Avtomatizirana izdelava 40 mm dolgih zobatih spojev ni bila mogoča, zato smo jih izdelali ročno. Tudi nanos lepila je bil izveden ročno. Za obe vrsti lepila je bil postopek lepljenja izveden v skladu z navodili proizvajalca.

V skladu z ugotovitvami iz testiranj prejšnjih nateznih testov smo v tej skupini testno postavitev nekoliko prilagodili. Prosti razpon med klešČami je bil zmanjšan na 500 mm. S tem smo zagotovili, da smo testirali manjši razpon izven območja zobatega spoja. Izmerili smo natezno trdnost in statični modul elastičnosti v nategu. Pri merjenju pomikov smo uporabili sistem za optično merjenje GOM. Teste smo spremljali z dvema fotoaparatoma Nikon D850 z resolucijo 5408×3600. Fotoaparata sta bila od preizkušanca oddaljena 600 mm.

Povprečna vrednost izmerjenega modula elastičnosti v nategu za vse preizkušance je bila 12140 MPa s standardno deviacijo 162 MPa. Srednja vrednost trdnosti vseh preizkušancev je bila 55.3 MPa. Vrednost se zelo ujema s predvideno trdnostjo, ki smo jo določili s preliminarno analizo z numeričnim modelom zobatega spoja. Glede na povprečno trdnost 18 mm dolgih zobatih spojev smo dosegli skoraj 50 % povečanje. Analiza ANOVA je pokazala, da med trdnostmi preizkušancev z lepiloma MUF in GP ni statistično značilne razlike. Izpostaviti je potrebno, da proizvajalec lepilo GP promovira kot primernejšega za uporabo na lesu bukve predvsem na podlagi boljše trajnosti in ne eksplicitno boljše nosilnosti zato smo do neke mere takšne rezultate tudi pričakovali. Kljub temu je bil delež porušitev po spoju v skupini GP preizkušancev v primerjavi s skupino MUF preizkušancev manjši kar govori v prid uporabe GP lepila. Glede na običajen raztros mehanskih lastnosti bukovine je bilo število preizkušancev relativno majhno, zato na osnovi teh rezultatov ne moremo sklepati zanesljivih zaključkov.

6.5.2 Upogibno preizkušanje lameliranih nosilcev

Upogibni testi so bili izvedeni na dveh skupinah lepljenih nosilcev, ki se med seboj razlikujejo v dolžini zobatih spojev, uporabljeni pri izdelavi lamel za nosilce. Tako smo v podjetju Hoja d.d. izdelali 10 nosilcev z zobatimi spoji dolžine 18 mm in 4 nosilce z zobatimi spoji dolžine 40 mm. Lamele za slednjo skupino smo izdelali ročno v podjetju Krovstvo in tesarstvo Štebe. Lamele so bile nato zlepljene v nosilce v podjetju Hoja d.d. Vsi nosilci so bili sestavljeni iz 10 lamel. Dolžina nosilcev je bila 3.6 m. Upogibni testi so bili izvedeni v skladu s standardom EN 408 (CEN, 2010).

6.5.2.1 Lamelirani nosilci z 18 mm dolgimi zobatimi spoji

Z upogibnimi testi smo izmerili upogibno trdnost nosilcev in upogibni lokalni ter globalni statični modul elastičnosti. Pomiki so bili izmerjeni z induktivnimi senzorji (LVDT) na sredini razpona in $2.5h$ levo in desno od sredine razpona nosilca. Minimalna upogibna nosilnost je znašala 45.9 MPa, maksimalna pa 88 MPa. Srednja vrednost je znašala 65.3 MPa. Vsi nosilci so se porušili v območju maksimalnih momentov in sicer v zobatem spoju. Na Sliki 6.5 je prikaz upogibnega testa enega izmed nosilcev tik pred porušitvijo in po porušitvi. Povprečna vrednost lokalnega modula elastičnosti 10 nosilcev je bila 13200 MPa, globalnega pa 14900 MPa. Visoke izmerjene mehanske lastnosti lepljenih lameliranih nosilcev dokazujejo dober potencial bukovega lesa v nosilnih konstrukcijah že brez posebnih modifikacij proizvodnje ali spremembe geometrije zobatih spojev. Karakteristična vrednost (5. percentila) izmerjenih upogibnih trdnosti (41.2 MPa), bi že lahko dosegli upogibni trdnostni razred na primer GL40. Za primerjavo, v standardu EN14080 je najvišji možni trdnostni razred GL32.

6.5.2.2 Lamelirani nosilci s 40 mm dolgimi zobatimi spoji

Kljub dejstvu, da so bile lamele za nosilce s 40 mm dolgimi zobatimi spoji izdelane ročno, smo z upogibnimi testi dokazali zelo visoke upogibne trdnosti. Najnižja med njimi je bila 80.3 MPa, najvišja pa

Figure 6.5: Beam with 18 mm long finger joints before failure (left) and after failure (right).
Slika 6.5: Nosilec z 18 mm dolgimi zobatimi spoji pred porušitvijo (levo) in po porušitvi (desno).

116.7 MPa. Srednja vrednost je bila 92.9 MPa z relativno majhno standardno deviacijo 16.8 MPa. Statične module elastičnosti smo merili z optičnim sistemom za merjenje deformacij in pomikov GOM na sprednji in zadnji strani nosilcev. Povprečni lokalni modul elasičnosti je znašal 19000 MPa, povprečni globalni modul elastičnosti pa 22000 MPa. S pomočjo optičnih meritev smo ocenili tudi strižni modul nosilcev. Povprečna vrednost strižnega modula je znašala 820 MPa, kar ustreza trdnostnemu razredu D40 (CEN, 2016b). Strižni modul stika med lamelami, K_{X}, smo določili ravno tako z optičnim sistemom GOM. Srednja vrednost izmerjenih modulov je bila 17.9 kN/cm^2. Vzorec 4 preizkušancev je majhen, česar se je potrebno zavedati pri interpretaciji rezultatov. Vsekakor pa so takšne meritve zelo obetavne in govorijo v prid uporabi bukovega lesa v konstrukcijske namene. Rezultati eksperimentalnih meritev so prikazani na Sliki 6.6, kjer je prikazana krivulja navpičnega pomika v odvisnosti od obtežbe F. Opazimo, da je do mejne sile, približno 80 kN, potek krivulje zelo linearen. Za nosilec z najvišjo trdnostjo pa je bil izmerjen nelinearen odziv. Glede na to, da smo pomike merili na sprednji in zadnji strani nosilca smo lahko preverili, da gre pravzaprav za geometrijsko in ne materialno nelinearnost, saj so bili izmerjeni različni navpični pomiki na sprednji in zadnji strani.

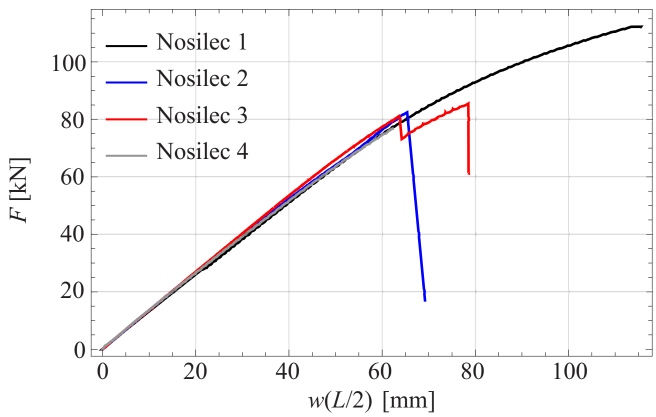

Figure 6.6: Measured load/displacement curve for vertical displacement at the mid-span of the beams.
Slika 6.6: Izmerjena krivulja obtežba/navpični pomik na sredini razpona za vse štiri nosilce.

6.6 Računski primeri

6.6.1 Analitična rešitev Euler-Bernoullijevega nosilca z zobatimi spoji

Z analitičnim modelom smo analizirali preprost primer dvoslojnega nosilca z enim zobatim spojem. Pri tem smo spreminjali lokacijo zobatega spoja znotraj celotnega razpona nosilca, x_{FJ}. Geometrija nosilca je prikazana na Sliki 6.7. Narejena je bila parametrična študija za različne togosti zobatega spoja K_{FJ}. Na Sliki 6.8 so prikazani rezultati notranjih osnih sil v spodnjem sloju, N^a, ter navpični pomik na sredini razpona nosilca, $w(L/2)$, v odvisnost od pozicije zobatega spoja x_{FJ}. Opazimo, da z višjo togostjo zobatega spoja vplivamo na maksimalni pomik nosilca. Vpliv zobatega spoja je najbolj izrazit, če je ta lociran na sredini nosilca. Pomiki na sredini nosilca se najbolj razlikujejo med seboj ravno tako pa je vpliv zobatega spoja zelo očiten tudi na diagramu notranjih osnih sil v sloju z zobatim spojem, kar seveda vpliva tudi na zgornji sloj, saj je, zaradi zagotavljanja globalnega ravnotežja, osna sila N^b nasprotno enaka sili N^a. Če je togost zobatega spoja zelo visoka, zobati spoj nima vpliva na obnašanje nosilca med obremenjevanjem.

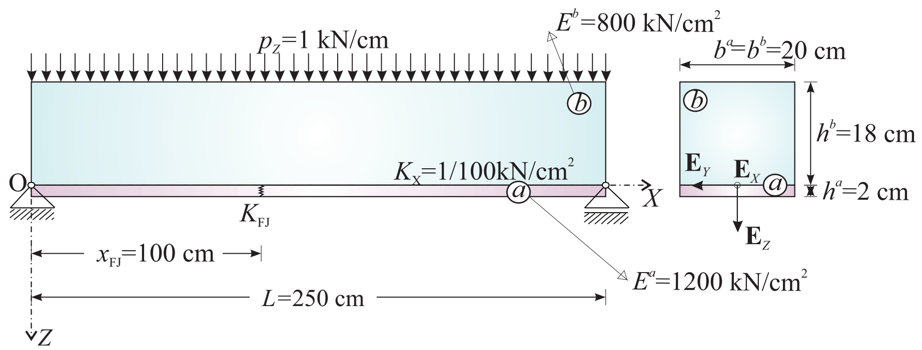

Figure 6.7: Geometric and material properties of the layers, position and magnitude of the loading and the finger joint and material properties of the interlayer contact and the finger joint.

Slika 6.7: Geometrijske in materialne lastnosti slojev, pozicije in velikosti obtežbe in zobatega spoja ter materialne lastnosti stika med sloji in zobatega spoja.

6.6.2 Numerična rešitev večslojnega nosilca z zobatimi spoji

Pripravljen numerični model smo najprej verificirali z modeli iz literature. Primerjavo rezultatov smo naredili na primeru štirislojnega nosilca, za katerega sta rezultate predstavila (Sousa Jr and Silva, 2010) in (Kroflič, 2012). Rezultate smo preverili tudi z našim analitičnim modelom in sicer za primer, kjer ni upoštevan strig. V numeričnem modelu smo kot vhodni podatek za strižni modul G upoštevali zelo visoko vrednost, $G = 10^5$ kN/cm^2. Primerjava treh zdrsov med štirimi sloji Δ^1_{X}, Δ^2_{X} in Δ^3_{X} na začetku nosilca ter navpični pomik w na sredini nosilca je prikazana v Tabeli 6.1. Vidimo, da so razlike med rezultati zelo majne oziroma zanemarljive.

Numerični model smo tudi validirali, in sicer tako, da smo izračunane rezultate numeričnega modela primerjali z izmerjenimi rezultati laboratorijskih upogibnih testov. Ker je bil odziv nosilcev v upogibu izrazito linearen, smo tudi v numeričnem modelu uporabili linearne materialne parametre, kakršni so

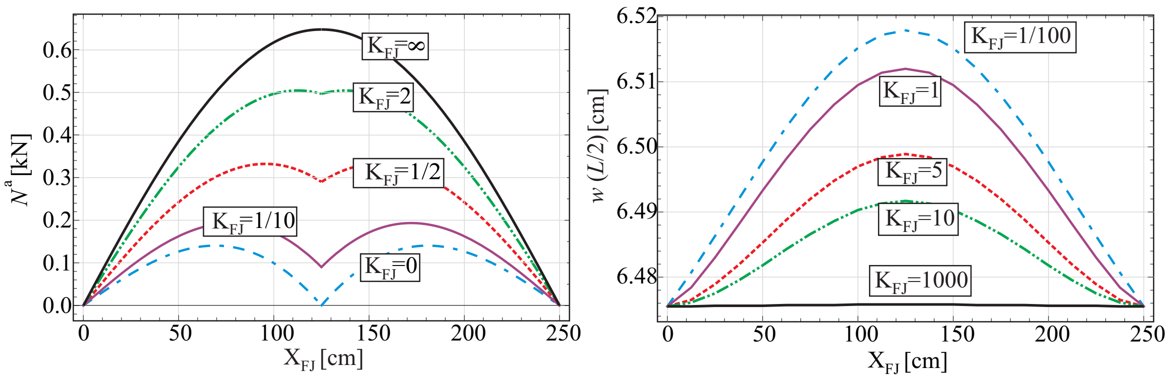

Figure 6.8: Axial force in the lower layer, N^a, and vertical displacement in the middle of the span, $w(L/2)$, of glued laminated beam, as a function of different finger-joint position and different finger-joint stiffness, K_{FJ}.

Slika 6.8: Osna sila v spodnjem sloju ,N^a, in navpični pomik na sredini razpona, $w(L/2)$, lepljenega slojevitega nosilca z zobatim spojem, kot funkcija različnih pozicij zobatega spoja, x_{FJ}, in različnih togosti zobatega spoja, K_{FJ}.

bili izmerjeni med laboratorijskimi testi za tri nosilce. Na Sliki 6.9 so prikazane krivulje numeričnih in eksperimentalnih navpičnih pomikov na sredini razpona v odvisnosti od obtežbe za tri nosilce skupaj z izračunanimi vrednostmi. Vidimo, da smo z numeričnim modelom in uporabo izmerjenih materialnih lastnosti lepo ujeli rezultate eksperimentalnih testov.

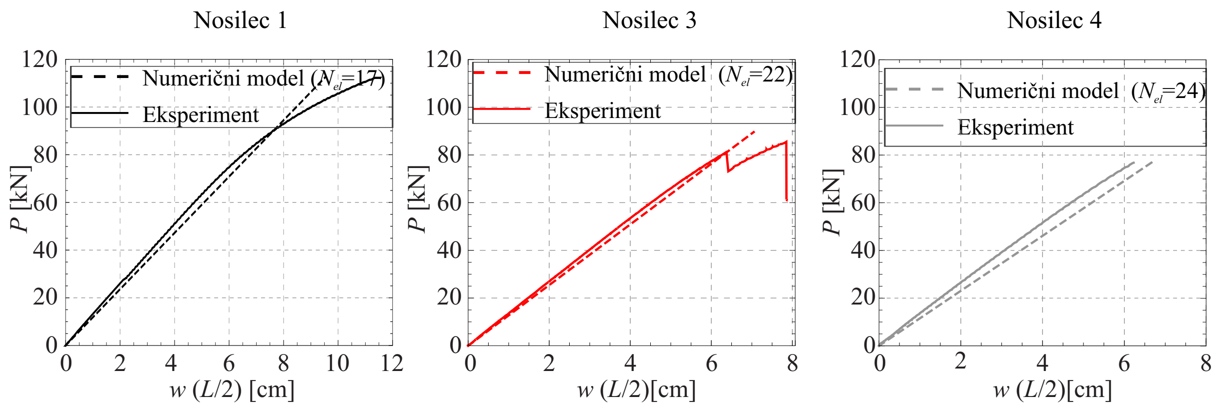

Figure 6.9: Comparison between the measured and calculated curve load with vertical displacement for Beam 1, Beam 3 and Beam 4.

Slika 6.9: Primerjava med izmerjeno in izračunano krivuljo obtežbe z navpičnim pomikom za Nosilec 1, Nosilec 3 in Nosilec 4.

6.6.3 Stohastična analiza deset slojnih nosilcev

Zaradi značilno velikega raztrosa materialnih parametrov bukovega lesa je smiselno, da nosilce analiziramo s stohastičnim pristopom. Na ta način pridobimo nekoliko realnejši pogled na mehanski odziv lepljenih nosilcev. Na osnovi geometrije Nosilca 2 je bilo narejenih 250 simulacij, kjer smo materialne

Table 6.1: Calculated interlayer slips Δ_X^j for $j = (1, 2, 3)$ at the begining of the four-layer beam and vertical displacement at the middle of the beam span calculated with the proposed analytical and numerical model and comparison with the results from the literature (Sousa Jr and Silva, 2010; Kroflič, 2012).
Preglednica 6.1: Zdrsi med sloji Δ_X^j za $j = (1, 2, 3)$ na začetku štirislojnega nosilca in navpični pomik na sredini razpona nosilca izračunani z izdelanim analitičnim in numeričnim modelom ter primerjava z rezultati iz literature (Sousa Jr and Silva, 2010; Kroflič, 2012).

	$\Delta_{\mathrm{X}}^{j=1}$ (0) [cm]	$\Delta_{\mathrm{X}}^{j=2}$ (0) [cm]	$\Delta_{\mathrm{X}}^{j=3}$ (0) [cm]	w (L/2) [cm]
Sousa, 2010	0.149301	0.214333	0.270896	3.82794
Kroflič, 2012	0.158872	0.215143	0.269841	3.83519
Numerical model, $N_{el} = 6$ (Timoshenko-Ehrenfest)	0.149301	0.214330	0.270896	3.82801
Analytical model (Euler-Bernoulli)	0.149301	0.214333	0.270896	3.82793
Error (Numerical vs. Analytical model) [%]	2.7 10^{-4}	1.4 10^{-3}	1.8 10^{-4}	-2.2 10^{-4}

parametre upoštevali stohastično. V Tabeli 6.2 so prikazane srednje vrednosti in standardne deviacije za posamezne vhodne podatke numeričnega modela pri čemer smo uporabili tako linearni kot tudi nelinearni konstitucijski zakon materiala. Poleg materialnih lastnosti smo kot stohastično upoštevali tudi debelino posamezne lamele v nosilcu. Slika 6.10 prikazuje rezultate simulacij. Na levem diagramu so prikazane

Table 6.2: Statistical values and distribution type of selected variables for simulations with non-linear constitutive material law.
Preglednica 6.2: Statistične vrednosti in tip porazdelitve izbranih spremenljivk za simulacije z nelinearnim konstitucijskim zakonom materiala.

Variable X	Distribution type	Mean value μ_{X}	Standard Deviation σ_{X}	Coefficient of variation
E_t	Normal	1878.5	182	0.01
$E_{t,\mathrm{FJ}}$	Log-Normal	1242	285	0.23
G	Normal	81.6	29.1	0.36
K_{X}	Normal	179.3	43.1	0.24
h^i [cm]	Normal	10.0	0.50	0.05

krivulje pomikov v odvisnosti od obtežbe. Raztros rezultatov je precejšen vendar je to pričakovan odziv nosilcev iz bukovega lesa. Na desnem diagramu je prikazana gostota verjetnosti porušnih napetosti, f_{lim}. Srednja vrednost izračunanih upogibnih trdnosti nosilcev je znašala 7.67 kN/cm^2 s standardno deviacijo 0.71 kN/cm^2, kar je približno 5 % nižje od izmerjenih upogibnih trdnosti. Srednja verjetnost izračunanih pomikov na sredini razpona (150 simulacij) je znašala 6.24 cm s standardno deviacijo 0.70 cm, kar je nekoliko manjše od povprečne vrednosti pomikov treh izmerjenih nosilcev. Ta je znašala 6.51 cm.

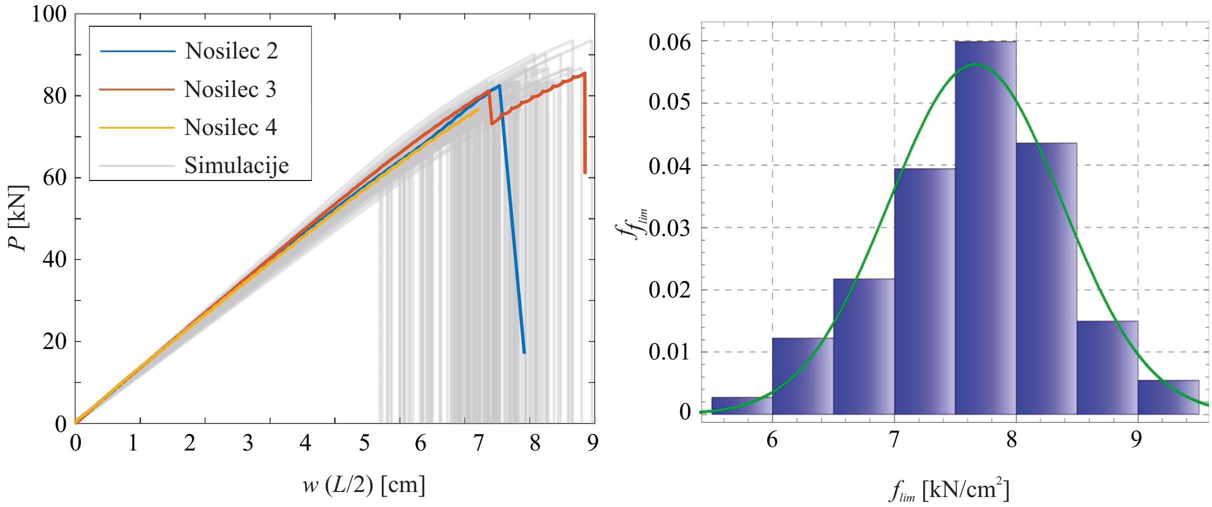

Figure 6.10: Load/vertical displacement curve for 250 simulations (left) and probability density function with histogram (right).
Slika 6.10: Krivulja obtežba/pomik za 250 simulacij skupaj z izmerjenimi nosilci (levo) in gostota verjetnosti s histogramom (desno).

6.7 Zaključki

V raziskavi smo na osnovi podatkov o visoki nosilnosti bukovega lesa optimizirali geometrijo zobatega spoja. S preliminarno analizo z analitičnim in numeričnim modelom smo ocenili pričakovano natezno trdnost za različne vrednosti geometrijskih parametrov zobatega spoja l, p in b_t. Za optimalne vrednosti, prilagojene mehanskim lastnostim bukovega lesa, so se izkazale naslednje: $l = 40$ mm, $p = 8$ mm in $b_t = 1.5$ mm. Hkrati smo analizirali vpliv lepila na trdnost. Izkazalo se je, da se vpliv lepila z dolžino zobatega spoja zmanjšuje. To pomeni, da lahko z dovolj dolgimi zobatimi spoji, uporabimo standardna konstrukcijska lepila, s tem pa se natezna trdnost bistveno ne zmanjša. Iz bukovih desk smo izdelali lamelirane lepljene nosilce z uporabo standardnih zobatih spojev ter zobatih spojev z optimizirano geometrijo. Z upogibnimi testi nosilcev smo dokazali, da se je srednja vrednost upogibne trdnosti nosilcev z optimiziranimi zobatimi spoji znatno povečala, in sicer za približno 42 % glede na lamelirane lepljene nosilce s standardnimi zobatimi spoji. Srednja vrednost upogibne nosilnosti nosilcev z optimiziranimi zobatimi spoji je znašala 92.9 MPa.

Pripravili smo tudi računska orodja za analizo lameliranih lepljenih nosilcev z upoštevanjem vpliva zobatih spojev. Z analitičnim modelom smo pripravili analitične izraze za kinematične in ravnotežne količine v slojih dvoslojnega lepljenega nosilca z zobatimi spoji in upoštevanim zdrsa med sloji. Za kompleksnejše primere, smo pripravili numerični model, kjer je možno modelirati lamelirane lepljene nosilce s poljubnim številom slojev in zobatih spojev. Ko smo primerjali rezultate numeričnega modela z eksperimentalnimi rezultati upogibnih testov se je pokazalo zelo dobro ujemanje. V numeričnem modelu je možno upoštevati tudi nelinerni konstitutivni zakon materiala. Bukov les je sicer z eksperimentalnimi testi izkazal linearno elastično obnašanje.

Z analitičnim in numeričnim modelom smo tudi stohastično analizirali lamelirane lepljene nosilce iz bukovine. S stohastično analizo dvoslojnega nosilca z zobatim spojem smo ocenili vpliv togosti stika in togosti zobatega spoja na navpični pomik na sredini razpona nosilca ter zdrs med slojema. Vpliv togosti stika med sloji je bolj opazen v primeru navpičnih pomikov medtem, ko je vpliv togosti zobatega spoja bolj očiten pri zdrsu med slojema. Z numeričnim modelom smo opravili podobno parametričbo analizo vpliva na navpični pomik na sredini nosilca za različne togosti stika med sloji deset slojnega nosilca s stohastičnimi podatki. Pokazali smo, da lahko z numeričnim modelom smo izračunamo verjetnost porušitve ob določenih obtežbah.

Pri tem kot originalne prispevke izpostavljamo:

- Analiza vplivov geometrijskih parametrov zobatega spoja ter izbire lepila na natezno trdnost spoja.
- Predlog in izdelava nove geometrije zobatega spoja, ki je prilagojena visokim mehanskim zahtevam bukovega lesa.
- Eksperimentalne meritve nateznih trdnosti in togosti različnih geometrij zobatih spojev z uporabo različnih tipov lepil pri spajanju desk iz slovenskega bukovega lesa.
- Izdelava lepljenih lameliranih nosilcev iz slovenskega bukovega lesa z različnimi geometrijami zobatih spojev in eksperimentalne meritve upogibne trdnosti, togosti ter strižnega modula in togosti stika med lamelami lepljenega nosilca.
- Pri tem smo dokazali visoke mehanske lastnosti bukovega lesa za uporabo v konstrukcijske namene, saj smo, glede na podatke iz literature, izmerili najvišjo upogibno trdnost nosilcev iz bukovega lesa.
- Priprava prvega analitičnega modela za lepljene lamelirane nosilce z upoštevanjem zdrsa med sloji ter upoštevanjem vpliva zobatih spojev v lamelah.
- Priprava prvega numeričnega modela za lepljene nosilce s poljubnim številom lamel ter poljubnim številom zobatih spojev.
- Stohastična analiza mehanskih lastnosti na osnovi analitičnega in numeričnega modela lepljenih lameliranih nosilcev iz bukovega lesa.
- Del izsledkov predstavljenega dela je objavljen v revijah, ki so indeksirane v SCI. Oba članka sta priložena v priponkah.

Eksperimentalne meritve in izračunani rezultati prispevajo k razširitvi baze podatkov in poznavanja obnašanja lepljenjih konstrukcijskih elementov iz bukovega lesa ter s tem lahko pripomorejo pri pripravi smernic za izdelavo lepljenih lameliranih nosilcev iz bukovega lesa.

REFERENCES

Adam, C., Furtmüller, T., 2019. Moderately large deflections of composite beams with interlayer slip. In Contributions to Advanced Dynamics and Continuum Mechanics, 1–17. Springer. doi:10.1007/978-3-030-21251-3_1.

Adam, C., Furtmüller, T., 2020. Flexural vibrations of geometrically nonlinear composite beams with interlayer slip. Acta Mechanica 231, 1: 251–271. doi:10.1007/s00707-019-02528-2.

Adekola, A. O., 1968. Partial interaction between elastically connected elements of a composite beam. International Journal of Solids and Structures 4, 11: 1125–1135. doi:10.1016/0020-7683(68)90027-9.

Aicher, S., 2003. Structural adhesive joints including glued-in bolts. In Thelardensson, S., Larsen, H. J., Eds., Timber Engineering, 333–363. Wiley, Chichester, England.

Aicher, S., Höfflin, L., Behrens, W., 2001. A study on tension strength of finger joints in beech wood laminations. Otto-Graf-Journal 12: 169.

Aicher, S., Klöck, W., 1991. Finger joint analysis and optimisation by elastic, nonlinear and fracture mechanics finite element computations .

Aicher, S., Klöck, W., 2001. Linear vs. quadratic failure criteria for inplane tension loaded wood based panels. Otto-Graf-Journal , Vol.12: 187–199.

Aicher, S., Ohnesorge, D., 2011. Shear strength of glued laminated timber made from European beech timber. European Journal of Wood and Wood Products 69, 1: 143–154. doi:10.1007/s00107-009-0399-9.

Aicher, S., Radović, B., 1999. Investigations on the influence of finger-joint geometry on tension strength of finer-jointed glulam lamellas. Holz als Roh- und Werkstoff 57: 1–11. doi:10.1617/s11527-006-9117-9.

Aicher, S., Reinhardt, H. W., 2006. Delamination characteristics and shear strength of bonded beech lamellas with red heartwood. Holz Roh-Werkst 65: 125–136.

AkzoNobel, 2017. Product information: Laminated beam MUF system GripPro^{TM} Design. Instructions for use, Version 2.

Ammann, S., bullet, S., Schlegel, Beyer, M., bullet, K., Aehlig, bullet, M., Lehmann, M., Heiko, b., Niemz, P., 2016. Quality assessment of glued ash wood for construction engineering. Holz als Roh- und Werkstoff 74. doi:10.1007/s00107-015-0981-2.

Blaß, H. J., Denzler, J., Frese, M., Glos, P., Linsenmann, P., 2005. Biegefestigkeit von Brettschnitholz in Buche. University of Karlsruhe, Germany. doi:10.5445/KSP/1000001371.

Bonet, J., Wood, R. D., 1997. Nonlinear continuum mechanics for finite element analysis. Cambridge University Press.

CEN, 2001. Finger Jointed Structural Timber - Performance Requirements and Minimum Production Requirements. Standard, European Committee for Standardization. (In English language).

CEN, 2003. EN 13183: 2003 Moisture content of a piece of sawn timber-Part 1: Determination by oven dry method. (In English language).

CEN, 2006. SIST EN 301: 2006 Lepila na osnovi fenolov in aminoplastov za nosilne lesene konstrukcije – Razvrstitev in zahteve.

CEN, 2010. EN 408: 2010+A1: 2012 Timber structures - Structural timber and glued laminated timber - Determination of some physical and mechanical properties. (In English language).

CEN, 2013a. Glued laminated timber - Performance Requirements and Minimum Production Requirements. Standard, European Committee for Standardization. (In English language).

CEN, 2013b. SIST EN 302-1: 2013 Lepila za nosilne lesene konstrukcije – Preskusne metode 1. del: Ugotavljanje vzdolžne natezne strižne obremenitve.

CEN, 2013c. SIST EN 302-2: 2013 Lepila za nosilne lesene konstrukcije – Preskusne metode 2. del: Določanje odpornosti lepljenega stika prosti razslojevanju – delaminaciji.

CEN, 2013d. SIST EN 302-3: 2013 Lepila za nosilne lesene konstrukcije – Preskusne metode 3. del: Ugotavljanje vzdolžne natezne strižne obremenitve.

CEN, 2013e. Timber structures – Glued laminated timber and glued solid timber – Requirements. Standard, European Committee for Standardization. (In English language).

CEN, 2016a. EN 14358: 2016 Timber structures-Calculation and verification of characteristic values. (In English language).

CEN, 2016b. EN 338: 2016 Structural timber - Strength classes. European Committee for Standardization. (In English language).

CEN, 2016c. EN 384: 2016 Structural timber-Determination of characteristic values of mechanical properties and density. (In English language).

CEN, 2017. SIST EN 15425: 2017 Lepila – Enokomponentni poliuretan za nosilne konstrukcije – Razvrstitev in zahtevane lastnosti.

Challamel, N., Girhammar, U. A., 2012. Lateral-torsional buckling of vertically layered composite beams with interlayer slip under uniform moment. Engineering structures 34: 505–513. doi:10.1016/j.engstruct.2011.10.004.

Challamel, N., Girhammar, U. A., 2013. Lateral-torsional buckling of partially composite horizontally layered or sandwich-type beams under uniform moment. Journal of Engineering Mechanics 139, 8: 1047–1064. doi:10.1061/(ASCE)EM.1943-7889.0000489.

Collin, F., Ehlbeck, J., 1992. Load bearing capacity of finger-joint connections in glulam constructions. Bauen mit Holz 94: 586–593.

Conner, A., 2001. Wood: adhesives. In Buschow, K., Ed., Encyclopedia of materials: science and technology. Elsevier Science, Ltd., Amsterdam; New York.

Cowper, G. R., 1966. The Shear Coefficient in Timoshenko's Beam Theory. Journal of Applied Mechanics 33, 2: 335–340. doi:10.1115/1.3625046.

Crocombe, A. D., Ashcroft, I. A., 2008. Simple Lap Joint Geometry, 3–23. Springer Berlin Heidelberg, Berlin, Heidelberg. doi:10.1007/978-3-540-79056-3_1.

Čas, B., 2004. Nelinearna analiza kompozitnih nosilcev z upoštevanjem zdrsa med sloji: doktorska disertacija. Doctoral Thesis, University of Ljubljana, Faculty of Civil and Geodetic Engineering. URL https://repozitorij.uni-lj.si/IzpisGradiva.php?lang=slv&id=1451.

Čas, B., Planinc, I., Schnabl, S., 2018. Analytical solution of three-dimensional two-layer composite beam with interlayer slips. Engineering Structures 173: 269–282. doi:10.1016/j.engstruct.2018.06.108.

Čas, B., Saje, M., Planinc, I., 2004. Non-linear finite element analysis of composite planar frames with an interlayer slip. Computers & Structures 82, 23: 1901–1912. doi:10.1016/j.compstruc.2004.03.070. Computational Structures Technology.

Danielsson, H., 2013. Perpendicular to grain fracture analysis of wooden structural elements: Models and Applications. Doctoral Thesis, Department of Construction Sciences. Structural Mechanics. Lund University., Lund, Sweenden. URL https://lup.lub.lu.se/record/3633863.

Davis, G., 1997. The performance of adhesive systems for structural timbers. International Journal of Adhesion and Adhesives 17, 3: 247–255. doi:10.1016/S0143-7496(97)00010-9.

Deng, S., Djukic, L., Paton, R., Ye, L., 2015. Thermoplastic–epoxy interactions and their potential applications in joining composite structures – A review. Composites Part A: Applied Science and Manufacturing 68: 121–132. doi:10.1016/j.compositesa.2014.09.027.

Derikvand, M., Pangh, H., 2016. A modified method for shear strength measurement of adhesive bonds in solid wood. BioResources 11, 1: 354–364. URL https://ojs.cnr.ncsu.edu/index.php/BioRes/article/view/BioRes_11_1_354_Derikvand_Shear_Strength_Measurement.

DeSalvo, G., Swanson, J., 1985. ANSYS Engineering Analysis System User's Manual. Release 18.1, Help System, Coupled Field Analysis Guide.

Desch, H. E., Dinwoodie, J., 2016. Timber Structure, Properties, Conversion and Use. Macmillan Education, UK. doi:10.1007/978-1-349-13427-4.

DIBt, 2019. Allgemeine bauafsichticlhe Zulassung Z-9.1-679. Misc. Pub FPL-1816. Madison, Wis. : U.S. Dept. of Agriculture, Forest Service, Forest Products Laboratory, 1962: 40 pages.

Ecsedi, I., Baksa, A., 2016. Analytical solution for layered composite beams with partial shear interaction based on Timoshenko beam theory. Engineering Structures 115: 107–117. doi:10.1016/j.engstruct.2016.02.034.

Ehlbeck, J., Colling, F., Görlacher, R., 1985a. Einfluß keilgezinkter Lamellen auf die Biegefestigkeit von Brettschichtholzträgern-Eingangsdaten für das Rechenmodell. Holz als Roh-und Werkstoff 43, 8: 369–373.

Ehlbeck, J., Colling, F., Görlacher, R., 1985b. Einfluß keilgezinkter Lamellen auf die Biegefestigkeit von Brettschichtholzträgern-Entwicklung eines Rechenmodells. Holz als Roh-und Werkstoff 43, 8: 333–337.

Ehlbeck, J., Colling, F., Görlacher, R., 1985c. Einfluß keilgezinkter Lamellen auf die Biegefestigkeit von Brettschichtholzträgern-Überprüfung des Rechenmodells mit Hilfe von Trägerversuchen. Holz als Roh-und Werkstoff 43, 8: 439–442.

Ehrhart, R., T.and Steiger, Palma, P., Frangi, A., 2018a. Mechanical properties of European beech glued laminated timber. In Proceedings. 5th international network on timber engineering research (INTER) - Meeting 51, (16 pp.). Tallin, Estonia.

Ehrhart, T., Fink, G., Steiger, R., Frangi, A., 2016. Strength grading of European beech timber for the production of GLT & CLT. In International Network on Timber Engineering Research: Proceedings of Meeting 49, volume 49, 29–44. Timber Scientific Publishing, KIT Holzbau und Baukonstruktionen. doi:10.3929/ethz-a-010795316.

Ehrhart, T., Steiger, R., Palma, P., Frangi, A., 2018b. Estimation of the tensile strength of European beech timber boards based on density, dynamic modulus of elasticity and local fibre orientation. World Conference on Timber Engineering 2018, Seoul, Republic of Korea. doi:10.3929/ethz-b-000286967.

Erdogan, F., Ratwani, M. M., 1971. Stress Distribution in Bonded Joints. Journal of Composite Materials 5: 378–393.

Focacci, F., Foraboschi, P., De Stefano, M., 2015. Composite beam generally connected: Analytical model. Composite Structures 133: 1237–1248. doi:10.1016/j.compstruct.2015.07.044.

Foraboschi, P., 2009. Analytical solution of two-layer beam taking into account nonlinear interlayer slip. Journal of engineering mechanics 135, 10: 1129–1146.

Fortuna, B., Azinović, B., Plos, M., Šuligoj, T., Turk, G., 2020. Tension strength capacity of finger joined beech lamellas. European Journal of Wood and Wood Products 78, 5: 985–994. doi:10.1007/s00107-020-01588-9.

Fortuna, B., Plos, M., Šuligoj, T., Turk, G., 2018a. Mechanical properties of Slovenian structural beech timber. In Proceedings of the 2018 World Conference on Timber Engineering. WCTE, Seoul, Republic of Korea.

Fortuna, B., Plos, M., Šuligoj, T., Turk, G., 2018b. Strength grading of structural timber. In Common Foundations 2018-uniSTem: 6th Congress of Young Researches in the field of Civil Engineering and Related Sciences. Udruga hrvatskih građevinskih fakulteta, Sveučilište u Splitu, Fakultet građevinarstva, arhitekture i geodezije, Faculty of Civil Engineering, Architecture and Geodesy, Split, Croatia. doi:10.31534/CO/ZT.2018.09.

Fortuna, B., Turk, G., Schnabl, S., 2021. Analytical solution of a composite beam with finger joints and incomplete interaction between the layers. Acta Mechanica 232, 11: 4405–4427. doi:10.1007/s00707-021-03061-x.

Foschi, R., Barrett, J., 1980. Glued-Laminated Beam Strength: A Model. Journal of the Structural Division 106: 1735–1754.

Foschi, R., Bonac, T., 1977. Load-slip characteristics for connections with common nails. Wood Science 9, 3: 118–123.

Franke, B., Schusser, A., Müller, A., 2014. Analysis of finger joints from beech wood. WCTE.

Frese, M., Blass, H., 2006. Characteristic bending strength of beech glulam. Materials and Structures 40: 3–13. doi:10.1617/s11527-006-9117-9.

Frihart, C., 2009. Adhesive Groups and How They Relate to the Durability of Bonded Wood. Journal of Adhesion Science and Technology 23, 4: 601–617. doi:10.1163/156856108X379137.

Galuppi, L., Royer-Carfagni, G., 2012. Laminated beams with viscoelastic interlayer. International Journal of Solids and Structures 49, 18: 2637–2645. doi:10.1016/j.ijsolstr.2012.05.028.

Girhammar, U. A., 2009. A simplified analysis method for composite beams with interlayer slip. International Journal of Mechanical Sciences 51, 7: 515–530. doi:10.1016/j.ijmecsci.2009.05.003.

Girhammar, U. A., Gopu, V. K. A., 1993. Composite beam-columns with interlayer slip—exact analysis. Journal of Structural Engineering 119, 4: 1265–1282. doi:10.1061/(ASCE)0733-9445(1993)119:4(1265).

Golum, G. H., 1973. Some modufied matrix eigenvalue problems. SIAM review 15, 2: 318–334. doi:10.1137/1015032.

Goodman, J. R., Popov, E. P., 1968. Layered Beam Systems with Interlayer Slip. Journal of the Structural Division 94: 2535–2548. URL https://hdl.handle.net/10217/204900.

Hozjan, T., Saje, M., SrpčIč, S., Planinc, I., 2013. Geometrically and Materially Non-Linear Analysis of Planar Composite Structures with an Interlayer Slip. Comput. Struct. 114–115: 1–17. doi:10.1016/j.compstruc.2012.09.012.

Hughes, T., Pister, K., 1978. Consistent linearization in mechanics of solids and structures. Computers & Structures 8, 3: 391–397. doi:10.1016/0045-7949(78)90183-9.

Kellar, J., 2010. Key issues in selecting the right adhesive. In Advances in Structural Adhesive Bonding, 3–19. Elsevier. doi:10.1533/9781845698058.1.3.

Khelifa, M., Celzard, A., Oudjene, M., Ruelle, J., 2016. Experimental and numerical analysis of CFRP-strengthened finger-jointed timber beams. International Journal of Adhesion and Adhesives 68: 283–297. doi:10.1016/j.ijadhadh.2016.04.007.

Knorz, M., Neuhaeuser, E., Torno, S., Kuilen, J. W., 2015. Influence of surface preparation methods on moisture-related performance of structural hardwood-adhesive bonds. International Journal of Adhesion & Adhesives 57: 40–48. doi:10.1016/j.ijadhadh.2014.10.003.

Ko, M., Goodman, J., Vandrebilt, M., Criswell, M., Bodig, J., 1972. Layered beam systems with interlayer slip. URL https://hdl.handle.net/10217/204900.

Konnerth, J., Gindl, W., Harm, M., Müller, U., 2006. Comparing dry bond strength of spruce and beech wood glued with different adhesives by means of scarf- and lap joint testing method. Holz als Roh- und Werkstoff 64: 269–271. doi:10.1007/s00107-006-0104-1.

Konnerth, J., Kluge, M., Schweizer, G., Miljkovic, M., Gindl-Altmutter, W., 2016. Survey of selected adhesive bonding properties of nine European softwood and hardwood species. European Journal of Wood and Wood Products 74: 809–819. doi:10.1007/s00107-016-1087-1.

Kos, J., 2013. Kakovost lepljenja z različnimi mešanicami utekočinjenega lesa in MUF lepila. Magistrska naloga, Biotechnical faculty, University of Ljubljana, Self-published. URL http://www.digitalna-knjiznica.bf.uni-lj.si/lesarstvo/du2_kos_jure.pdf.

Kroflič, A., Saje, M., Planinc, I., 2011. Non-linear analysis of two-layer beams with interlayer slip and uplift. Computers & structures 89, 23-24: 2414–2424. doi:10.1016/j.compstruc.2011.06.007.

Kroflič, A., 2012. Nelinearna analiza večslojnih kompozitnih konstrukcij. Doctoral Thesis, University of Ljubljana., Ljubljana.

Kržan, M., Azinović, B., Fortuna, B., 2019. Hybrid glulam beam made of beech and spruce laminations–experimental and numerical investigation. In Proceedings of CompWood 2019 Conference, 89–89. Växjö, Sweden.

Lehmann, M., 2019. Personal communication.

Lolić, D., Zupan, D., Brojan, M., 2020. A consistent finite element formulation for laminated composites with nonlinear interlaminar constitutive law. Composite Structures 247: 112445. doi: 10.1016/j.compstruct.2020.112445.

Milner, H., Tan, H., 2001. Modelling deformation in nailed, thin-webbed timber box beams. Computers & Structures - COMPUT STRUCT 79: 2541–2546. doi:10.1016/S0045-7949(01)00138-9.

Milner, H. R., Yeoh, E., 1991. Finite Element Analysis of Glued Timber Finger Joints. Journal of Structural Engineering 117, 3: 755–766. doi:10.1061/(ASCE)0733-9445(1991)117:3(755).

Müller, U., Veigel, S., Follrich, J., Gabriel, J., Gindl, W., 2009. Performance of One Component Polyurethane in Comparison to Other Wood Adhesives.

Newmark, N. M., 1951. Test and analysis of composite beams with incomplete interaction. Proceedings of Society for Experimental Stress Analysis 9, 1: 75–92. URL https://ci.nii.ac.jp/naid/10004543145/en/.

Norris, C. B., 1962. Strength of orthotropic materials subjected to combined stresses. Technical report Report No. 1816, US Forest Products Laboratory, Madison (WI),USA.

Patton-Mallory, M., Cramer, S. M., 1987. Fracture mechanics: a tool for predicting wood component strength. Forest Product Journal 37, 7/8: 39–47.

Peperko, J., 2006. Tradicionalna gradnja lesenih stavb na Dolenjskem: diplomsko delo (visokošolski strokovni študij). B.s. thesis, Biotecnical Faculty, University of Ljubljana. URL https://repozitorij.uni-lj.si/IzpisGradiva.php?lang=slv&id=133.

Planinc, I., 1998. Račun kritičnih točk konstrukcij s kvadratično konvergentnimi direktnimi metodami. Doctoral Thesis, University of Ljubljana, Ljubljana.

Plos, M., Fortuna, B., Straže, A., Turk, G., 2018a. Visual grading of beech wood. Proceedings of the 2018 World Conference on Timber Engineering, Seoul, Republic of Korea.

Plos, M., Fortuna, B., Šuligoj, T., Turk, G., 2018b. Beech as construction wood. In Common Foundations 2018-uniSTem: 6th Congress of Young Researches in the field of Civil Engineering and Related Sciences. Udruga hrvatskih građevinskih fakulteta, Sveučilište u Splitu, Fakultet građevinarstva, arhitekture i geodezije, Faculty of Civil Engineering, Architecture and Geodesy, Split, Croatia. doi:10.31534/CO/ZT.2018.25.

Plos, M., Fortuna, B., Šuligoj, T., Turk, G., 2022. From Visual Grading and Dynamic Modulus of European Beech (Fagus sylvatica) Logs to Tensile Strength of Boards. Forests 13, 1. doi:10.3390/f13010077. URL https://www.mdpi.com/1999-4907/13/1/77.

Qiu, L., Zhu, E., Van de Kuilen, J., 2014. Modeling crack propagation in wood by extended finite element method. European Journal of Wood and Wood Products 72, 2: 273–283. doi:10.1007/s00107-013-0773-5.

Ranzi, G., Bradford, M., 2006. Analytical solutions for the time-dependent behaviour of composite beams with partial interaction. International Journal of Solids and Structures 43, 13: 3770–3793. doi:10.1016/j.ijsolstr.2005.03.032.

Rassam, H. Y., Goodman, J., et al., 1970. Buckling behavior of layered wood columns. Wood Science 2, 4: 238–46.

Reissner, E., 1972. On one-dimensional finite-strain beam theory: The plane problem. Journal of Applied Mechanics and Physics (ZAMP) 23: 795–804. doi:10.1007/BF01602645.

Rodman, U., 2009. Analiza nosilnosti prostorskih okvirnih konstrukcij z upoštevanjem materialnih in geometrijskih nepopolnost. Doctoral Thesis, University of Ljubljana., Ljubljana.

Saje, M., Planinc, I., Turk, G., Vratanar, B., 1997. A kinematically exact finite element formulation of planar elastic-plastic frames. Computer Methods in Applied Mechanics an Engineering 144: 125–151.

Sandhaas, C., 2012. Mechanical behaviour of timber joints with slotted-in steel plates. Doctoral Thesis, Technical University Delft, Delft, Netherlands. URL http://resolver.tudelft.nl/uuid:df5dbd8f-d19e-407d-aadd-48ad29a5fe97.

Sandhaas, C., Sarnaghi, A., van de Kuilen, J., 2019. Numerical modelling of timber and timber joints: computational aspects. Wood Science and Technology 54 (2020), 1: 31–61. doi:10.1007/s00226-019-01142-8.

Schnabl, S., 2007. Analiza obnašanja kompozitnih nosilcev pri požaru. Doctoral Thesis, University of Ljubljana., Ljubljana.

Schnabl, S., Planinc, I., 2011. The effect of transverse shear deformation on the buckling of two-layer composite columns with interlayer slip. International Journal of Non-Linear Mechanics 46, 3: 543–553. doi:10.1016/j.ijnonlinmec.2011.01.001.

Schnabl, S., Saje, M., Turk, G., Planinc, I., 2007. Locking-free two-layer Timoshenko beam element with interlayer slip. Finite Elements in Analysis and Design 43, 9: 705–714. doi:10.1016/j.finel.2007.03.002.

Sebera, V., Pečnik, J., Azinović, B., Milch, J., Huč, S., 2021. Wood-adhesive bond loaded in mode II: experimental and numerical analysis using elasto-plastic and fracture mechanics models. Holzforschung 75, 7: 655–667. doi:10.1515/hf-2020-0141.

Serrano, E. Adhesive joints in timber engineering - modelling and testing of fracture properties. Doctoral Thesis, Division of Structural Mechanics, LTH, Lund University, Lund, Sweden. URL https://lup.lub.lu.se/record/41135,.

Serrano, E., 2001. Glued-in rods for timber structures—An experimental study of softening behaviour. Materials and Structures 34: 228–234. doi:10.1007/BF02480593.

Serrano, E., 2003. Mechanical Performance and Modelling of Glulam. In Thelandersson, S., Larsen, H. J., Eds., Timber Engineering, 333–363. Wiley, Chichester, England.

Siciliano, A. F., Škec, L., Jelenić, G., 2021. Closed-form solutions for modelling the rotational stiffness of continuous and discontinuous compliant interfaces in two-layer Timoshenko beams. Acta Mechanica 232, 7: 2793–2824. doi:10.1007/s00707-021-02958-x.

da Silva, L., Campilho, R., 2012. Advances in Numerical Modelling of Adhesive Joints. Springer, Berlin, Heidelberg. doi:10.1007/978-3-642-23608-2_1.

da Silva, L., das Neves, P., Adams, R., Spelt, J., 2009. Analytical models of adhesively bonded joints—Part I: Literature survey. International Journal of Adhesion and Adhesives 29, 3: 319–330. doi:10.1016/j.ijadhadh.2008.06.005.

Simo, J., 1985. A finite strain beam formulation. The three-dimensional dynamic problem. Part I. Computer Methods in Applied Mechanics and Engineering 49, 1: 55–70. doi:10.1016/0045-7825(85)90050-7.

Smith, M., 2009. ABAQUS/Standard User's Manual, Version 6.9. Dassault Systèmes Simulia Corp, United States.

Sousa Jr, J., Silva, A., 2010. Analytical and numerical analysis of multilayered beams with interlayer slip. Engineering Structures 32: 1671–1680. doi:10.1016/j.engstruct.2010.02.015.

Sterley, M., Gustafsson, P., 2012. Shear fracture characterization of green-glued polyurethane wood adhesive bonds at various moisture and gluing conditions. Wood Material Science & Engineering 7, 2: 93–100. doi:10.1080/17480272.2012.662997.

Šernek, M., 2018. Reologija in kinetika utrjevanja lepil za les. Class Lecture.

Šernek, M., Resnik, J., Kamke, F., 1999. Penetration of liquid urea-formaldehyde adhesive into beech wood. Wood and Fiber Science 31, 1: 41–48.

Šernek, M., Kutnar, A., 2009. Proučevanje vpliva količine katalizatorja na utrjevanje urea-formaldehidnega in melamin-urea-formaldehindega lepila z diferenčno dinamično kalorimetrijo. Les:revija za lesno gospodarstvo 61, 2: 47–53.

Timoshenko, S. P., 1921. On the correction for shear of the differential equation for transverse vibrations of prismatic bars. The London, Edinburgh, and Dublin Philosophical Magazine and Journal of Science 41, 245: 744–746. doi:10.1080/14786442108636264.

Tran, V. D., Oudjene, M., Méausoone, P.-J., 2014. FE analysis and geometrical optimization of timber beech finger-joint under bending test. International Journal of Adhesion and Adhesives 52. doi: 10.1016/j.ijadhadh.2014.03.007.

Tran, V. D., Oudjene, M., Méausoone, P.-J., 2015. Experimental and numerical analyses of the structural response of adhesively reconstituted beech timber beams. Composite Structures 119: 206–217. doi: 10.1016/j.compstruct.2014.08.013.

Ugovšek, A., Šernek, M., 2012. Proučevanje vpliva količine katalizatorja na utrjevanje urea-formaldehidnega in melamin-urea-formaldehindega lepila z diferenčno dinamično kalorimetrijo. Les:revija za lesno gospodarstvo 64, 1/2: 6–11.

Ülker, O., 2016. Wood Adhesives and Bonding Theory. doi:10.5772/65759.

Vratanar, B., Saje, M., 1998. A consistent equilibrium in a cross-section of an elastic-plastic beam. International Journal of Solids and Structures ASCE 36, 7: 311–337. doi:10.1007/BF01602645.

Washizu, K., 1994. Variational Methods in Elasticity and Plasticity. Pergamon Press, Paris.

Westermayr, M., Stapel, P., Van de Kuilen, J. W., 2018. Tensile and Compression Strength of Small Cross Section Beech (Fagus s.) Glulam Members. International council for building research INTER/51-12-2, Tallinn, Estonia.

Wolfram Research, I. Mathematica, Version 11.2. Champaign, Illinois,2017.

Wu, P., Zhou, D., Liu, W., 2016a. 2-D elasticity solutions of two-layer composite beams with an arbitrarily shaped interface. Applied Mathematical Modelling 40, 2: 1477–1493. doi:10.1016/j.apm.2015.06.034.

Wu, P., Zhou, D., Liu, W., Wan, L., Liu, D., 2016b. Elasticity solution of two-layer beam with a viscoelastic interlayer considering memory effect. International Journal of Solids and Structures 94: 76–86. doi:10.1016/j.ijsolstr.2016.05.007.

Xu, R., Wang, G., 2013. Bending solutions of the Timoshenko partial-interaction composite beams using Euler-Bernoulli solutions. Journal of Engineering Mechanics 139, 12: 1881–1885. doi:10.1061/(ASCE)EM.1943-7889.0000614.

Xu, R., Wu, Y.-F., 2009. Analytical study of beams strengthened by adhesively bonded reinforcement with variable properties using state space method. Composites Science and Technology 69, 11-12: 1912–1918. doi:10.1016/j.compscitech.2009.04.011.

ZAG. ZAG cerificates. URL https://www.zag.si/si/certifikati/befe3de5c194f6ecf0e2c35e239fcfa3. Accessed: 2022-03-20.

ZGS, 2020. Poročilo Zavoda za gozdove Slovenije o gozdovih za leto 2020 (Annual report on Slovenian forests). Technical report Publication 2020, Slovenian Forests Service, Ljubljana, Slovenia.

Zienkiewich, O., Taylor, R., 1991. The finite element method. Volumen 2. McGraw-Hill, London.

Appendices / Priloge

Two articles, already published in the SCI indexed journals:

1. FORTUNA, Barbara, AZINOVIĆ, Boris, PLOS, Mitja, ŠULIGOJ, Tamara, TURK, Goran. Tension strength capacity of finger joined beech lamellas. European journal of wood and wood products. [Print ed.]. 2020, letn. 78, avg., str. 985-994, ilustr. ISSN 0018-3768. DOI: 10.1007/s00107-020-01588-9.
   Link to the full paper: https://rdcu.be/cWz2a

2. FORTUNA, Barbara, TURK, Goran, SCHNABL, Simon. Analytical solution of a composite beam with finger joints and incomplete interaction between the layers. Acta mechanica. Nov. 2021, vol. 232, iss. 11, str. 4405-4427, ilustr. ISSN 0001-5970. https://link.springer.com/article/10.1007/s00707-021-03061-x, DOI: 10.1007/s00707-021-03061-x
   Link to the full paper: https://rdcu.be/cWz3w

“Blank page.”